R-09-22

# SR-Site groundwater flow modelling methodology, setup and results

Jan-Olof Selroos, Svensk Kärnbränslehantering AB

Sven Follin, SF GeoLogic AB

December 2010

**Svensk Kärnbränslehantering AB**
Swedish Nuclear Fuel
and Waste Management Co

Box 250, SE-101 24 Stockholm
Phone +46 8 459 84 00

SKB

ISSN 1402-3091
SKB R-09-22
ID 1271844
Updated 2013-08

# SR-Site groundwater flow modelling methodology, setup and results

Jan-Olof Selroos, Svensk Kärnbränslehantering AB

Sven Follin, SF GeoLogic AB

December 2010

*Keywords*: Hydrogeology, Groundwater, Modelling, Excavation, Operation, Temperate, Periglacial, Glacial, Forsmark, Safety assessment.

**Update notice**

The original report, dated December 2010, was found to contain both factual and editorial errors which have been corrected in this updated version. The corrected factual errors are presented below.

**Updated 2013-08**

| Location | Original text | Corrected text |
|---|---|---|
| Page 25, Table 2-2, column 4, rows 1, 2 and 5 | Wrong data in table | Table updated with correct data |
| Page 25, Table 2-2, column 5, rows 1–15 | Wrong data in table | Table updated with correct data |
| Page 25, Table 2-2, column 6, line 6 | (–7.0, 1.2) | (–6.7, 1.2) |
| Page 25, Table 2-3, column 3, rows 1–5 | Wrong data in table | Table updated with correct data |
| Page 25, Table 2-3, column 5, rows 1–5 | Wrong data in table | Table updated with correct data |
| Page 26, Table 2-4, column 5, rows 1–10 | Wrong data in table | Table updated with correct data |

The updated tables show the correct input values used in the modelling presented in the original version of this report; i.e. all results are identical between the original and the up-dated versions of the report.

# Preface

The work presented in the current report is to a great extent a compilation and summary of results presented in more detailed reports describing the hydrogeological modelling performed as part of SR-Site. The modelling has been planned, managed, and evaluated within the SKB hydrogeology discipline-specific group HydroNet. The work and collaborative spirit of all HydroNet members is truly acknowledged.

The authors of the present report have borrowed, and built on, text and figures from the more detailed reports freely when details of the individual modelling studies are summarised and results exemplified. However, higher-level statements made and conclusions drawn, in a SR-Site context, in the present report are the sole responsibility of the authors.

*Jan-Olof Selroos*

Manager Hydrogeological Modelling SR-Site

# Abstract

As a part of the license application for a final repository for spent nuclear fuel at Forsmark, the Swedish Nuclear Fuel and Waste Management Company (SKB) has undertaken three groundwater flow modelling studies. These are performed within the SR-Site project and represent time periods with different climate conditions. The simulations carried out contribute to the overall evaluation of the repository design and long-term radiological safety. Three time periods are addressed; the Excavation and operational phases, the Initial period of temperate climate after closure, and the Remaining part of the reference glacial cycle.

The present report is a synthesis of the background reports describing the modelling methodology, setup, and results. It is the primary reference for the conclusions drawn in a SR-Site specific context concerning groundwater flow during the three climate periods. These conclusions are not necessarily provided explicitly in the background reports, but are based on the results provided in these reports. The main results and comparisons presented in the present report are summarised in the SR-Site Main report.

# Sammanfattning

I Svensk Kärnbränslehanterings (SKB) ansökan om ett slutförvar för använt kärnbränsle i Forsmark ingår tre olika grundvattenmodelleringsstudier. Studierna har utförts inom projekt SR-Site och hanterar grundvattenströmning under perioder med olika klimatförhållanden. Dessa är Byggnations- och driftskedena, den Initiala perioden av tempererade förhållanden efter förvarets förslutning, samt den Återstående perioden av referensglacialcykeln. Beräkningsresultaten från de utförda simuleringarna ingår i bedömningsunderlaget inom design och långsiktig säkerhet.

Föreliggande rapport sammanfattar de tre modelleringsstudiernas uppställning, genomförande och resultat. Rapporten utgör huvudreferens för SR-Site vad gäller slutsatser angående frågeställningar som är kopplade till grundvattenströmning under de tre klimatperioderna. Dessa slutsatser finns inte nödvändigtvis redovisade i de tre grundvattenmodelleringsstudierna, även om underlaget för slutsatserna redovisas i dessa. De väsentligaste resultaten och jämförelserna som redovisas i denna rapport sammanfattas i SR-Site:s huvudrapport.

# Contents

# 1 Introduction

## 1.1 Background of the SR-Site project and its relation to the present report

As a part of the license application for a final repository for spent nuclear fuel, the Swedish Nuclear Fuel and Waste Management Company (SKB) has performed the SR-Site project. The objective of SR-Site is to assess the long term safety of a KBS-3 type repository located at Forsmark in Northern Uppland of Sweden.

SR-Site contains a main report, here denoted the SR-Site Main report /SKB 2011/, and a set of primary references, here denoted the Level II reports. These include among others, with specific relevance for the current report, the Climate report /SKB 2010a/, Data report /SKB 2010b/, Geosphere process report /SKB 2010c/, and Radionuclide transport report /SKB 2010d/. In addition, there are a number of additional references, here denoted Level III reports. Within the hydrogeological modelling of the bedrock, a series of four Level III reports are produced. Three of these are background reports that describe simulations of the operational phase or different post-closure climate situations. The fourth, the present report, is a synthesis of these background reports, providing the primary reference for the Hydrogeological modelling performed in support of SR-Site. It is noted that the present report also draws conclusions in a SR-Site specific context; these conclusions are not necessarily provided explicitly in the background reports, but are based on the results provided in these reports.

The present report serves as a reference for the Data report concerning hydrogeological data used within SR-Site. The report also serves as a primary reference for the SR-Site Main report concerning results obtained within the different hydrogeological model applications. Specifically, the results obtained within the three Level III background reports are here put in a SR-Site context. The main results and comparisons presented in this report are summarised in the SR-Site Main report; here more details are provided.

## 1.2 Objectives

The main objectives of the report are to:

- Provide an integrated account of all hydrogeological modelling performed as part of SR-Site. This is to serve as a benefit to readers who want an integrated description of all hydrogeological modelling performed.
- Summarise the hydrogeological modelling strategy and model setups used in SR-Site, specifically how the different time periods, scales, and model tools relate to each other.
- Provide a rationale for the hydrogeological base cases and variants defined for the different hydrogeological model applications.
- Provide an evaluation and discussion of the results obtained in the different hydrogeological model applications.
- Present additional analyses, results and comparisons of importance for SR-Site not included in the Level III reports.

## 1.3 Relation to SDM-Site

The hydrogeological description in SR-Site is based on the site descriptive model SDM-Site, and is essentially identical to SDM-Site concerning hydrogeological conceptualisation and parameterisation. A few minor changes have been made and are motivated and reported in the present report when the different model applications are introduced.

## 1.4 Outline of report

The outline of the report is as follows: Chapter 1 presents the background and objectives of the report as well as a description of how the results of the hydrogeological modelling are used in subsequent analyses within the SR-Site project. Chapter 2 is a brief summary of the hydrogeological model in SDM-Site and hence the primary input used in the modelling presented here. Chapter 3 describes the modelling methodology as well as the time periods analysed and model domains utilised. Chapter 4 through 6 present the three different modelling applications. Within each chapter, the analyses requested by SR-Site are provided, and the various base cases and alternatives used in the modelling studies are presented along with the results. Chapter 7 presents an integration between the different model applications and disciplines within SR-Site not reported in the Level 3 reports. Chapter 8 provides a summary of the main results for further use in SR-Site.

## 1.5 Usage of results from hydrogeological modelling within SR-Site

The hydrogeological modelling of the bedrock serves several assessment activities within SR-Site. First, the results are as such a description of the hydrogeological conditions during different assessment phases. Second, various sets of results are exported to other disciplines such as radionuclide transport calculations, hydrogeochemistry, and biosphere analyses. The specific usages of the hydrogeological results are highlighted in the relevant chapters below (Chapters 4 through 6) and summarised in Section 7.4.

A key notion of the hydrogeological analyses is highlighted already in this introductory text. While hydrogeology within safety assessment applications traditionally has been focussed on delivering output data and conditions for use within transport calculations of radionuclides escaping from the repository, the hydrogeological analyses within SR-Site devote particular attention to the evolution of hydrogeochemical conditions in the geosphere driven by changes in the climate and surface system. This is because hydrogeochemical conditions in the bedrock have a significant bearing on the long-term performance of the buffer. Hence, the geosphere needs to be assessed both in terms of its affect on the engineered barriers as well as its own performance as a barrier. Thus, the classical view of the geosphere as a barrier only, serving as a prerequisite for containment or isolation of the repository, is not strictly relevant. Both transport from the surface to the repository, and for certain assumptions and conditions, from the repository to the surface is studied.

Given the hydrogeological evolution driven by a changing climate, the geosphere is a dynamic system from hydrogeological and hydrogeochemical points of view. The present report tries to convey this notion of a dynamic system; it illustrates how the effects of climate have been described as a cycle of different phases each with associated hydrogeological conditions and processes, and how these have been conceptualised in numerical models. How the findings of each climate phase provide input to subsequent assessment analyses and robust safety cases arguments is also described. The analyses of various uncertainties are described along with how these inform safety assessment and supporting arguments.

## 1.6 Setting of the Forsmark site

The Forsmark area is located in northern Uppland within the municipality of Östhammar, about 120 km north of Stockholm (Figure 1-1). The candidate area for site investigation is located along the shoreline of Öregrundsgrepen. It extends from the Forsmark nuclear power plant and the access road to SFR in the north-west (SFR is an existing repository for short-lived radioactive waste) to Kallrigafjärden in the south-east (Figure 1-1). It is approximately 6 km long and 2 km wide. The north-western part of the candidate area was selected as the target area/volume for the complete site investigation work /SKB 2005b/ (Figure 1-2).

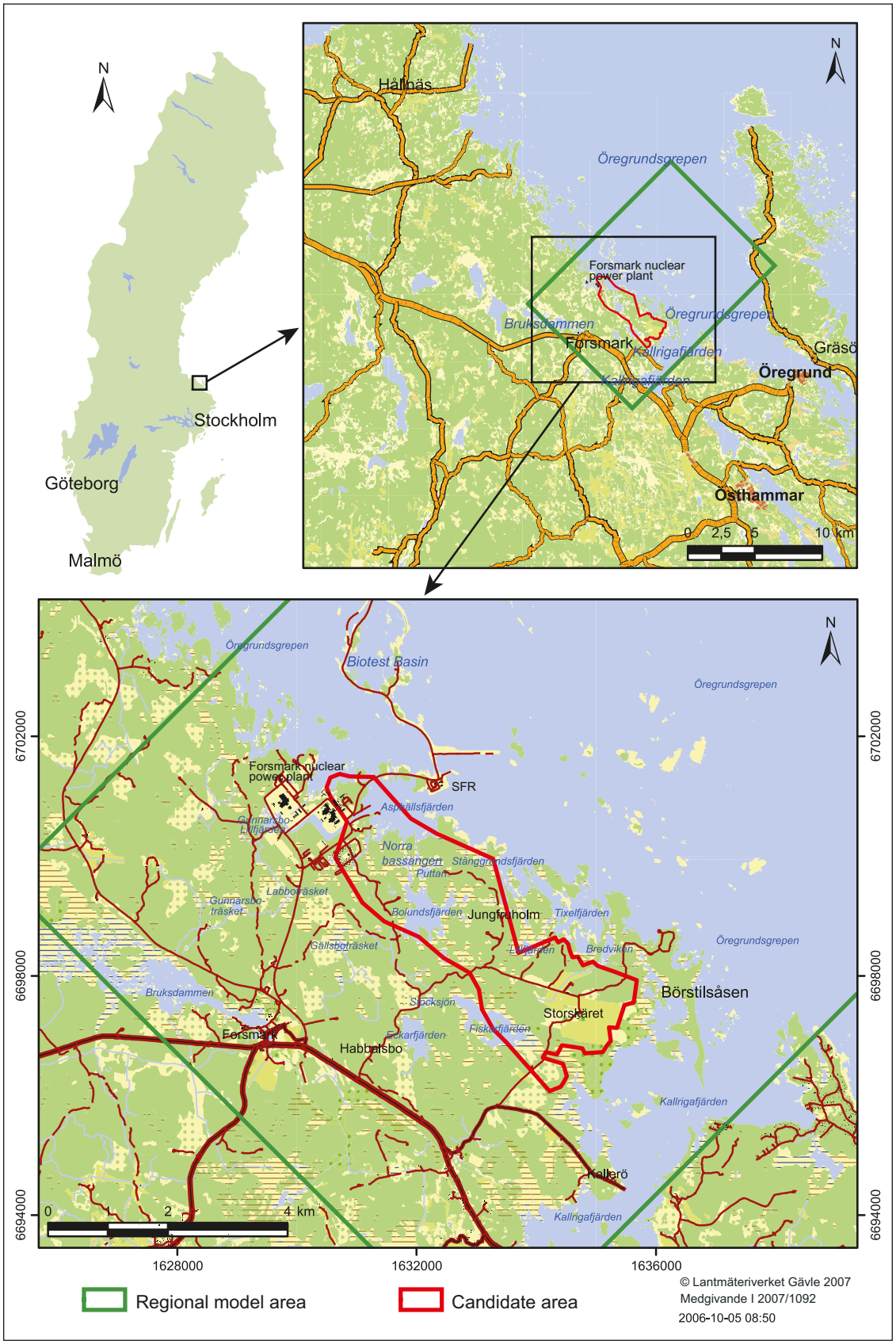


***Figure 1-1.*** *The red polygon shows the size and location of the candidate area for site investigations at Forsmark. The green rectangle indicates the size and location of the regional model area used in SDM-Site.*

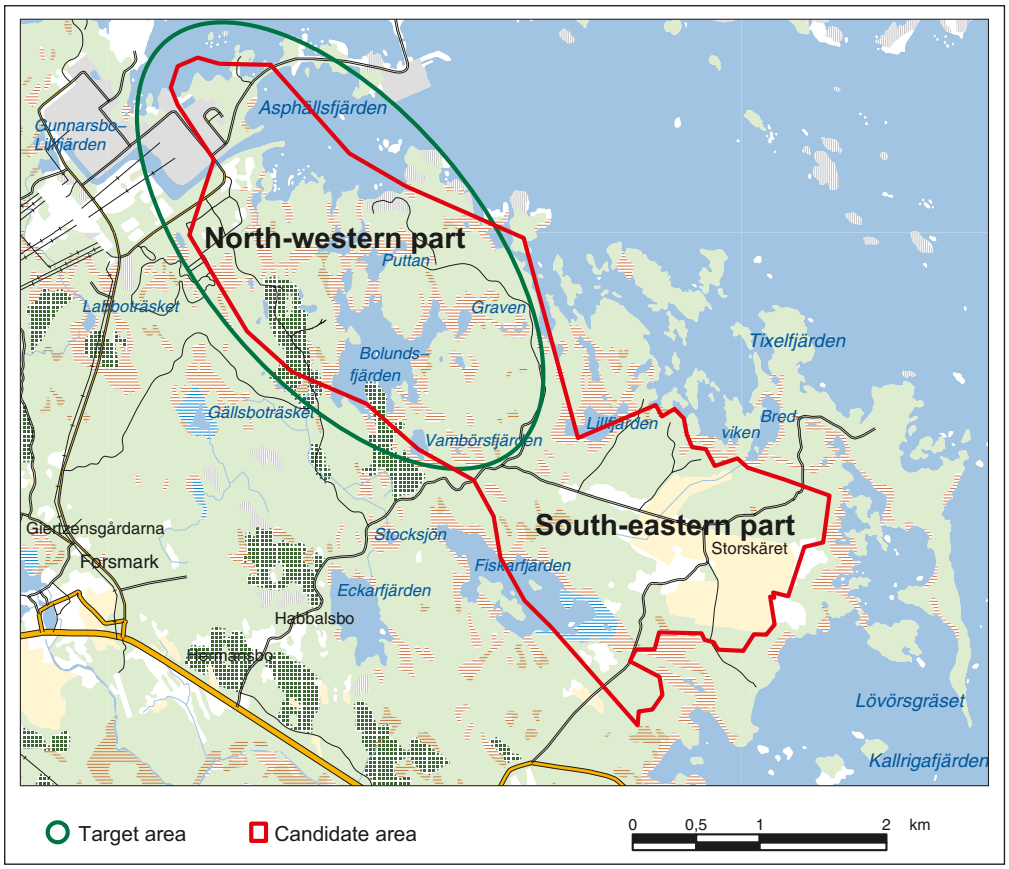


***Figure 1-2.*** *The north-western part of the candidate area was selected as the target area/volume for the complete site investigation work.*

The Forsmark area consists of crystalline bedrock that belongs to the Fennoscandian Shield, one of the ancient continental nuclei of the Earth. The bedrock at Forsmark in the south-western part of this shield formed between 1.89 and 1.85 billion years ago during the Svecokarelian orogeny /SKB 2005a/. It has been affected by both ductile and brittle deformation. The ductile deformation has resulted in large-scale, ductile high-strain belts and more discrete high-strain zones, the orientation of which is indicated in Figure 1-3. Tectonic lenses, in which the bedrock is less affected by ductile deformation, are enclosed between the ductile high strain belts. The candidate area is located in the north-westernmost part of one of these tectonic lenses. This lens extends from north-west of the nuclear power plant south-eastwards to the area around Öregrund (Figure 1-3). The brittle deformation has given rise to reactivation of the ductile zones in the colder, brittle regime and the formation of new brittle fracture zones of variable size.

The current ground surface in the Forsmark region forms a part of the sub-Cambrian peneplain in south-eastern Sweden. This peneplain comprises a relatively flat topographic surface with a gentle dip towards the east that formed more than 540 million years ago. The bedrock is covered by a few metres of Quaternary deposits (glacial till mainly). The ground surface is characterised by small-scale topography at low altitude (Figure 1-4). The most elevated areas to the south-west of the candidate area are located at c 25 m above the Swedish Ordnance Datum RHB 70. The whole area is located below the highest coastline associated with the last glaciation, and large parts of the candidate area emerged from the Baltic Sea only during the last 2,000 years. Both the flat topography and the still ongoing shore-level displacement of c 6 mm/y strongly influence the current landscape (Figure 1-4). Sea bottoms are continuously transformed into new terrestrial areas or freshwater lakes, and lakes and wetlands are successively infilled by peat. The average specific discharge (net precipitation) is approximately 150 mm/y /SKB 2008/.

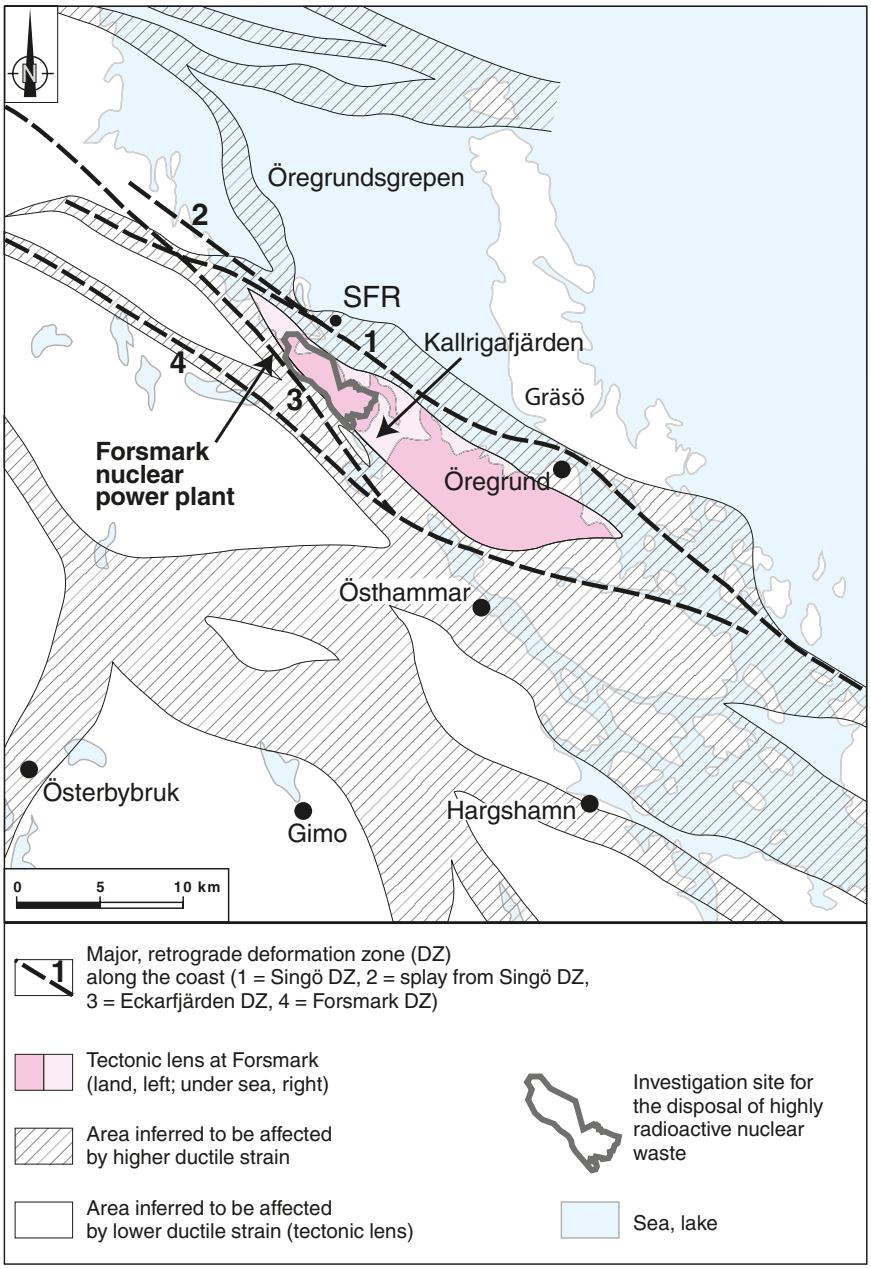


***Figure 1-3.*** *Tectonic lens at Forsmark and areas affected by strong ductile deformation in the area close to Forsmark.*


***Figure 1-4.*** *Photographs from Forsmark showing the flat topography and the low-gradient shoreline with recently isolated bays due to land uplift. Top: looking south from SFR across Asphållsfjärden. Bottom: looking north-east from the centre of the candidate area.*

# 2 Hydrogeological modelling within SDM-Site

## 2.1 Primary data

The north-western part of the candidate area was selected as the target area/volume for the complete site investigation work, see Figure 2-1. The hydrogeology of the bedrock is summarised in /Follin 2008/ and presented in more detail in /Follin et al. 2007a, b, 2008/.

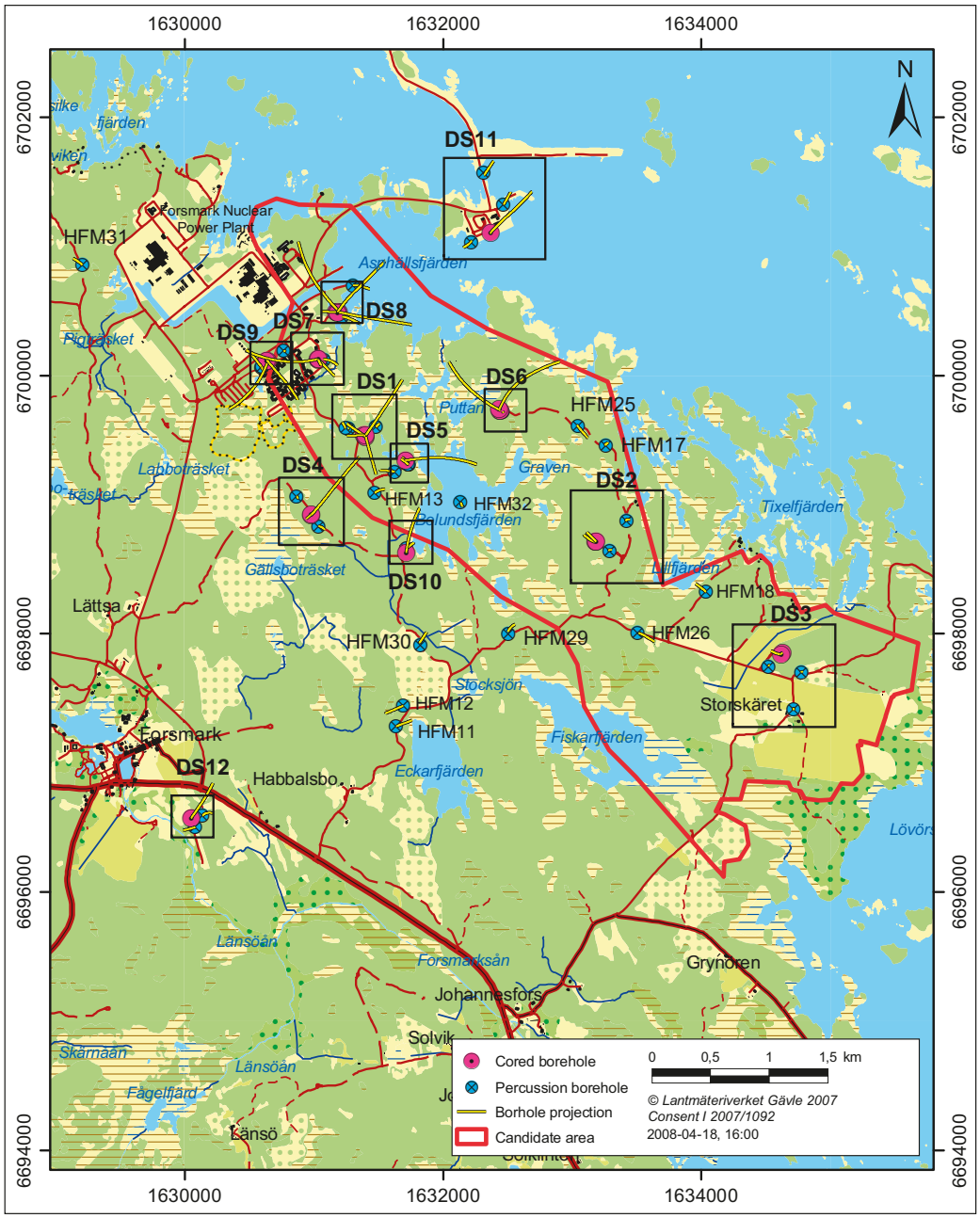


***Figure 2-1.*** *Map showing the 25 core-drilled and the 38 percussion-drilled boreholes produced during the site investigation at Forsmark between years 2002–2007. The projection of the boreholes on the ground surface due to their inclination is also shown. The ellipse indicates the target area/volume. (Modified after Figure A-1 in /Follin 2008/.)*

Table 2-1 lists the 25 cored boreholes shown in Figure 2-1. These are investigated with the Posiva Flow Log (PFL) method and the Pipe String System (PSS) method. The hydraulic data acquired from these tests are used to parameterise the deterministically defined deformation zones and the fracture networks contained in the rock mass volumes in between the deformation zones. In SKB's approach to hydraulic assessment, the former are referred to as Hydraulic Conductor Domains (HCD), whereas the latter are referred to as Hydraulic Rock mass Domains (HRD), see Section 3.4.1 for details.

The 38 percussion-drilled boreholes shown in Figure 2-1 are investigated by means of open hole pumping tests in combination with impeller flow logging (HTHB method). The hydraulic data acquired from these tests are used to parameterise the horizontal to sub-horizontal sheet joints that occur in the uppermost150 m of the bedrock within the north-western part of the tectonic lens. This part of the flow model domain is called the shallow bedrock aquifer, see /Follin 2008/ for details.

The fractured rock mass volumes between the deterministically modelled deformation zones are divided into six fracture domains, FFM01–FFM06 based on the fracture frequency of *all* fractures /Olofsson et al. 2007/. The key fracture domains in the target area/volume aimed for a deep repository; FFM01 and FFM06, occur below fracture domain FFM02, see Figure 2-2 and Figure 2-3.

At Forsmark, the HRD geometries are identical to the geometries of the fracture domains. However, the six fracture domains are refined in the hydrogeological modelling based on the differences observed in the frequency of flowing fractures (conductive fracture frequency) versus depth, see /Follin 2008/ for details. The primary data used for this refinement come from the difference flow logging measurements carried out with the PFL method, see /Follin et al. 2007a/ for details. In summary, three of the six fracture domains are split into two sub-units each (FFM03–FFM05) and two fracture domains are split into three sub-units each (FFM01 and FFM06). One fracture domain was kept unchanged (FFM02).

Structural-hydraulic data from twelve cored boreholes /Follin et al. 2007a/ are used in the detailed hydrogeological modelling of the target area/volume. The twelve boreholes are drilled at different locations and in different orientations in the rock mass volumes surrounding the repository. Figure 2-4 shows a view of the borehole locations with upper layers transparent.

**Table 2-1. List of the cored boreholes at Forsmark tested with the PFL and PSS methods. (Modified after Table B-4 in /Follin et al. 2008/.)**

| Borehole | PFL | PSS | Bottom elevation of borehole (m) | Borehole | PFL | PSS | Bottom elevation of borehole (m) |
|---|---|---|---|---|---|---|---|
| KFM01A | X | X | –982 | KFM07A | X | | –819 |
| KFM01B | | X | –479 | KFM07B | | X | –238 |
| KFM01C | | X | –333 | KFM07C | X | | –494 |
| KFM01D | X | X | –612 | KFM08A | X | X | –759 |
| KFM02A | X | X | –987 | KFM08B | | X | –166 |
| KFM02B | X | X | –565 | KFM08C | X | | –781 |
| KFM03A | X | X | –987 | KFM08D | X | | –751 |
| KFM03B | | X | –88 | KFM09A | | X | –621 |
| KFM04A | X | X | –796 | KFM09B | | X | –472 |
| KFM05A | X | X | –825 | KFM10A | X | X | –338 |
| KFM06A | X | X | –826 | KFM11A | X | X | –716 |
| KFM06B | X | X | –93 | KFM12A | | X | –511 |
| KFM06C | | X | –781 | | | | |

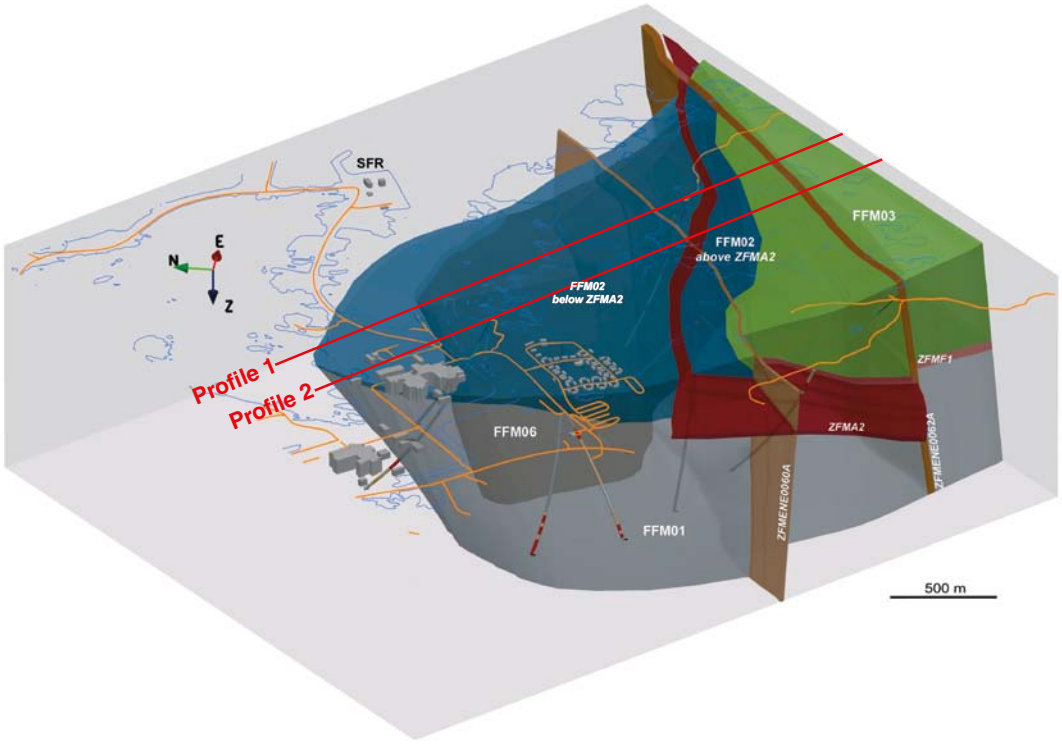


***Figure 2-2.*** *Three-dimensional view to the East-North-East showing the relationship between deformation zone ZFMA2 (red) and fracture domain FFM01-03 and FFM06. Profile 1 and 2 are shown as cross-sections in Figure 2-3.*

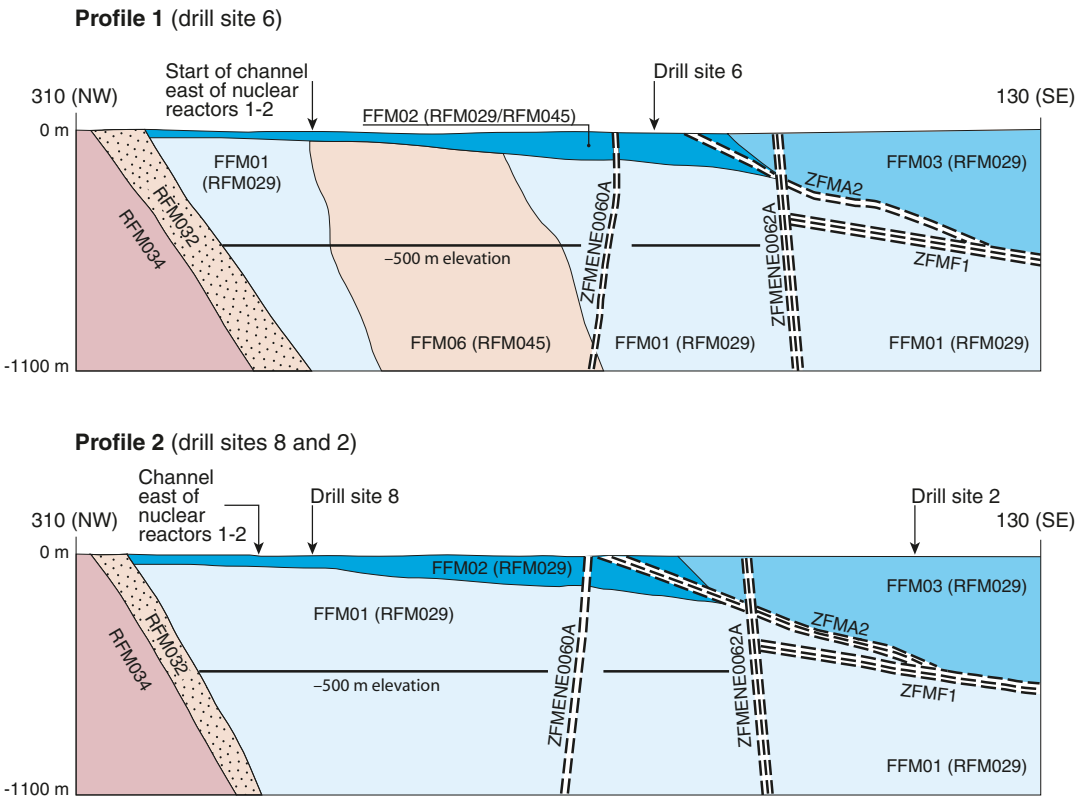


***Figure 2-3.*** *Simplified profiles in a NW-SE direction that pass through drill sites 2 and 8 (lower profile) and drill site 6 (upper profile), cf. Figure 2-2 The key fracture domains FFM01, –02 and –06 occur in the footwall of zones ZFMA2 (gently dipping) and ZFMF1 (sub-horizontal). The major steeply dipping zones ZFMENE0060A and ZFMENE0062A are also included in these images.*

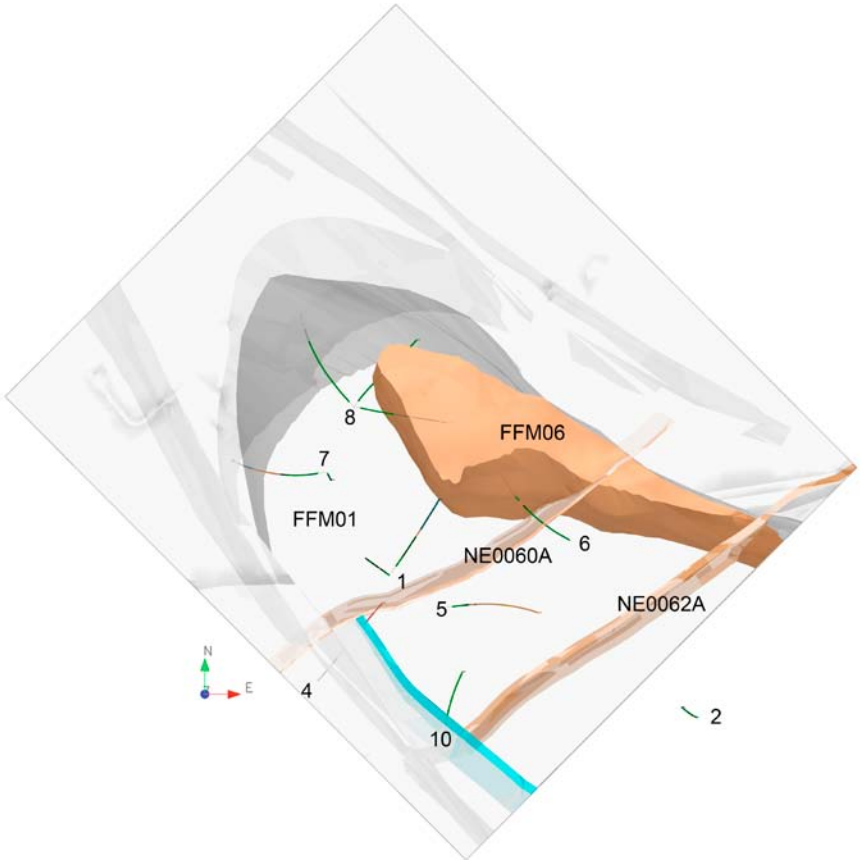


***Figure 2-4.*** *View of the target area/volume with the regolith and FFM02 transparent showing the key fracture domains, FFM01 (transparent) and FFM06 (brownish). The lines represent cored boreholes and the labels represent drill site numbers (1, 2, 4–8, 10). NE0060A and NE0062A are two major deformation zones, see Figure 2-3.*

Figure 2-5 shows examples of PFL data[1] from four cored boreholes, KFM01D and KFM06A–8A, located at drill sites 1, 6, 7 and 8, respectively. As can be seen in the plots, the bedrock has a high frequency of conductive fractures above –200 m, whereas below –400 m the frequency of conductive fractures decreases significantly. The decrease in PFL fracture transmissivity is not as significant as the decrease in PFL fracture frequency, although the highest PFL fracture transmissivity values are clearly observed above –200 m. These observations are commented in more detail in the text below. For the sake of clarity, it is noted that a casing is installed in the cored boreholes, which prohibits a detailed characterisation of the uppermost 100 m of bedrock with the PFL and PSS methods. Instead, the hydraulic characterisation of the uppermost bedrock is made with the HTHB method as described above. A detailed description of the three different test methods, PFL, PSS and HTHB, is found in /Follin et al. 2007a/.

[1] The flow rate at an intersecting flowing fracture is measured twice with the PFL method; first at natural head conditions and second with pumped head conditions. The difference in flow rate, $\Delta Q$ [$L^3T^{-1}$], is divided by the difference in head, $\Delta h$ [L], and the ratio defines the specific capacity, $\Delta Q/\Delta h$ [$L^2T^{-1}$], at the fracture intercept. In SKB's database, Sicada, the specific capacity at an intersecting flowing fracture determined with the PFL method is called fracture transmissivity, $T$ [$L^2T^{-1}$]. More information on this matter is found in /Follin et al. 2007a/ and in the SR-Site Data report /SKB 2010b, Section 6.6/.

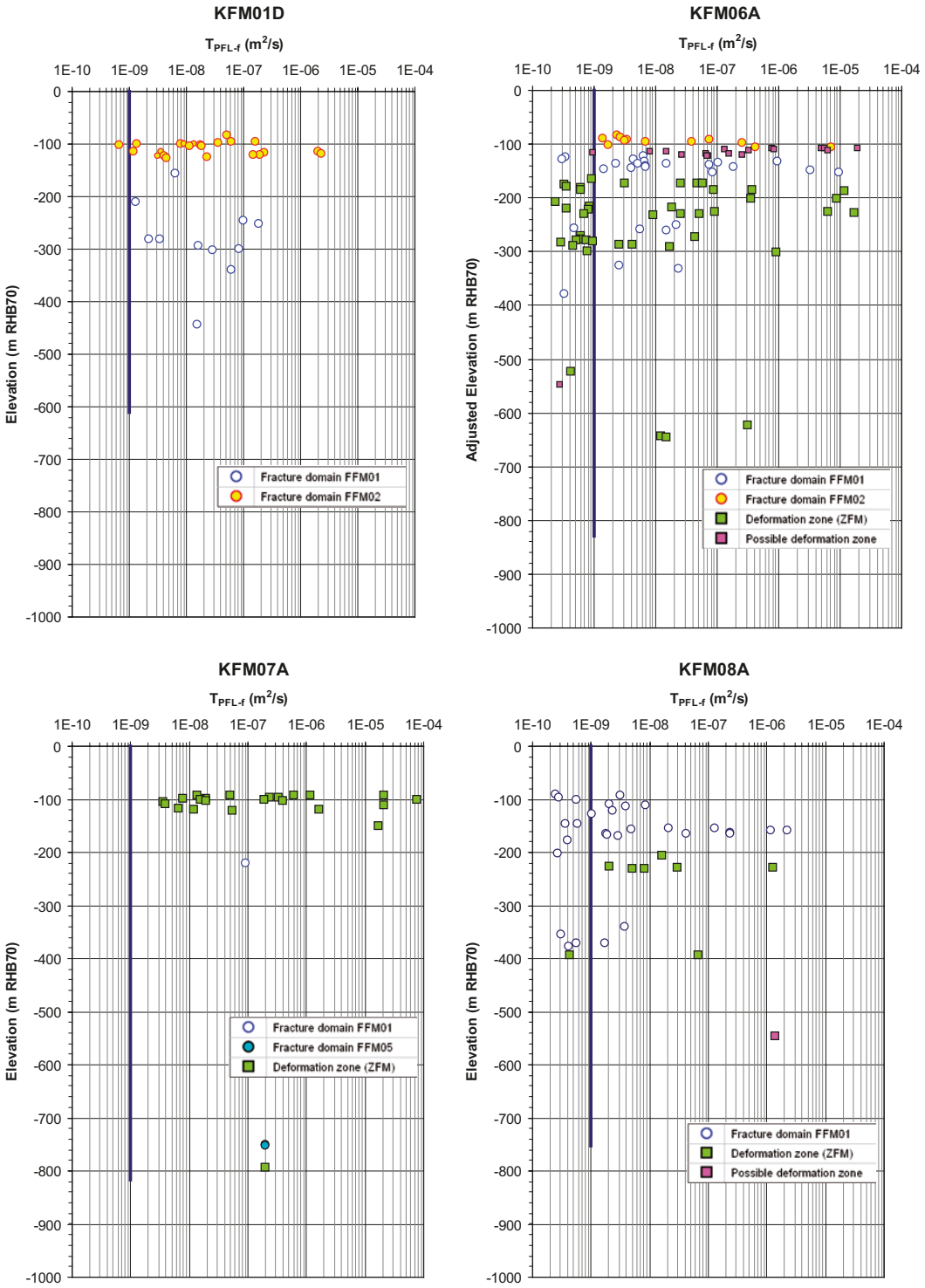


***Figure 2-5.*** *Specific capacity data of flowing fractures in the cored boreholes KFM01D, KFM06A, KFM07A and KFM08A detected with the PFL method. The data are coloured with regard to their structural classification and the blue lines indicate the typical detection limit reported from the investigations in the Forsmark area, $1{\cdot}10^{-9}$ m²/s. The lengths of the blue lines correspond to the depths investigated with the PFL method. In Sicada, the specific capacity data determined with the PFL method are called PFL fracture transmissivity data, which explains the x-axis caption $T_{PFL}$.*

## 2.2 Hydraulic characteristics of the deformation zones (HCD)

The in-plane transmissivities of the deterministically modelled deformation zones are obtained by a summation of the PSS and PFL measurements from the intersection boreholes. The summation of the PSS and PFL measurements is made between the upper and lower bounds of each deformation zone intercept. The results are shown in Figure 2-6, where the transmissivities are coloured with regard to the orientations of the zones. Here, G means gently dipping and the steeply dipping zones are denoted by their strike direction. The deformation zones with no measurable flow are assigned an arbitrary low transmissivity value of $1 \cdot 10^{-10}$ m$^2$/s in order to make them visible on the log scale. The transmissivity data that are marked up by slightly larger squares with a white cross in the centre represent data that were acquired during the verification phase, see /Follin et al. 2008/ for details.

As can be seen in the figure, there is a considerable lateral heterogeneity in the in-plane deformation zone transmissivity, but there is also a significant decrease in deformation zone transmissivity with depth, where the gently dipping zones have the highest transmissivities regardless of elevation followed by the steeply dipping WNW zones.

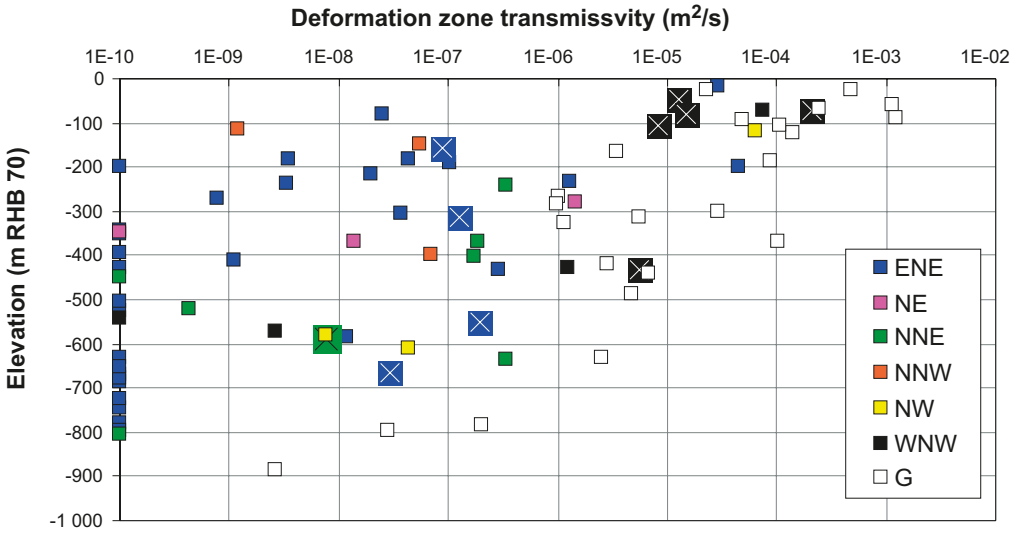


***Figure 2-6.*** *Scatter plot of the in-plane transmissivity data versus depth for the deterministically modelled deformation zones. The transmissivities are coloured with regard to the orientations of the deformation zones. G means gently dipping and the steeply dipping zones are denoted by their strike direction. Data denoted by ☒ come from KFM08D, KFM11A, KFM12A, HFM34, HFM36 and HFM37 and where obtained at the very end of SDM-Site and used for hypothesis testing, see /Follin et al. 2008/ for details.*

## 2.3 Hydraulic characteristics of the fracture domains (HRD)

The hydraulic conductivity estimated from measurements conducted with the PSS method ($K_{PSS}$) and the Terzaghi corrected conductive fracture frequency and the fracture transmissivity distribution estimated from measurements using the PFL method ($P_{10,PFL,corr}$) are also used to describe the permeability of the rock mass volumes between the deterministically modelled deformation zones.

Figure 2-7 shows a cumulative distribution function plot of 151 $\log_{10}(K_{PSS})$ data measured with a packer spacing (test scale) of 20 m[2] in the depth interval –400 to –700 m. Approximately 90% of the PSS data set (151 measurements) have values below –10.4 (or $4 \cdot 10^{-11}$ m/s), which is the robust lower measurement limit of the PSS method. This implies a conductivity-thickness product that is consistent with the PFL detection limit.

Figure 2-8 shows all PFL data acquired in the target area/volume in the rock mass volumes between the deterministically modelled deformation zones, see Figure 2-4. Above –200 m, the conductive fracture frequency is much higher than below this elevation. In fact, there are hardly any conductive fractures below –400 m. The decrease in specific capacity (or PFL fracture transmissivity, cf. footnote #1 in Section 2.1) is not as significant as the decrease in frequency, although the highest PFL data are clearly observed above –200 m. These observations are confirmed by the measurements conducted with the PSS method shown in Figure 2-7. Table 2-1 lists the boreholes that are tested with both methods.

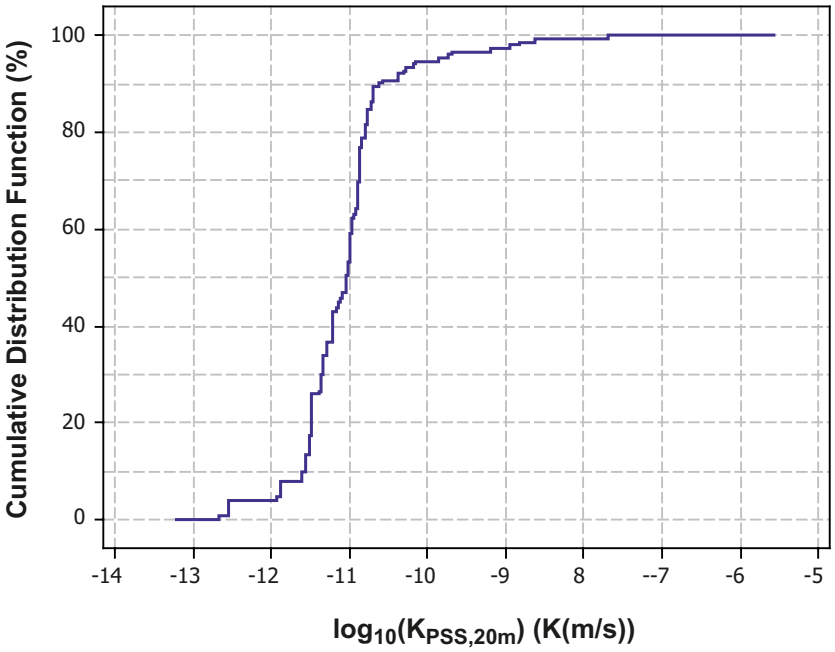


***Figure 2-7.*** *Cumulative distribution plot of 151 $log_{10}(K_{PSS})$ data measured with a packer spacing (test scale) of 20 m between elevations –400 m to –700 m within the target area/volume at Forsmark. The robust lower measurement limit of the PSS method is $4 \cdot 10^{-11}$ m/s (log(K) = –10.4).*

[2] A telescopic approach is used for the single-hole hydraulic testing with the PSS method at Forsmark. Each borehole is measured with consecutive 100-m long, 20-m long and 5-m long packer intervals beginning with the longest packer interval. Non-flowing 100-m long packer intervals were not studied with 20-m long packer intervals, etc. The telescopic measurement approach saves time but it assumes that low transmissive sections are correctly characterised. To display a cumulative plot of all 20 m sections a uniform distribution of transmissivity ($T$) is assumed in each low-transmissive 100 m section and the corresponding five unmeasured 20 m sections are a assigned a hydraulic conductivity ($K$) as follows: $K_{PSS,20m} = T_{100m}/5/20$ m.

It is noted that the PFL data occurring around –450 m are observed in the cored borehole KFM02A at drillsite 2, see Figure 2-1 and the lower image in Figure 2-3. This segment of KFM02A intersects the rock mass volume sandwiched in between two deformation zones, ZFMA2 and ZFMF1, and is not part of the planned repository volume. In conclusion, the fractured rock mass volumes between the deterministically modelled deformation zones look very different above and below approximately –400 m elevation.

Figure 2-9 shows two types of Terzaghi[3] corrected fracture frequencies in the target area/volume; open fractures (fractures that have visible apertures) and flowing fractures detected with the PFL method. Figure 2-9 shows also the measured specific capacities of the flowing fractures. At repository depth, the geometric mean of the Terzaghi corrected frequency of flowing fractures detected with the PFL method is very low, approximately 0.005 fractures per metre (5/km). The geometric mean of the specific capacity is also low, approximately $6.5 \cdot 10^{-9}$ m$^2$/s. The product of these two values suggest an equivalent hydraulic conductivity of approximately $3.3 \cdot 10^{-11}$ m/s for 200-m blocks of rock located below –400 m elevation.

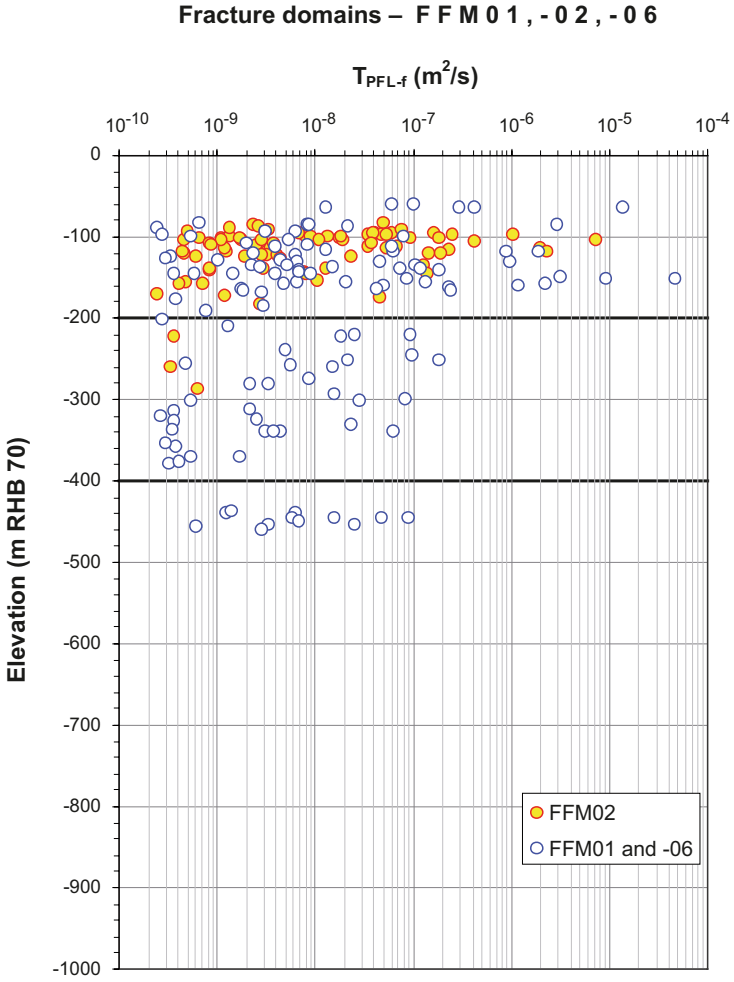


***Figure 2-8.*** *Specific capacity data of the flowing fractures detected with the PFL method in boreholes KFM01A, –01D, –02A, –04A to –08A, –08C and –08D outside deformation zones within the target area/volume (fracture domains FFM01–02 and –06). In Sicada, the specific capacity data determined with the PFL method are called PFL fracture transmissivity data, which explains the x-axis xcaption $T_{PFL}$.*

[3] Terzaghi correction is a common method used to mitigate orientation bias.

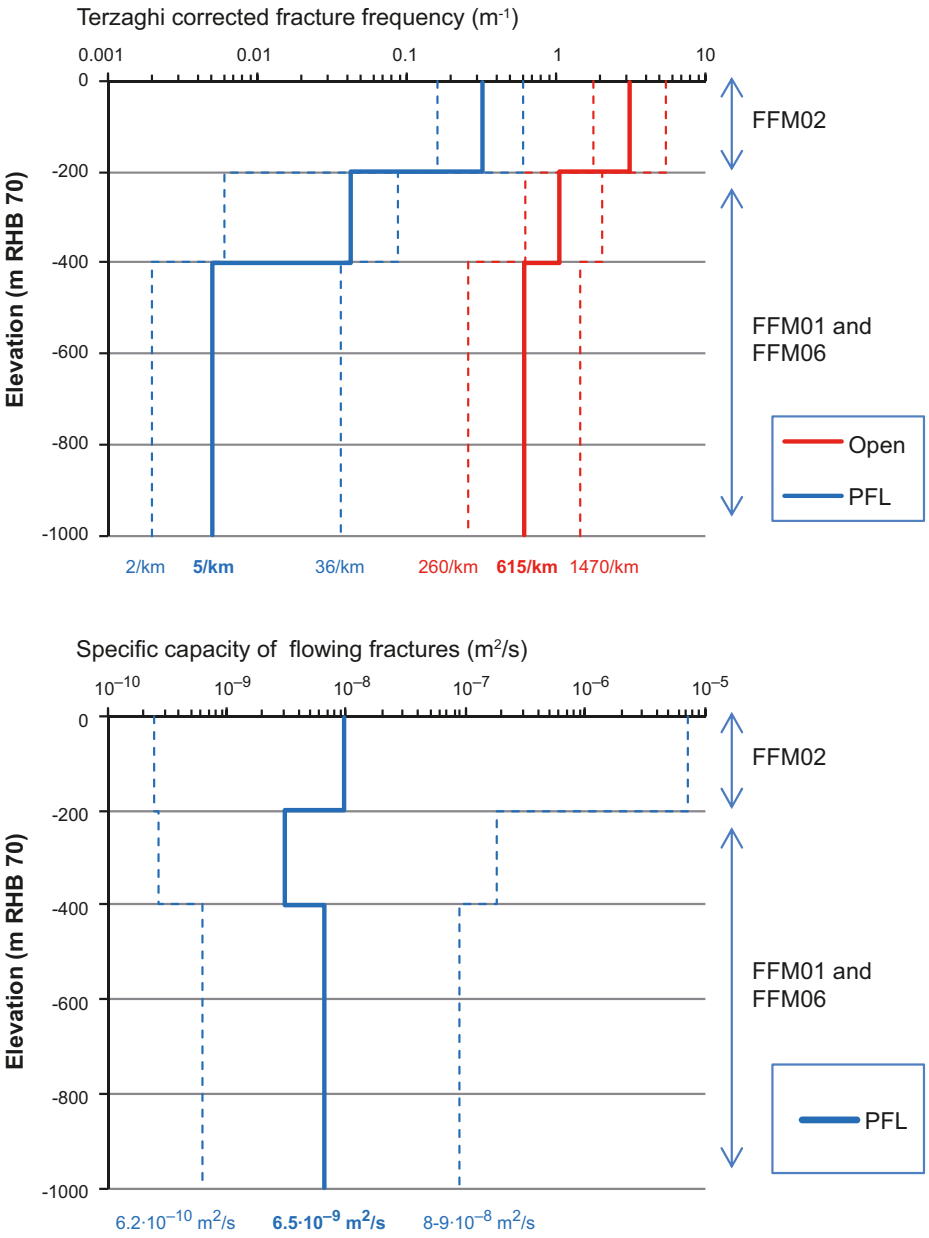


***Figure 2-9.*** *Top: Terzaghi corrected frequencies of open fractures and of the flowing fractures detected with the PFL method. Bottom: Specific capacities of the flowing fractures detected with PFL method. The thicker lines represent the geometric means over all boreholes and the thinner lines represent the spread between individual boreholes, i.e. the minimum and maximum values observed in any borehole.*

## 2.4 Parameter values for groundwater flow modelling

Field measurements suggest that the value of the hydraulic diffusivity is locally very high in the bedrock at Forsmark, particularly in the shallow bedrock aquifer (sheet joints and the gently dipping deformation zones/fractures). High transmissivities and low storativities in these structures imply little or no delay in the hydraulic responses to different kinds of pressure disturbances in the bedrock that overlay the bedrock at repository depth.

### 2.4.1 Deformation zones

An exponential trend model for the depth dependency of the in-plane deformation zone transmissivity $T$ [$L^2T^{-1}$] is suggested in SDM-Site. The depth trend model may be written as:

$$T(z) = T(0)\ 10^{z/k} \qquad (2\text{-}1)$$

where $T(z)$ [$L^2T^{-1}$] is the deformation zone transmissivity, $z$ [L] is elevation relative the Swedish Ordnance Datum RHB 70, $T(0)$ [$L^2T^{-1}$] is the expected value of the transmissivity of the deformation zone at zero elevation, and $k$ [L] is the depth interval that gives an order of magnitude decrease of the transmissivity.

The value of $T(0)$ can be estimated by inserting a measured value [$z'$, $T(z')$] in (2-1):

$$T(0) = T(z')\ 10^{-z'/k} \qquad (2\text{-}2)$$

In the case of several measurements at different locations in the same zone, the geometric mean of the calculated values of $T(0)$ is used as an effective value, $T_{eff}(0)$ in Equation 2-1. With this approach, the effect of conditioning to a measurement is to extrapolate the conditioned value over the entire extent of the deformation zone laterally, but not more than 100 m vertically.

/Follin et al. 2007a/ provide values of $T(z)$ of all deterministically modelled deformation zones used in SDM-Site. The value of $k$ deduced from the measured data is 232.5 m.

Lateral heterogeneity is simulated in SDM-Site by adding a log-normal random deviate to the exponent in (2-1):

$$T(z) = T(0)\ 10^{z/k+N(0,\ \sigma_{\log(T)})} \qquad (2\text{-}3)$$

where $\sigma_{\log(T)} = 0.632$. This value implies a 95% confidence interval in the lateral spread in $\log(T)$ of about 2.5 orders of magnitude. Furthermore, a nugget covariance model is assumed that is conditioned on measured transmissivity data.

The transmissivity model shown in Equation 2-3 requires, in principle, a stochastic approach with several model realisations. For the sake of clarity, the calibrated deterministic base model realisation derived in SDM-Site corresponds to the case where $\sigma_{\log(T)} = 0$.

Values of the kinematic porosity $\phi_f$ [–] of the deformation zones are calculated from the ratio between the transport aperture and the geological thickness:

$$\phi_f = (e_t)_f / b_f \qquad (2\text{-}4)$$

where $(e_t)_f$ is the fracture transport aperture [L], and $b_f$ is the geological thickness [L]. In SDM-Site, the fracture transport aperture is modelled based on Äspö Task Force 6c results /Dershowitz et al. 2003/, which assume a power-law function between the fracture aperture and the fracture transmissivity $T_f$ [$L^2T^{-1}$]:

$$(e_t)_f = a\ (T_f)^b \qquad (2\text{-}5)$$

The values of the parameters $a$ and $b$ in Equation 2-5 used in SDM-Site are defined in /Dershowitz et al. 2003/, where $a = 0.46$ and $b = 0.5$. /Stephens et al. 2007/ provide values of the geologic thickness of all deterministically modelled deformation zones.

### 2.4.2 Fracture domains

Groundwater flow in the sparsely fractured repository host rock at Forsmark is conceived to occur in discrete fracture networks (DFN). Hydrogeological DFN models explicitly model the fractures through which the groundwater flows and are characterised by structural-hydraulic quantities associated with these fractures such as orientation, size, intensity, transmissivity, and aperture. By definition, hydrogeological DFN modelling invokes Monte Carlo simulations (multiple realisations) as the fracture quantities are described statistically.

It is noted that in the hydrogeological discrete fracture network (DFN) modelling, the PFL data are not treated as fracture transmissivities but as specific capacities. This because the testing is performed over several days, hence it is an effective hydraulic property of the network connectivity. That is, the actual transmissivity value interpreted at the borehole will be close to the value of "the bottleneck" in the network of flowing fractures carrying water to the pumped borehole. Section 6.6 in the Data report describes in detail how the hydrogeological DFN (Hydro-DFN) modelling is performed and calibrated.

The hydrogeological DFN parameters used in SDM-Site for FFM01 and FFM06 are tabulated in Table 2-2.

Table 2-3 and Table 2-4 show the corresponding parameters used for FFM02 and FFM03–FFM05, respectively. In these tables, the values of $P_{32,open}$ represent the Terzaghi corrected linear frequencies of open fractures, $P_{10,open,corr}$. The statistical distributions mentioned briefly in Table 2-2, Table 2-3 and Table 2-4 are described greater detail in /Follin 2008/.

Further, the three transmissivity models; semi-correlated, correlated and uncorrelated, are shown in Table 2-5.

**Table 2-2. Parameters values used in SDM-Site for fracture domains FFM01 and FFM06.**

| Elevation (m RHB 70) | Fracture set name | Orientation poles: Fisher (trend, plunge), conc. κ (°,°, –) | Size model, power-law ($r_0$, $k_r$) (m, –) | Intensity, ($P_{32,open}$), valid size interval: ($r_0$, 564 m) ($m^2/m^3$) | Transmissivity model (Table 2-5) |
|---|---|---|---|---|---|
| > –200 | NS | (292, 1) 17.8 | (0.038, 2.50) | 0.073 | Semi-correlated: ($a,b,\sigma_{logT}$) = (6.3 · $10^{-9}$, 1.3, 1.0); |
| | NE | (326, 2) 14.3 | (0.038, 2.70) | 0.319 | |
| | NW | (60, 6) 12.9 | (0.038, 3.10) | 0.107 | Correlated: ($a,b$) = (6.7 · $10^{-9}$, 1.4); |
| | EW | (15, 2) 14.0 | (0.038, 3.10) | 0.088 | |
| | HZ | (5, 86) 15.2 | (0.038, 2.38) | 0.543 | Uncorrelated: ($\mu_{logT}$, $\sigma_{logT}$) = (–6.7, 1.2) |
| –200 to –400 | NS | As above | As above | 0.142 | Semi-correlated: ($a,b,\sigma_{logT}$) = (1.3 · $10^{-9}$, 0.5, 1.0); |
| | NE | As above | As above | 0.345 | |
| | NW | As above | As above | 0.133 | Correlated: ($a,b$) = (1.6 · $10^{-9}$, 0.8); |
| | EW | As above | As above | 0.081 | |
| | HZ | As above | As above | 0.316 | Uncorrelated: ($\mu_{logT}$, $\sigma_{logT}$) = (–7.5, 0.8) |
| < –400 | NS | As above | As above | 0.094 | Semi-correlated: ($a,b,\sigma_{logT}$) = (5.3 · $10^{-11}$, 0.5, 1.0); |
| | NE | As above | As above | 0.163 | |
| | NW | As above | As above | 0.098 | Correlated: ($a,b$) = (1.8 · $10^{-10}$, 1.0); |
| | EW | As above | As above | 0.039 | |
| | HZ | As above | As above | 0.141 | Uncorrelated: ($\mu_{logT}$, $\sigma_{logT}$) = (–8.8, 1.0) |

**Table 2-3. Parameters values used in SDM-Site for fracture domain FFM02.**

| Elevation (m RHB 70) | Fracture set name | Orientation poles: Fisher (trend, plunge), conc. κ (°,°, –) | Size model, power-law ($r_0$, $k_r$) (m, –) | Intensity, ($P_{32,open}$), valid size interval: ($r_0$, 564 m) ($m^2/m^3$) | Transmissivity model (Table 2-5) |
|---|---|---|---|---|---|
| > –200 | NS | (83, 10) 16.9 | (0.038, 2.75) | 0.342 | Semi-correlated: ($a,b,\sigma_{logT}$) = (9.0 · $10^{-9}$, 0.7, 1.0); |
| | NE | (143, 9) 11.7 | (0.038, 2.62) | 0.752 | |
| | NW | (51, 15) 12.1 | (0.038, 3.20) | 0.335 | Correlated: ($a,b$) = (5.0 · $10^{-9}$, 1.2); |
| | EW | (12, 0) 13.3 | (0.038, 3.40) | 0.156 | |
| | HZ | (71, 87) 20.4 | (0.038, 2.58) | 1.582 | Uncorrelated: ($\mu_{logT}$, $\sigma_{logT}$) = (–7.1, 1.1) |

**Table 2-4. Parameter values used in SDM-Site for fracture domains FFM03–FFM05. Transmissivity is increased by a factor 2 for fracture domain FFM04.**

| Elevation (m RHB 70) | Fracture set name | Orientation poles: Fisher (trend, plunge), conc. κ (°,°, –) | Size model, power-law ($r_0$, $k_r$) (m, –) | Intensity, ($P_{32,open}$), valid size interval: ($r_0$, 564 m) ($m^2/m^3$) | Transmissivity model (Table 2-5) |
|---|---|---|---|---|---|
| > –400 | NS | (292, 1) 17.8 | (0.038, 2.60) | 0.091 | Semi-correlated: ($a$,$b$,$\sigma_{logT}$) = (1.3 · $10^{-8}$, 0.4, 0.8); |
| | NE | (326, 2) 14.3 | (0.038, 2.50) | 0.253 | |
| | NW | (60, 6) 12.9 | (0.038, 2.55) | 0.258 | Correlated: ($a$,$b$) = (1.4 · $10^{-8}$, 0.6); |
| | EW | (15, 2) 14.0 | (0.038, 2.40) | 0.097 | |
| | HZ | (5, 86) 15.2 | (0.038, 2.55) | 0.397 | Uncorrelated: ($\mu_{logT}$, $\sigma_{logT}$) = (–7.2, 0.8) |
| < –400 m | NS | As above | As above | 0.102 | Semi-correlated: ($a$,$b$,$\sigma_{logT}$) = (1.8 · $10^{-8}$, 0.3, 0.5); |
| | NE | As above | As above | 0.247 | |
| | NW | As above | As above | 0.103 | Correlated: ($a$,$b$) = (7.1 · $10^{-9}$, 0.6); |
| | EW | As above | As above | 0.068 | |
| | HZ | As above | As above | 0.250 | Uncorrelated: ($\mu_{logT}$, $\sigma_{logT}$) = (–7.2, 0.8) |

**Table 2-5. Transmissivity models defined in SDM-Site for hydrogeological DFN modelling.**

| Type | Description | Relationship | Parameters |
|---|---|---|---|
| Correlated | Power-law relationship | $\log(T) = \log(a\, r^{b})$ | $a$, $b$ |
| Uncorrelated | Log-normal distribution about a specified mean | $\log(T) = \mu_{log(T)} + \sigma_{log(T)}$ N(0,1) | $\mu_{log(T)}$, $\sigma_{log(T)}$ |
| Semi-correlated | Log-normal distribution about a power-law correlated mean | $\log(T) = \log(a\, r^{b}) + \sigma_{log(T)}$ N(0,1) | $a$, $b$, $\sigma_{log(T)}$ |

For the region outside the six fracture domains FFM01–FFM06, i.e. on a regional scale, there is no site-specific DFN information available in the rock mass volumes between deformation zones in SDM-Site. The approximate values of homogeneous CPM properties (hydraulic conductivity ($K$), kinematic porosity ($\phi$), and flow-wetted fracture surface area per unit volume of rock mass ($a_r$)) used in SDM-Site are given in Table 2-6. A depth dependency is suggested in accordance with the depth zonations used for fracture domains FFM01 and FFM06, see Table 2-2.

**Table 2-6. Homogeneous continuum properties used in SDM-Site for the rock mass volumes outside the six fracture domains FFM01-FFM06.**

| Elevation | CPM properties outside FFM01–FFM06 | | |
|---|---|---|---|
| (m RHB 70) | $K$ (m/s) | $\phi$ (–) | $a_r$ ($m^2/m^3$) |
| > –200 | 1 · $10^{-7}$ | 1 · $10^{-5}$ | 0.60 |
| –200 to –400 | 1 · $10^{-8}$ | 1 · $10^{-5}$ | 0.30 |
| < –400 | 3 · $10^{-9}$ | 1 · $10^{-5}$ | 0.30 |

## 2.5 Hydrogeochemical description

SDM-Site concluded that the occurrence of horizontal sheet joints of high transmissivities in the uppermost 100 m of bedrock have a profound effect on the percolation depth of the fresh water recharge that started approximately 1,100 years ago as a result of the ongoing shoreline displacement process during Holocene time. In effect, the salinity of the fracture water in the uppermost 100 m of bedrock is generally lower than the salinity of the fracture water below this depth. The increase in fracture water salinity is fairly moderate between –100 and –800 m elevation, where the fracture water salinity is approximately 1% by weight (c. 10 g of total dissolved solids per litre). Below this elevation, the fracture water salinity could be expected to increase significantly with depth.

The chemical composition of near-surface groundwater samples gathered in the uppermost 100 m of bedrock reveals that chemical reactions (water-rock interactions) have a profound effect on the composition of the infiltrating rain water. Therefore, the chemical composition of rain water considered in the palaeohydrological groundwater flow modelling was substituted by a modified water composition called Altered Meteroric water. The characteristic composition of this reference water is described in /Laaksoharju et al. 2008/ and in /Salas et al. 2010/.

Besides reactions, the transport of Altered Meteoric water is also affected by matrix diffusion. The matrix porewater data used for modelling come from three boreholes drilled in the target volume, see /Laaksoharju et al. 2008, Waber et al. 2009/ for details. The key bedrock matrix transport properties governing the penetration length (depth) of a non-sorbing fracture water component are the effective diffusivity and matrix porosity.

The interaction between the fracture water salinity and the matrix porewater salinity is also dependent on the spacing between the flowing fractures. At Forsmark, the intensity (frequency) of conductive (flowing) fractures varies considerably with depth within the target volume (Table 2-2 and Figure 2-9). The two types of water, the fracture water and the matrix porewater, should be more alike in the densely fractured bedrock close to surface than in the sparsely fractured bedrock at repository depth, and this is also what the data show as described in the references cited above. At even larger depths, the water circulation is low and the system may become diffusion controlled. Hence, the fracture water and the matrix porewater are more alike.

SDM-Site concluded that the initial hydrochemical conditions of the fracture water at the start of the flow simulations at 8000 BC can be modelled by mimicking the present-day depth trends in matrix porewater salinity within the target volume and outside this volume, respectively, see /Follin 2008/ for details. Hence, the modelled changes in the top boundary condition during Holocene time between 8000 BC and 2000 AD are sufficient to create differences between the fracture water and matrix porewater that resemble the observed differences /Follin 2008/. The key hydrological changes are the intrusion of Littorina Sea water, that began approximately 6500 BC, and the subsequent flushing by Altered Meteoric water that started approximately 900 AD, see /Follin 2008/ for details. In principle, these palaeohydrological phenomena have a greater effect on the near-surface fracture water salinity than on the matrix porewater salinity at repository depth.

# 3 Hydrogeological modelling within SR-Site

## 3.1 Time periods assessed

In SR-Site, three different time periods are analysed as part of the assessment. These are the Excavation and operational phases, the Initial period of temperate climate after closure, and the Remaining part of the reference glacial cycle.

During the excavation and operational phases, the tunnels will be at atmospheric pressure and the inflow of water to the open repository will depend on the hydraulic properties of the intersecting, water conducting fractures. The inflow may result in a redirection of flow and in changes of the groundwater flow pattern, potentially resulting in drawdown of the water table, infiltration of near-surface waters into the deeper parts of the bedrock, and in upconing of saline water from depth. The actual impacts primarily depend on the permeability distribution of the rock, the repository layout and on the tightness of the underground construction, which in turn depends on the grouting efficiency. In order to assess the magnitude of these impacts, groundwater flow simulations, based on the hydrogeological models developed as part of Site description Forsmark /SKB 2008/, are performed. The overall objective has been to assess the effects of an open repository on site hydrogeological and hydrogeochemical conditions.

The hydrogeological evolution during the temperate period after repository closure involves two distinct time intervals. The first is that for saturation of the repository once pumping of the open tunnels has ceased. The subsequent time interval deals with the evolution of the saturated repository during the remaining part of the period with temperate climate conditions. The actual impacts primarily depend on the permeability distribution of the bedrock (fracture network connectivity and hydraulic properties of the fractures), the repository layout and the associated permeability of the backfilled tunnels, and the prevailing boundary conditions. At Forsmark, the primary hydraulic driving forces for groundwater flow during periods with temperate climate conditions are flushing of terrestrial areas due to precipitation combined with the ongoing shoreline displacement. In order to assess the magnitude of these impacts, groundwater flow simulations, based on the hydrogeological models developed as part of Site description Forsmark /SKB 2008/**,** are performed. The overall objective is to assess the effects of a temperate climate on site hydrogeological and hydrogeochemical conditions in the presence of a backfilled repository.

The evolution for the remaining part of the reference glacial cycle is handled in a more stylised manner within the hydrogeological analysis. Bedrock hydrogeology during periods with both periglacial (permafrost) and glacial climate conditions are addressed, but the analyses performed are more of a bounding nature than trying to accurately predict the future evolution. The actual impacts primarily depend on the permeability distribution (fracture network connectivity and hydraulic properties of the fractures), and the prevailing boundary conditions (it is noted that the repository is not included in the model, and hence the hydraulic characteristics of the backfilled tunnels do not influence the model results). The primary hydraulic driving force for groundwater flow during periods of periglacial and glacial conditions is the hydraulic gradient resulting from the existence of an ice sheet. In order to assess the magnitude of these impacts, groundwater flow simulations, based on the hydrogeological models developed as part of Site description Forsmark /SKB 2008/ are performed. The overall objective is to assess the effects of glacial and periglacial (permafrost) climate conditions on site hydrogeological and hydrogeochemical conditions.

## 3.2 A few key concepts of groundwater flow in fractured rock

Below, a few key concepts used in the modelling are briefly introduced in order to facilitate the discussion in subsequent sections of the report. The concepts are central for the present flow modelling studies given relevant site characteristics and types of analyses performed. However, the concepts are not exhaustive if a complete description of groundwater flow and solute transport in fractured rocks is to be presented.

- **Density driven flow**
  Salt transport in flowing fractures gives rise to variations in groundwater salinity and hence fluid density. The fluid density is also affected by temperature differences. The density variations create density-driven flows. These flows are accounted for in the flow modelling by considering buoyancy effects in the mass balance equation.

- **Rock Matrix Diffusion (RMD)**
  Solutes are transported in the flowing (mobile) water in the fractures primarily by advection. Diffusion between the mobile fracture water and the immobile water in the rock matrix is denoted Rock Matrix Diffusion (RMD). In a hydrogeological context, RMD is an important process for individual groundwater constituents and salinity. Without the retention implied by RMD, models will not be able to reproduce the hydrogeochemical evolution and measured data correctly. For example, transport of dilute water from surface to depth will not be correctly described without the incorporation of RMD.

- **Flow-related transport resistance (*F*)**
  The flow-related transport resistance is an entity, integrated along flow paths, that quantifies the flow-related (hydrodynamic) aspects of the possible retention of solutes transported in a fractured medium. The flow-related transport resistance can be defined in a number of ways which are interchangeable according to the basic definitions of hydraulic parameters characterising the system. In its most intuitive, although not necessarily most generalised, form the flow-related transport resistance is defined as the ratio of flow-wetted surface and flowrate. The definitions used in the present work for different type of model applications are given in Section 3.4.4. The flow-related transport resistance governs nuclide migration, salt diffusion into and out from the matrix, as well as oxygen ingress. An increase in flow-wetted surface, for a given flowrate, yields a higher *F* and hence more retention of transported solutes. The conductive fracture frequency is related to the available flow-wetted surface; a higher conductive fracture frequency implies a higher flow-wetted surface. A comprehensive description of the flow-related transport resistance is given in e.g. /Crawford 2008/.

- **Darcy flux (*q*)**
  The Darcy flux is a macroscopic entity defined as the groundwater flow rate per unit area, i.e. specific discharge, $q$ [$LT^{-1}$]). It is typically calculated as the product of hydraulic conductivity and hydraulic gradient. The Darcy flux is in the present work calculated for deposition hole positions in the repository. It is mainly used as a comparison entity between different model applications and codes. Hence, the Darcy flux needs to be defined in a consistent manner between ECPM and DFN models; the definitions used are given in Section 3.4.4. For the DFN models, it is noted that the Darcy flux is derived based on the flowrate in all fractures intersecting a deposition hole, and averaged over a suitable length scale [$L^2T^{-1}$].

- **Equivalent flowrate (*Qeq*)**
  The equivalent flow rate is used as input to the nearfield radionuclide transport code COMP23 /SKB 2010g/. The equivalent flow rate is a fictitious flow rate of water that carries a concentration equal to that at the interface between the nearfield and farfield models. The value of Qeq is dependent on the geometry of the contact area, the water flux, the flow porosity, and the diffusivity. The equivalent flowrate is calculated in the groundwater flow models in a corresponding manner as the Darcy flux; i.e. based on the flowrate at deposition hole positions. The equations used for calculation of the equivalent flowrates presenterd here are given in /Joyce et al. 2010/.

- **DFN, ECPM and CPM groundwater flow models**
  Hydrogeological discrete fracture network (DFN) models explicitly model fractures through which groundwater flows and are characterised by the stochastic nature of the structural-hydraulic quantities associated with these fractures. The flow and transport properties of hydrogeological DFN models can be up-scaled to equivalent continuous porous medium (ECPM) properties. That is, the ECPM approach honours the intrinsic heterogeneity and anisotropy of hydrogeological DFN models on the scale of resolution of the chosen computational grid. Since each ECPM model is based on a particular underlying stochastic hydrogeological DFN realisation, the ECPM models also are stochastic. Uncertainties relating to spatial variability in the geometrical and/or hydraulic properties are quantified by means of multiple realisations. Homogeneous (deterministic) continuous porous medium (CPM) models typically have constant hydrogeological properties within each given sub-domain. That is, the CPM approach is useful for describing groundwater flow in less heterogeneous media, e.g. Quaternary deposits, or in the rock mass volumes far away from the bed-

rock region in focus. Finally, it is noted that the flow-related transport resistance can be calculated directly in a discrete (DFN) model, whereas additional assumptions on the flow-wetted surface need to be made in continuum models.

- **FPC and EFPC**
  Two geometrical criteria, the Full Perimeter Criterion (FPC) and the Extended Full Perimeter Criterion (EFPC), are applied in the groundwater flow modelling for SR-Site as a means to reject unfavourable deposition hole positions based on fracture geometry solely.

  The FPC criterion handles steeply dipping fractures and the EFPC criterion handles gently dipping fractures; the criteria are defined as /Munier 2006/:
  1. Full perimeter criterion (FPC) – a deposition hole is excluded if it is intersected by the hypothetical extension of a fracture that intersects the full perimeter of the corresponding deposition tunnel.
  2. Extended full perimeter criterion (EFPC) – a deposition hole is excluded if its full perimeter is intersected by a fracture that also intersects the full perimeter of four or more neighbouring deposition holes in the same deposition tunnel.

  It is noted that the two definitions in /Munier 2006/ refer to deposition hole positions and that the key geometrical criterion adopted in the groundwater flow modelling for SR-Site is "FPC or EFPC", which implies three possibilities of rejection. It is also noted that SR-Site uses the definitions in /Munier 2010/ rather than the definitions in /Munier 2006/; i.e., except for the groundwater flow modelling. The key difference between /Munier 2010/ and /Munier 2006/ is that in /Munier 2010/, the rejection is based on fracture intersections with canister positions rather than with deposition hole positions; the canisters have a smaller diameter than the deposition holes (cf. Figure 3-7). Second, in the SR-Site Main report, the notation is changed such that the EFPC acronym encompasses both steeply and gently dipping fractures.

- **Reference waters**
  It is assumed that the mixing of several so-called reference (or end-member) water types contribute to the groundwater composition /Laaksoharju et al. 2008/. Conceptually, the reference water types reflect important aspects of changes in the climate and evolution of the hydrogeological conditions (palaeohydrology). In the flow modelling of the intial temperate period after closure, the reference water mass fractions on the top boundary vary with time according to the position of the shoreline, see also Section 3.4.4.

## 3.3 Codes used in the modelling

Two codes for simulation of groundwater flow are used in SR-Site; these are DarcyTools and ConnectFlow. Both codes are capable of simulating density-driven groundwater flow in sparsely fractured rock. Also, both codes include matrix diffusion of salt and/or of solutes such as e.g. individual groundwater constituents or (fractions of) reference waters.

The codes supplement each other and essentially solve the same problems, i.e. the same equations. However, ConnectFlow has the capability of an explicit representation of fractures, i.e. an option to solve flow and transport using Discrete Fracture Network (DFN) models. The DFN parts can also be up-scaled to Equivalent Continuous Porous Medium (ECPM) models. DarcyTools is an ECPM model code, also utilising up-scaling of DFN models. In addition, both codes can have Continuous Porous Medium (CPM) descriptions included.

Below, the codes and their capabilities are briefly summarised providing references to key code documents. The text is a shortened and slightly modified version of a more comprehensive text found in the SR-Site Model Summary report /SKB 2010g/ where also QA aspects of the modelling work are elaborated.

### 3.3.1 ConnectFlow

ConnectFlow is the suite of Serco's groundwater modelling software /Serco 2008a/ that includes the NAMMU /Serco 2008b/ continuous porous medium (CPM) module and the NAPSAC /Serco 2008c/ Discrete Fracture Network (DFN) module. ConnectFlow is also the name given to the concept of embedding CPM and DFN sub-models into a combined CPM/DFN model. A further module, GeoVisage, is a dedicated 3D visualisation application for interpreting the results from ConnectFlow. Hence, ConnectFlow is a very flexible tool for modelling groundwater flow and transport in both fractured and porous media on a variety of scales.

ConnectFlow allows the modelling of a wide range of physical processes of relevance to SR-Site such as: transient groundwater flow; saturated and unsaturated groundwater flow; coupled groundwater flow and salt transport; transport of reference waters including rock matrix diffusion; coupled groundwater flow and heat transport; variable-density flow and transport in fracture networks, and radionuclide transport.

ConnectFlow has a long track-record of being used in the SKB programme. Developments have been made to suit the needs of site modelling and safety assessment calculations. The current role of the software in SKB safety assessment applications has been illustrated in the SR-Can interim assessment /Hartley et al. 2004/ as well as in the SR-Can assessment /Hartley et al. 2006/. The use of ConnectFlow within SR-Site is a natural progression from its application in the site-descriptive modelling /Follin 2008/.

The capabilities of ConnectFlow are described in the Technical Summary Document /Serco 2008a/. A full description of the verification of NAMMU and NAPSAC are given in /Serco 2008d, 2008e/. Testing of combined models is reported in the ConnectFlow Verification Manual /Serco 2008f/. Each release of ConnectFlow is verified by running a full test set for all modules of the software with over 200 test cases. In SR-Site, ConnectFlow version 9.6 is used.

### 3.3.2 DarcyTools

DarcyTools is a computer code for simulation of flow and transport in porous and/or fractured media. The fractured media in mind is a fractured rock and the porous media the soil cover on the top of the rock.

DarcyTools is a general purpose code for this class of problems, but the analysis of a repository for spent nuclear waste is the main intended application.

A number of novel features are introduced in DarcyTools. The most fundamental is the method to generate grid cell properties (DarcyTools is an ECPM code); a fracture network, with properties given to each fracture, is represented in the computational grid. This method is shown to result in very accurate anisotropy and connectivity properties. Another key feature is the grid system; an unstructured Cartesian grid which accurately represents objects, read into the code as CAD-files, is used in DarcyTools.

DarcyTools builds upon earlier development of groundwater flow models carried out during the last twenty years; many of these developments and applications are related to studies performed at the Äspö Hard Rock laboratory. The development work on DarcyTools was initiated in early 2001. In SR-Site, DarcyTools version 3.4 is used.

Three main documents /Svensson et al. 2010, Svensson 2010, Svensson and Ferry 2010/ describe the code and its use in detail. /Svensson et al. 2010/ provides a description of concepts and methods used. /Svensson and Ferry 2010/ is a User's Guide that describes all input parameters. These input parameters make up the so called CIF (Compact Input File), which is written in XML format. DarcyTools also includes a Fortran input file, where more advanced features (transient boundary conditions, new source/sink terms, etc) can be introduced. Tecplot has been selected as the standard tool for post processing. Input files for Tecplot are readily generated. /Svensson 2010/ deals with verification, validation and demonstration. About thirty test cases, many of which have an analytical solution, are used to ensure that the equations are solved correctly. When a new major version of the code is released, all test cases are updated and checked to ensure both consistency with the old version and to make sure that the new version is correct. A number of comparisons with field data are included in /Svensson 2010/.

## 3.4 Modelling strategy, domains and models used for different time periods

### 3.4.1 Hydrogeological systems approach

Figure 3-1 indicates the time period handled by each bedrock flow modelling study and where the results are presented in this report. The three studies employ different computer codes and modelling teams. The studies conducted by /Svensson and Follin 2010/ and /Vidstrand et al. 2010/ are made with DarcyTools, whereas the study by /Joyce et al. 2010/ is made with ConnectFlow.

The studies share the same systems approach and hydrogeological input (parameter database) to support conceptual integration, to allow for consistency checks of the reported flow simulations and to provide a good modelling strategy. In SKB's systems approach, the geosphere is divided into three hydraulic domains denoted by HCD, HRD and HSD, see Figure 3-2:

- HCD (Hydraulic Conductor Domains) represents the deterministically modelled deformation zones.
- HRD (Hydraulic Rock mass Domain) represents the less fractured bedrock in between the deformation zones.
- HSD (Hydraulic Soil Domain) represents the regolith (Quaternary deposits).

General assumptions, simplifications and uncertainties related to the hydrogeological modelling, specifically the usage of discrete fracture network models to represent the HRD, are discussed in more detail in the SR-Site Data report /SKB 2010b, Section 6.6/.

In Figure 3-3, the relation between the hydrogeological model presented in SDM-Site /Follin 2008/, i.e. the *base model simulation*, and the models used in SR-Site are exemplified. A *hydrogeological base case* model is derived within the temperate phase modelling. This model is essentially identical to the SDM-Site model, which also was derived using the modelling tool ConnectFlow (CF), but with slight modifications to incorporate features specific to SR-Site, e.g., repository structures. This model is in turn exported to the other two phases, and modified on two accounts. First, modifications are made specific to the other modelling tool DarcyTools (DT), and second, modifications and/or additional parameterisations are made specific to the problems addressed. Within these other phases studied, the central cases are denoted *base cases* in order to clearly separate them from the central ConnectFlow case (hydrogeological base case) used within the temperate period simulations.

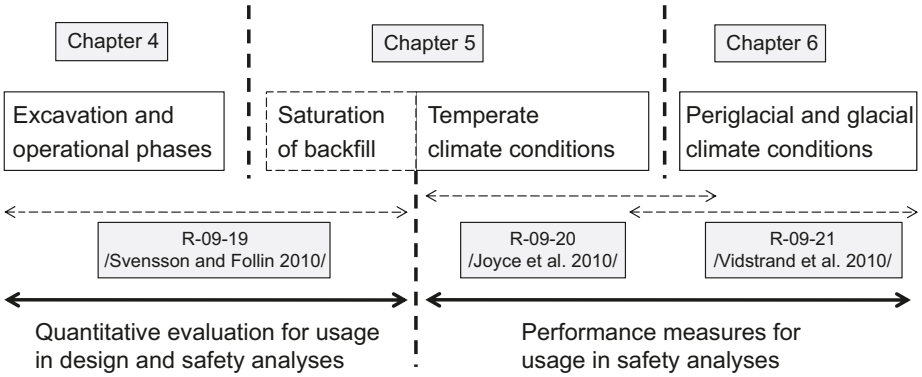


***Figure 3-1.*** *Overview of flow modelling made with respect to the safety functions related to the bedrock.*

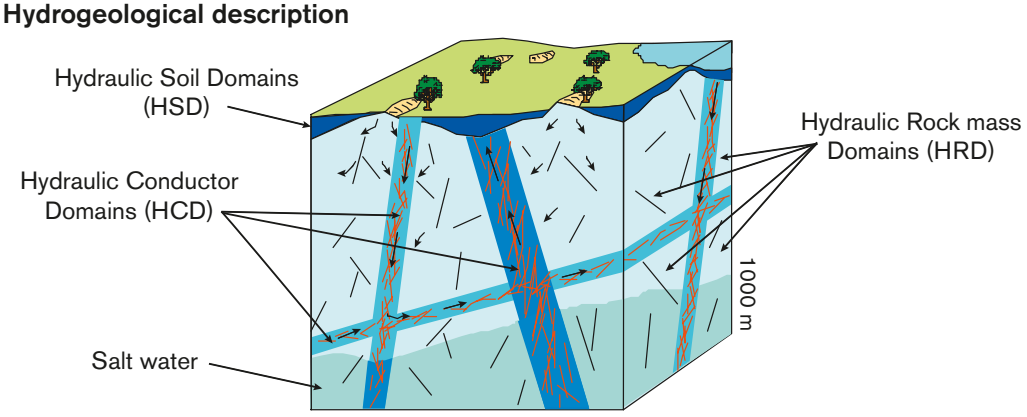


***Figure 3-2.*** *Cartoon showing SKB's systems approach used in SDM-Site and SR-Site.*

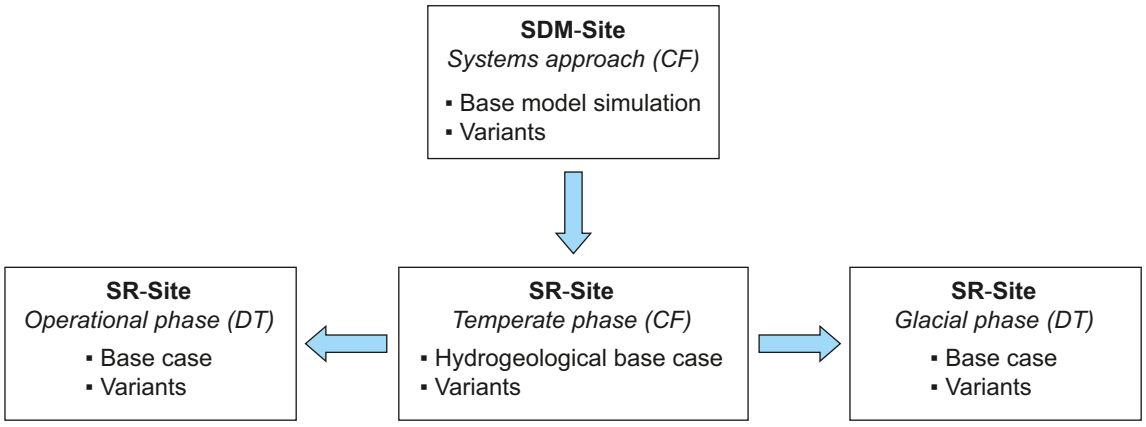


***Figure 3-3.*** *Relation between SDM-Site's base model simulation and SR-Site's hydrogeological base case in /Joyce et al. 2010/ and the base cases in /Svensson and Follin 2010/ and /Vidstrand et al. 2010/, respectively. Here, CF is short for ConnectFlow and DT is short for DarcyTools.*

/Joyce et al. 2010/ simulate groundwater flow both in a discrete form (discrete fracture network, DFN), and in an up-scaled form (equivalent continuous porous medium, ECPM, and continuous porous medium, CPM). /Svensson and Follin 2010/ and /Vidstrand et al. 2010/ both use up-scaled models, i.e. the ECPM/CPM approaches. In addition, /Svensson and Follin 2010/ use a variant of the ECPM approach called the equivalent discontinuous porous medium (EDPM) approach, see /Svensson and Follin 2010/ for details.

DFN models provide distributions of the detailed flow patterns around the deposition holes, but usually support a limited range of physical processes that can be modelled, such as multi-phase flow. ECPM/CPM models are more appropriate for modelling complex coupled processes, but usually involve some averaging of fracture properties and geometries. Hence, the different approaches are used in parallel to assess a range of issues in a complementary fashion.

### 3.4.2 Initial and boundary conditions

The three model periods are characterised by different initial and boundary conditions.

- The excavation and operational phase is characterised by an initial condition identical to today's conditions; i.e. hydrogeological conditions at the end of the site investigation phase. The appropriate flow boundary conditions for this phase are atmospheric pressure in the open tunnels.
- The initial period of the temperate climate after closure (saturation of the repository once pumping of the open tunnels has ceased) is characterised by initial conditions coinciding with the conditions at the end of the previous phase. The boundary conditions during the remaining period of the temperate phase assumes a fully saturated system and are governed by the shoreline displacement; specifically, above the shoreline a net precipitation (flux) is prescribed on the top surface of all terrestrial parts of the model, whereas a fixed pressure is prescribed below the shoreline.
- The remaining part of the reference glacial cycle is characterised by the presence of permafrost and ice sheets. The initial conditions are thus strictly the conditions that prevail at the end of the temperate phase; however, as a full glacial cycle is not modelled, but rather sub-sets of the cycle, see Section 3.4.5 and Chapter 6 below, the initial conditions, to a certain extent, need to be hypothesised. The flow boundary conditions are governed by the presence or absence of an ice sheet and permafrost.

Initial and boundary conditions are described in more detail below in Sections 4.2, 5.2, and 6.2, respectively for the different modelling applications.

### 3.4.3 The excavation and operational phases

Figure 3-4 illustrates the setup of the groundwater flow model of the excavation and operational phases conducted by /Svensson and Follin 2010/ using the DarcyTools code. Key components of this modelling are:

- A need to resolve scales from individual canister deposition holes to the regional scale. This is accomplished using an unstructured grid, which allows for a spatially varying resolution of the computational grid.
- A capability to calculate the detailed inflows to the repository, including analyses of grouting efficiency and canister failures.
- An analysis of the disturbance of the water table (drawdown) and the upconing of more saline water appearing at depth is performed as a function of the grouting efficiency. Both a free groundwater surface and variable-density flow are incorporated in the analysis.
- A simplification of the hydration process of the initially unsaturated backfill material is adopted.
- Spatially varying ECPM properties are derived through up-scaling of deformation zones and discrete fracture network (DFN) realisations generated in the groundwater flow modelling of the temperate climate conditions conducted by /Joyce et al. 2010/, see Section 3.2.4.

The domain used in the modelling by /Svensson and Follin 2010/ is the same as utilised in the hydro-geological modelling within SDM-Site, see Figure 3-5.

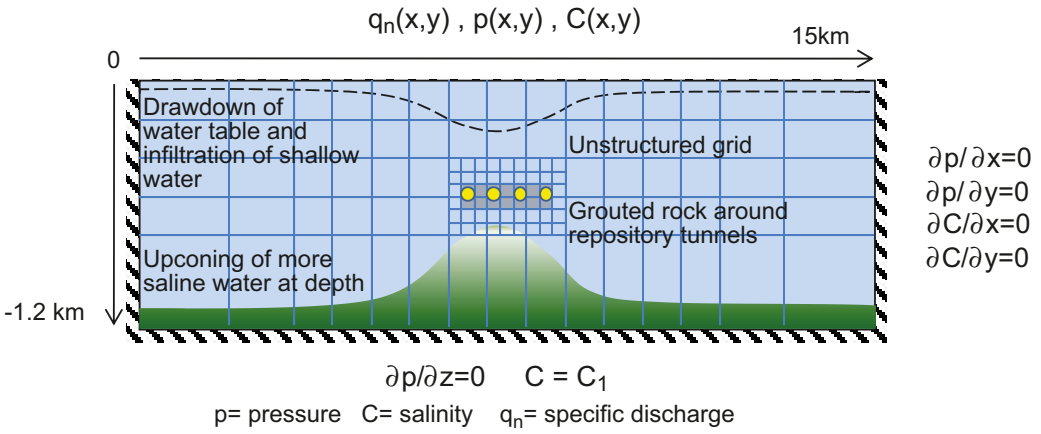


***Figure 3-4.*** *2D-cartoon showing the main characteristics of the groundwater flow model of the excavation and operational phases studied by /Svensson and Follin 2010/ using the DarcyTools code.*

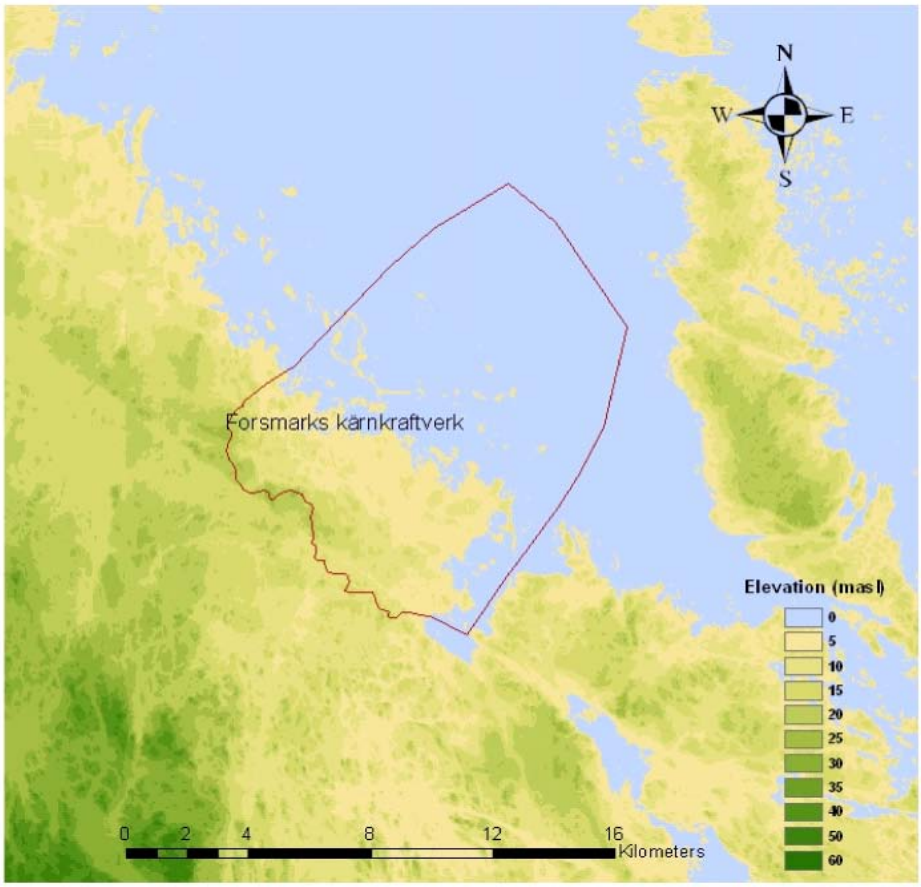


***Figure 3-5.*** *Regional topography in the Forsmark area based on a digital elevation model with a 20 m grid scale. The regional model domain used for groundwater flow modelling is shown by the red line. (Geographic data © Lantmäteriverket Gävle 2007. Consent I 2007/1092).*

### 3.4.4 The initial period of temperate climate after closure

Figure 3-6 illustrates the setup of the groundwater flow modelling of the initial period of temperate climate after closure conducted by /Joyce et al. 2010/. In order to meet the requirements of SR-Site, /Joyce et al. 2010/ use a methodology where a mixture of model scales and flow concepts (continuum and discrete) of the fractured rock are invoked using the ConnectFlow code:

- on the repository scale, a DFN flow concept is used, and
- on a site scale, both DFN and ECPM/CPM flow concepts us are used,
- on the regional scale, ECPM/CPM flow concepts are used.

The pressure solutions of the transient and variable-density regional-scale flow model are used as boundary conditions for the steady-state, fixed-density repository-scale and site-scale flow models. Particle tracking is conducted both forwards and backwards to yield performance measures of discharge pathways from the repository to the surface, and of recharge pathways from surface to repository depth, respectively. Only forward particle tracking is shown in Figure 3-6.

Each calculation starts with the generation of a realisation of the hydrogeological DFN of the rock mass volumes between the deformation zones. Second, the generated DFN realisation is either coupled to a realisation of heterogeneity of transmissivity within each deformation zone or, as in the base case, coupled to a realisation of deterministic depth trend of transmissivity within each deformation zone, see Sections 2.4.1 and 2.4.2 for details. This combined realisation of HRD and HCD then provides the underlying discrete fracture network for each of the three model scales including the upscaling to ECPM properties. Hence, each model realisation involves a suite of simulations on three scales

based on a consistent underlying DFN realisation. Likewise, the same DFN realisations underlie the calculations of operational and glacial phases via export of the fracture properties to the DarcyTools code. This provides consistency across the operational and post-closure climate phases such that local hydrogeological and hydrogeochemical conditions at individual deposition holes can be compared across the entire suite of simulations.

1. Regional Scale (output: p, C and ρ)

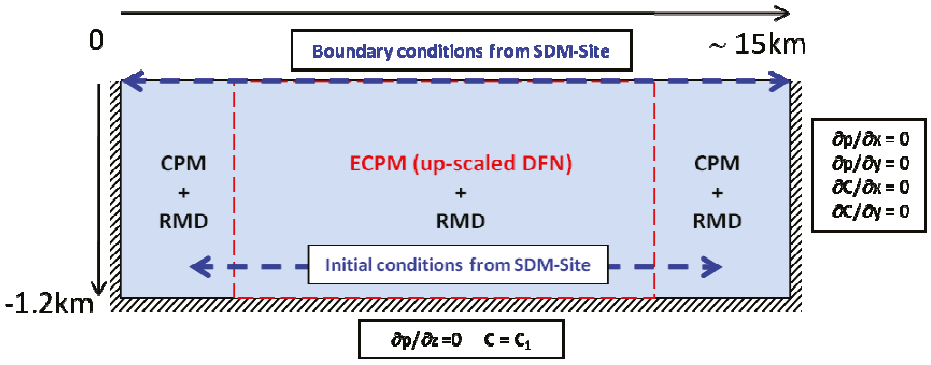


2. Repository Scale (output: q, $Q_{eq}$, $t_w$ and F)

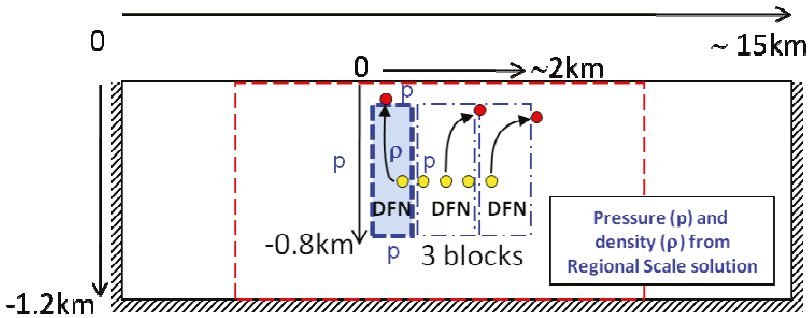


3. Site Scale output: (continuation of $t_w$ and F and particle exit locations)

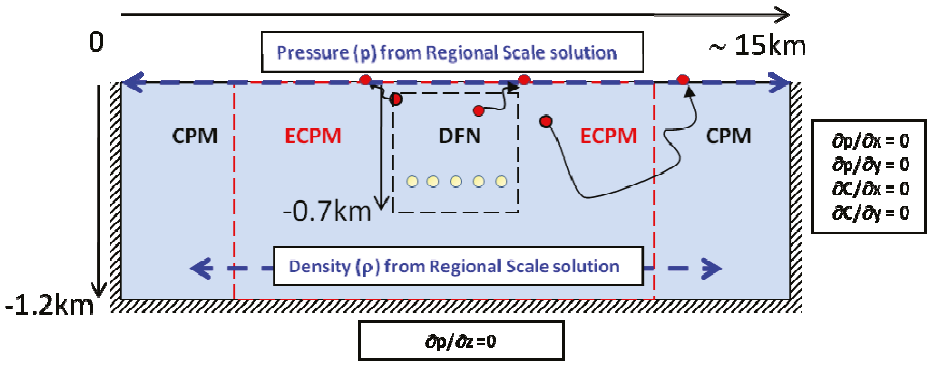


***Figure 3-6.*** *Three cartoons showing the setup of the groundwater flow model of the initial period of temperate climate after closure using ConnectFlow /Joyce et al. 2010/. In the upper and lower cartoons, the size of the model domain is identical to that used in SDM-Site (cf. Figure 3-5). The modelled blocks shown in the remaining (middle) cartoon encompass three different deposition areas. The flow solutions of the regional-scale model provide boundary conditions for the repository and site- scale models. The particle tracking starts at repository depth within the repository-scale model and continues in the site-scale model to yield the desired performance measures. Only forward tracking is shown here.*

### *Regional-scale model*

The setup of the regional-scale model in SR-Site is, in essence, identical to the setup used in SDM-Site (see Appendix G in /Joyce et al. 2010/ for details). The setup of the regional-scale model in SR-Site may be summarised as follows.

In the regional-scale model, variable-density pressure solutions are derived for a transient flow model that is based on continuous porous media (ECPM and CPM) properties. The ECPM properties are derived by means of up-scaling of the discrete fracture network (DFN) realisations treated in the repository-scale and site-scale models. It is noted that the regional-scale model does not include the repository structures, but they are included when the connected fracture network is assessed prior to up-scaling.

Groundwater flow is simulated between 8000 BC and 12,000 AD[4]. Between 8000 BC and 1000 AD, the repository area is submerged and mainly covered by marine water (Littorina Sea). Between 1000 AD and 12,000 AD, terrestrial conditions prevail and the groundwater above the repository is subjected to flushing by meteoric water. The predicted shoreline displacement between today and 12,000 AD results in a total vertical displacement of the site of approximately 40 m upwards /SKB 2010a/. The advective transport of salt in the regional-scale model is subjected to rock matrix diffusion (RMD) using a double-porosity model.

The output data from the regional-scale model consist of pressures ($p$ [M $T^{-2}$ $L^{-1}$]), salinities ($C$ [$MM^{-1}$]), concentrations of groundwater constituents ($C$ [$MM^{-1}$]), fractions of reference waters ($f_i$ [–]), and fluid densities ($\rho$ [$ML^{-3}$]) at predefined time slices.

The output data from the regional-scale model are used in SR-Site as follows:

- The pressures and densities are used to define initial and boundary conditions for the groundwater flow modelling carried out on the more detailed model scales, i.e. the repository-scale and the site-scale models, see below.
- The salinities and fractions of reference waters are used as input to the analysis of the chemical conditions in proximity to the repository during the initial period of temperate climate conditions after closure, i.e. between 2000 AD and 9000 AD, as well as during the submerged conditions following forthcoming periglacial and glacial climate conditions, i.e. results from the modelled period between 8000 BC and 1000 AD.

### *Repository-scale embedded CPM/DFN model*

In the repository-scale model, steady state flow solutions are derived for the predefined time slices treated in the regional-scale model. The flow solutions assume fixed pressures on the model domain boundaries and a fixed, yet spatially varying, fluid density field throughout the model domain. Both the boundary pressures and fluid density distributions are obtained from the regional-scale model at the relevant time slice. The pressure field calculated is the one consistent with the fixed distribution of fluid density and boundary conditions. Hence, there is no advective transport of salt and no matrix diffusion of salt in the repository-scale model. This simplification may imply a bias when particle tracking is performed. Therefore, a test and evaluation of the simplification is performed in Section 5.4.9.

The physical dimensions of the repository-scale model domain are limited because of the computational constraints involved. Therefore, three blocks are used, see Figure 3-6. For each block, the groundwater flow solution is based on a discrete representation of the fractured bedrock surrounding the repository, i.e. the deformation zones and rock mass in between. It is noted that some of the implemented repository features are also modelled in a discrete fashion, i.e. ramp, shafts, central area and transport tunnels, whereas others are modelled as continuous porous media (CPM), i.e. deposition holes, deposition tunnels and main tunnels. The CPM objects are formally coupled to the discrete repository features and to the DFN through an embedding approach where continuity of both pressure and mas flux is ensured by the use of constraint equations, see /Joyce et al. 2010/ for details.

[4] It is noted that the initial period of temperate climate conditions after closure is assumed to end at approximately 10,000 AD in the reference evolution of SR-Site; thus the hydrogeological modelling by /Joyce et al. 2010/ covers a slightly longer period. This choice is made in order to assess the effects of the shoreline displacement up to the point in time when the shoreline retreats beyond the model domain.

The output data from the repository-scale model consist of two types of performance measures:

- Darcy fluxes ($q$ [$LT^{-1}$]) and equivalent flow rates ($Q_{eq}$ [$L^3T^{-1}$]) at the deposition-hole positions, and
- Cumulative advective travel times ($t_w$ [T]) and flow-related transport resistances ($F$ [$TL^{-1}$]) of released particles.

The output data from the repository-scale model are used in SR-Site as follows:

- The equivalent flow rates are used for buffer erosion and canister corrosion analyses as well as for the near-field radionuclide transport calculations.
- The advective travel times and flow-related transport resistances are used for far-field radionuclide transport calculations.

In the particle tracking calculations, three release paths for radionuclide are considered (Figure 3-7):

1. A fracture intersecting the deposition hole, i.e. the Q1 path.
2. The excavation damaged zone (EDZ), if such a zone exists, located below the floor of the deposition tunnel that runs above the deposition holes, i.e. the Q2 path.
3. A path through the backfilled tunnel and into a fracture intersecting the deposition tunnel, i.e. the Q3 path. The Darcy flux associated with this path is the flux in the fracture intersecting the deposition tunnel.

Individual particles are released at each deposition hole position, i.e. three particles per deposition hole, and the flow pathways are tracked, see /Joyce et al. 2010/ for details. It is noted that for the Q3 path, the fracture intersecting the deposition tunnel, is identified through particle tracking of the particle released in the Q3 position.

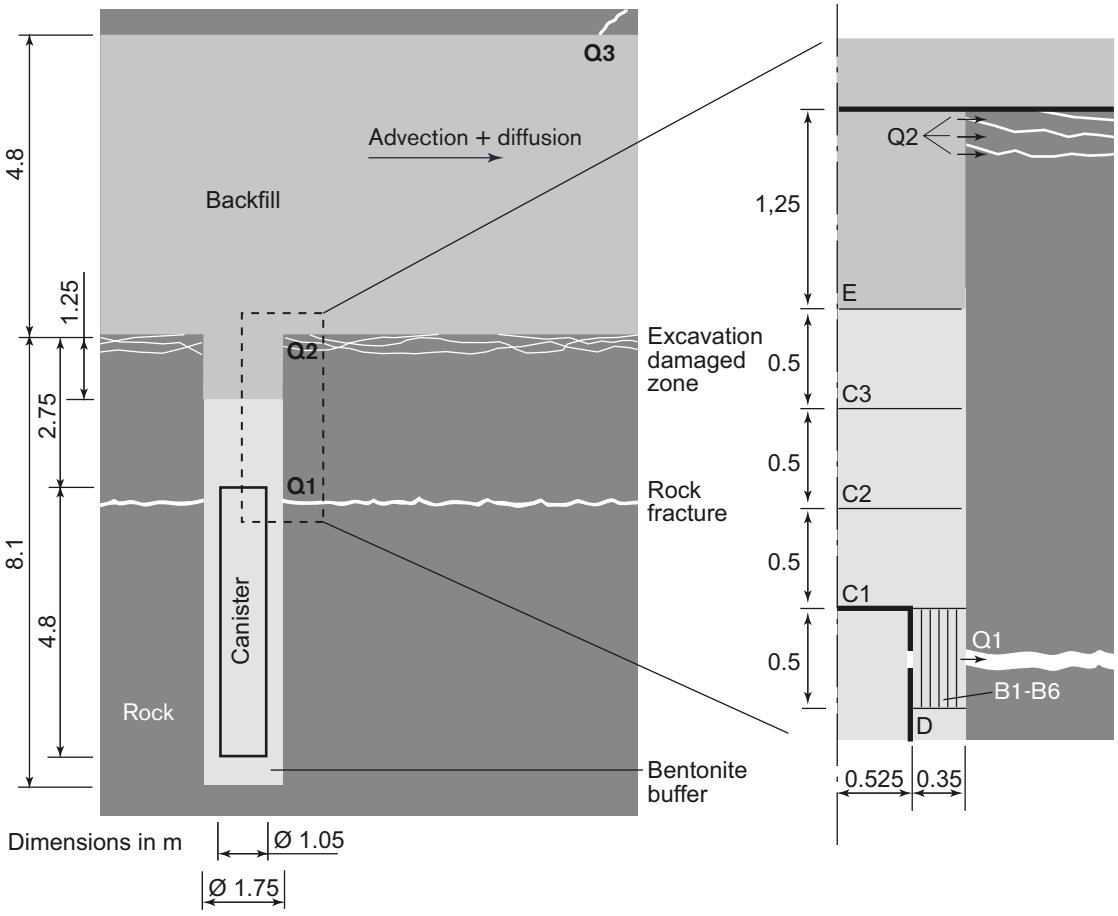


***Figure 3-7.*** *The transport release paths to a fracture intersecting the deposition hole (Q1), to the excavation damaged zone (Q2), and to a fracture intersecting the deposition tunnel (Q3), respectively. All values are in metres.*

### *Site-scale embedded DFN/ECPM model*

The cumulative values of $t_w$ and $F$ of each particle together with its exit location on the side or top of the studied repository-scale blocks are propagated to the site-scale model for continued particle tracking to the biosphere. For this purpose, the site-scale model domain is as large as the regional-scale model domain and uses a DFN representation on the site-scale to maintain the same conceptual model for the majority of the groundwater pathway, although some long pathways may have to be continued through parts of the model where a ECPM/CPM are used for practical reasons. In order to extend the DFN model to the site-scale, the representation of the repository has to be simplified. This is adequate for the purpose of the site-scale model which is to complete the far-field pathways, not to calculate detailed near-field performance measures.

In the site-scale model, steady-state flow solutions are derived for the predefined time slices treated in the regional-scale model using the same methodology as previously described for the repository-scale model. The site-scale model uses a mixture of flow modelling concepts:

- The DFN approach is used throughout the target area/volume.
- In regions where there are DFN properties defined outside the target volume, the ECPM approach is used.
- In regions where there are no DFN properties defined outside the target area, a CPM approach is used.
- A top layer of Quaternary deposits, HSD, is also represented by a CPM approach.

The DFN/ECPM/CPM regions are formally coupled through an embedding approach where continuity of both pressure and mass flux is ensured by the use of constraint equations, see /Joyce et al. 2010/ for details.

In the repository-scale model, particles are also back-tracked from the deposition hole locations in order to assess recharge pathways. The recharge particle pathways extend into the site-scale model in a corresponding manner as for the discharge pathways. Using the recharge paths and an analytical solution for solute transport, an assessment of the potential for penetration of dilute water to repository depth during temperate climate conditions is made, see /Joyce et al. 2010, Appendix F/.

### *Performance measures*

For the three different release paths Q1–Q3 discussed above, various performance measures are calculated. Below, the notation of /Joyce et al. 2010/ is used.

In a DFN representation, the performance measures are defined as:

1. Travel-time, $t_r = \sum_f \frac{e_{tf} w_f \delta l}{Q_f}$, where $\delta l$ is a step length along a path of $f$ steps, each between a pair of fracture intersections, $e_{tf}$ is the fracture transport aperture, $w_f$ is the flow width between the pair of intersections, and $Q_f$ is the flow rate between the pair of intersections in the fracture.
2. Equivalent flux at the release point, $U_r$. For a fracture intersecting the deposition hole, the equivalent flux is calculated as $U_{r1} = \frac{1}{w_c} \sum_f \frac{Q_f}{\sqrt{a_f}}$ where $a_f$ is the area of the fracture plane intersecting the deposition hole, and $w_c$ is the deposition hole height. Corresponding fluxes are defined for the Q2 and Q3 paths, see /Joyce et al. 2010/ for details. (It is noted that this equivalent flux is considered a Darcy flux when compared to corresponding fluxes calculated within the excavation and operational phase /Svensson and Follin 2010/ or within periods with periglacial and glacial climate condition /Vidstrand et al. 2010/.)
3. Equivalent flow rate at the release point, $Q_{eq}$. The definitions of the equivalent flow rates for the three different release paths Q1–Q3 are provided in /Joyce et al. 2010/.
4. Flow pathway length, $L_r = \sum_f \delta l$.
5. Flow-related transport resistance, $F_r = \sum_f \frac{2_{wf} \delta l}{Q_f} = \sum_f \frac{2t_{rf}}{e_{tf}}$, where $t_{rf}$ is the travel time in a fracture along the path.

In a CPM/ECPM representation, the performance measures are defined as:

1. Travel-time, $t_r = \sum_l \frac{\phi \delta l}{q}$, where $\delta l$ is a step length, for example through one finite-element, along a path of $l$ steps, $\phi$ is the kinematic porosity, and $q$ is the Darcy flux;
2. Equivalent flux at the release point, $U_r$. (It is noted that this equivalent flux is considered a Darcy flux when compared to corresponding fluxes calculated within the excavation and operational phase /Svensson and Follin 2010/ or within periods with periglacial and glacial climate condition /Vidstrand et al. 2010/.)
3. Equivalent flow rate at the release point, $Q_{eq}$. The definitions of the equivalent flow rates for the three different release paths Q1–Q3 are provided in /Joyce et al. 2010/.
4. Flow pathway length, $L_r = \sum_l \delta l$.
5. Flow-related transport resistance, $F_r = \sum_l \frac{a_r \delta l}{q}$, where $a_r$ is the flow-wetted fracture surface area per unit volume of rock. This is a measure of the potential for retention and retardation of radionuclides within the rock.

The subscript "*r*" indicates "rock". That is, the cumulative values of the associated performance measures represent only those parts of the flow pathways that are in the rock (HRD and HCD). There is no contribution from the flow pathways that pass through the EDZ or tunnel backfill.

The contribution from legs of flow pathways within the EDZ and tunnels are computed as separate performance measures and distinguished by an "*EDZ*" or "*t*" subscript, respectively. It is noted that no flow-related transport resistance is assumed in tunnels or in the EDZ.

The results from the simulations are used to produce ensemble statistics for the performance measures, as well as locating the discharge areas. The ensemble statistics are calculated over the set of 6,916 deposition hole positions; one ensemble each for the Q1, Q2, and Q3 release paths of each deposition hole, respectively. Multiple realisations are considered, thus allowing for an assessment of uncertainty in the ensemble statistics.

To avoid particles becoming stuck in regions of stagnant flow, they are not started if the initial volumetric flow rate per unit width is less than $1 \cdot 10^{-6}$ m$^2$/y for Q1 and Q2, and if the initial Darcy flux is less than $1 \cdot 10^{-6}$ m/y for Q3. Moreover, not all deposition hole positions are intersected by a fracture. This applies to the Q1 release.

### 3.4.5 The remaining part of the reference glacial cycle

The groundwater flow modelling of the base case is divided into three stages, pre-LGM[5], LGM and post-LGM. During the pre-LGM stage, the ice grows and both unfrozen and frozen (permafrost) conditions are considered in front of the advancing ice sheet margin, see Figure 3-8. During the LGM stage, the model domain is completely covered by a thick ice sheet for thousands of years. Finally, during the post-LGM stage, submerged conditions are considered in the periglacial area while the ice sheet margin retreats.

[5] LGM is a standard acronym used to denote the glacial maximum of the last glaciation (Weichsel), cf. the **Climate report**.

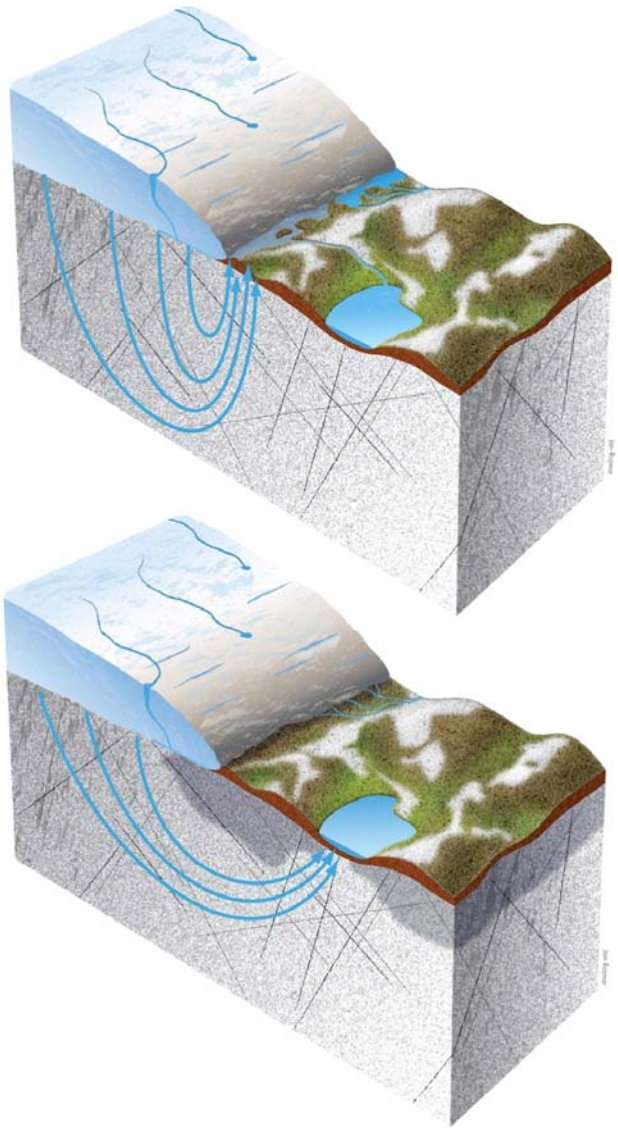

***Figure 3-8.*** *Groundwater discharge for an advancing ice sheet margin occurs predominantly close to the margin if there is no permafrost in the periglacial area (top) and in taliks if there is permafrost in the periglacial area. (bottom).*

Key components of the modelling in /Vidstrand et al. 2010/ are:

- The capability of using an unstructured grid, which allows for a spatially varying resolution of the computational grid. This feature allows for a super-regional model domain, see Figure 3-9, which is needed given the spatial extent of the ice sheet.
- The capability to model heat flow and the development of permafrost. This allows for a physically more realistic simulation of transient changes in permeability due to freezing during periglacial and glacial climate conditions.
- The inclusion of variable-density flow. The evolution of the flushing and upconing of more saline water appearing at depth are analysed for the studied stages, i.e. pre-LGM, LGM and post-LGM. In total, the three stages comprise approximately 19,000 years, where the period of complete ice coverage lasts approximately 17,000 years.
- The inclusion of spatially varying ECPM properties. These are derived through up-scaling of deformation zones and discrete fracture network (DFN) realisations using the specifications provided in the groundwater flow modelling of the temperate climate conditions conducted by /Joyce et al. 2010/, see Section 3.2.4.

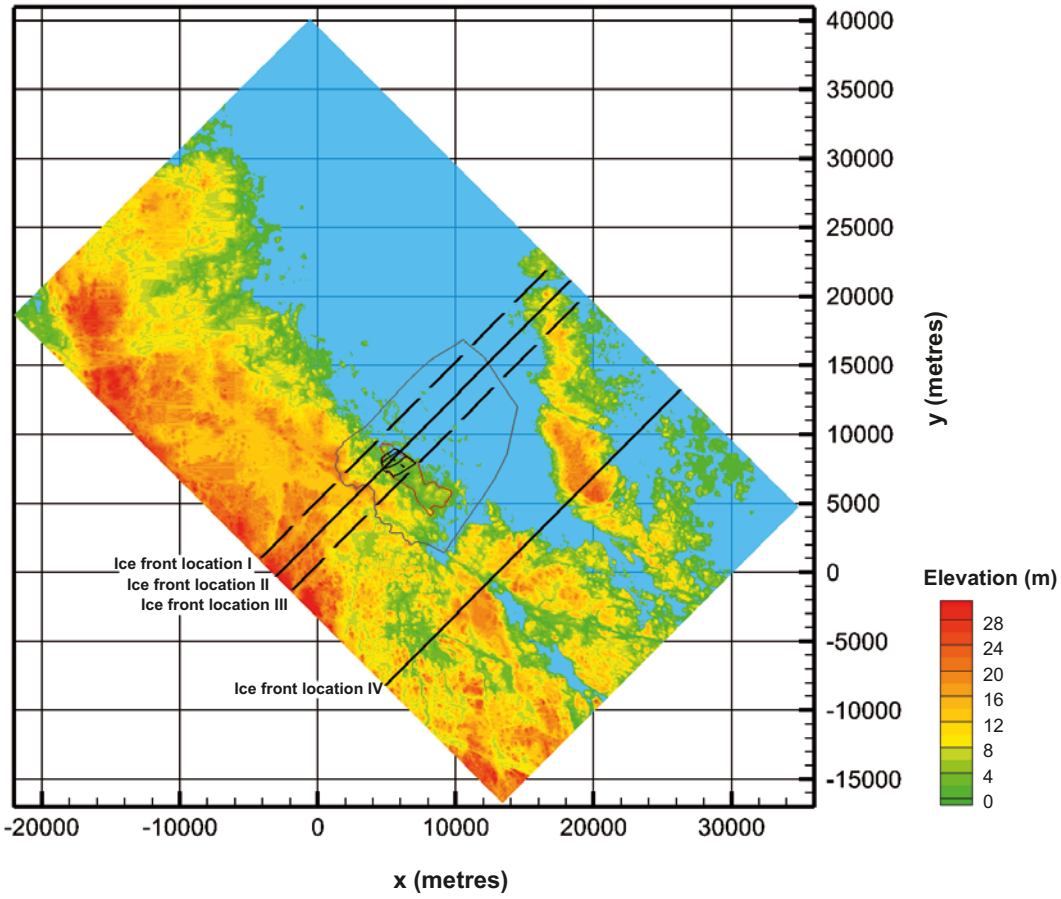


***Figure 3-9.*** *Map showing the present-day topography at Forsmark and the positions of ice front locations IFL I-IV for a NW-SE orientation of the flow model domain studied by /Vidstrand et al. 2010/. The large polygon in the centre shows the model domain used for groundwater flow modelling in SDM-Site, cf. Figure 3-5. The small polygon inside the large polygon shows the location of the investigated candidate area. The repository area is located in the north-western part of the small polygon. The y-axis points towards north.*

The key output parameters from the flow simulation are the pressures ($p$ [$ML^{-1}T^{-2}$]), Darcy fluxes ($q$ [$LT^{-1}$]) and the salinities ($C$ [$MM^{-1}$]) at repository depth for six predefined ice front locations denoted by IFL 0 plus IFL I-V, see Figure 3-9. In the model, IFL II corresponds to a situation when the ice sheet margin is right above the repository, IFL 0 corresponds to a situation when the advancing ice sheet margin is far upstream of the model domain, and IFL V corresponds to a situation when the ice front location has reached the LGM, i.e. far downstream of the model domain, see /SKB 2010a/. The simulated evolution of the Darcy flux and the salinity at repository depth during the three stages are monitored at five measurement localities, denoted by numbers 1–5 in Figure 3-10.

The pressure and salinity solutions of /Vidstrand et al. 2010/ are exported to the study by /Joyce et al. 2010/, since the repository layout and the excavation damage zone are not explicitly resolved within the model studied by /Vidstrand et al. 2010/. Hence, the basis for detailed calculations of performance measures use a methodology consistent with that used for the temperate phase. In the model of /Joyce et al. 2010/, performance measures are thus calculated by means of particle tracking also for glacial climate conditions using the provided pressures as boundary conditions and using the internal distribution of salinity (fluid density). The results of /Joyce et al. 2010/ are used in the far-field radionuclide transport calculations /SKB 2010d, 2011/ and in the buffer erosion/canister corrosion analyses /SKB 2011/.

Further, in /Joyce et al. 2010/, particles are also back-tracked from the deposition hole locations in order to assess recharge pathways during glacial climate conditions. Using the recharge pathways and an analytical solution for solute transport, an assessment of potential for penetration of glacial meltwater to repository depth is made /Joyce et al. 2010, Appendix F/.

Finally, particle tracking is also performed in /Vidstrand et al. 2010/. One particle is released at each deposition hole position when the ice sheet margin reaches ice-front locations II and IV during the pre-LGM stage simulations. All particles are tracked backwards and forwards as a means to identify their recharge and discharge locations in the super-regional model, respectively. Fracture water and matrix porewater salinities as well as flow path lengths, advective travel times, and flow-related transport resistances of particles travelling from the surface to repository depth are exported to the hydrogeochemical modelling carried out by /Salas et al. 2010/ and /Sidborn et al. 2010/.

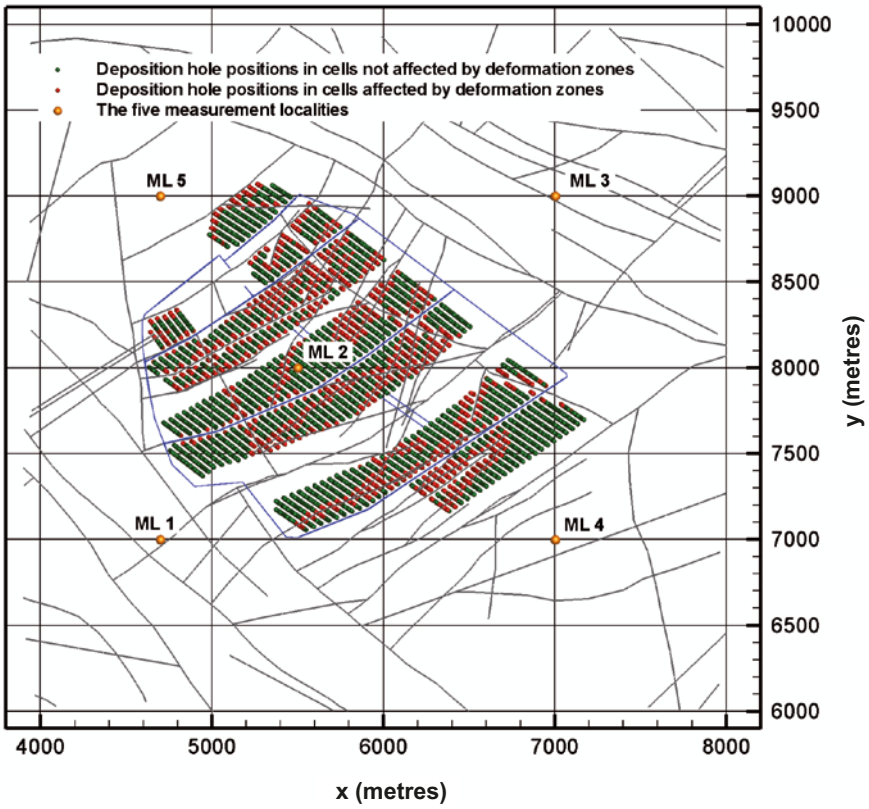


***Figure 3-10.*** *Plane view of the repository layout at –465 m elevation (the blue lines represent major tunnels). The repository has 6,916 deposition hole positions. These are coloured according to their structural location, i.e. whether the computational grid cell in DarcyTools is intersected by a deformation zone (HCD) or fully put inside the rock mass volumes between the deformation zones (HRD). (The deformation zones are shown as grey lines. It is noted that tunnels and deposition holes are not included in the model, but just shown in the figure for context.) The simulated evolution of the Darcy fluxes and the salinities are monitored at five measurement localities denoted by ML 1–5. The y-axis points towards north.*

# 4 The excavation and operational phases

## 4.1 Analyses performed to address specific questions within SR-Site

Below, the different cases of the excavation and operational phases studied by /Svensson and Follin 2010/ are listed. It is indicated where the results of each case are intended to be used within the subsequent analyses in SR-Site.

- **Drawdown of the groundwater table, infiltration of shallow surface water, and upconing of deep saline groundwater.** During the excavation and operational phases, the repository tunnels will be at atmospheric pressure. Hence, a hydraulic gradient will develop and water will flow towards the tunnels. The inflow implies a drawdown of the groundwater table above the repository with possible changes of the water composition at repository depth. The drawdown may cause infiltration of shallow surface water (including seawater intrusion), as well as upconing of deep saline groundwater from below. The simulation results are intended as an input to (i) analyses of ecological and other types of environmental consequences, and (ii) analyses of the groundwater chemistry at repository depth during the mentioned phases.
- **Inflow calculations.** Depending on which tunnels are kept open and which are closed, and also depending on the grouting efficiency, the inflow rate will vary in space and time. The simulation results are primarily intended as an input to Repository Engineering, but also as an input to analyses of buffer and backfill (mechanical) erosion during backfilling of the deposition holes and tunnels.
- **Inflow rejection criteria.** Inflow rejection criteria are proposed as a means to avoid unsuitable conditions during deposition of canisters. However, an assessment of the long-term safety of the repository typically reveals that canister deposition holes associated with the highest groundwater flow (Darcy flux) during saturated conditions yield the most severe consequences in terms of erosion of the buffer and subsequent copper corrosion. As a correlation is expected between the inflow rate during open conditions and the groundwater flow during saturated conditions, it is of interest to avoid canister deposition holes with high inflow rates. The simulation results are primarily intended as an input to the assessment of the merits of applying inflow rejection criteria during the operational phase, and identification of potential merits for the long-term safety.

## 4.2 Base case

The base case of /Svensson and Follin 2010/ is, in principle, identical to the hydrogeological base case described in Section 5.2 in that they are based on the same realisations of HRD fractures and HCD properties. However, a few minor modifications are made in the parameterisation vis-à-vis the hydrogeological base case. Some of the modifications are motivated by the difference in focus, whereas others are due to the fact that a different computer program is used in the groundwater flow modelling of the excavation and operational phases than in SDM-Site and in the modelling of the initial period of temperate climate after closure. In short, the two programs use different flow concepts, different mass transport concepts and different principles in the up-scaling of discrete fracture networks (DFN) to equivalent continuous porous media (ECPM).

The code DarcyTools /Svensson et al. 2010/ is used in the different cases of the excavation and operational phases studied by /Svensson and Follin 2010/. The following modifications are made in the model set-up in comparison with the base model simulation in SDM-Site and the hydrogeological base case described in Section 5.2:

- The hydrogeological model of the uppermost 20 m of the model domain is treated in a simplistic fashion in comparison with the set-up used in SDM-Site and in the hydrogeological base case. The simplification is evaluated by /Mårtensson and Gustafsson 2010/, who use a very detailed description of the Quaternary deposits in their environmental impact assessment flow modelling study.

- The exchange of salt between the immobile (matrix) and mobile (fracture) pore systems in DarcyTools is based on the one-dimensional multi-rate diffusion model[6] suggested by /Haggerty and Gorelick 1995/. The concept of a multi-rate diffusive exchange between the matrix and the fractures ranges from short-term diffusion (fast exchange rate) into/out of the stagnant pools of water nearby the flowing fractures, to the long-term diffusion (slow exchange rate) into/out of the less permeable rock (matrix) elsewhere. Since the exchange rates vary significantly between the mobile pore system and the short-term immobile pore system vis-à-vis the long-term immobile pore system, a variable-density flow system will never be at perfect equilibrium and gravity effects can be expected when other forces are weak, relatively speaking. A detailed description of the concepts and methodology of the implementation of the multi-rate diffusion model in DarcyTools is found in /Svensson et al. 2010/. It is noted that the void space in the matrix is assumed to be ten times greater than the void space in the fractures in the work by /Svensson and Follin 2010/. Ten time constants (exchange rate coefficients) are used to model the diffusion process. The time constant governing the short-term diffusion into/out of the stagnant pools of water nearby the flowing fractures is set to $1 \cdot 10^{-3}$ $s^{-1}$, whereas the time constant governing the long-term diffusion into/out of the less permeable rock matrix is set to is set to $1 \cdot 10^{-10}$ $s^{-1}$. The chosen settings imply a time scale of less than one hour for the fast diffusive exchanges and approximately 300 years for the slow diffusive exchanges. These values of the time constants are consistent with the time frame modelled by /Svensson and Follin 2010/.
- Hydrodynamic dispersivity (dispersion length) is not considered in the DarcyTools code. The classic continuum concept of longitudinal and transverse dispersion is replaced by the notion that it is sufficient to work with a fine grid discretisation of the underlying discrete fracture network realisation. That is, the equation for mass (salt) transport in DarcyTools handles advection and diffusion solely. It is thus assumed that macro-scale dispersion is captured by the explicit representation of variability in the ECPM approach, and that sub-scale dispersion is considered less important. It is noted that DarcyTools uses an unstructured computational grid that allows for spatially varying grid refinements including complex underground constructions and grid discontinuities. The usage of the latter feature in SR-Site is discussed in Chapter 7.

The requirements of SR-Site on the hydrogeological modelling of the excavation and operational phases may be summarised as follows:

- Three scenarios (operation stages A–C) of the repository development are studied (Figure 4-1), i.e. not all parts of the repository are in operation (depressurised) at the same time. The first stage, stage A, lasts for 15 years, stage B lasts for 15 years and stage C lasts for 20 years. Hence, the total operation time is 50 years.
- Three levels of grouting efficiency, I–III, are studied for each operation stage A–C (Table 4-1).
- For the modelling of the saturation process following the closure of the operational phase, the backfill material is assumed to have hydraulic properties similar to Friedland Clay /Börgesson et al. 2006/.
- Two thresholds of the inflow rate to any deposition hole are analysed as a means to quantify the effect of using hydraulic criteria for rejecting a deposition hole:
  Q1: Deposition hole inflow is greater than 0.1 L/min.
  Q2: Deposition hole inflow is greater than 1% of the total inflow to the deposition tunnel (including its deposition holes).

Details of the model setup include:

- The salinity and pressure during the simulation of the excavation and operational phases are fixed on the lateral sides of the model domain implying unaffected steady-state conditions a few kilometres away from the modelled repository.
- The location and geometry of the modelled repository is imported from /SKB 2009b/.

[6] The groundwater flow modelling in SDM-Site is conducted with ConnectFlow /Follin et al. 2007b, 2008/. Unlike DarcyTools, ConnectFlow does not apply the multi-rate diffusion model suggested by /Haggerty and Gorelick 1995/. Instead, a single-rate diffusion model is used that is based on a method developed by /Carrera et al. 1998/ and enhanced by /Hoch and Jackson 2004/. The approach implemented in ConnectFlow combines an approximation that is accurate for small times with one that is accurate for long times, to give a representation of the diffusion into the rock matrix that is accurate for all times.

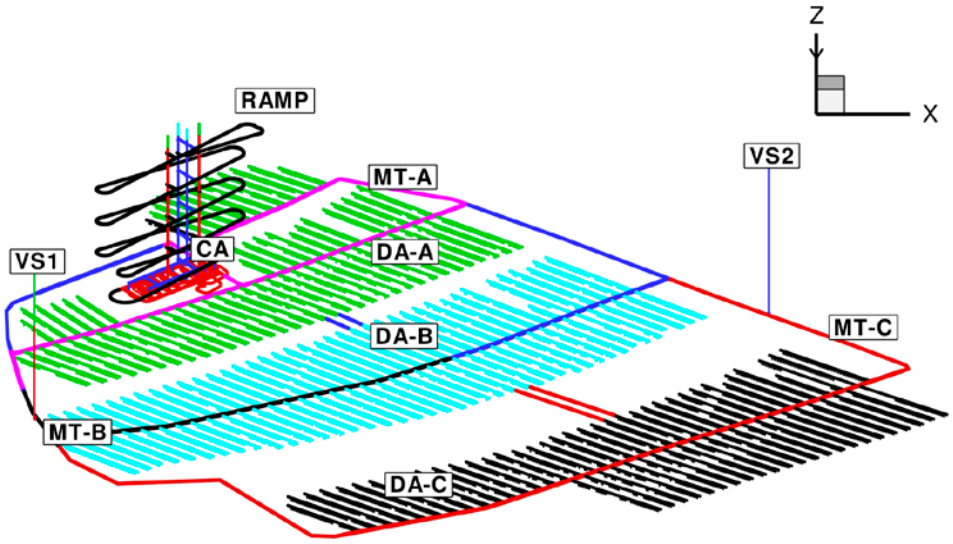


***Figure 4-1.*** *Definition of different parts of the studied repository layout (D2) at Forsmark. The modelling reported here considers three operation stages, A–C, and three possible grouting levels for each stage. The three stages are indicated by green, turquoise and pink colours. DA = deposition area, MT= transport and main tunnel, VS = ventilation shaft, CA = central area. The deposition tunnels are shown as branches to the main tunnels and the canister holes are drilled from the bottom of the deposition tunnels.*

**Table 4-1. Definition of the studied levels of grouting efficiency.**

| Level | Definition |
|---|---|
| I | The hydraulic conductivity of all cells in contact with the repository has a maximum value of $1 \cdot 10^{-7}$ m/s. |
| II | The hydraulic conductivity of all cells in contact with the repository has a maximum value of $1 \cdot 10^{-8}$ m/s. |
| III | The hydraulic conductivity of all cells in contact with the repository has a maximum value of $1 \cdot 10^{-9}$ m/s except where the modelled ungrouted hydraulic conductivity is $10^{-6}$ m/s or greater. At these positions the hydraulic conductivity has a maximum value of $1 \cdot 10^{-8}$ m/s. |

The baseline hydrogeological and hydrochemical conditions at the start of the operational phase need to be self-consistent with the model implementation within DarcyTools and consistent with the SDM-Site hydrogeological model. To ensure this the following steps are taken:

- The model is first run for natural conditions from 8000 BC to present day conditions. The initial conditions of the water salinity at 8000 BC are the same as those used for SDM-Site. These imply a spatially varying interface between fresh and saline groundwaters, where the depth to the interface is shallower within the target area/volume than elsewhere within the regional model domain due to the lower effective hydraulic conductivity within the tectonic lens.
- The boundary conditions used during Holocene time (8000 BC–2000 AD) are also the same as those used for SDM-Site. They consist of a recharge-discharge boundary condition on the top surface and no flow through the sides and bottom of the model. The bottom of the model is located at –1,200 m and has a fixed salinity of approximately 3% based on the initial values of the reference water fractions considered in SDM-Site. The salinity on the top boundary varies with time according to the elevation of the sea with regard to the elevation of the ground surface during the Holocene.
- The geometry and hydraulic properties of discrete geological features in the bedrock such as deformation zones, sheet joints and fracture network realisations are the same as in the SDM work. The specific features used are imported from the groundwater flow modelling of the temperate period carried out by /Joyce et al. 2010/. (It is noted that the up-scaling from discrete properties to ECPM properties is made within DarcyTools, see /Svensson et al. 2010/ for details.)
- Present-day lakes, wetlands, main surface water (stream) runoff and groundwater chemistry are loosely used as "calibration targets" for the modelled evolution of the hydrological and hydrochemical conditions during Holocene time. The simulated conditions at 2000 AD are used as reference for the identification of disturbances caused by the subsequent flow modelling of the excavation and operational phases.

## 4.3 Variants

Seven cases are studied as a means to study the sensitivity of the base model simulation to variations in the geometrical and hydraulic properties other than the impact of different levels of grouting efficiency.

1. The number of possible deposition holes is reduced by removing the deposition holes failing the Full Perimeter Criterion (FPC) and the Extended Full Perimeter Criterion (EFPC) criterion /Munier 2006/. Based on a new flow solution, it is studied which deposition holes fail the inflow rejection criteria.
2. A single deposition tunnel. This case illustrates the magnitude of the simulated inflow rates to a partially excavated repository.
3. A stochastic representation of the deformation zone properties together with another (second) realisation of the stochastic Hydro-DFN model.
4. No salinity. This case is used to study whether there is a difference in the simulated inflow rates if there are no contrasts in the fluid density.
5. The HRD outside the candidate area is modelled as a continuous porous medium (CPM) in SDM-Site, with hydraulic properties as specified in Table 2-6. For the sake of SR-Site, the HRD outside the candidate area is also modelled as an equivalent continuous porous medium (ECPM) using a preliminary Hydro-DFN model developed for the bedrock around SFR /Öhman and Follin 2010/ (see Table A-1 in Appendix A).
6. The amount of sea water recharge to the modelled repository is investigated by reducing the vertical hydraulic conductivity in the sediments below the Baltic Sea by two orders of magnitude. This case is combined with the previous case (a preliminary Hydro-DFN model developed for the bedrock around SFR).
7. Simultaneous operation of two repositories, a final repository for spent nuclear fuel and SFR, the existing repository for short-lived radioactive waste approximately one km north of the investigated candidate area (see Figure A-1 in Appendix A).

Cases 1–3 are of interest for the operation of a final repository since they describe the sensitivity of the inflow rates to late changes in the usage of the planned repository (Case 1), a partially excavated repository (Case 2), and a spatial variability in the hydraulic properties (Case 3).

Cases 4–6 are of interest for the operation of a final repository; however the main objective for their inclusion is invoked by Case 7, i.e. to study the potential hydraulic interference due to a simultaneous operation of two repositories.

It is not feasible to carry out the sensitivity study for all operation stages and grouting levels. For the sake of simplicity, a modified setup of the base case is used as a reference:

- All construction parts of the repository layout are held open at the same time.
- The grouting efficiency is fixed to level II, see Table 4-1.

## 4.4 Results

### 4.4.1 Drawdown of the groundwater table, infiltration of shallow surface water, and upconing of deep saline groundwater

Results are produced for all variants above. However, here only a set of key illustrations are presented for operation stage C and grouting level II. Operation stage C implies the largest inflows and hence the strongest perturbation of the initial salinity field. Also, since operation stage C is the last stage, the chemical conditions have already to some extent been perturbed during the first two operation stages. The drawdown is relatively small with maximum values around one metre except for the Central Area (CA) of the repository, where a drawdown around ten metres is obtained /Svensson and Follin 2010/.

Figure 4-2 shows the simulated salinity before and after the construction and operation of the repository with conditions during operation stage C. It is observed that a dilution has occurred around most parts of the repository. That is, fresh water has been drawn towards repository depth due to the lowering of the groundwater table. A corresponding upconing does occur, but water with higher salinity is found only around the Central area with ramp and shafts. The reason is likely due to this being a discharge area, and also that there are structures connected to depth within this area. It is also noted that surface water with a higher salt content may infiltrate into the bedrock from the brackish Baltic Sea.

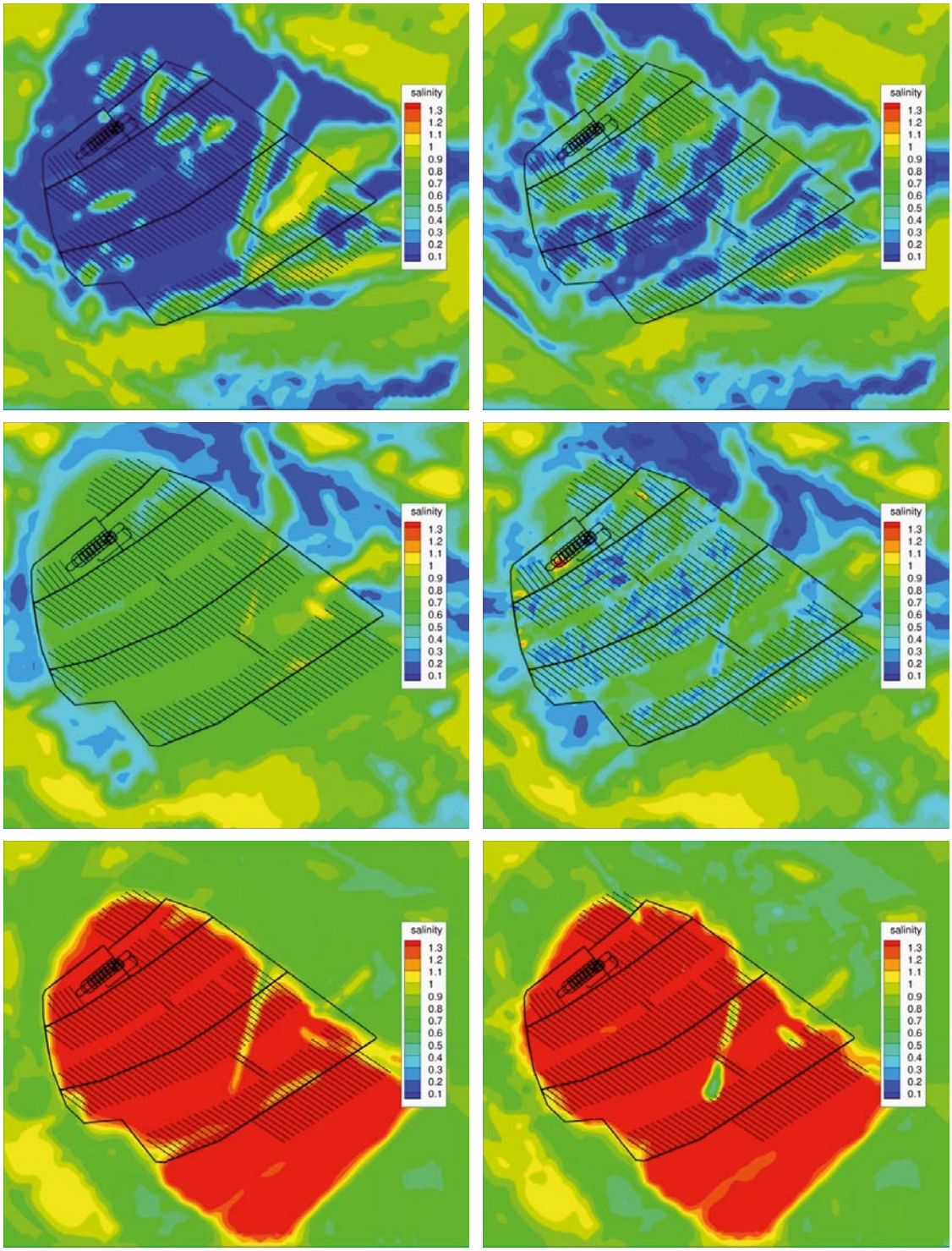


***Figure 4-2.*** *Simulated salinity at –300 m, –465 m and –600 m elevation. Left: Pre-repository conditions. Here, the repository is shown for context only. Right: Conditions at the end of operation stage C for grouting level II. The values shown in the legend are expressed in percent by weight.*

The recharge area for water entering the repository is assessed by backward particle tracking. The results shown in Figure 4-3 indicate that most of the recharge to the repository is located right above the facility, i.e. within a small radius of influence as expected. The black dots indicate the particle positions after ten days. These imply high transport velocities in the flowing fractures close to the repository. It should be noted that transport velocity is linearly related to the reciprocal value of kinematic porosity and that the kinematic porosity values applied in /Svensson and Follin 2010/ are derived from the relationship between transport aperture and fracture transmissivity shown in Equation 2-5. This equation is based on results presented in /Dershowitz et al. 2003/ for the Äspö Task Force Task 6c project. In the model implementation, the ECPM grid cell kinematic porosities derived by /Svensson and Follin 2010/ vary roughly between $5 \cdot 10^{-5}$ and $1 \cdot 10^{-3}$, which can be considered low values, hence the estimated recharge advective travel times are at the low end of the plausible range.

A discussion about the derivation of grid cell kinematic porosity in DarcyTools and its implication for travel time simulations is found in see Section 4.6 of /Svensson and Follin 2010/. Below, Section 5.4.8 provides a sensitivity analysis on fracture transport aperture based on a compilation of tracer test data by /Hjerne et al. 2010/.

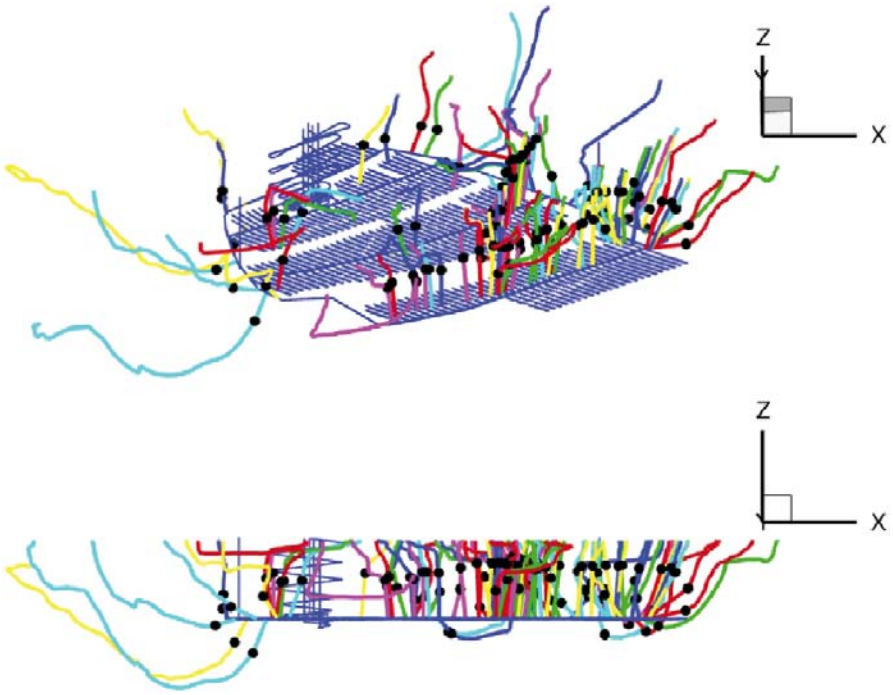


***Figure 4-3.*** *Flow paths of 100 randomly selected particles traced by means of reversed particle tracking. The black dots indicate the particle positions after ten days (see Section 5.4.8 for a discussion on kinematic porosity). The x-axis points towards East.*

### 4.4.2 Inflow calculations

The calculated inflow during the different operation stages and grouting levels are presented in Table 4-2. The total inflow varies from 8 to 51 L/s depending on the stage of operation (A–C) and the level of grouting efficiency (I–III). For the stage illustrated in Figure 4-2, i.e. operation stage C and grouting level II, the inflow is 28 L/s. The ramp passes through the sheet joints (shallow bedrock aquifer) /Follin 2008/; hence the large inflows for the case with a low grouting efficiency.

The inflow distribution to the repository for grouting level II during operation stage C is shown in Figure 4-4. The inflows mainly occur at the boundaries of the repository. This is due to the fact that the largest horizontal hydraulic gradients are found at the boundaries between the repository and the outside rock volumes since the pressure between all open tunnels is close to atmospheric.

**Table 4-2. Calculated inflow rates (L/s) to different parts of the repository for three levels of grouting efficiency (I–III) and three stages of operation (A–C). CA = central area, DA = deposition area, MT = transport and main tunnels, VS = ventilation shaft.**

| | Grouting level I | | | Grouting level II | | | Grouting level III | | |
|---|---|---|---|---|---|---|---|---|---|
| | Operation stage | | | Operation stage | | | Operation stage | | |
| Part of repository | A | B | C | A | B | C | A | B | C |
| CA | 4 | 4 | 5 | 2 | 2 | 2 | 1 | 1 | 1 |
| DA-A | 6 | – | – | 4 | – | – | 3 | – | – |
| DA-B | – | 8 | – | – | 6 | – | – | 3 | – |
| DA-C | – | – | 9 | – | – | 8 | – | – | 4 |
| RAMP | 16 | 17 | 17 | 6 | 6 | 6 | 2 | 2 | 2 |
| MT-A | 6 | 6 | 7 | 4 | 4 | 5 | 2 | 2 | 2 |
| MT-B | – | 1 | 1 | – | 1 | 1 | – | 0 | 0 |
| MT-C | – | – | 9 | – | – | 5 | – | – | 2 |
| VS1 | 1 | 1 | 1 | 1 | 1 | 0 | 0 | 0 | 0 |
| VS2 | – | 2 | 2 | – | 1 | 1 | – | 0 | 0 |
| **Total** | **33** | **39** | **51** | **17** | **21** | **28** | **8** | **8** | **11** |

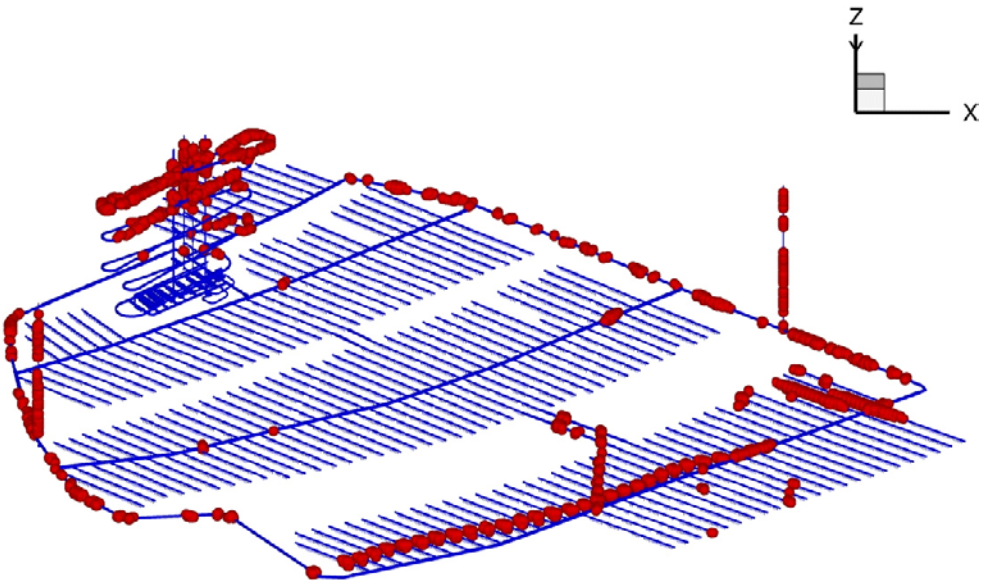


***Figure 4-4.*** *Cells with an inflow rate greater than 0.1 L/min are marked up by spheres. Operation stage C and grouting level II.*

In the base case, each deformation zone has a unique but homogeneous value of hydraulic conductivity including a constant depth trend (cf. the hydrogeological base case in /Joyce et al. 2010/). The sensitivity in inflow is tested by applying a second realisation of the underlying fracture network combined with heterogeneous deformation zones (Variant 3 in Section 4.3). Heterogeneity is represented by dividing the deformation zones into smaller pieces and assigning spatially varying properties according to Equation 2-3, see Figure 4-5. In this comparison, grouting level II is used in combination with the condition that the whole repository is kept open. Resulting values are thus not directly comparable to the model set-up behind Table 4-2. The base case realisation with homogeneous deformation zones yields an inflow rate of 31.2 L/s, whereas the second realisation yields an inflow rate of 33.4 L/s. This value indicates that hydraulic heterogeneity in the deformation zones alters the total inflow compared to hydraulically homogeneous deformation zones by approximately 10%.

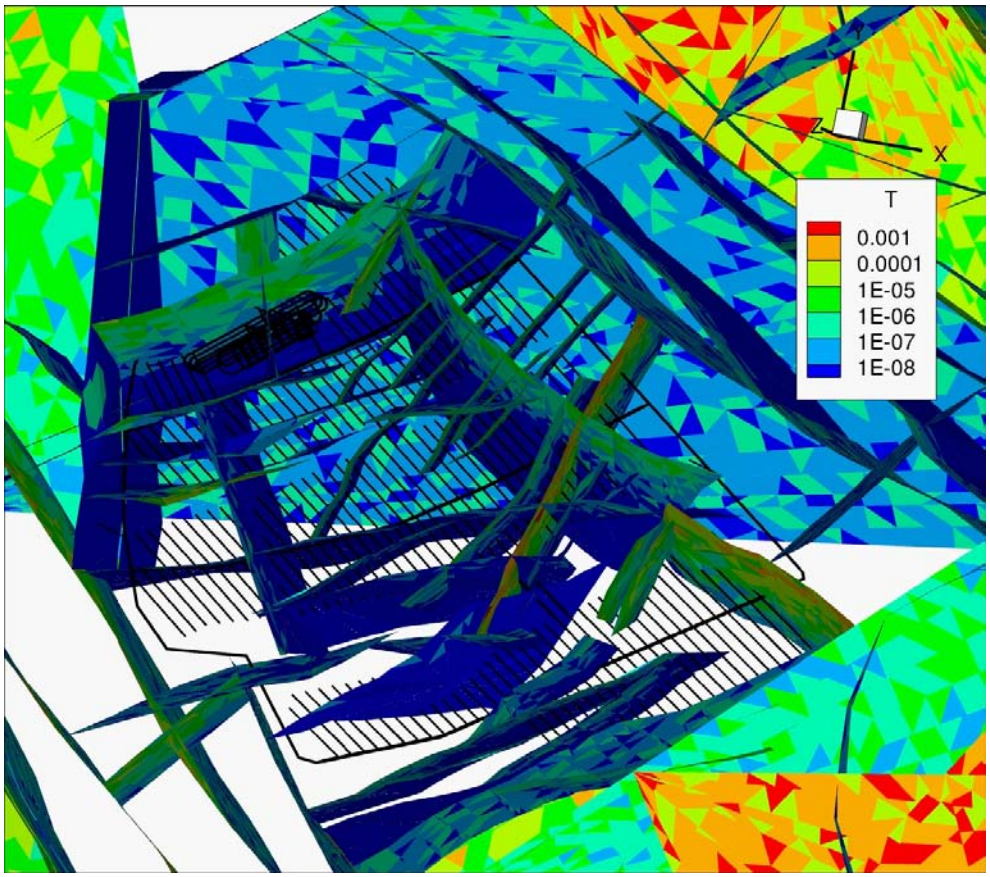


***Figure 4-5.*** *Visualisation of the repository layout at –465 m elevation and the transmissivity of deterministically modelled deformation zones nearby for the third variant and sensitivity test, see Section 4.3. Some zones are deleted in this visualisation for the sake of visibility. The y-axis points towards north.*

### 4.4.3 Inflow rejection criteria

According to the design premises /SKB 2009a/, the total volume of water flowing into a deposition hole, for the time between when the buffer is exposed to inflowing water and saturation, should be limited to ensure that no more than 100 kg of the initially deposited buffer material is lost due to piping/erosion. This implies, according to the present knowledge, that this total volume of water flowing into an accepted deposition hole must be less than 150 $m^3$. It is judged that this design premise is met provided that the specified inflow criteria, Q1, Q2 and "Q1 or Q2", are met, see Section 4.2.

/Svensson and Follin 2010/ analyse the two inflow rejection criteria (see Section 4.2) for the base case realisation using two types of equivalent porous media models, the traditional ECPM approach and an elaborated approach named EDPM (equivalent discontinuous porous medium, see /Svensson and Follin 2010/ for details). In the EDPM approach, grid cells not intersected by fractures are removed from the computational grid rather than giving them arbitrary low values as in the ECPM approach.

The modelling with the ECPM approach suggest that 157 deposition holes fail the Q1 criterion, 867 fail the Q2 criterion, and 874 deposition holes fail the combined criterion "Q1 or Q2". Thus, the Q2 criterion is responsible for the majority of the failing deposition hole positions using the ECPM approach. Further, /Svensson and Follin 2010/ show that 121 deposition holes fail both the combined "Q1 or Q2" criterion and the "FPC or EFPC" criterion (this criterion is discussed in detail in /Munier 2006/ and presented also in Section 3.2).

The corresponding results for the elaborated EDPM approach are: 88 fail the Q1 criterion, 368 fail the Q2 criterion and 372 fail the combined criterion "Q1 or Q2". Also, it is shown that 141 deposition holes fail both the "Q1 or Q2" criterion and the "FPC or EFPC" criterion. Since one would expect the deposition holes failing the "Q1 or Q2" criterion to be correlated to the holes failing also the "FPC or EFPC" criterion, it is observed that there is a greater overlap between these groups for the EDPM approach (372 vs.141) than for the ECPM approach (874 vs.121). The ECPM approach simply identifies too many inflows according to the Q2 criterion.

In conclusion, less deposition hole positions fail the different inflow criteria if the sparsely fractures rock is treated as a discontinuous porous medium. Figure 4-6 shows the 157 and 88 deposition hole positions (out of a total of 6,916) that fail inflow criterion Q1 using the two approaches for the base case realisation. It is noted that /Svensson and Follin 2010/ conclude that there appears to be substantial variability between realisations when number and location of deposition holes rejected by inflow criteria are considered. For instance, a second realisation /Svensson and Follin 2010/ obtained 211 failing deposition hole positions (as compared to 157 in the first realisation) using the ECPM approach, and 144 failing deposition hole positions (as compared to 88 in the first realisation) using the EDPM approach. However, this variability between realisations is reasonable given the low geometric mean of the conductive fracture frequency and the strong impact of large random features.

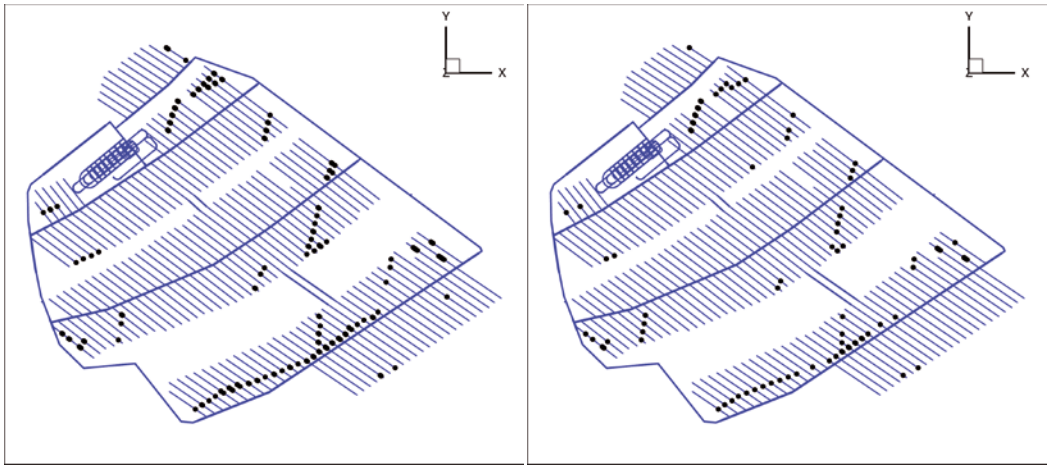


***Figure 4-6.*** *Left: Illustration of the 157 deposition hole positions that fail inflow criterion Q1 using the ECPM approach. Right: Illustration of the 88 deposition hole positions that fail inflow criterion Q1 using the EDPM approach. The plots look alike but in the ECPM approach many positions that fail lie next to each other.*

As explained above, there is also an interest to evaluate to what extent high inflow rates during the operational phase are correlated to deposition holes with high Darcy fluxes in the discrete fractures intersecting the deposition holes during saturated conditions. If this is the case, avoiding deposition holes with high inflow rates would also have potential implications for long term safety. In order to investigate this, the elaborated EDPM approach is used. The results of the correlation analyses are assessed in Chapter 7.

### 4.4.4 Variants

A single deposition tunnel open rendered a slight increase in the inflow rates to some of the other open parts of the repository layout. This is due to higher pressure gradients to those parts when only one deposition tunnel is present.

Heterogeneous deformation zones in combination with a second realisation of the underlying Hydro-DFN model rendered slightly different inflow rates in some parts of the repository, especially in the deposition areas. However, the total inflow is about the same as for the Base case.

Groundwater salinity appears to have little or no impact on the inflow rates. Likewise, neither an extended Hydro-DFN, nor a calibrated flow model for an extended SFR in operation appears to have any significant impact on the inflow rates to a repository in the target volume. The pressure interference between the two open repositories and backward particle tracks from the repositories are shown in Figure 4-7.

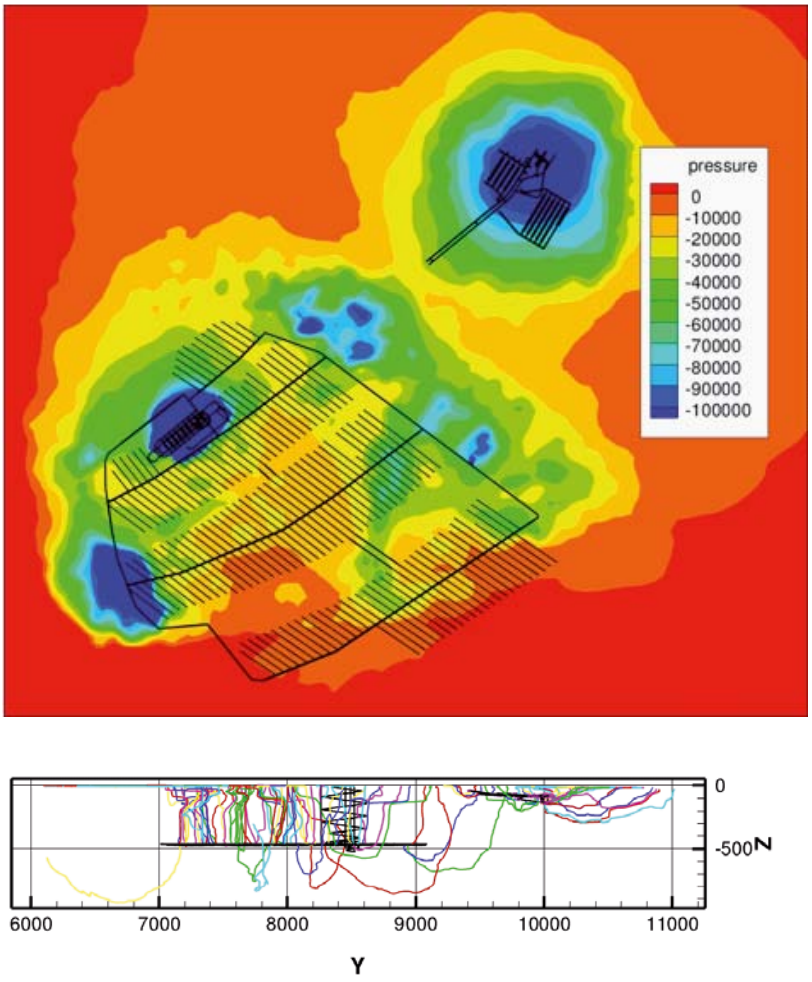


***Figure 4-7.*** *Top: Horizontal view showing the pressure interference (Pa) at –150 m elevation for a simultaneous operation of an extended SFR and a deep repository in the target volume. Bottom: Transparent cross-section with backward particle tracking trajectories. The starting positions of these trajectories have inflow rates greater than 0.1 L/min.*

## 4.5 Assumptions, simplifications and uncertainties

Main assumptions, simplifications and uncertainties related to the study of the excavation and operational phase are:

- It is argued that the simulated changes in chemical composition around the repository reported by /Svensson and Follin 2010/ may be too large. Detailed calculations of the near-surface effects of an open repository carried out with the MIKE-SHE modelling tool /Mårtensson and Gustafsson 2010/ within the Environmental Impact Assessment (EIA) reveal that the simplistic handling of the surface hydrology and near-surface hydrogeology in the groundwater flow calculations carried out with the DarcyTools modelling tool overestimates the area of influence of the drawdown of the water table by a factor of two and also overestimates its magnitudes above the repository. This observation demonstrates that the spatial distribution and the magnitude of the drawdown of the water table is not a function of the inflow to the repository only (which is considered reasonable), but also a function of the boundary conditions on the top boundary of the model domain and the hydraulic properties of the Quaternary deposits and the uppermost part of the bedrock (the shallow bedrock aquifer /Follin 2008/). Thus, since the drawdown of the water table affects the movement of shallow and deep waters of different chemical compositions, it is argued that the final calculated perturbation of the initial chemical composition may also be too large. Furthermore, if an alternative relationship between transmissivity and aperture yielding larger apertures had been used, see Section 5.4.8, also a smaller perturbation of the chemical composition had been observed. Based on these observations, it is argued within SR-Site that the uncertainty in groundwater chemistry (salinity) during the Excavation and operational phase does not need to be propagated to further analyses.
- The ECPM approach is used for calculation of total inflows. This method likely over estimates total inflows. Also, the comparison with MIKE SHE indicates that total inflows are over estimated. Hence, it is argued within SR-Site that the presented inflows are conservative estimates.

# 5 The initial period of temperate climate after closure

## 5.1 Analyses performed to address specific questions within SR-Site

Below, the different cases of /Joyce et al. 2010/ performed with relevance for the periods with temperate climate conditions are listed. In addition, the saturation calculation of /Svensson and Follin 2010/ is included. Finally, it is indicated where the results produced by each case are used within the subsequent analyses of SR-Site.

- **Saturation**. In the simulations of /Joyce et al. 2010/, the back-filled repository is assumed saturated. However, the analysis of the temperate period formally starts when the repository is closed; i.e. prior to full saturation. In order to assess the simplification of assuming full saturation, an assessment of the saturation process is conducted. The results of the saturation calculations presented here are used in a comparative sense when the saturation of buffer and backfill are analysed in Section 10.3.8 of the SR-Site Main report.
- **Hydrogeochemical evolution**. The groundwater chemistry, here represented as fractions of different reference waters, is calculated in the regional-scale model utilising a porous medium representation of the discrete fracture network /Joyce et al. 2010/. Due to the shoreline displacement process and infiltration of meteoric water, the groundwater chemistry will change with time. The results are used within the hydrogeochemistry assessment in Section 10.3.7 of the SR-Site Main report.
- **Discharge locations in the biosphere.** The discharge locations of particles transported advectively through the system from all canister deposition hole locations are calculated. The analysis is first performed in the site-scale model for every 1,000 years (i.e. from 0 AD to 12,000 AD) in order to support the identification of discharge locations in the biosphere, see Section 10.3.3 of the SR-Site Main report for details. Furthermore, discharge locations are calculated in the combined repository and site-scale models including a detailed representation of the repository structures for a few selected snapshots-in-time. These flow paths are used when some of the performance measures are calculated, see bullet below. Due to the shoreline displacement process, the discharge locations will move in time and generally follow the retreating shoreline.
- **Performance measures.** The main performance measures used in the subsequent radionuclide transport calculations are the Darcy flux (and associated equivalent flow rates) and flow-related transport properties along flow paths. These are calculated for each deposition hole location (Darcy flux and equivalent flow rates) and associated flow path from deposition hole location to the biosphere (flow-related transport resistance and advective travel time). Due to the shoreline displacement, these measures will also change with time. The results are used as input for the buffer erosion and canister corrosion analyses (Sections 10.3.11, 10.3.13, 10.4.8 and 10.4.9 of the SR-Site Main report, respectively) and for radionuclide transport calculations, see Chapter 13 of the SR-Site Main report.
- **Penetration of meteoric water.** The recharge of meteoric water in combination with the shoreline displacement implies a gradual dilution of the originally more saline water. As dilute water has negative effects on the buffer and backfill stability, it is of interest to assess the possibilities for dilute water to reach repository depth considering the hydrogeological flow and transport conditions. This is done using the flow-related transport properties described above in conjunction with analytical transport estimates. The results are used within the hydrogeochemistry assessment in Section 10.3.7 of the SR-Site Main report.
- **EDZ, spalling and crown space.** The intended properties of the repository are defined in /SKB 2010e/ and /SKB 2010f/; however, it is of interest to assess consequences in terms of the performance measures if the intended repository properties are not achieved. The results of these sensitivity analyses are mainly used in Chapter 13 (Radionuclide Transport) of the SR-Site Main report.

- **SDM-Site related model variants.** The hydrogeological base case properties of the geosphere are defined through SDM-Site Forsmark /Follin 2008/. However, it is of interest to assess consequences in terms of the performance measures if the geosphere is assumed to be characterised by other cases or properties identified as relevant in the SDM-Site work. The results of these sensitivity analyses are used for the buffer erosion and canister corrosion analyses (Sections 10.3.11, 10.3.13, 10.4.8 and 10.4.9) and for radionuclide transport, see Chapter 13 of the SR-Site Main report.
- **Unsealed boreholes.** Boreholes are drilled in close proximity to or into the repository rock volume both during the characterisation phase and during construction. In case the sealing of these boreholes does not function as intended, or if a borehole is abandoned and forgotten, the boreholes may affect the groundwater flow and transport characteristics. Variant cases incorporating completely unsealed boreholes are performed to bound the importance of such boreholes. The result of this analysis is also used as input to the Future Human Action scenarios, see Section 14.2 of the SR-Site Main report.

## 5.2 Hydrogeological base case

The hydrogeological base case is, in essence, identical to the so called base model simulation of the site-descriptive model (SDM-Site Forsmark /Follin 2008/) and described briefly in Chapter 2 of this report. However, a few minor modifications are made to this model within SR-Site and are highlighted below.

- The effective diffusivity of solutes in the matrix is reduced from $1 \cdot 10^{-13}$ m$^2$/s to $4 \cdot 10^{-15}$ m$^2$/s. (It is noted that the chloride ion is the key constituent in the salt transport modelling.)
- The specification of the rock matrix diffusion parameters for solute transport is changed, primarily for the specific flow-wetted fracture surface area per unit volume of rock below –200 m elevation in the key hydraulic rock mass domains at Forsmark, FFM01 and FFM06. Specifically, the flow-wetted fracture surface area used in the palaeohydrogeological simulations is kept constant within each hydraulic rock domain based on the fracture frequency. This implies lower values of the flow-wetted fracture surface area relative to SDM-Site.
- The initial conditions for two of the five reference waters used in the palaeohydrogeological simulations (Old Meteoric and Glacial) are changed to include a variation with distance from a conductive fracture within the matrix.
- Grid dispersivities (dispersion lengths) are modified slightly for the region outside the candidate area, i.e. in the part handled as a homogeneous and isotropic continuous porous medium (CPM) to ensure numerical stability. The longitudinal dispersion length in the coarser part of the grid is increased from 40 m to 50 m, and the transverse dispersion length in the coarse part of the grid is increased from 5 m to 10 m.
- The identification of the connected discrete fracture network on the regional-scale was made to include a representation of the repository and smaller-scale fractures down to radius of 0.4 m in a volume surrounding the repository, while fractures with radius greater than 5.6 m are created over the hydraulic rock mass domains covered by the candidate area, FFM01 to FFM06.
- The shoreline displacement curve is updated to also include the evolution during the temperate period considered (2000 AD–12,000 AD).

The boundary conditions used on the regional-scale for SR-Site are the same as those used for SDM-Site. They consist of a recharge-discharge boundary condition on the top surface and no flow through the sides and bottom of the model. The bottom of the model is located at –1,200 m elevation and has a hydrochemical boundary condition set to the initial values of the reference water fractions. The reference water fractions on the top boundary vary with time according to the elevation of shoreline with regard to the topography of the ground surface. On the scales with finer resolution, i.e. site-scale and repository-scale, boundary conditions are taken from the regional-scale model for different time slices as explained in Section 3.4.4.

The numerical techniques adopted for the applications on the different scales are presented in Section 3.4.4 above. Details on the numerical implementation are given in /Joyce et al. 2010/.

It is noted that the base model simulation in SDM-Site uses a homogeneous HCD and a single realisation of the HRD. In SR-Site, the hydrogeological base case consists of the base model simulation plus 10 realisations:

- Homogeneous HCD + r1 of HRD,
- r1 of HCD + r1 of HRD,
- r2 of HCD + r2 of HRD,
- …
- r10 of HCD + r10 of HRD.

where rn denotes realisation n.

The hydrogeological base case is furthermore implemented as a set of models on three different scales, see Section 3.4.4, with focus on the quantities of interest at each scale. However, it is emphasised that each model scale is a representation of the same hydrogeological base case, and each is derived from the same set of properties and fractures. The regional-scale model is concerned with the large scale evolution of pressure and reference water distribution over time from 8000 BC to 12,000 AD. The site-scale model uses a DFN to provide a more detailed representation of the site for carrying out particle transport calculations. The repository-scale model uses a CPM representation of the main tunnels, deposition tunnels and deposition holes within the site-scale DFN to provide detailed performance measures for the initial portions of the particle transport pathways. Since the HRD and, in some cases, the HCD are based on stochastic properties, the hydrogeological base case is represented as a number of realisations. Each realisation forms part of the hydrogeological base case.

## 5.3 Variants

### 5.3.1 Alternative DFN transmissivity-size relationships

It is assumed that there is some correlation between fracture size and fracture transmissivity /Follin 2008, Appendix C/. The hydrogeological base case defines a semi-correlated relationship between fracture size and transmissivity. The variants in this section examine two alternative relationships, fully correlated and uncorrelated.

The details of the different correlation models are given in /Joyce et al. 2010/. Two issues are highlighted here. First, for the semi-correlated model, the assigned transmissivity value for any fracture is limited to two standard deviations on either side of the mean by resampling values outside of this range. For the uncorrelated model, the maximum values for each fracture set are limited to the maximum deformation zone transmissivities with corresponding inclinations, fracture domains and depth zones. Second, the procedure described above implies that different realisations of the fracture network will result due to the resampling. Thus, the different hydraulic correlation models in general also imply different realisations of the fracture geometrical properties.

### 5.3.2 Inclusion of possible deformation zones

Forty-three possible deformation zones (PDZ) were identified in the single-hole geological interpretations. /Follin et al. 2007b/ established that only ten of these corresponded with a hydraulic test above the detection limit. Of these, six were found to be gently dipping zones in the top 150 m of bedrock and considered to be already represented by the implementation of the near-surface sheet joints, leaving four PDZs above the hydraulic detection limit at or close to repository depth. The deformation zones are one of the main groundwater flow conduits and therefore it is important to investigate the influence of these additional possible deformations zones.

As a variant in SR-Site, four possible deformation zones are added to the model and handled in the same way as the deterministically modelled deformation zones.

### 5.3.3 Unmodified vertical hydraulic conductivity

During the calibration and confirmatory testing of the SDM-Site base model simulation, the vertical conductivity of the ECPM representation of the HRD above an elevation of –400 m was reduced by a factor of ten in order to provide a better fit to chemistry and interference test data. This reduction is also used for the ECPM in the hydrogeological base case for SR-Site. However, no corresponding change is made to the properties of the fractures in the DFN representation of the HRD, leading to a possible inconsistency in flows between the DFN and CPM in the site-scale model.

This variant removes the modification of the vertical conductivity of the ECPM used in the regional and site-scale models.

### 5.3.4 Extended spatial variability

The hydrogeological base case uses an HRD model from SDM-Site that covers the repository site area, based on the data available. Outside this area, the rock is modelled as a CPM with homogeneous and isotropic properties for each depth zone. However, this greatly reduces the effect of outcropping sub-vertical deformation zones on particle exit points. Limited additional data from investigations at SFR /Öhman and Follin 2010/ allows for a tentative parameterisation of a DFN in the area otherwise modelled as a CPM, see Appendix A.

This variant keeps the hydrogeological base case DFN but adds fractures, based on the additional data, to cover the area to the boundaries of the regional model. This is used to provide a full ECPM for the regional-scale and site-scale models. In addition, the area of the DFN in the site-scale model is extended northwards beyond the Singö deformation zone, which may provide an important discharge location.

### 5.3.5 Tunnel variants

Once the repository has been closed, the deposition tunnels will be backfilled with low permeability material, typically bentonite, which may consolidate over a period of time. This consolidation of the backfill may leave a crown space between the top of the backfill and the top of the tunnel. The crown space may lead to extra flow in the repository and provide additional transport pathways for particles. It is noted that in reality a crown space is considered unlikely or even impossible to develop with a swelling backfill. However, a variant considers a case with a crown space included.

Repository construction can cause local damage in the surrounding rock, known as an excavation damaged zone (EDZ). The hydrogeological base case represents the EDZ as a continuous layer below all deposition, main and transport tunnels and shafts (shafts are represented as equivalent fractures, and the EDZ as fractures intersecting and orthogonal to these) with a thickness of 0.3 m and a transmissivity of $1.0 \cdot 10^{-8}$ m$^2$/s, consistent with the design premise /SKB 2010e/. However, it is considered justified to consider how transmissive an EDZ would need to be in order to significantly affect performance measures, hence two variants are considered with higher transmissivity values of $1.0 \cdot 10^{-7}$ m$^2$/s and $1.0 \cdot 10^{-6}$ m$^2$/s, respectively. Evidence suggests that repository construction would lead to no continuous EDZ developing at all /SKB 2011, Section 10.2.2/, and so a third variant is considered with no EDZ present.

### 5.3.6 Effect of boreholes

The purpose of this variant is to assess the effect on groundwater flow and performance measures of the presence of one or more hypothetical boreholes. The boreholes represent boreholes drilled during characterisation or construction of the repository; the sealing properties of the boreholes are assumed completely degraded. Such boreholes may also represent the result of Future Human Actions (FHA).

### 5.3.7 Glacial conditions

Boundary conditions from the glacial model described in Section 6 are used to assess flow and transport characteristics for cases with the ice sheet front in close proximity to the repository footprint utilising the models derived for use otherwise in the temperate period. The results of this analysis are discussed in conjunction with the presentation of periglacial and glacial simulations of the next chapter.

### 5.3.8 Additional analyses performed

Two additional analyses are performed in order to shed light on some aspects of the model results. These are a sensitivity analysis of the impact of the assumed transmissivity-aperture relationship on calculated results, and an assessment of the groundwater circulation and flow path characteristics.

## 5.4 Results

### 5.4.1 Saturation

The time scale of saturation is estimated using the DarcyTools code based on the methodology described above and detailed in /Svensson and Follin 2010/. The inflow is calculated separately for each excavation and operational phase; for an explanation of the different phases, see Chapter 4.

In Figure 5-1, the inflow is shown as a function of time. A rapid initial inflow is followed by an asymptotic regime where the inflow gradually decreases. Based on the calculations, /Svensson and Follin 2010/ conclude that it will take several hundred years for the repository to reach full saturation. The temperate period is on the order of 10,000 years, hence this initial period of unsaturated conditions covers only a small part of it, and the assumption of saturated conditions within the rest of the simulations of the temperate period can be defended.

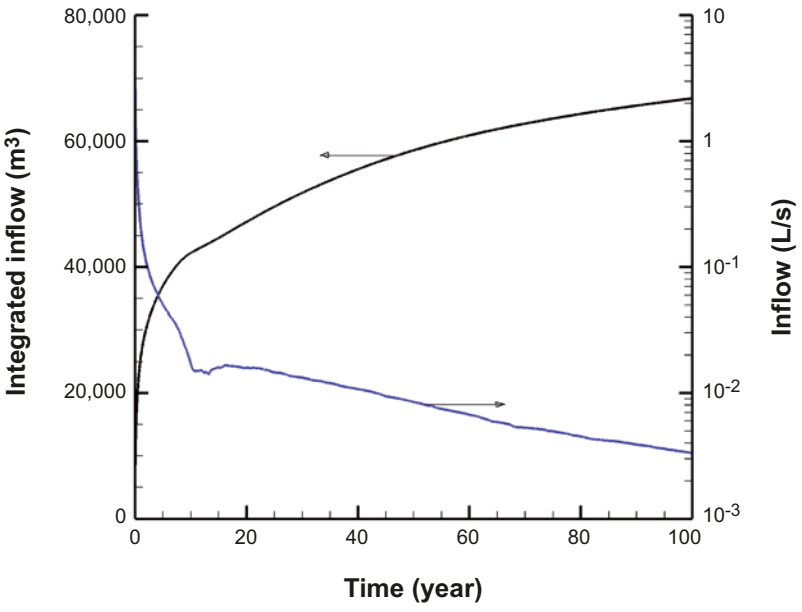


***Figure 5-1.*** *Inflow rate [L/s] and cumulate inflow [$m^3$] for stage A (see Section 4.2 for a definition of the different stages). The perturbation at about 10–15 years is a model effect caused by the change in specific storage when the unsaturated backfill becomes saturated.*

In order to study differences in saturation characteristics between different parts of the repository, an analysis is made where slow, intermediate and fast tunnel sections, in terms of saturation, are identified based on the pressure distribution after 100 days of saturation. The result is shown in Figure 5-2 in terms of integrated inflow per meter of tunnel. Approximately 4.1 $m^3/m$ of water is needed to fully saturate the void space of the backfill in the tunnels. The results indicate that after 50 years the fast tunnel has reached 3.7 $m^3/m$, whereas the slow tunnel only has reached 2.9 $m^3/m$. The intermediate tunnel has reached 3.1 $m^3/m$. The transient evolution is quite different for slow and fast tunnels, but since the integrated inflow curves converge, the time to reach full saturation coincides for all tunnels. To reach full saturation takes approximately 150 years for all tunnels (not shown in figure).

The water that saturates the backfilled repository structures originates predominantly from the top of the model domain. The reasoning behind this conclusion is twofold. First, the only available free source of water in the model is the recharge at the surface. This enters the model either as net precipitation (meteoric water with an altered chemical composition) or as water from the Baltic Sea (sea water with an altered chemical composition). Second, the permeability of the bedrock is much lower below repository depth than above. In principle, the contrast in kinematic porosity between the backfill and the bedrock suggests that the entire volume of mobile water in the bedrock above repository depth equals the volume of water required to reach full saturation.

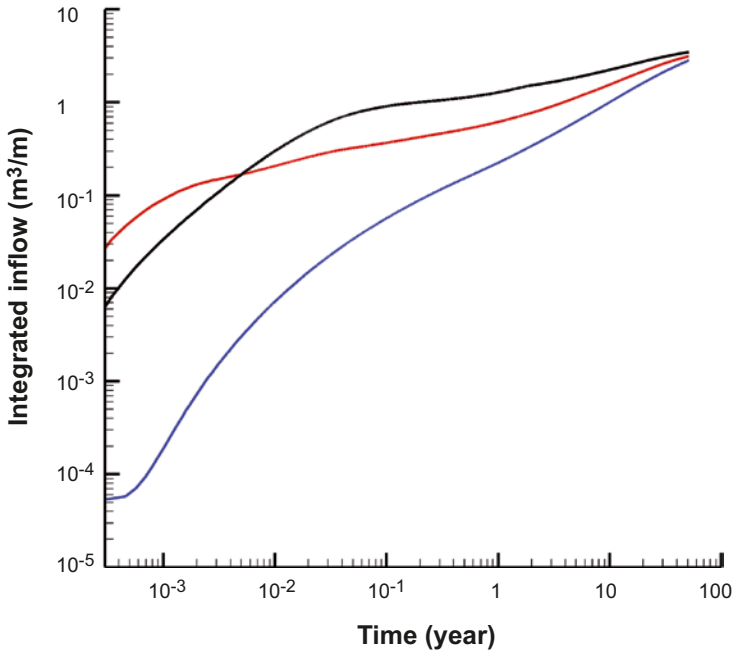


***Figure 5-2.*** *Integrated inflow [$m^3/m$] for three different tunnel sections with different saturation rates; black = fast, red = intermediate, and blue = slow.*

### 5.4.2 Hydrogeochemical evolution

The evolution of groundwater flow and hydrogeochemistry for the temperate period from 8000 BC to 12,000 AD is modelled. The initial condition is expressed in terms of reference waters which are assumed to contribute to the groundwater composition in the Forsmark area. The chosen initial condition is Deep Saline Water at depth, with the less saline groundwater above being a mixture of Deep Saline Water, Old Meteoric Waters and Glacial Melt Water. Figure 5-3 shows the location of a slice through the regional-scale model domain; in Figure 5-4, the distribution of Meteoric Water at 2000 AD and 9000 AD is shown for this vertical slice. The important deformation zones ZFMA2 and ZFMENE0060 in the region of the repository and the repository structures are also shown for context in Figure 5-3.

In Figure 5-4, the distribution of concentrations at 2000 AD is comparable to that found in the site-descriptive model, with concentrations (maximum concentration fraction of over 0.9) highest at the very top of the slice. The depth of the highest concentrations increases steadily from 2000 AD through to 9000 AD until it reaches the full depth of the model. Thus, it can be concluded that the domain over time will be subject to more dilute water conditions also at depth. This will have implications on repository performance as discussed below. In Figure 5-5, the corresponding plots for the Littorina water is shown; here it is seen that the Littorina water that initially occupies the domain is flushed out over time.

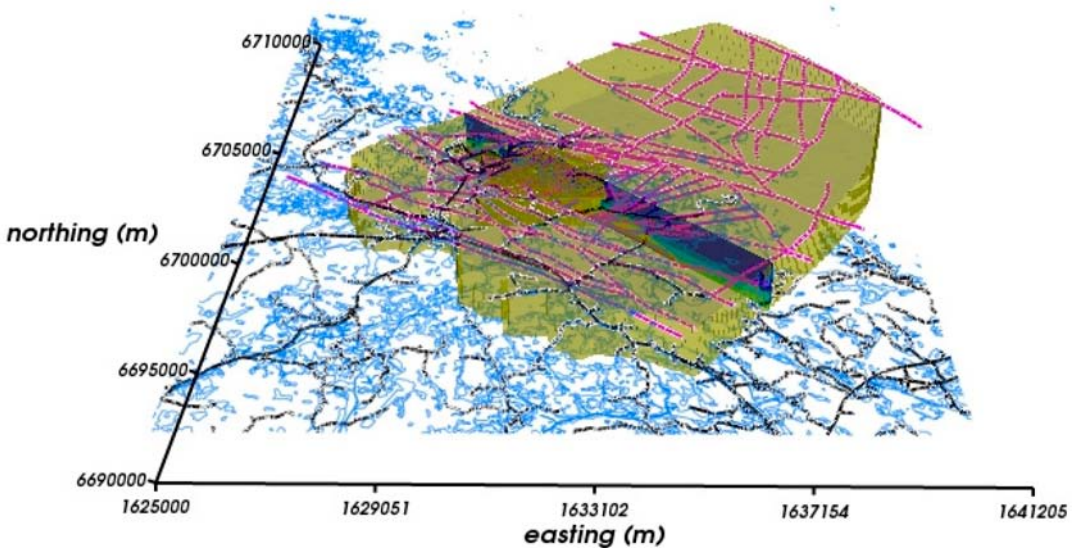


***Figure 5-3.*** *The location of the north-west to south-east vertical slice used in the fractional distributions plots below.*

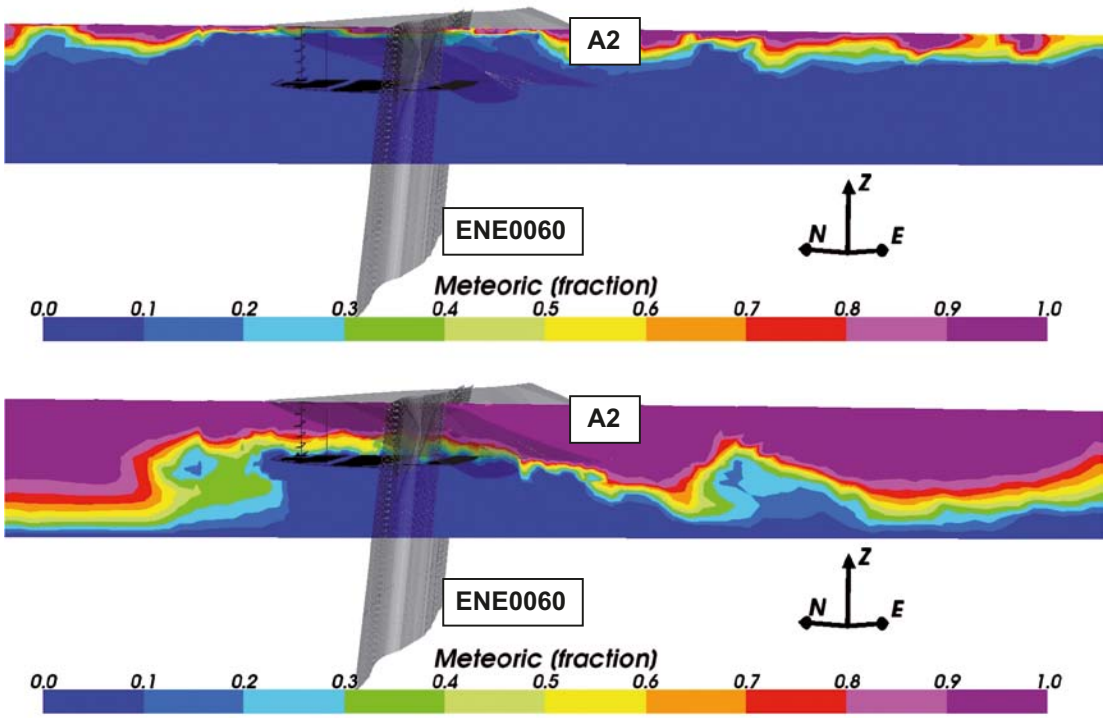


***Figure 5-4.*** *Vertical slices (north-west to south-east) of the distributions of mass fractions of the Meteoric water for the regional-scale model. From the top: Distributions at 2000 AD and 9000 AD. The model domain is 1,200 m deep.*

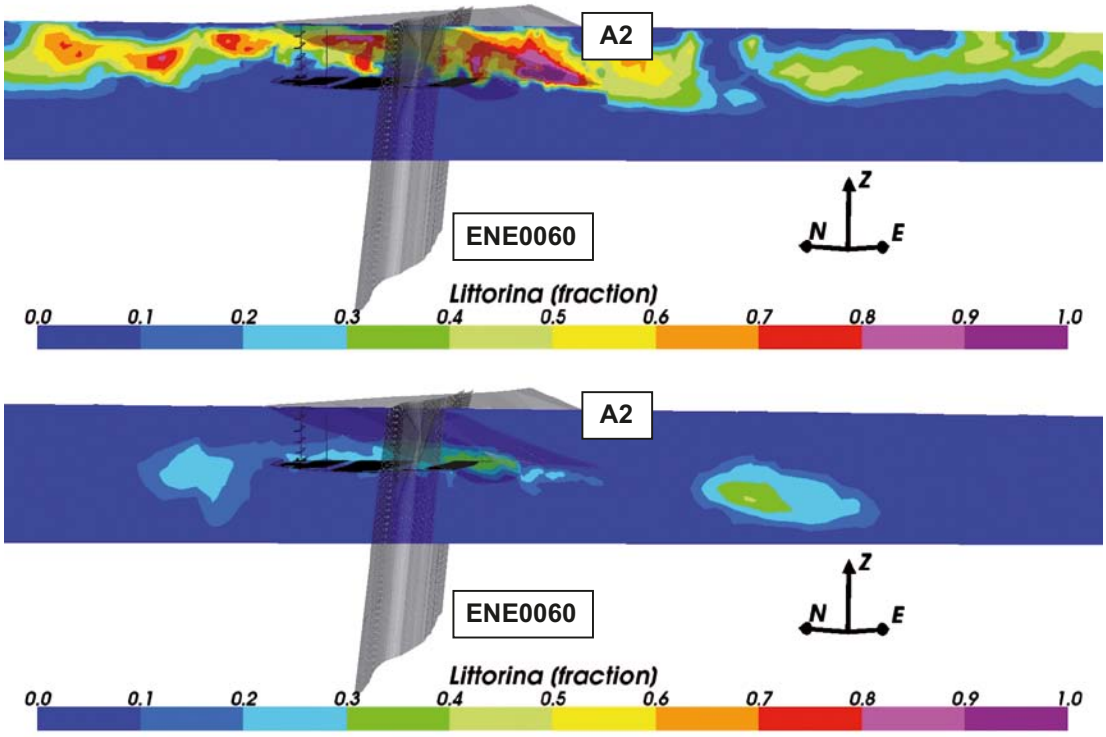


***Figure 5-5.*** *Vertical slices (north-west to south-east) of the fractional distributions of the Littorina water for the regional-scale model. From the top: Distributions at 2000 AD and 9000 AD. The depth of the model depth is 1,200 m.*

### 5.4.3 Discharge locations in the biosphere

Figure 5-6 shows the discharge point evolution in time. Particles are released in steady-state velocity fields at times from 0 AD to 12,000 AD in the site-scale model. The repository is included in a simplified manner expressed as equivalent fractures in the site-scale model. The discharge points of particles released at earlier times (0 AD, 1000 AD and 2000 AD) are located onshore near the repository and show a very slight migration toward the 2000 AD shoreline with release time. The near-future discharge locations (3000 AD, 4000 AD and 5000 AD) follow the retreating shoreline. The far-future discharge locations (6000 AD through to 12,000 AD) congregate on the north-eastern model boundary. This may be interpreted such that the model domain should be extended further to the northeast. However, the boundary is consistent with the boundary of the SDM model domain and corresponds to a bathymetric depression in the Baltic Sea. Thus, extending the model domain would not necessarily change the discharge location pattern. However, as discussed in Section 13.2.2 of the SR-Site Main report, a minor change in discharge locations would not affect the derived biosphere objects for use in subsequent dose calculations. It is also noted that discharge locations do not vary significantly between realisations as shown in /Joyce et al. 2010/ when multiple realisations are studied in the repository-scale model. Hence, it can be concuded that the discharge locations are governed mainly by the deterministic deformation zones and the topography.

In /Joyce et al. 2010/, it is shown that the Darcy flux at the starting locations, and properties along the flow paths (travel time and flow-related transport resistance) are essentially unchanged between different release times. A slight trend may be observed indicating that the results divide into two groups, those before 2000 AD and those after (i.e. when the site is under the sea and afterwards). These later times generally have higher Darcy fluxes and slightly lower flow-related transport resistances. However, from 3000 AD there is again a small increase in flow-related transport resistance with time; i.e. within the second group there is a slight trend towards higher values with time. It is noted that even with the trend, the flow-related transport resistance values of the second group (i.e. after 2000 AD) are still lower than the values of the first group (i.e. prior to 2000 AD).

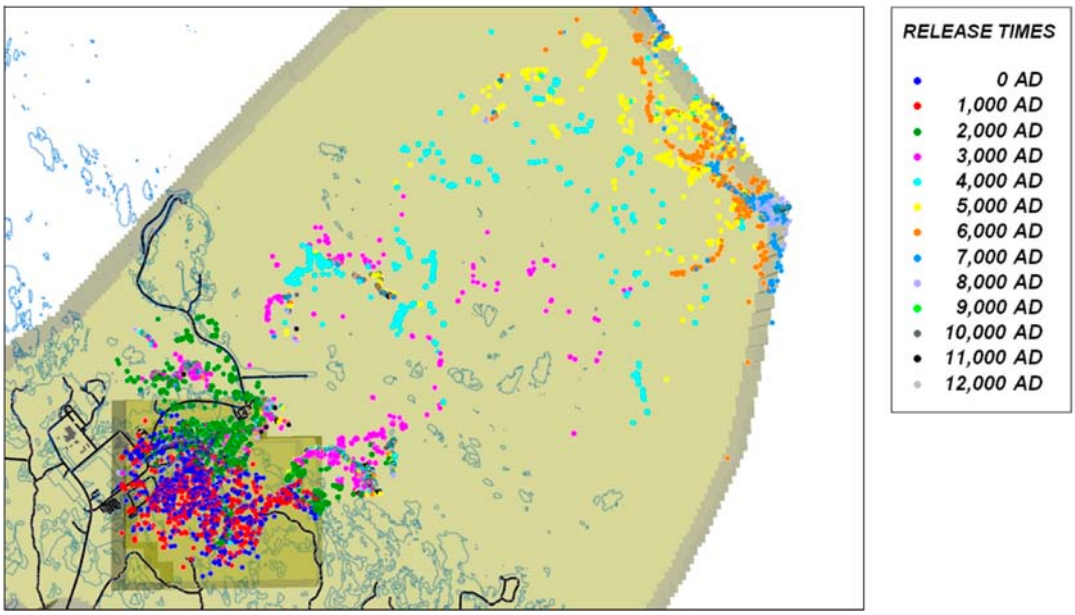


***Figure 5-6.*** *Discharge locations for particles (Q2 path) successfully reaching the top boundary of the site-scale hydrogeological base case model (89%–97%) for releases every 1,000 years from 0 AD to 12,000 AD. The model domain is shown in beige.*

### 5.4.4 Performance measures

The performance measures are calculated for four steady-state velocity fields at different times; these are 2000 AD, 3000 AD, 5000 AD and 9000 AD. A multitude of results are available in /Joyce et al. 2010/ for the multiple times and for multiple realisations representing the hydrogeological base case presented. In addition, the effect of branching along flow paths is assessed in a variant calculation by the use of multiple particles per start position. Furthermore, results can be analysed in terms of spatial variability among different particle start locations within the same realisation. Here, only a small subset of the results is presented for illustrative purposes.

In Figure 5-7 the flow-related transport resistance ($F$) is shown at the starting location for the released particles; i.e. the final $F$ value at the end of the path is shown at the start location. It is seen that both low and high (in a relative sense) values are found distributed over the repository. No clear trend of more or less favourable conditions within the repository is readily discerned; i.e. no part of the repository is found to be clearly associated with the lower or higher values of the calculated flow-related transport resistance.

In Figure 5-8 a scatter plot between Darcy flux ($q$) and flow-related transport resistance ($F$) for those particles that reach the surface (24% of all deposition hole locations) is shown. A negative correlation between the two entities is observed, even if a spread exists. Specifically, the deposition hole positions with the highest Darcy fluxes are associated with paths with low $F$ values relative to the positions with low Darcy fluxes. This pattern is valid for all release times.

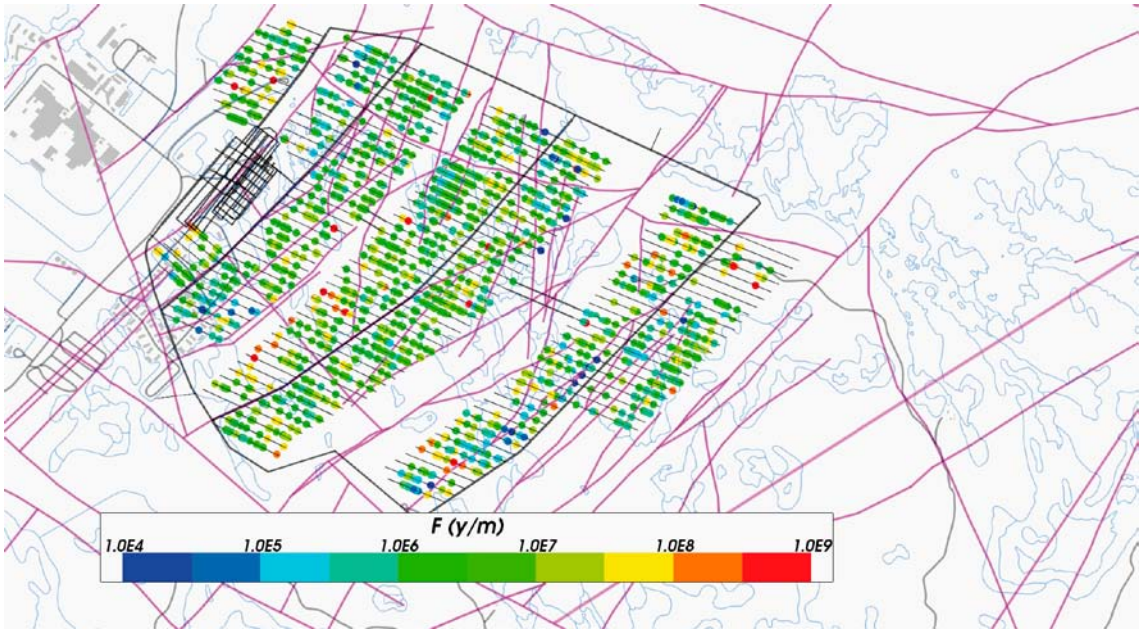


***Figure 5-7.*** *Starting locations coloured by $\log_{10}(F)$ for particles released at 2000 AD (Q1 path) and successfully reaching the top boundary (24%). The HCD model at z= –470 m (purple), roads and buildings (black) and shoreline (blue) are also shown.*

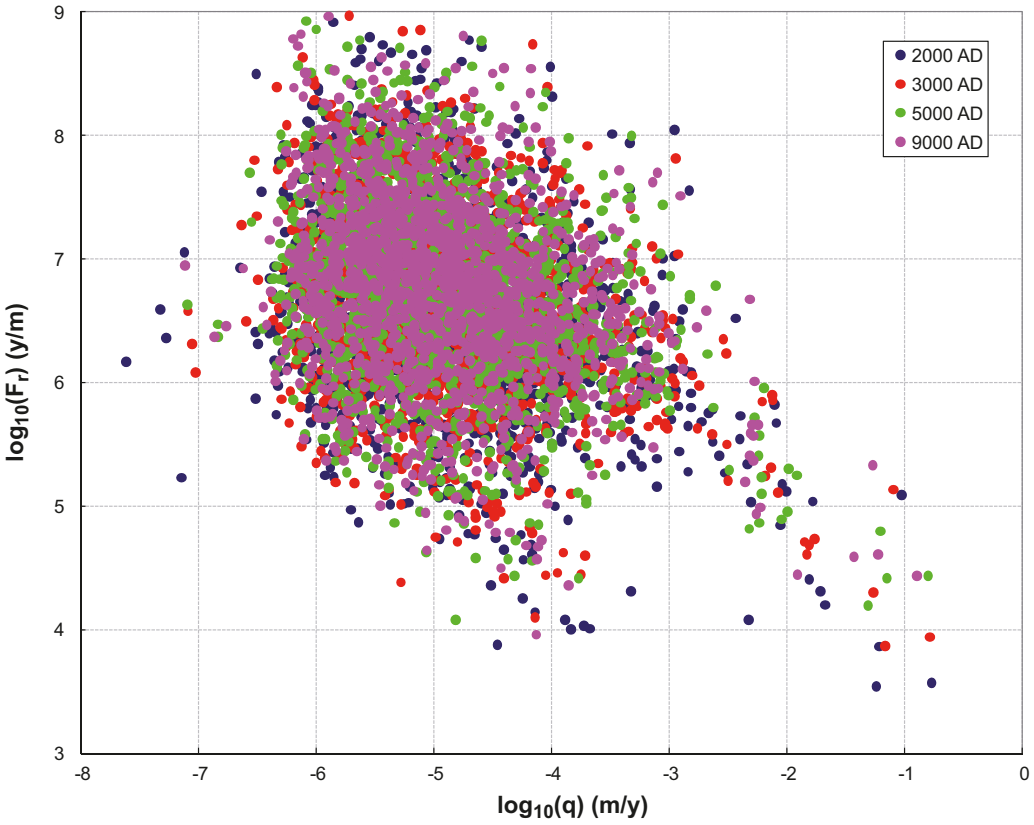


***Figure 5-8.*** *Scatter plot of flow-related transport resistance (F) versus Darcy flux (q) for Q1 particles released at 2000 AD, 3000 AD, 5000 AD and 9000 AD that successfully reach the top boundary (24%).*

As indicated above when assessing discharge locations, some flow paths tend to become longer as the shoreline is displaced. This generally implies longer travel times and larger flow-related transport resistance values with time as indicated by Figure 5-9 below.

The definition of the flow-related transport resistance ($F$) is straight forward in a discrete model; in a continuum model, additional assumptions need to be made. Thus it is of interest to assess how much contribution to the overall $F$ is accumulated in the continuum representation (ECPM+CPM) of the domain. Figure 5-9 shows that for the later release times, the $F$ values are shifted to somewhat higher values when the continuum representation is included. This is particularly true for the later times (5000 AD and 9000 AD). Thus, the results indicate that during the earlier times most discharge in fact takes place within the DFN representation of the model. For the subsequent radionuclide transport calculations, only the discrete (DFN) contribution will be included.

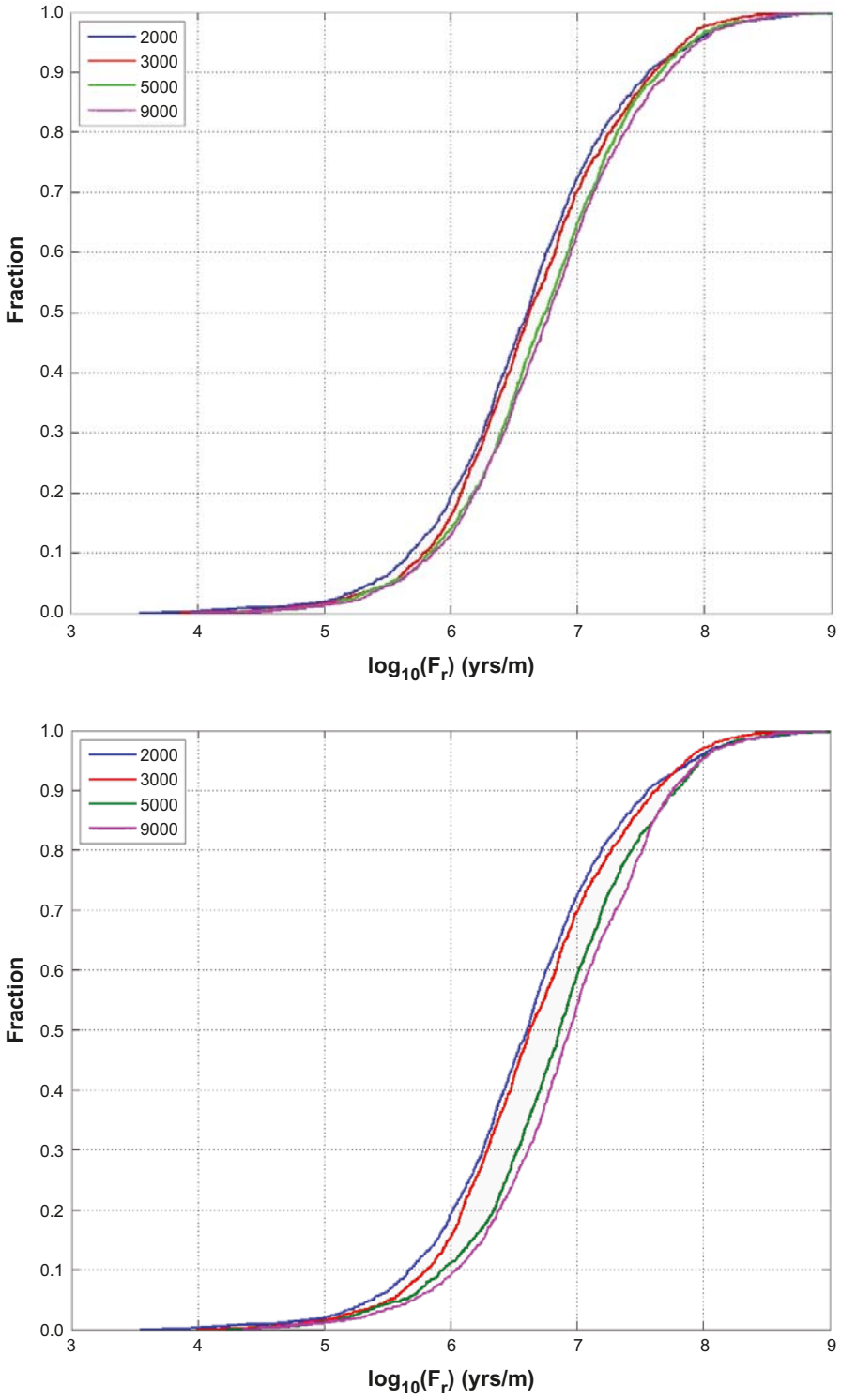


***Figure 5-9.*** *Cumulative distribution function plots of flow-related transport resistance (F) for the Q1 path in the hydrogeological base case for the particles successfully reaching the model top boundary (24%) released at 2000 AD, 3000 AD, 5000 AD and 9000 AD. The top plot shows the contribution from the DFN part of the model only, whereas the bottom figure includes the contribution also from the ECPM and CPM parts.*

In SR-Site, the Extended Full Perimeter Criterion (EFPC) is adopted when consequences are evaluated, see Section 3.2. In Figure 5-10, the effect of applying different criteria is illustrated for the Darcy flux in fractures intersecting deposition holes. The figure illustrates that roughly 70 per cent of deposition hole locations do not have a flowing fracture intersecting the deposition hole. When the "FPC or EFPC" criterion is applied, only about 20 per cent of deposition hole positions intersected by a flowing fracture remain; i.e. the criterion lead to rejection of roughly 10 per cent of the deposition holes. Also seen in the figure is that the remaining distribution is shifted towards lower Darcy flux values. Hence, the application of the criterion will have positive consequences for assessment calculations.

In the hydrogeological base case realisation, all deformation zones are assumed to have only a depth trend of transmissivity, but otherwise constant properties. However, the discrete fracture network is stochastic. In additional realisations, also the deformation zone properties are assumed to be characterised by spatial variability (heterogeneity). In Figure 5-11, bar and whisker plots of the flow-related transport resistance ($F$) for the Q3 path are shown for the hydrogeological base case realisation and the additional ten realisations (the Q3 path is exemplified because it exists for all deposition hole positions, even those without a Q1 path). It is seen that the median and upper percentiles are quite stable between realisations, whereas some realisations, e.g., r1, r5 and r9, are characterised by a lower tail, i.e. a lower 5$^{th}$ percentile. Corresponding results are observed for the advective travel time; however, the Darcy flux is more stable between realisations. Also, for all performance measures, the Q1 path is characterised by less variability between realisations than the Q2 and Q3 paths, respectively. The reason is that performance measures for migration through the rock for the Q1 path necessarily include a section of path through the fractures surrounding each deposition hole, which might be of low transmissivity, whereas for Q2 and Q3 the EDZ and tunnels provide a by-pass to large stochastic fractures or deformation zones with relatively large flows. Hence, performance measures for the Q2 and Q3 paths are more sensitive to the locations and transmissivities of the scarce features that vary between individual realisations.

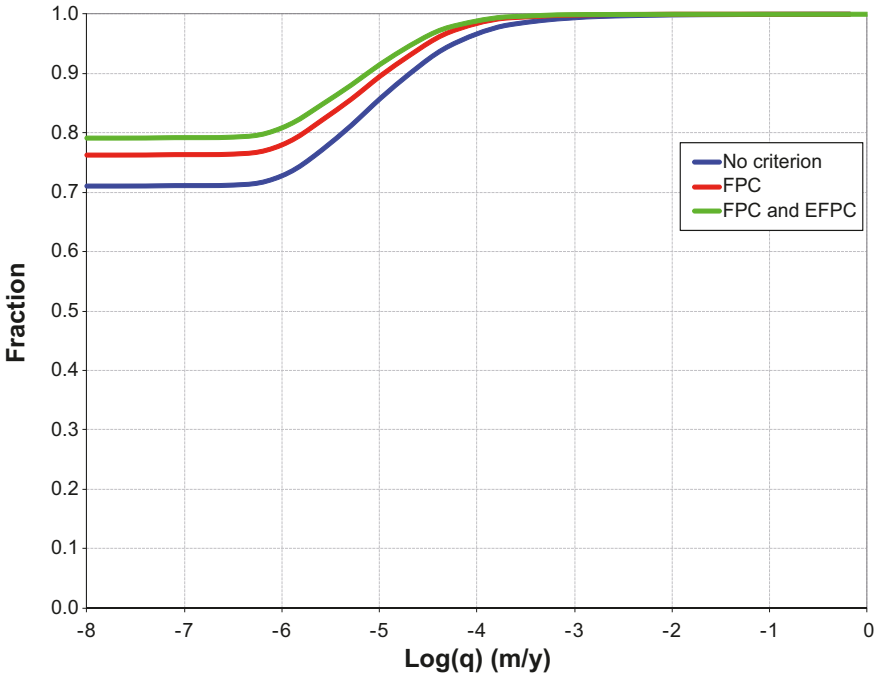


***Figure 5-10.*** *Cumulative distribution plot of Darcy flux (q) for the Q1 path at 2000 AD based on all deposition hole locations and applying different deposition hole rejection criteria. "FPC and EFPC" in the figure legend denotes that the "FPC or EFPC" criterion is applied.*

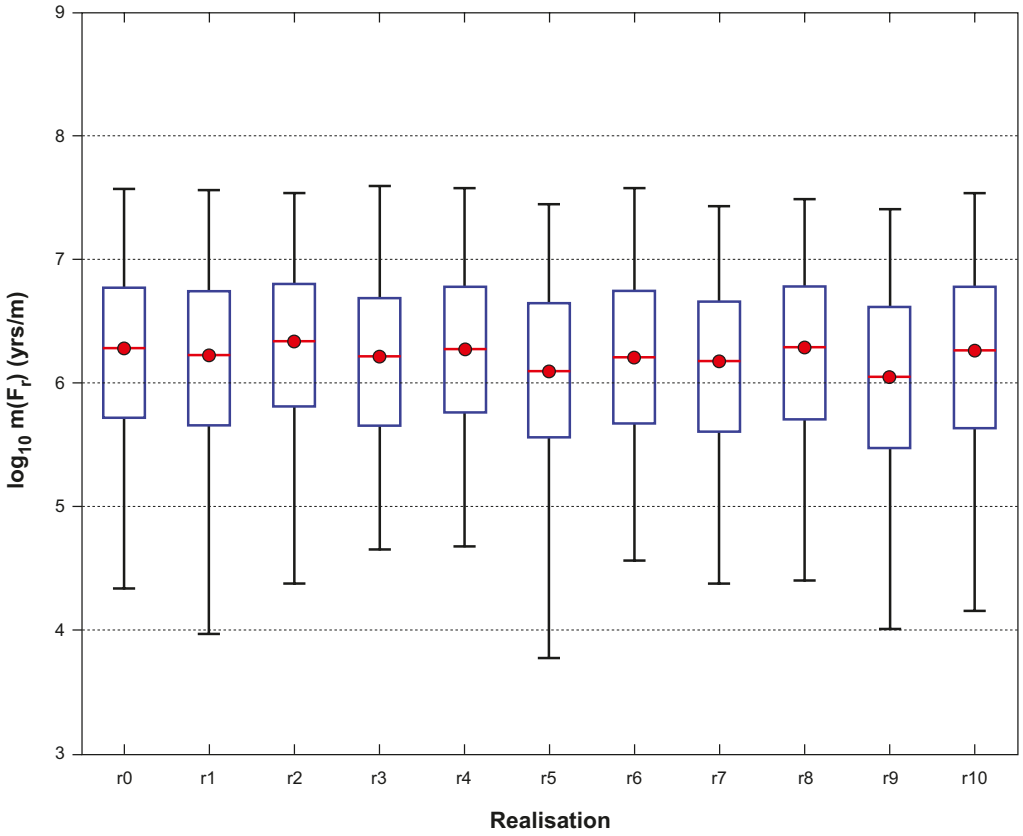


***Figure 5-11.*** *Bar and whisker plots of flow-related transport resistance (F) for the Q3 path in the hydro-geological base case realisation (r0) and 10 stochastic realisations of the HCD and HRD (r1 to r10) for the particles successfully reaching the model top boundary released at 2000 AD. The statistical measures are the median (red), 25$^{th}$ and 75$^{th}$ percentile (blue bar) and the 5$^{th}$ and 95$^{th}$ percentile (black "whiskers").*

In order to assess the effect of branching along the flow paths on the advective travel time and flow-related transport resistance, a variant with multiple particles (ten) released per start point in the particle tracking has been analysed. Only the 25 per cent of start points with highest Darcy flux are used in the comparison. The ten particles can choose different flow paths due to a stochastic choice (weighted by flow rate) at each fracture intersection. The results indicate that the branching has negligible effects on the ensemble statistics of the analysed performance measures. This suggests that the large number of starting locations provide a sufficient sampling of the available flow pathways or there is very little dispersion of particles along their paths, i.e. the paths may be dominated by relatively few flow channels. However, if only a single deposition hole position is considered, the branching may have some effects. This has not been further addressed in /Joyce et al. 2010/ since it can be assumed conservative to neglect spreading along individual flow paths in the assessment calculations.

### 5.4.5 Penetration of dilute water

In principle, the future groundwater chemistry is provided by the regional-scale groundwater flow simulation reported above. However, the regional-scale simulation is terminated at 12,000 AD and, furthermore, has a fairly coarse discretisation which does not allow an assessment of the groundwater chemistry evolution on a deposition hole scale. Thus, an alternative assessment of the evolution of the groundwater chemistry, and specifically the potential for penetration of dilute water, is made since dilute groundwater may cause erosion of the buffer and the backfill.

In order to assess the potential for penetration of dilute water, a simplified approach is adopted. An injection of meteoric water along those recharge pathways that originate close to the surface within the regional-scale model is considered; it is assumed that the infiltrating water has zero salinity; note that this is a pessimistic assumption as discussed in Section 2.5. Also, in this simplified calculation, it is assumed that the matrix and fracture water salinity is in equilibrium at the start of the simulations; the relevance of this assumption is also discussed in Section 2.5. The flow field and recharge flow paths of year 2000 AD are used. Along the flow paths, the only mitigating process considered is the out diffusion of matrix water affecting the penetration of the meteoric water front. For each deposition hole, the time required for the groundwater salinity to fall below ten per cent of the initial water concentration is calculated. Figure 5-12 shows the distribution of these times for all deposition hole positions. The present-day salinity at the site is approximately 10 g/L; ten per cent of the initial concentration thus corresponds to 1 g/L, which is well above the criterion of 0.3 g/L which is assumed to represent dilute conditions with potential buffer erosion problems. The vertical lines represent the assumed approximate duration of the temperate period; i.e. 10,000 year for the base case, and 60,000 years for the Global warming variant. It is observed that slightly more than two per cent of the deposition hole positions experience dilute conditions within the Global warming variant, whereas approximately one per cent experience dilute conditions during the first ten thousand years of the initial temperate period.

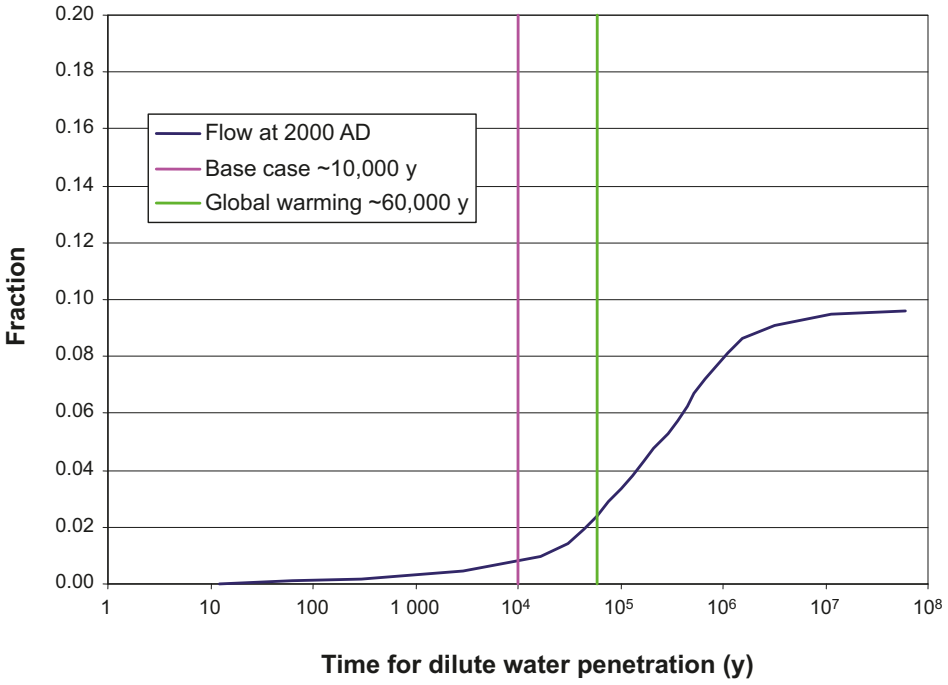


***Figure 5-12.*** *Temporal distribution for all deposition holes to obtain ten per cent of the initial water concentration. The green line shows that slightly more than two per cent of the deposition holes experience dilute conditions within the Global warming variant. The purple line shows that approximately one per cent of the deposition holes experience dilute conditions during the first ten thousand years of the initial temperate period.*

It is noted that the quantification above is a likely conservative assessment of the salinity evolution. First, a steady-state velocity field is chosen as representative for the full time duration. In reality, advective transport processes may imply transport of salt from greater depths to the more shallow parts of the system. Second, in reality the dilute water may be influenced by other mitigating processes than out-diffusion of salt only. For example, reactions with fracture surface minerals may change the water composition /Salas et al. 2010/. It is also noted that canister deposition hole positions that are poor for dilution do not necessarily correlate with the positions with low flow-related transport resistance for discharge.

### 5.4.6 EDZ and crown space in deposition tunnels

There is ample evidence (SR-Site Main report Section 10.2.2) that a potential excavation damaged zone (EDZ) formed during excavation will be kept below the maximum allowed transmissivity as set out by the design premises. Furthermore, empirical data suggest that a continuous EDZ will not develop at all /SKB 2011, Section 10.2.2/. Given that the occurrence of the EDZ currently can only be assessed by indirect measurements, an EDZ according to the design premises, i.e. with an axial transmissivity of $10^{-8}$ m$^2$/s, is used as a basic assumption within SR-Site. However, it is also explored in SR-Site how transmissive an EDZ needs to be in order to significantly impact other safety functions. In addition, the impact of no axially continuous EDZ at all is also examined.

In the hydrogeological base case model, a continuous EDZ is implemented in all tunnels (deposition, main, transport and access tunnels and shafts) under the tunnel floor. The EDZ has a transmissivity value of $T=1\cdot10^{-8}$ m$^2$/s and a thickness of 0.3 m. In order to assess the sensitivity in performance measures on tunnel properties, four alternative cases are analysed. Two of these have higher EDZ transmissivities ($T=1\cdot10^{-7}$ m$^2$/s and $T=1\cdot10^{-6}$ m$^2$/s, respectively), one case has no EDZ, and the final case has the base case EDZ properties, but is combined with a crown space under the tunnel ceiling implemented for the deposition and main tunnels. The crown space results from a consolidation of the backfill material. In the model, the crown space is implemented as a 0.1 m thick zone with a high conductivity value ($K=1\cdot10^{-3}$ m/s) and a porosity equal to unity.

Darcy flux for the Q2 path is shown in Figure 5-13. Since the Q2 path corresponds to the EDZ path, no result exists by definition for the case with the EDZ removed. The figure clearly shows, as expected, that an increase in the EDZ transmissivity implies an increase in the associated Darcy flux. The crown space, on the other hand, implies no change in the Darcy flux in the EDZ. The same holds true for the other release paths; i.e. the crown space has a marginal influence on the estimated Darcy fluxes.

Corresponding results for the flow-related transport resistance for the Q3 path are shown in Figure 5-14. The case with no EDZ provides the most favourable conditions. The reason is that with no EDZ present, particles tend to travel more in the fractured rock, and hence accumulate their flow-related transport resistance ($F$) values (no retention is assumed in the EDZ). Conversely, with an increased EDZ transmissivity or a crown space, less favourable conditions prevail and the flow-related transport resistance distributions are shifted towards lower values. Corresponding results of the flow-related transport resistance are observed for the other release paths (not shown here), but the differences are less dramatic than for the Q3 path.

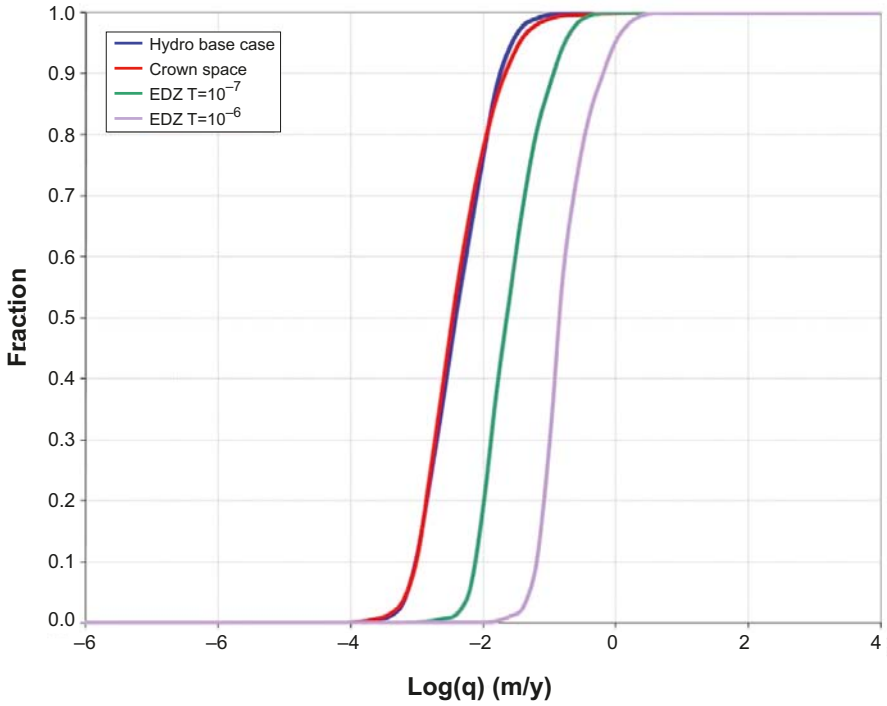


***Figure 5-13.*** *Cumulative distribution function plot of the Darcy flux (q) for the Q2 path for the hydrogeological base case model, the crown space model, the EDZ T=1·10⁻⁷ m²/s case, and the EDZ T=1·10⁻⁶ m²/s case for the particles successfully reaching the model (82–84%) top boundary, released at 2000 AD. (Modified after Figure 6-32 in /Joyce et al. 2010/.)*

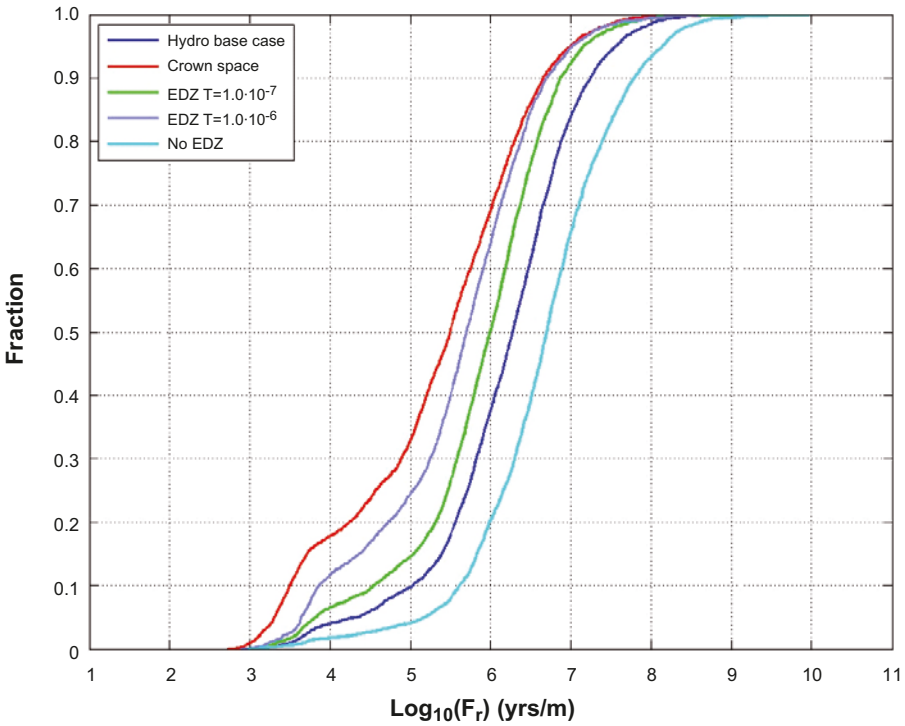


***Figure 5-14.*** *Cumulative distribution function plot of flow-related transport resistance (F) for the Q3 path for the hydrogeological base case model, the crown space model, the EDZ T=1·10⁻⁷ m²/s model, the EDZ T=1·10⁻⁶ m²/s model and the no EDZ model for particles successfully reaching the model top boundary (68% hydrogeological base case, 81% crown space, 64% EDZ T=1·10⁻⁷, 53% EDZ T=1·10⁻⁶, 52% no EDZ).*

### 5.4.7 SDM-Site related model variants

A number of variants related to site characteristics and motivated in the SDM-Site report /Follin 2008/ are judged necessary to be assessed also within SR-Site. These are briefly summarised below.

#### *Alternative DFN transmissivity-size relationships*

The hydrogeological DFN modelling for SDM-Site /Follin et al. 2007/ treated three kinds of transmissivity-size correlation models; fully correlated, uncorrelated and semi-correlated. It was found that the fully correlated and semi-correlated models reproduced the numbers and shape of the distributions of measured specific capacities with the Posiva Flow Log reasonably well, giving a wedge shaped distribution characteristic of having a transmissivity-size correlation, whereas the simulated distribution for the uncorrelated model was flatter and less representative. For this reason, the hydrogeological base case in SR-Site is based on the semi-correlated relationship between transmissivity and size as propagated by SDM-Site. However, to quantify uncertainties, the alternative relationships, i.e. the fully correlated and the uncorrelated models, are also investigated in SR-Site as variant cases.

Besides the recommendation of SDM-Site, there are two other motivations for using a semi-correlated relationship between fracture transmissivity and fracture size as the basis for the hydrogeological base case in SR-Site. First, large (long) structures tend to be thicker than small (short) structures and hence contain more fractures which are likely to form connections. Second, for the realistic case where fracture surfaces are rough, then fractures of larger area are more likely to contain connected openings. Together, these relationships suggest some kind of positive correlation between fracture transmissivity and fracture size. For instance, large deformation zones are often found to be thicker and more transmissive than small and thin deformation zones.

The particle tracking results reported by /Joyce et al. 2010/ indicate that the performance measures (Darcy flux and the flow-related transport resistance) are dependent on the chosen transmissivity-size relationship with up to about half an order of magnitude variation between variants. Results for the Darcy flux are shown in Figure 5-15.

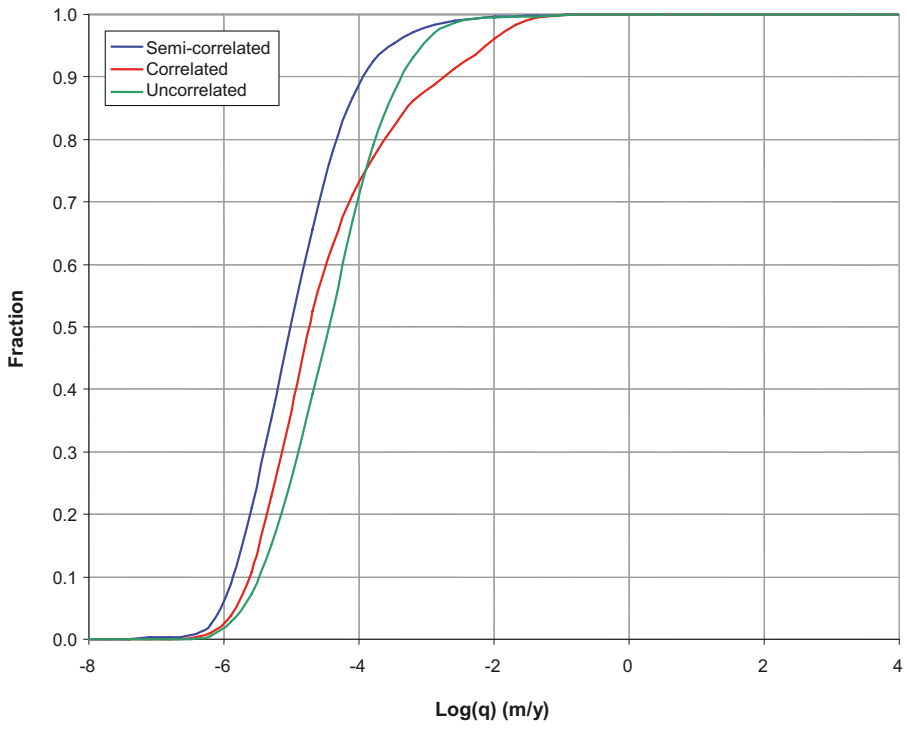


***Figure 5-15.*** *Cumulative distribution plot of the Darcy flux (q) for the correlated and uncorrelated transmissivity-size relationships compared to the hydrogeological base case (semi-correlated) for the Q1 release path at 2000 AD. (Modified after Figure 6-28 in /Joyce et al. 2010/.) The cumulative distributions are based on the Q1 particles successfully reaching the model top boundary (24% semi-correlated, 32% correlated, 27% uncorrelated).*

It is noted in Figure 5-15 that the semi-correlated model provides the lowest Darcy fluxes at the deposition hole positions. This is explained by the fact that the uncorrelated model tends to have higher transmissivity values for small fractures than the other models, which have some correlation between size and transmissivity by definition, and so more flow percolates down to these small fractures. Furthermore, most of the fractures intersecting deposition holes are small due to the fact that there are more of them. This implies that for most deposition holes the uncorrelated model gives the highest Darcy flux values, which is reflected by the higher median value in Figure 5-15. However, some holes are intersected by larger fractures. Where these occur, the highest transmissivity values are obtained in the correlated model. Thus, for the correlated model, high Darcy flux values can be observed at a number of discrete locations, and a high end tail results. The Darcy flux at the deposition hole positions for the correlated and uncorrelated models are shown in Figure 5-16. It is observed that the correlated case has higher Darcy flux values at a number of discrete locations.

It is not obvious why the median value of the Darcy flux is higher in the correlated than in the semi-correlated model. However, a number of factors may contribute such as the small dataset with which to constrain the DFN model at depth, differences in calibration and also the fact that the different models constitute different realisations of the network. Thus, one may conclude that the three models reflect the uncertainty in the conceptual model and in the interpretation of data used in the calibration.

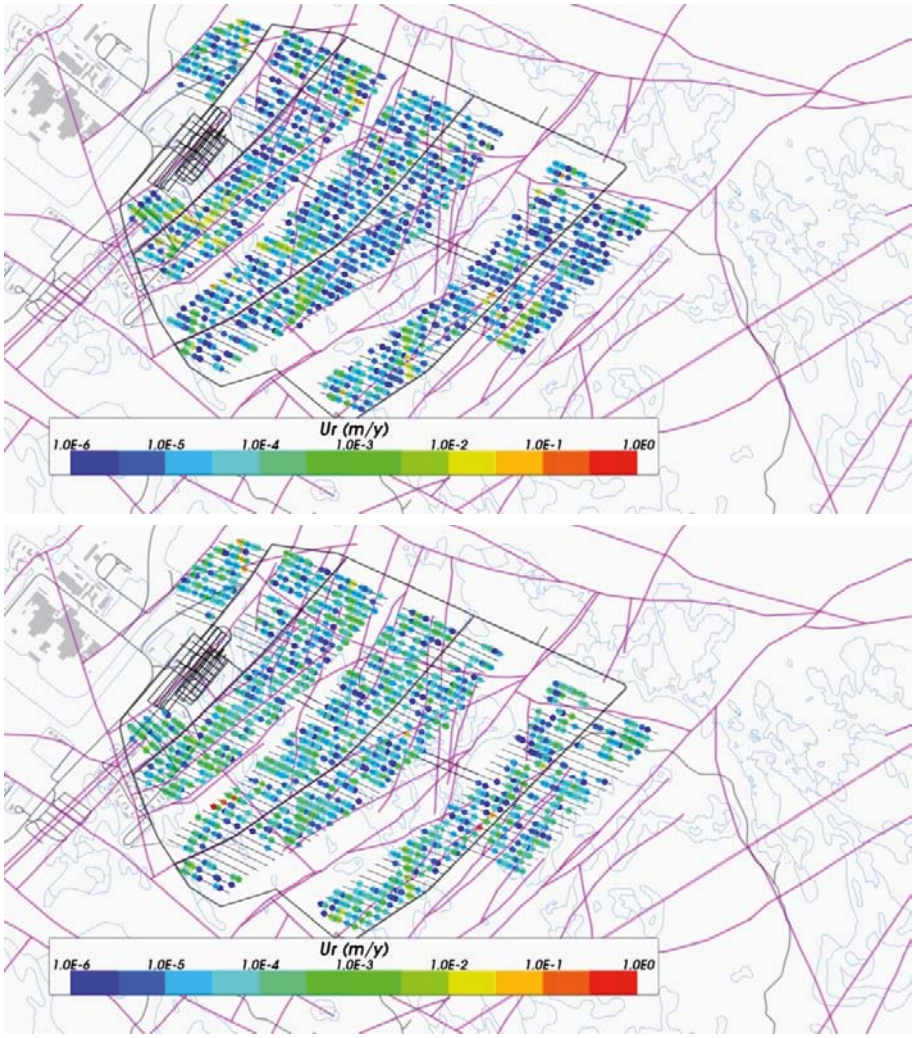


***Figure 5-16.*** *Starting locations coloured by $\log_{10}(q)$ for Q1 particles successfully released at 2000 AD. Top: correlated case (32%) and Bottom: uncorrelated case (27%). The HCD model at z= –470 m (purple), roads and buildings (black) and shoreline (blue) are also shown.*

### *Possible deformation zones*

As a variant case for SR-Site, four possible deformation zones (PDZ) identified in SDM-Site are added to the HCD model and treated in the same way as the deterministically modelled deformation zones. Three realisations of stochastic properties are generated for the possible deformation zones to represent lateral heterogeneity. These are combined with the corresponding realisations of the HCD and HRD fractures generated for the hydrogeological base case. Figure 5-17 shows the possible deformation zones relative to the repository structures. Some of them intersect the repository structures and may provide potential flow pathways.

The simulated discharge locations for the three PDZ realisations show little variation between realisations and are similar to those for the hydrogeological base case. The modelled possible deformation zones have little effect also on the performance measures.

### *Unmodified vertical hydraulic conductivity*

During the calibration and confirmatory testing of the SDM-Site base model simulation, the vertical hydraulic conductivity of the ECPM representation of the HRD above an elevation of –400 m was reduced by a factor of ten in order to provide a better fit to chemistry and interference test data. This modification is also used for the ECPM representation in the regional and site-scale hydrogeological base case models for SR-Site. However, no corresponding change is made to the properties of the fractures in the DFN representation in the site-scale model, leading to a possible inconsistency in flows between the DFN and ECPM in the site-scale model. Therefore, as a variant case for SR-Site, the modification of the vertical hydraulic conductivity of the ECPM representation used in the regional and site-scale models is removed.

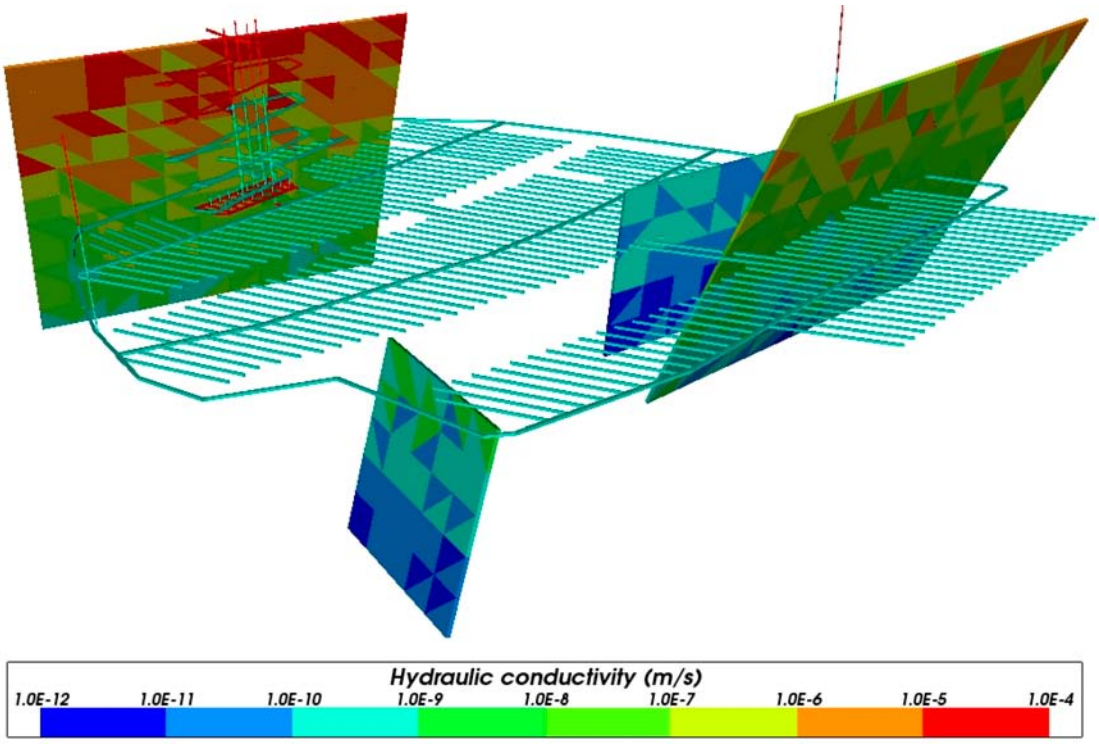


***Figure 5-17.*** *Realisation 1 of the possible deformation zones in relation to the repository structures.*

The simulated discharge locations for the unmodified vertical hydraulic conductivity variant case are similar to those for the hydrogeological base case. The cumulative distribution function plots showing the Darcy flux and the flow-related transport resistance compare well with the corresponding plots for the hydrogeological base case suggesting that the site-scale model is insensitive to the adopted change in the vertical hydraulic conductivity in the ECPM. It is noted that when flow-related transport resistance is compared, only contributions in the explicit DFN parts are accounted for. The DFN parts of the models are identical for the two compared cases; thus, the difference between the unmodified vertical hydraulic conductivity case and the hydrogeological base case is the pressure boundary conditions and densities imported from the regional-scale model.

#### *Extended spatial variability*

The HRD model developed for SDM-Site essentially covers the repository site area. Outside this area, there was little or no information available to support any elaborate description of rock mass properties. Therefore, the bedrock outside the repository area was modelled as a CPM with homogeneous and isotropic properties for each depth zone. The hydrogeological base case in SR-Site is no different in this regard.

As a model variant for SR-Site, the volume treated as a CPM in the hydrogeological base case is replaced by a DFN description of the HRD. The additional DFN data required for this variant case come from the investigations at SFR /Öhman and Follin 2010/. This information is used as the basis for generating regional-scale DFN realisations. By means of up-scaling this provides a full ECPM representation for the regional-scale and site-scale models. In addition, the area of the DFN in the site-scale model is extended northwards beyond the Singö deformation zone, which may provide an important discharge location. Both models retain the existing HSD. However, the repository-scale model is not included in the analysis.

For the extended spatial variability case, more particles seem to exit closer to the repository, which is reasonable given the improved representation of discrete features. However, the cumulative distribution function plots showing the Darcy flux and the flow-related transport resistance do not differ significantly from the corresponding plots for the hydrogeological base case, thus suggesting that the extended spatial variability case has only a moderate effect on performance measures. It is noted that recharge pathways of the extended spatial variability case are used within the hydrogeochemical analyses presented in the SR-Site Main report, Section 10.4.7, when penetration of oxygenated water is studied for glacial conditions.

### 5.4.8 Porosity sensitivity

Advective travel time depends on the transport apertures of the fractures. In the hydrogeological base case model, aperture and transmissivity follow the relationship

$$e_t = 0.5T^{0.5} \qquad (5\text{-}1)$$

where $e_t$ is fracture transport aperture and $T$ is fracture transmissivity. This was also the relationship used for SDM-Site /Follin 2008/, but with the coefficient 0.46 instead of the rounded off value 0.5 used in SR-Site.

The relationship in Equation 5-1 is based on experiences from Äspö Hard Rock Laboratory /Dershowitz et al. 2003/ and hence not a site-specific relationship. Also, it is noted that the relationship strictly provides a hydraulic aperture as explained in /Hjerne et al. 2010/ even though used for transport calculations in SDM-Site and SR-Site. Furthermore, the advective travel times calculated in /Joyce et al. 2010/ using Equation 5-1 appear fast. Hence a sensitivity study is warranted.

In /Hjerne et al. 2010/, a compilation of tracer tests performed by SKB is presented. Different types of fracture apertures are derived based on the available data, and best fit relationships to the data are presented.

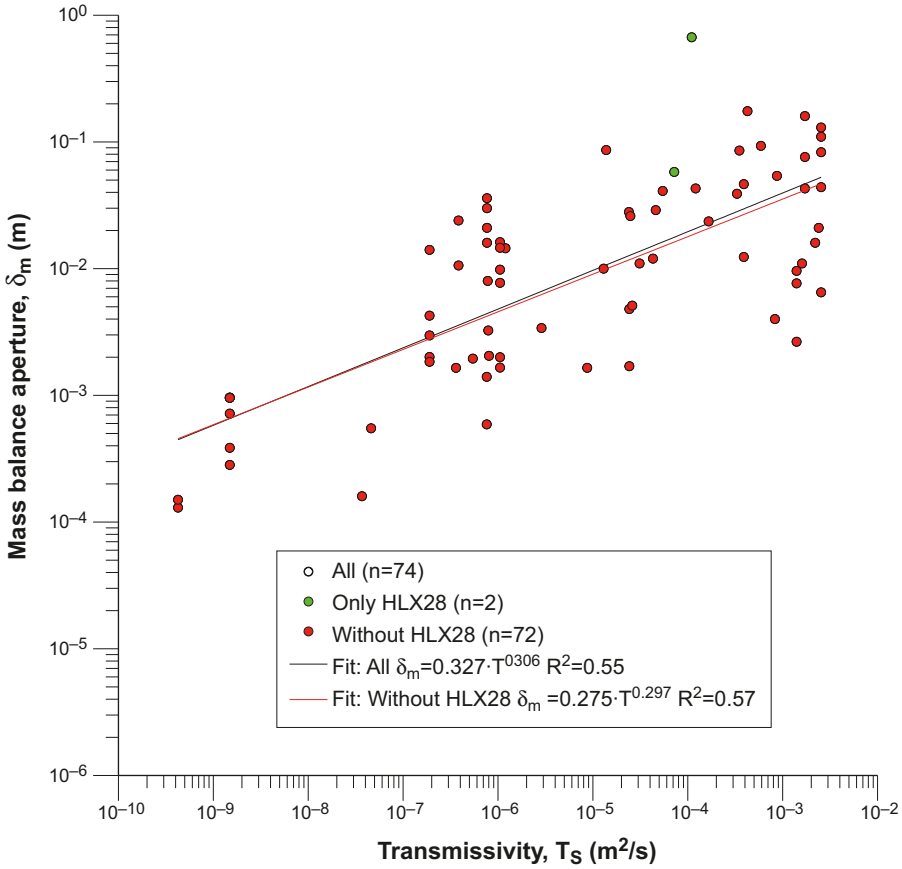


***Figure 5-18.*** *Best fit to tracer test data with or without inclusion of tracer test HLX28 (at Laxemar).*

The fit without the Laxemar test in borehole HLX28 (a test result that came late in the project) is here approximated as

$$e_t = 0.28T^{0.3} \qquad (5\text{-}2)$$

with notation as above. Using the transmissivity distribution of the fractures intersecting deposition holes in the hydrogeological base case simulation, cumulative distributions of the different aperture-transmissivity relationships can be produced, see Figure 5-19. In this figure, cumulative distribution functions of different types of fracture aperture-transmissivity relationships used in SR-Site and additional relationships presented in /Hjerne et al. 2010/ are shown.

It is noted in Figure 5-19 that the relationship based on tracer test data yields larger apertures than the relationship used in SR-Site. Also, it is noted that the two relationships based on tracer tests with or without the tracer test HLX28 at Laxemar yields very similar cumulative distribution functions.

The SR-Site relationship is fairly close to the theoretical relationship applicable for flow in fractures with constant apertures as given by the cubic law, i.e. $e_t = 0.01172\ T^{0.333}$. Thus, the relationship derived by /Hjerne et al. 2010/ can be considered to be an upper aperture bound. This is supported by two arguments. First, in conducted tracer tests, fractures (flow paths) with preferential properties for tracer transport are chosen. Hence, the derived apertures should be on the larger side. Second, as shown in the SR-Site Data report /SKB 2010b/, site-specific apertures estimated based on electrical resistivity measurements also show smaller apertures than the values derived by /Hjerne et al. 2010/ (but larger than the values obtained using the SR-Site relationship).

In Figure 5-20, the advective travel time distributions for the hydrogeological base case and the case based on relationship suggested by /Hjerne et el. 2010/ are shown for the Q1 path. It is observed that the Hjerne relationship gives about an order of magnitude increase in the median travel time values compared to the hydrogeological base case. The shortest travel time values are increased by approximately a factor of 2, and the longest by approximately a factor of 70. Thus, the effect of this bounding variant aperture-transmissivity relationship has some impact on the travel time distribution.

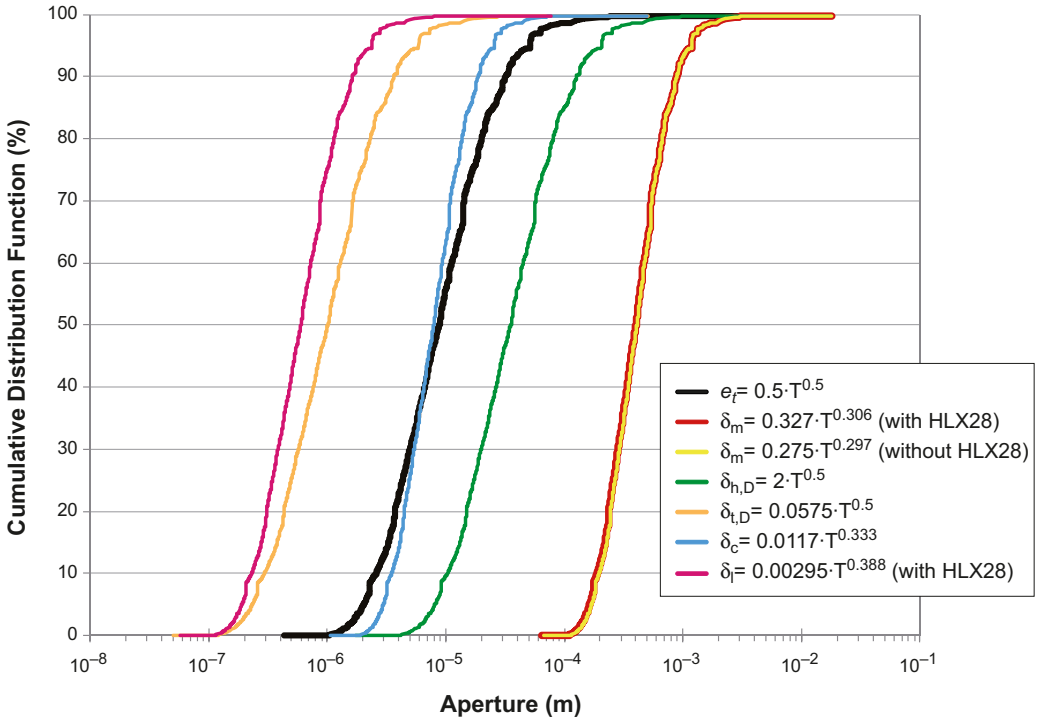


***Figure 5-19.*** *Cumulative distribution function plot of apertures based on the aperture-transmissivity relationship used in SR-Site and additional relationships presented in /Hjerne et al. 2010/. Note that /Hjerne et al. 2010/ use the notation δ for aperture. (90 per cent of the transmissivity values of the fractures intersecting deposition holes are in the range $1.6 \cdot 10^{-11}$ to $1.1 \cdot 10^{-8}$ $m^2/s$.)*

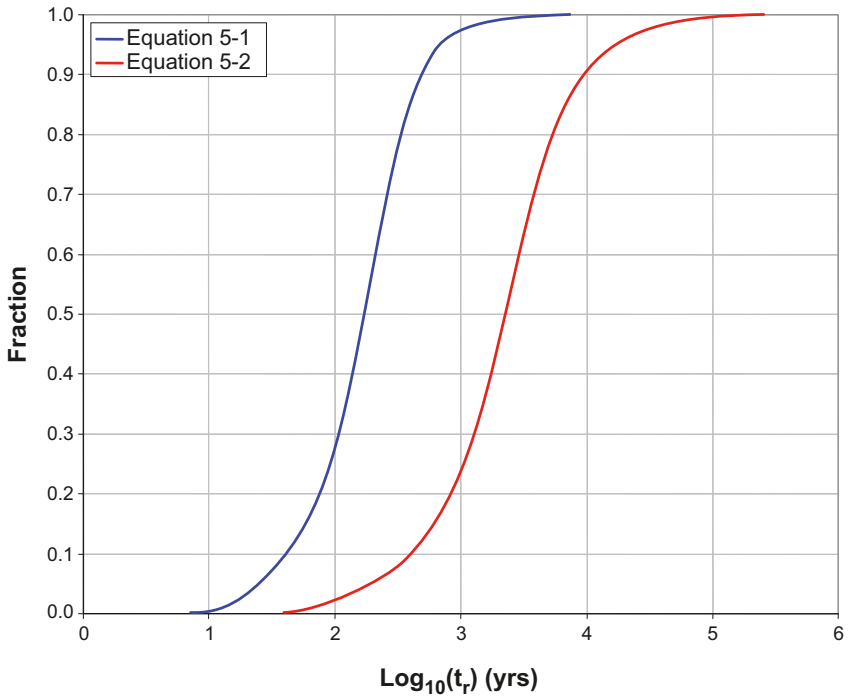


***Figure 5-20.*** *Cumulative distribution function plots of advective travel time ($t_r$) in the hydrogeological base case model using the standard $e_t$ to T relationship and the /Hjerne et al. 2010/ relationship for the Q1 particles successfully reaching the model top boundary (24%), released at 2000 AD.*

It is noted that in the simulations of the excavation and operational phase, see Chapter 4, and in the simulation of the reference glacial cycle, see Chapter 6, a slightly different form of the aperture-transmissivity relationship has been used (a coefficient 0.46 instead of 0.5 is used; 0.5 is an approximate value). This difference is sub-ordinate to other approximations and simplifications in the modelling.

It is noted that also the hydrogeochemical evolution and dilute water penetration are dependent on the assumed aperture-transmissivity relationship. However, these sensitivities are considered smaller than for advective travel time since both depend also on diffusional processes. Considering e.g. penetration of dilute water, see Figure 5-12, it is observed that after 10,000 years only 1% of deposition holes experience dilute conditions even with the shortest advective travel times indicated by Figure 5-20.

### 5.4.9 Groundwater circulation and flow path characteristics

In Section 5.4.3, it is shown that discharge locations for present day and near-future conditions are located in close proximity to the repository footprint, implying fairly vertical flow paths from the repository to the surface. It is important to verify that these paths are not an artefact of the modelling methodology but in fact real attributes of site characteristics. Below, a few issues with relevance for the vertical nature of these paths are addressed.

#### *Modelling of salinity*

One possible concern is whether the use of a distribution of salinity calculated from a transient palaeohydrogeological model of variable density reference water calculations to provide the fluid density for a steady-state snap-shot model of groundwater flow and particle transport is consistent with the underlying fully coupled transient calculations.

To address this concern, flow paths are calculated in a steady-state regional-scale ECPM model with a fixed distribution of density at 2000AD and using the consistent pressure. The flow paths are calculated using a mass-conserving method available in ConnectFlow /Cordes and Kinzelbach 1992, Serco 2011/. This approach to variable density flow is consistent with what is done in the hydrogeological base case model, albeit the calculation in the hydrogeological base case is performed with a DFN model on the site-scale.

The resulting flow paths are compared with flow paths calculated directly in the regional-scale model based on reference water transport for the solution at 2000AD. Hence, the test is whether the transfer of boundary conditions itself could bias flow paths in some way for the same conceptual model. Figure 5-21 shows that the recharge and discharge locations for the two sets of flow paths are consistent, and so the transfer of fluid density boundary conditions seems valid. Uncertainty remains as to how appropriate it is to use a fluid density field from an ECPM model (derived from the same underlying DFN realisation) in a calculation of a time slice of the pressure and flow field in the underlying DFN model. A DFN model has less connectivity by its very nature; if transient coupled variable density flow calculations in a large DFN model could be achieved, then the resulting density field would likely be more discontinuous.

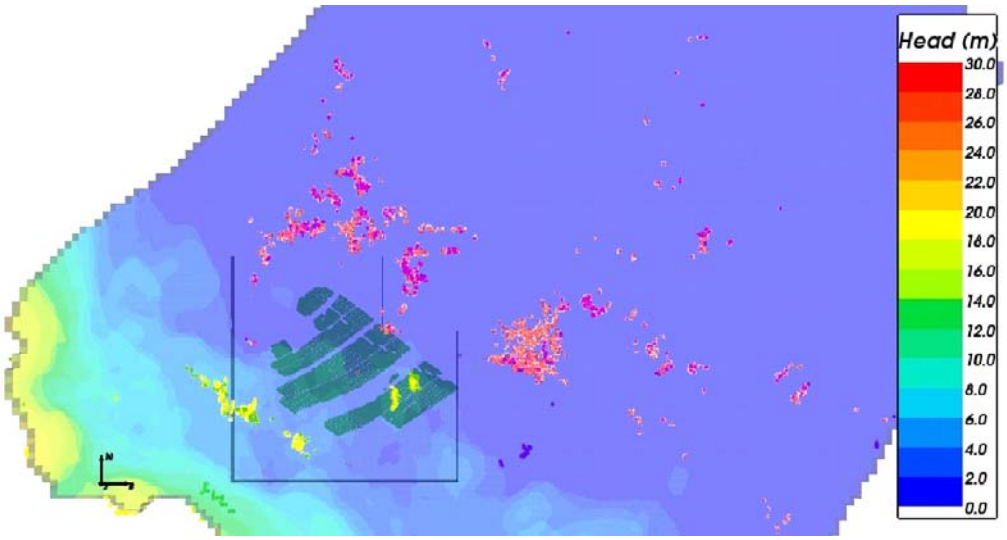


***Figure 5-21***. *Orange and green points are discharge and recharge locations, respectively, in an ECPM model based on a fully coupled regional-scale simulation at 2000AD. Pink and yellow points are discharge and recharge locations, respectively, in an ECPM model based on a steady-state snap-shot calculation using the same density and boundary conditions as used in the hydrogeological base case simulation.*

### *Patterns of recharge and discharge to the repository at 2000AD*

Under steady-state conditions at 2000AD, models predict that the groundwater circulation to the repository is quite localised. Recharge from the surface comes from seepage into several NW zones to the south: mainly ZFMNW0003, ZFMNW0017, and ZFMNW1200. The flow paths are along and, to some extent, down through a series of steeply and gently dipping ENE zones (ZFMA2 and ZFMENE0060A-C being major ones, but also ZFMENE0159A, ZFMENE2325A, and ZFMENE2320 may contribute). Discharge is at the topographic lows that are very close to the site, i.e. the sea around SFR and the Singö zone, and potentially Bolundsfjärden which is almost at sea level (~0.4 m). Figure 5-22 illustrates these areas and deformation zones. The existence of the sheet joints (and their associated hydrogeological characteristics) is an important concept for the regional-scale groundwater flow, but there are several steep and moderately inclined deformation zones that slice through the tectonic lens, and these are important transport pathways through and from the repository.

Furthermore, in Figure 5-23 a handful of the flow paths with smallest flow-related transport resistance ($F$) values for a release under 2000AD flow conditions are exemplified. The results are based on a DFN model in the site scale. The results indicate that the flow paths are steep but not vertical. Figure 5-23 also illustrates that the vertical paths with the lowest $F$ values are those that link the North East of the repository directly to the sea (0 m head) via ZFMWNW0044, and those that link the South East of the repository directly to Bolundsfjärden (0.4 m head) via ZFMENE0401A.

Based on this analysis, it is concluded that the fairly vertical flow paths are well substantiated and supported by the discrete nature of the open connected fracture system and the existence of known deformation zones.

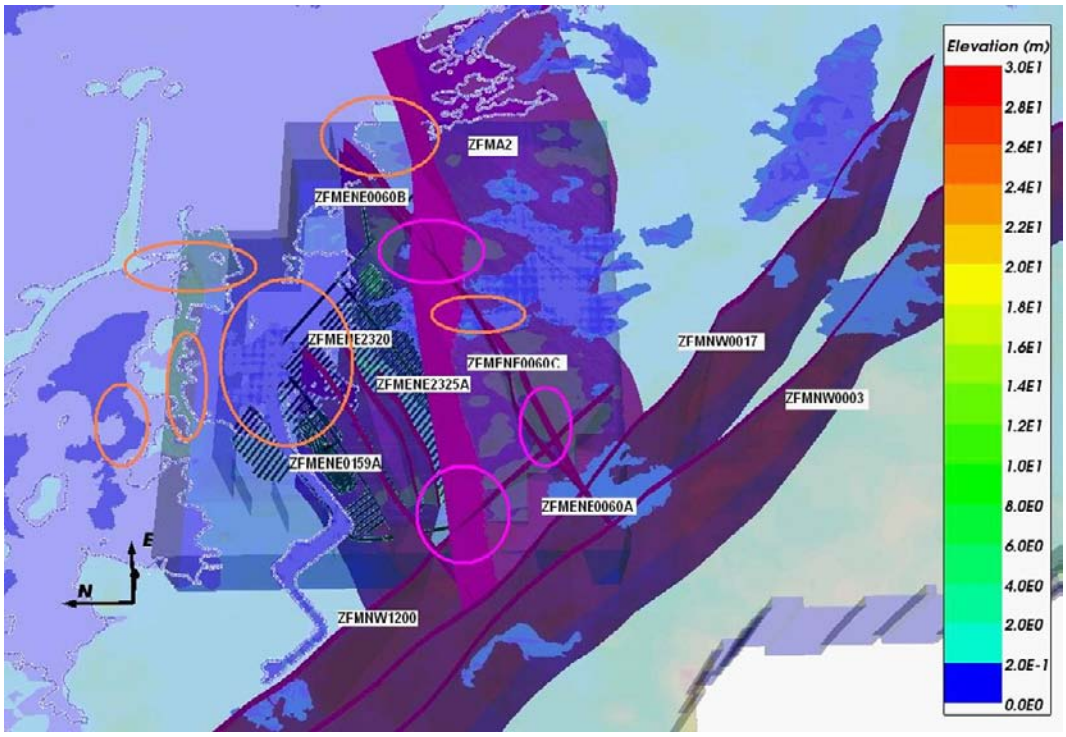


***Figure 5-22***. *Illustration of key recharge areas (pink) and discharge areas (orange) for the repository together with key deformation zones for relevant deep groundwater circulation.*

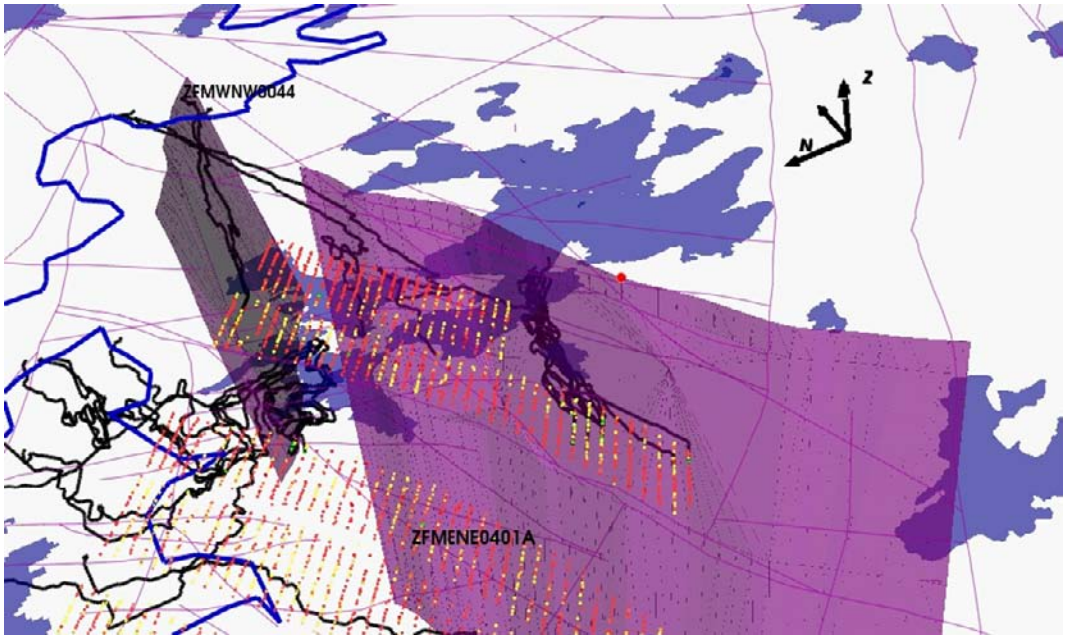


***Figure 5-23***. *Some of the steeply dipping deformation zones and steep flow paths that they give rise to.*

## 5.5 Assumptions, simplifications and uncertainties

Main assumptions, simplifications and uncertainties related to the study of the initial period of temperate climate after closure are:

- The time scale for saturation is probably over estimated based on results presented in /Enssle and Poppei 2010/. This is due to the simplification adopted in DarcyTools where the non-linear capillary suction effects of the backfilling material are neglected. According to /Enssle and Poppei 2010/, saturation-dependent values of the specific storage enables a dynamic evolution of the hydration process and a method for the implementation in DarcyTools is derived. The pressure build-up proceeds more rapidly for saturation-dependent values of the specific storage. However, the time for full saturation may not be very different between the two methods. The saturation times reported by /Svensson and Follin 2010/ are within the range of values obtained from modelling where the hydrology of the backfill is treated in more detail and where also the buffer is included (see Section 10.3.8 of the SR-Site Main report).
- The hydrogeochemical evolution of individual reference waters is dependent on the chosen initial and boundary conditions. The evolution of salinity, which depends on the reference water composition, is hence also associated with some uncertainty; however, it is argued that this uncertainty is smaller than the uncertainty of the individual reference waters since the salinity is an integrated entity (summation of individual reference water constituents). The modelled salinity development of generally more dilute conditions during the temperate period is considered an evolution with a high degree of certainty.
- Discharge locations may be excessively dominated by the location of the shoreline due to the continuum representation in the outer parts of the domain where particles tend to discharge at later times. For a discrete representation, the discharge locations may be more influenced by outcropping deformation zones or fractures. This issue is examined by the extended spatial variability variant, see SDM-Site related model variants below for details.
- The uncertainty in performance measures of the hydrogeological base case is addressed both through multiple realisations and multiple particles per start location. The results indicate that branching (assessed by multiple particles per start location) implies no uncertainty, whereas there is some variability between realisations. Thus, it is judged that multiple realisations need to be assessed in subsequent analyses within SR-Site.
- The uncertainty in results due to the conceptual model chosen, i.e. a discrete representation where the parameterisation of the discrete model has been done according to the methodology developed as part of the site descriptive modelling /Follin 2008/, is assessed by adopting a different conceptual model representation. In /Longcheng et al. 2010/, the channel network modelling tool CHAN3D is applied to the temperate conditions of the Forsmark site, and the corresponding performance measures as in /Joyce et al. 2010/ have been calculated. In CHAN3D, the model is parameterised using the statistics of block-conductivity values resulting from up-scaling of the original hydro-geological DFN model. The results indicate that the reported median performance measures are very similar, whereas the spread of results is smaller in CHAN3D than in the ConnectFlow application. These results are consistent with findings in an earlier assessment (SR 97) as reported by /Selroos et al. 2002/; i.e. discrete models tend to exhibit more spreading than continuum representations.
- Out of the different performance measures, only the advective travel time is dependent on porosity or aperture. An alternative aperture-transmissivity relationship, derived based on field data from tracer tests, has been explored. The results indicate a shift towards longer travel times by approximately an order of magnitude for the median travel time. The effect of this uncertainty is judged negligible, and conservative, for subsequent analyses of solute transport. Concerning the hydrogeochemical evolution, it is noted that a change in porosity by a factor of ten could have some effects; however, in the regional-scale analyses by /Joyce et al. 2010/ where the evolution of reference waters is analysed, a calibration of porosity is made by multiplying the porosity resulting from the up-scaling of the underlying DFN model by a factor of ten (it is noted that the change in porosity in the regional-scale model is motivated by the truncation in fracture size used in the model, not uncertainty in transmissivity-aperture relationship per se). Thus, also the evolution of hydrogeochemistry is judged to be representative for further use within SR-Site.

- The assessment of penetration of dilute water should be considered an approximate quantification. First, the flow field at 2000 AD is used; i.e. the temporal development in flow characteristics is not accounted for. Second, no mixing or water-rock interactions are considered, which clearly may affect the water chemistry evolution. Thus, the reported numbers should be seen as very rough estimates rather than precise predictions of a future evolution. However, the presented numbers of deposition hole locations experiencing dilute conditions are deemed appropriate for use in subsequent analyses of buffer erosion and canister corrosion as they are likely pessimistic estimates. The site understanding presented in Section 2.5, based on collected data, indicates that dilute waters do not penetrate to repository depth. However, as the simplified analysis conducted here indicates, it is hard to defend that not a few deposition holes could experience dilute conditions.
- No additional uncertainties are identified in the cases with modified repository properties relative to the simulations with base case properties. The extent of the crown space is purely hypothesised. In reality, a crown space is considered unlikely or even impossible to develop with a swelling backfill, see Section 10.3.8 of the SR-Site Main report. Furthermore, the implemented properties of the EDZ are also believed to be pessimistic. Thus, the cases addressed are pessimistic variants, and no additional uncertainties relative to the simulations with base case repository properties are identified. The cases with modified repository related properties are of interest to propagate to subsequent radionuclide transport calculations since system performance is affected.
- The uncertainty in performance measures of the SDM-Site related hydrogeological base case parameterisation (parameter heterogeneity) is addressed through a number of model variant simulations. Among the four variant cases studied, it is primarily the "Alternative DFN transmissivity-size relationship" variant cases that suggest any substantial additional variability (uncertainty). The results for this variant case indicate that the performance measures of the semi-correlated relationship utilised in the hydrogeological base case model in general are more favourable than the other two correlation models. Thus it is important to propagate the other correlation models to assessment calculations. The results of the extended spatial variability variant case indicate that the effect of representing the full domain in a discrete fashion changes the discharge location pattern to a certain extent. Specifically, the incorporation of the additional discretely modelled fractures causes more particles to discharge close to the repository. However, since the base case parameterisation already contains discharge locations close to the repository, it is argued that this variant does not warrant further consideration in the subsequent analyses. In summary, the uncertainty in transmissivity-size relationship implies that all three correlation models need to be propagated for subsequent analyses of buffer erosion, canister corrosion and radionuclide transport. The other SDM-Site related variants do not warrant further consideration in the assessment.
- It is noted that the calculated flow-related transport resistance ($F$) values are to be used unmodified in subsequent radionuclide transport and oxygen penetration calculations. In SR-Can, $F$ values were divided by a factor of ten to account for channelling. In SR-Site no such channelling factor is used based on motivations provided in /SKB 2010d/ and summarised in /SKB 2010b/. First, fracture-to-fracture variability is generally larger than within-fracture variability in aperture. Second, fluid can only enter and leave fractures on a limited area, significantly constraining the meander of flow paths. Third, substantial portions of the non-contacting fracture surface area outside of the dominant flow channels may still be accessible by diffusion within the fracture pore space and thus provide additional surface area for radionuclides to interact with the rock matrix. The results obtained using the alternative conceptual model inherent in CHAN3D also support the use of an unmodified $F$ value. In CHAN3D, the flow-wetted surface is not given through the discrete fractures in the model but rather estimated based on conductive fracture frequency. Thus, similar estimates of $F$ in both modelling tools indicate that the distribution of the flow-related transport resistance should not be modified in the discrete application.
- The uncertainties related to the assessment of open boreholes stem from the representation of the boreholes in the model. The boreholes are introduced as high permeability features in the model that end 10 m below ground surface. Also, a freshwater density is assigned to the entire borehole, which is a conservative assumption in terms of hydraulic driving forces. These simplifications are not judged to have any implications on the analyses performed given the purpose of the analyses.

# 6 Evolution for the remaining part of the reference glacial cycle

## 6.1 Analyses performed to address specific questions within SR-Site

Below, the different cases of /Vidstrand et al. 2010/ performed with relevance for the periods with periglacial and glacial climate conditions are listed. In addition, the calculations of /Joyce et al. 2010/ using boundary conditions from the glacial models are included. It is indicated where the results produced by each case are intended to be used within the subsequent analyses of SR-Site.

- **Hydrogeological evolution.** The changes in Darcy Flux ($q$) and advective (fracture) water salinity ($C$) at repository depth relative to temperate climate conditions ($q_{temp}$ and $C_{temp}$) are simulated on a super-regional scale. To a lesser extent, the exchange of salt between the advective (fracture water) salinity and diffusive (matrix porewater) salinity is also looked at. It is noted that the groundwater chemistry is represented by salinity alone.
- **Recharge and discharge locations in the biosphere.** Recharge and discharge locations are identified using forward and backward particle tracking from positions representing the deposition hole position within the repository footprint. The particle tracking is performed for steady-state velocity fields representing different ice front locations relative to the location of the repository. The results on discharge locations in the biosphere are intended for the dose calculation in the biosphere.
- **Performance measures.** The key performance measures are (i) the Darcy flux ($q$) at the deposition hole positions, and (ii) the advective travel time ($t_w$) and the flow-related transport resistance ($F$) along flow paths passing through these positions. The latter two are obtained from forward and backward particle tracking. The results intended for radionuclide transport calculations are obtained from the combined repository-scale and site-scale model of /Joyce et al. 2010/, which simulates groundwater flow through an explicit representation of the repository structures using boundary conditions from the super-regional scale model.
- **Penetration of glacial melt water.** Recharge of glacial meltwater implies a gradual dilution of the originally more saline water. As dilute water has negative effects on the buffer and backfill stability, it is of interest to assess the possibilities of dilute water reaching repository depth considering the hydrogeological flow and transport conditions. This is done utilising the flow-related transport results (performance measures) from the repository-scale and site-scale models described in /Joyce et al. 2010/ using boundary conditions from the super-regional scale model in conjunction with analytical transport estimates.
- **EDZ and crown space.** In the application of glacial boundary conditions in the repository-scale and site-scale models including an explicit representation of the repository, an assessment of modified properties of the excavation damaged zone (EDZ) is performed. Also, an assessment of the impact of a crown space in the tunnel is made. The crown space is caused by a consolidation of the tunnel backfill material. The analysis is performed utilising the combined repository-scale and site-scale model of /Joyce et al. 2010/, which simulates groundwater flow through an explicit representation of the repository structures, using boundary conditions from the super-regional scale model. These results are intended to be used in radionuclide transport calculations.
- **Site related variants.** Some properties of the site, with specific relevance to glacial conditions, as well as the glacial conditions as such are uncertain. The impacts of alternative parameterisations related to these issues are assessed in order to judge their importance. For example, the transmissivity of all deformation zones and fractures that strike towards northwest is changed based on the results from the rock mechanics modelling conducted for SR-Site /Hökmark et al. 2010, Lönnqvist and Hökmark 2010/.
- **Comparison of the Darcy flux at different time slots during glaciation and deglaciation.** Various model simplifications are made in /Vidstrand et al. 2010/ and /Joyce et al. 2010/ that do not conform fully to the expected reference evolution described in /SKB 2010a/. In order to obtain an appreciation of the evolution of groundwater flow for an advancing and retreating ice sheet margin, methods to combine all simulated "climate events" (states) are presented and exemplified. The objective is to find reasonable simplifications of the complex temporal evolution of the Darcy flux for subsequent handling in radionuclide transport calculations within the safety assessment.

## 6.2 Base case

The reference evolution in /SKB 2010a/ has permafrost conditions in front of an advancing ice sheet margin. However, results for this case cannot be exported to the repository-scale and site-scale models of /Joyce et al. 2010/ as the hydraulic properties of the geosphere change continuously due to the presence of permafrost. Therefore, a Glacial Case without Permafrost in front of an advancing ice sheet margin constitutes a base case for all models (variant cases) treated in /Vidstrand et al. 2010/ including a Glacial Case with Permafrost in front of an advancing ice sheet margin. The different flow simulations conducted by /Vidstrand et al. 2010/ are listed in Table 6-1.

Another reason for the Glacial Case without Permafrost as a base case is that this case produces the largest hydraulic gradients at the ice sheet margin, hence the greatest effects on the studied performance measures with regard to Darcy flux and fracture (advective) salinity at repository depth.

**Table 6-1. Overview of flow simulations. The main scenarios, A and B, are divided into five cases (a)–(e). The bullets indicate the particular conditions modelled with each case considered. Case (a) constitutes a base case in /Vidstrand et al. 2010/.**

| | **A. Glacial conditions without permafrost** | |
|---|---|---|
| | *Pre-LGM stage* | *LGM stage* |
| (a) | • Ice sheet movement from northwest.<br>No permafrost in front of the ice sheet margin.<br>Undistorted permeability conditions. | • Entire model domain is covered by an ice sheet<br>Undistorted permeability conditions.<br>*Post-LGM stages*<br>• Submerged conditions in the ice free area.<br>Undistorted permeability conditions. |
| | **Variants** | |
| | *Pre-LGM stage* | *LGM and Post-LGM stages* |
| (b) | • As in (a), but ice sheet movement from north. | • – |
| (c) | • As in (a), but distorted permeability conditions. | |
| | **B. Glacial conditions with permafrost** | |
| | *Pre-LGM stage* | *LGM and Post-LGM stages* |
| (d) | • Ice sheet movement from northwest.<br>Permafrost in front of the ice sheet margin as well as 2 km below the tip (tongue) of the ice sheet margin<br>Undistorted permeability conditions. | • – |
| | **Variants** | |
| | *Pre-LGM stage* | *LGM and Post-LGM stages* |
| (e) | • As in (d), but no permafrost tongue. | • – |

The following modifications are made in the model setup in comparison with the base case described in Section 4.2:

- The model parameter governing the short-term diffusion into/out of the stagnant pools of water nearby the flowing fractures is set to $4 \cdot 10^{-7}$ $s^{-1}$, whereas the parameter governing the long-term diffusion into/out of the less permeable rock matrix away from the fracture is set to is set to $4 \cdot 10^{-12}$ $s^{-1}$. The latter value implies a time scale of approximately 8,000 years for the remotest diffusive exchange.
- Scoping calculations by /Vidstrand et al. 2010, Appendix D/, suggest that it is the matrix porewater close to the flowing fractures, i.e. within a distance of a few metres, that will interact with the chemistry of fracture water during 10,000 years. Hence, the salinity of the matrix porewater further away from the fracture surfaces will remain unaffected by the diffusive exchange. As indicated in Figure 2-9, the geometric mean of the conductive fracture frequency of flowing fractures detected with the PFL method below –400 m elevation is approximately 0.005 $m^{-1}$, which implies a block size between flowing fractures of approximately 200 m.
- The model domain size is increased in order to accommodate the intended simulations. This is necessary as the even elevation of ice sheet profile away from the ice sheet margin overrides the topographic water divides that prevail during temperate climate conditions.
- The initial conditions of the water salinity considered for the simulation of (i) temperate climate conditions, (ii) glacial climate conditions without permafrost, and (iii) glacial climate conditions with permafrost are all different from one another. In principle, the derivation of the initial conditions for the temperate case starts with the same salinities as those used for SDM-Site at 8000 BC. However, depending on glacial case considered, the flow model is run until steady state with different top boundary conditions, see /Vidstrand et al. 2010/ for details. Present-day lakes, wetlands, main surface water (stream) runoff and groundwater chemistry are not used as "calibration targets". Thus, the term temperate is not to be understood as 2000 AD, but rather as a time slot in the future when the ice sheet margin is close to, but still outside, the model domain.
- The boundary conditions on the top boundary vary depending on the glacial case considered. A pressure equal to 92% of the weight of the ice sheet thickness is specified on the top boundary below the ice. Elsewhere, the pressure is set to zero in all terrestrial parts and to the hydrostatic pressure below the ice-free sea and lakes. The salinity on the top boundary is set to zero. The bottom of the model is located at –2,000 m elevation and is a no-flow boundary with a fixed salinity of approximately 7.2% based on the initial values of the reference water fractions considered in SDM-Site. All vertical sides of the model domain are no-flow boundaries.
- The geometry and hydraulic properties of deterministically modelled geological features such as deformation zones and sheet joints are imported from the hydrogeological base case defined in groundwater flow modelling of the temperate period carried out by /Joyce et al. 2010/.
- The geometry and hydraulic properties of stochastically modelled hydraulic features such as discrete fracture networks (DFN) are not imported from /Joyce et al. 2010/ but generated by /Vidstrand et al. 2010/. The statistical distributions are identical to those used by /Joyce et al. 2010/ for the generation of DFN realisations of the hydrogeological base case. However, a single realisation is studied in the work reported by /Vidstrand et al. 2010/, whereas /Joyce et al. 2010/ study several realisations and /Svensson and Follin 2010/ study two realisations.

## 6.3 Variants

The variants studied by /Vidstrand et al. 2010/ are listed in Table 6-1, where they are denoted as cases (b), (c) and (e).

### 6.3.1 N-S ice advance direction

Based on the historic data provided in /SKB 2010a/, a NW-SE orientation of the model domain is conceived to be the most appropriate orientation to study for an advancing ice sheet margin. (The most appropriate retreat direction is probably somewhat more parallel to S-N.) The simulations carried out by /Vidstrand et al. 2010/ include a case (b), where a N-S ice advance direction is used as a variant and sensitivity test.

### 6.3.2 THM properties

Isostasy is not accounted for in the study by /Vidstrand et al. 2010/. However, the potential impact on groundwater flow of an uneven surface loading at the ice sheet terminus (the fore-bulge phenomenon) is addressed by incorporating a case (c), where a change in fracture transmissivity is used as a variant and sensitivity test. It is noted that the change in transmissivity applied by /Vidstrand et al. 2010/ exceeds the change suggested in the hydro-mechanical modelling within the SR-Site project /Lönnqvist and Hökmark 2010, Hökmark et al. 2010/, see Section 10.4.4 of the SR-Site Main report.

### 6.3.3 Permafrost tongue

The Base case, i.e. the Glacial Case without Permafrost, is accompanied by a Glacial Case with Permafrost. As the speed of the advancing ice sheet margin during glaciation is greater than the rate of the thawing of the permafrost layer in periglacial area in front of the ice sheet margin, a tongue of trapped permafrost is created close to the ice sheet margin. A case (e) with no permafrost tongue close to the ice sheet margin is studied as a variant and sensitivity test to the Glacial Case with Permafrost.

## 6.4 Results

### 6.4.1 Hydrogeological evolution

Permafrost is a key process to consider as it reduces the permeability of subsurface materials to water flux. Permafrost does not develop instantaneously, however. Its development is a transient process. The performance of the freezing algorithm used by /Vidstrand et al. 2010/ to modify Holocene hydraulic conductivity values as a function of temperature is illustrated in Figure 6-1. The input to the permafrost model is obtained from the ground surface temperature time series described in /SKB 2010a/.

A discontinuous permafrost layer is considered in /Vidstrand et al. 2010/, which implies that the permafrost layer contains more or less unfrozen sections depending on the local boundary conditions and material properties. Probable locations for taliks (unfrozen spots in the permafrost layer) are estimated from the forecasted landscape development carried out in the SR-Site project based on the shoreline displacement at Forsmark.

Figure 6-2 suggests insignificant differences in Darcy flux between the two cases of permafrost conditions studied at the ice sheet margin, i.e. cases (d) and (e). It is noted that the oscillations near the peak in Figure 6-2 reflect transient effects at the top boundary due to the transient hydraulic properties of the permafrost.

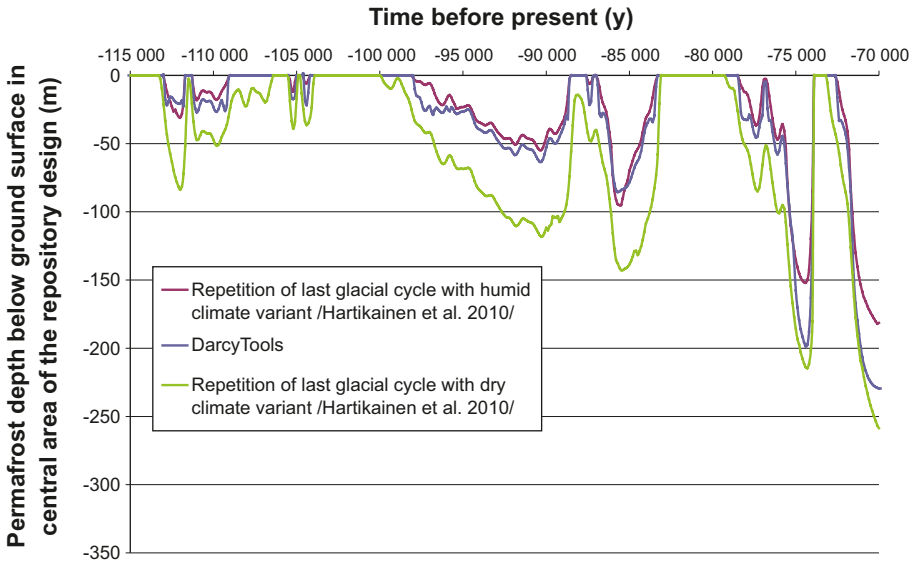


***Figure 6-1.*** *Permafrost depth simulated with DarcyTools in comparison with the two main cases in /Hartikainen et al. 2010/.*

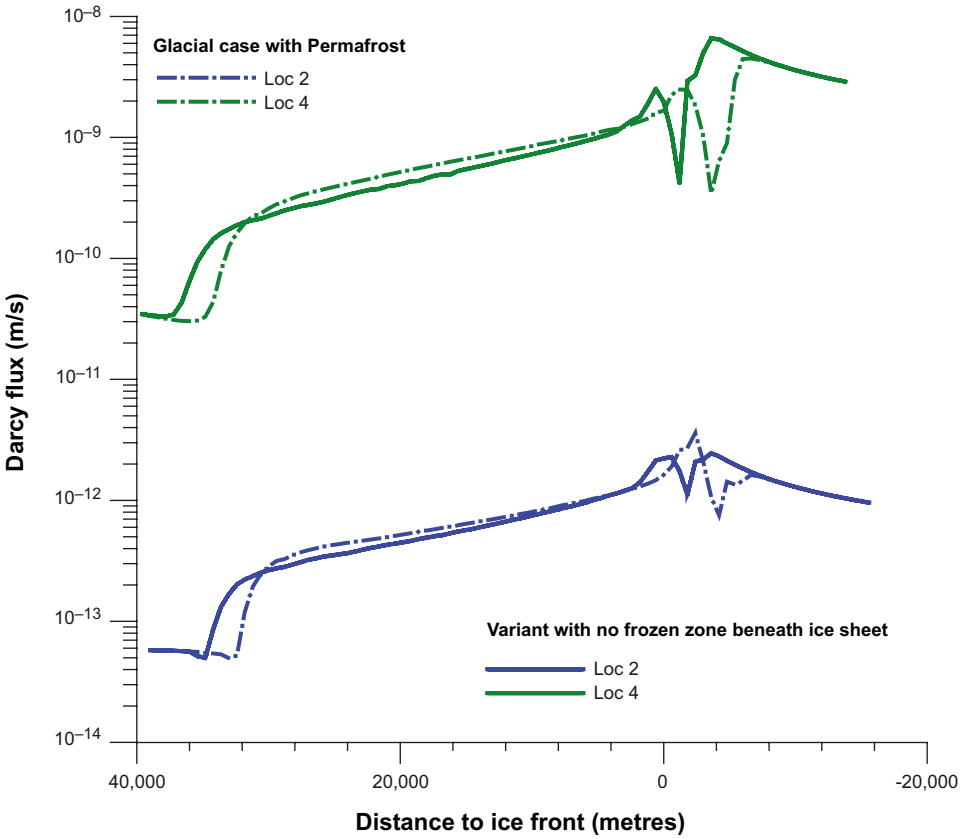


***Figure 6-2.*** *Comparison of the Darcy flux at ML 2 and ML 4 for two of the permafrost models studied; case (d) Glacial with Permafrost and a 2 km long tongue of permafrost behind the ice sheet margin (dashed lines), and case (e) Glacial with Permafrost but no tongue of permafrost (Solid lines). Positive distance values mean that the ice sheet margin has not yet arrived at the measurement locations.*

Figure 6-3 shows Darcy fluxes for a NW-SE vertical cross section through the potential repository area. Three cases are shown. The upper most cross-section represents temperate conditions (IFL 0). The cross-section in the middle represents an advancing ice sheet margin at IFL II without permafrost in the periglacial area. The bottom most cross-section represents an advancing ice sheet margin at IFL II with permafrost conditions in the periglacial area. The Darcy flux pattern corresponds to the existence of deformation zones.

Figure 6-4 shows the salinity field for a NW-SE vertical cross section through the potential repository area. Three cases are shown. The upper most cross-section represents temperate conditions (IFL 0). The cross-section in the middle represents an advancing ice sheet margin at IFL II without permafrost in the periglacial area. The bottom most cross-section represents an advancing ice sheet margin at IFL II with permafrost conditions in the periglacial area. Figure 6-5 shows the same salinity fields but for a horizontal plane placed at –465 m through the target volume.

In summary, Figure 6-3 and Figure 6-4 show that the hydraulic pressure at the bottom of the ice sheet distorts the temperate conditions and causes glacial meltwater to recharge and flush the advective system. In effect, the more saline water in the fractures is pushed forwards and upwards (upconing). The reason for the high salinity near the ground surface is that the permafrost hinders discharge at the top boundary (cf. the bottom most image in Figure 6-3), except where taliks (unfrozen ground) occur.

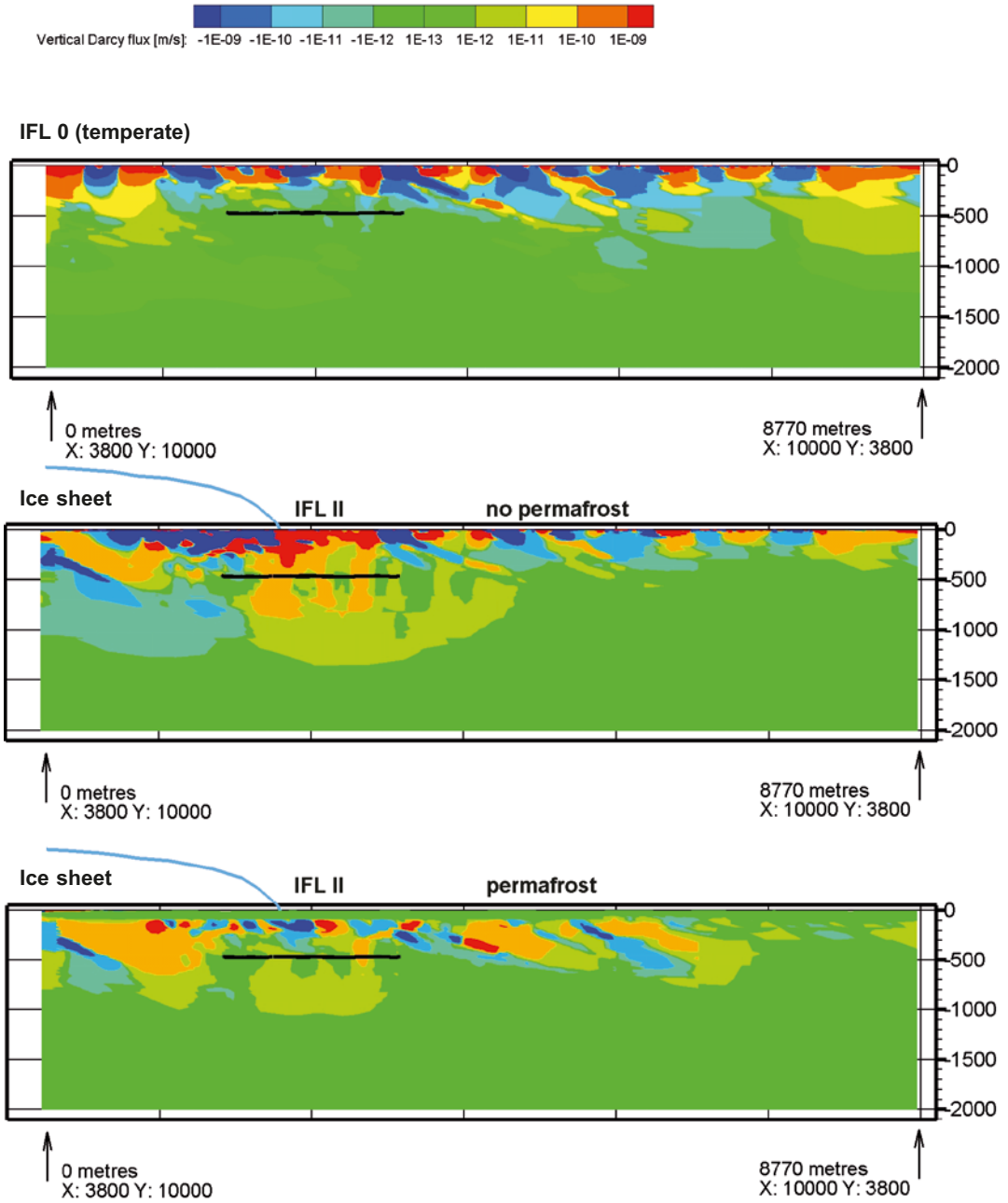


***Figure 6-3.*** *Top: Darcy flux during temperate conditions mapped on a cross-section parallel to the direction of the ice sheet movement during glaciation. The images in the middle and at the bottom show the Darcy fluxes when the ice sheet margin is at IFL II for the Glacial Case without Permafrost (middle) and for the Glacial Case with Permafrost (bottom). The position of the ice sheet profile is illustrated with a blue curve. IFL II is located close to the centre of the repository area. Negative values represent downward directed fluxes.*

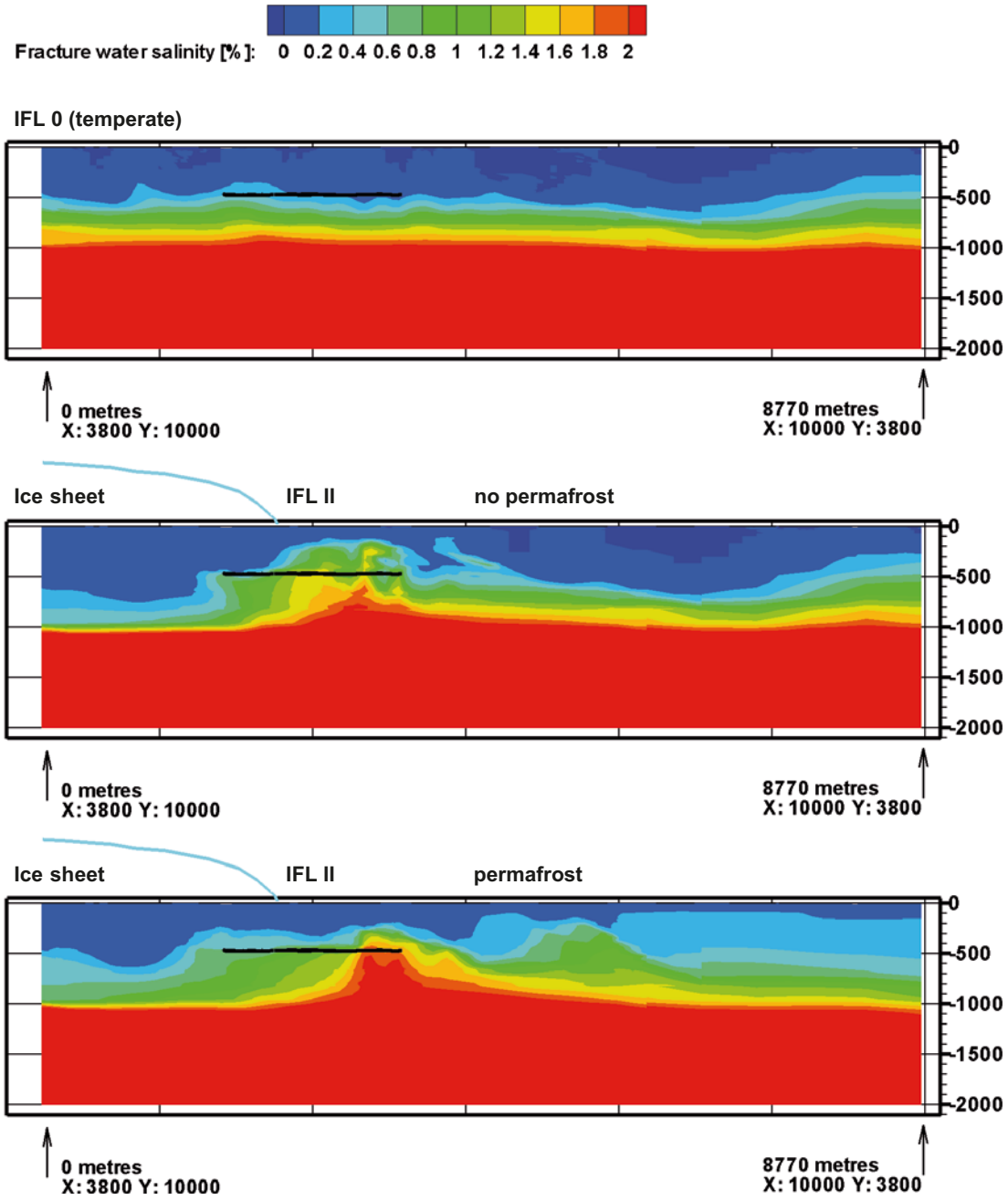


***Figure 6-4.*** *Top: Fracture (advective) water salinity during temperate conditions mapped on a cross-section parallel to the direction of the ice sheet movement during glaciation. The images in the middle and at the bottom show the fracture water salinity when the ice sheet margin is at IFL II for the Glacial Case without Permafrost (middle) and for the Glacial Case with Permafrost (bottom). The position of the ice sheet profile is illustrated with a blue curve. IFL II is located close to the centre of the repository area.*

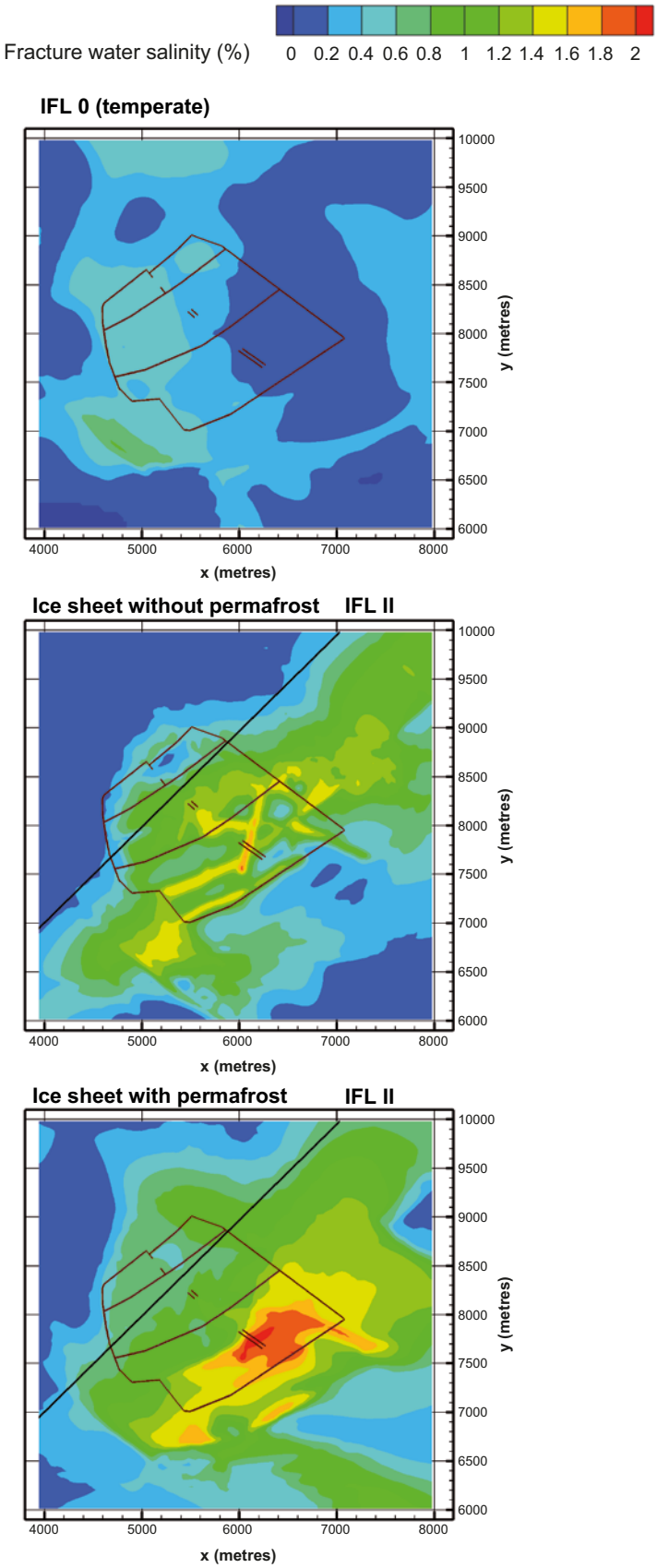


***Figure 6-5.*** *Top: Fracture (advective) water salinity during temperate conditions mapped on a horizontal plane located at –465 m. The images in the middle and at the bottom show the fracture water salinity when the ice sheet margin is at IFL II for the Glacial Case without Permafrost (middle) and for the Glacial Case with Permafrost (bottom). The black thin lines represent main repository tunnels. IFL II is located close to the centre of the repository area.*

The changes in Darcy flux and fracture water salinity during the simulated period (IFL 0 → IFL V → IFL 0) are monitored at the five measurement localities ML 1–5 and expressed as ratios relative to the corresponding initial, temperate values, see Figure 6-6 and Figure 6-8. It is recalled that the term temperate in /Vidstrand et al. 2010/ is not to be understood as 2000 AD, but rather as a time slot in the future when the ice sheet margin is close to, but still outside, the flow model domain, i.e. IFL 0.

In Figure 6-6, it is seen that the Darcy flux increases dramatically during the two ice front passages. The immediate shift to low and constant values at the start of the period of complete ice coverage is an artifact of the instantaneous shift in ice sheet gradient at the same moment. In reality, a more smooth transition is expected. For the Glacial Case with Permafrost, slightly different shapes of the curves are obtained during glacial advance, see Figure 6-7 . However, for the remaining parts of the cycle, the curves are identical to those shown in Figure 6-6 as there is no permafrost during these periods.

The normalised change in the salinity development is shown in Figure 6-8. The passage during glaciation (pre-LGM) is characterised by an initial upconing followed by an out flushing resulting in lower salinities than during the initial temperate conditions. However, during the subsequent stage, i.e. when the site is completely covered by the ice sheet (LGM), a gradual increase in fracture water salinity at repository depth occurs. This gain of the "salt water interface" is due to an accommodation of the buoyancy forces to the very weak top boundary condition of an almost uniform ice sheet thickness, and to the slow, but continuous advective transport of salt from below. It is recalled that the fracture water salinity at great depth is assumed to be undisturbed (fixed) at all times in the flow model. The data support for this assumption is presented in SDM-Site.

The passage during deglaciation (post-LGM) is also characterised by an upconing and flushing event, but the effects are considerably smaller than during the advance. The reason for this is twofold; (i) the speed of the retreating ice sheet margin is twice as fast as the speed of the advancing ice sheet margin (100 m/y versus 50 m/y), and (ii) the subglacial area in front of the retreating ice sheet margin is submerged. These conditions reduce the duration and the magnitude of the hydraulic gradient across the ice sheet margin significantly.

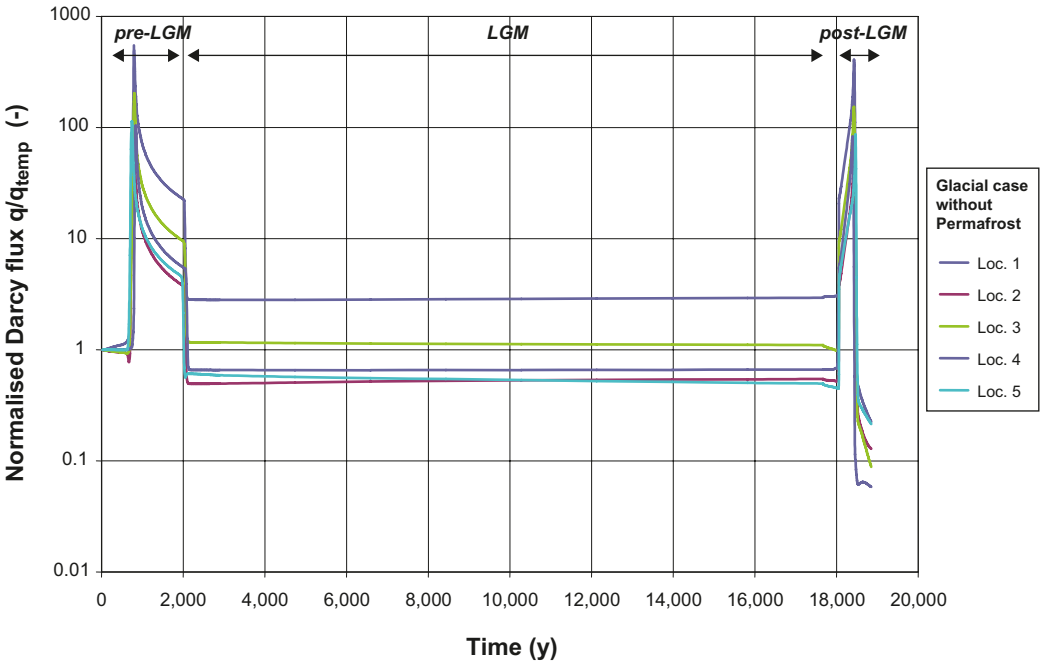


***Figure 6-6.*** *Plot showing the normalised change in Darcy flux, ($q/q_{temp}$), at ML 1–5 during approximately 19,000 years for the Glacial Case without Permafrost. ML 1 is located close to a steeply dipping deformation zone.*

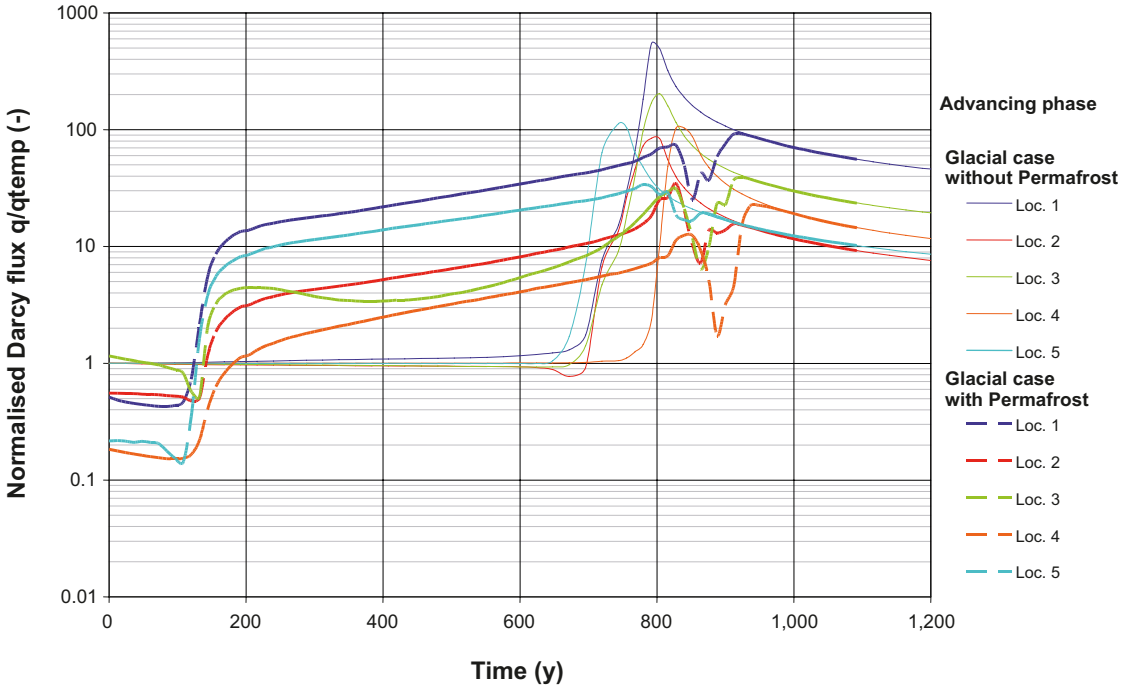


***Figure 6-7.*** *Close-up of the plot in Figure 6-6 showing the normalised change in Darcy flux, ($q/q_{temp}$), at ML 1–5 during glaciation (pre-LGM). Besides the Glacial Case with Permafrost (solid lines), the evolution of the Glacial Case without Permafrost (dashed lines). Beyond t = 1,000 years the two scenarios are identical.*

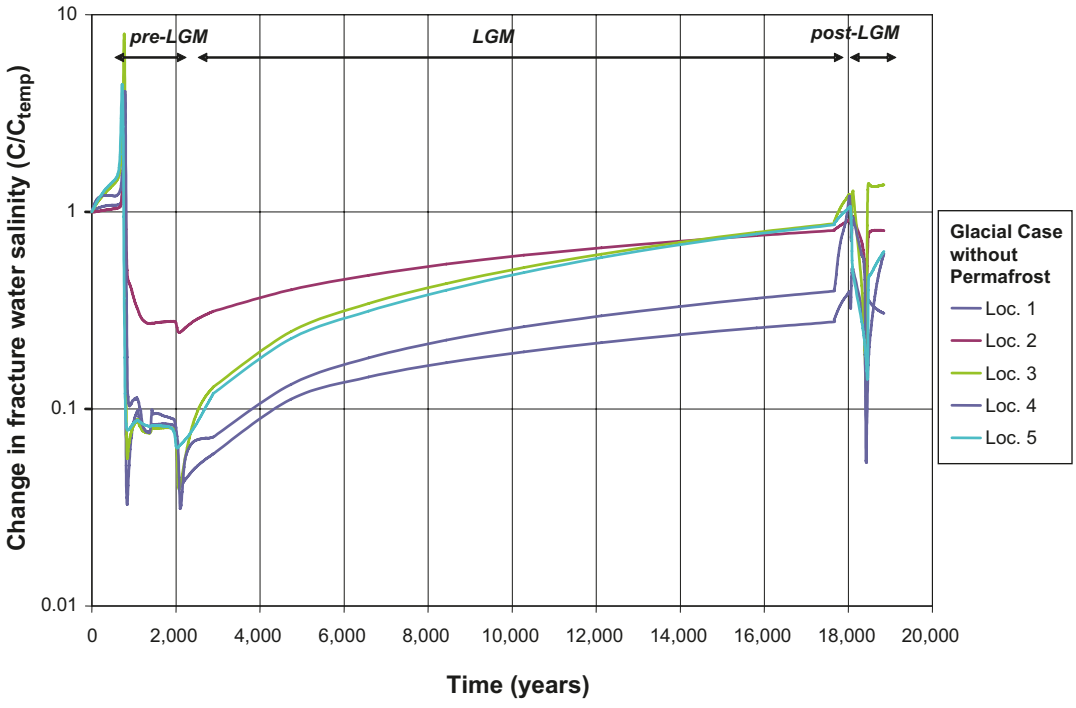


***Figure 6-8.*** *Plot showing the normalised change in salinity, ($C/C_{temp}$), at ML 1–5 during approximately 19,000 years for the Glacial Case without Permafrost.*

Figure 6-9 shows the simulated difference in flushing as a function of the average speed of the retreating ice sheet margin. A retreat speed of 300 m/y yields less flushing than a retreat speed of 100 m/y. It is noted that the average speed of the retreating ice sheet margin considered for the reference evolution in /SKB 2010a/ is 300 m/y; i.e. three times the speed considered in /Vidstrand et al. 2010/. Second, the retreating ice sheet profile considered for the reference evolution in /SKB 2010/ is significantly thinner and less steep at the ice sheet margin than the ice sheet profile considered in /Vidstrand et al. 2010/, which is a theoretical maximum. Thus, the conditions considered by /Vidstrand et al. 2010/ exaggerate the impact of the ice sheet; still the results indicate that the fracture water salinities are more or less restored during the simulated period (IFL 0 → IFL V → IFL 0). In conclusion, low fracture water salinities, i.e. dilute conditions, are mainly found in conjunction with the ice front passages. The results presented in Figure 6-8 indicate that fracture water salinities reach values below ten per cent of the values at temperate conditions for a limited period of time only.

Regarding the exchange of salt between the fracture water and the matrix porewater, the exchange appears to be from the matrix porewater to the fracture water for a limited period of time only coinciding with the passages of the ice sheet margin. During the long period of complete ice coverage the conditions are the opposite, see Figure 6-10, although it is noted that a quasi-equilibrium between fracture and matrix waters exists. The reason for not a full equilibrium developing is that there is a constant advective transport of salt in the fractures from the bottom boundary of the model. Furthermore, the results indicate that it takes roughly 3,000 years to establish this quasi-equilibrium after flushing has occurred. This also implies that it is the matrix close to the fracture surface that is included in the model rather than the matrix further away. Also noted is that the fracture water salinity in this transient simulation does not go below approximately 0.1% (i.e. approximately 1 g/L) at any time. In Section 6.4.4, where penetration of glacial melt water to repository depth is analysed using a steady-state velocity field representative of the flushing period, it is shown that matrix diffusion effects delay the penetration of dilute water such that it takes thousands of years to obtain dilute conditions (0.3 g/L) in more than a few percent of deposition holes (approximately 4% at 1000 years).

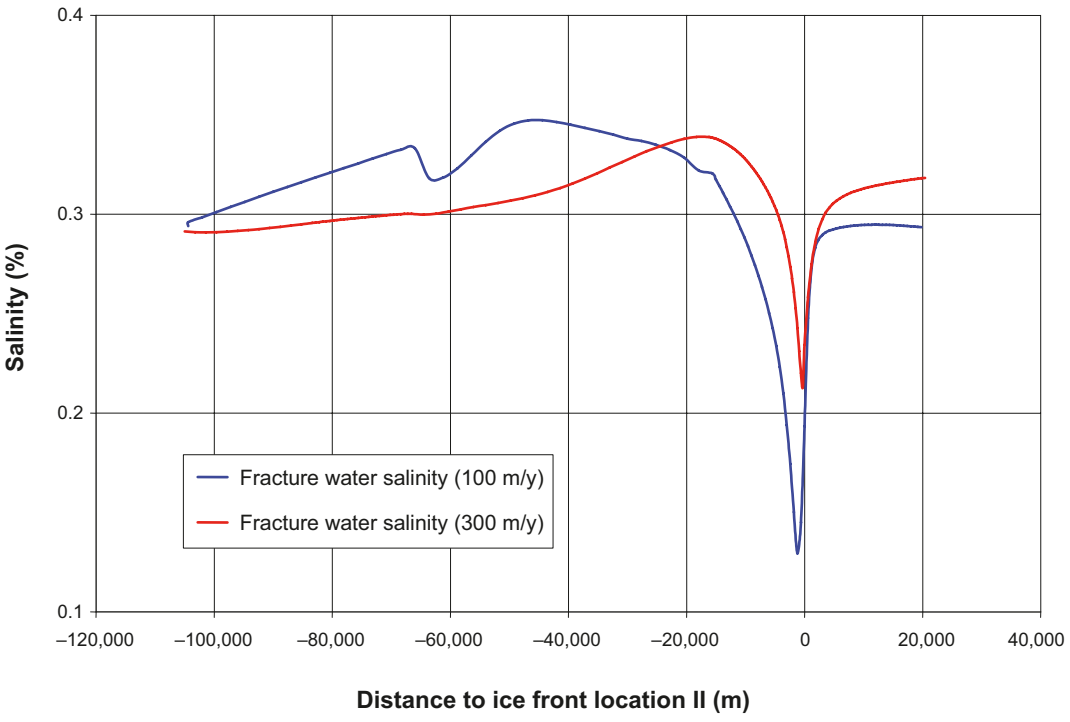


***Figure 6-9.*** *Plot showing the difference in flushing as a function of the average speed of the retreating ice sheet margin at ML 2. A retreat speed of 300 m/y yields lesser flushing. (The ice sheet margin moves from left to right in this plot.)*

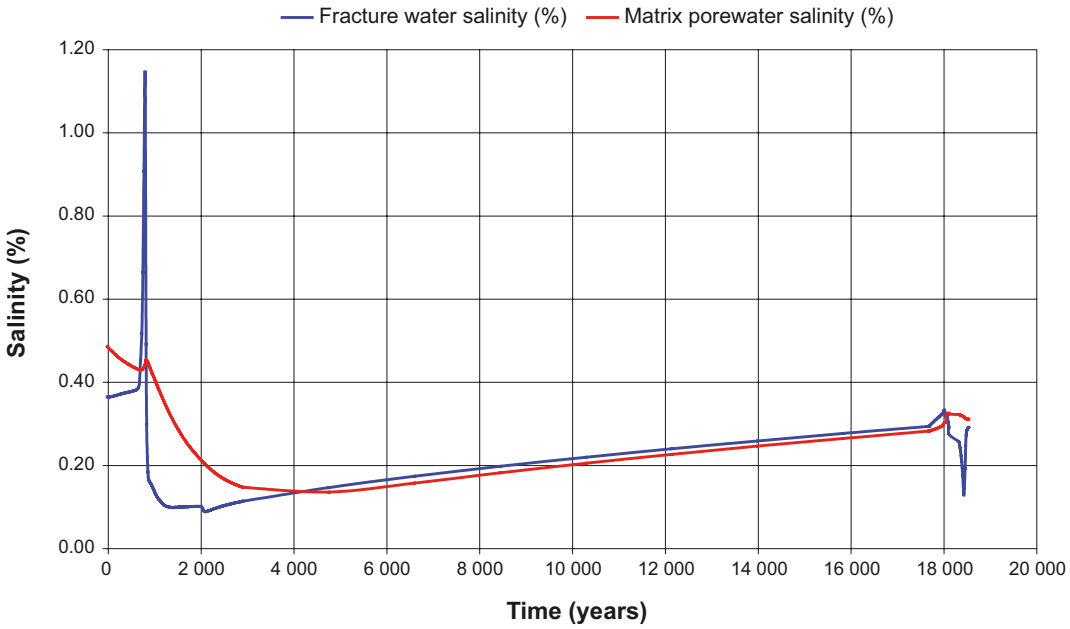


***Figure 6-10.*** *Plot showing the fracture water and matrix porewater salinities at ML 2 during approximately 19,000 years for the Glacial Case without Permafrost.*

### 6.4.2 Recharge and discharge locations in the biosphere

The top image in Figure 6-11 shows the recharge and discharge locations when the ice sheet margin reaches ice front location II for the glacial case without permafrost, and the bottom image shows the corresponding results for the glacial case with permafrost. For both cases, a number of particles recharge at the upstream boundary of the model domain, which suggests that the model domain is too short to give a fully undisturbed view of all recharge locations for a fixed Darcy flux field. Nevertheless, it may be concluded that the present-day topographic water divides are significantly diminished during glacial conditions. In contrast, the discharge locations are predominantly found well within the physical boundaries of the model domain and often very close to the ice sheet margin. The differences seen between the two glacial cases are largely caused by the permafrost. For the Glacial case with permafrost, there are two centres of discharge:

- The deformation zone model that exists within the regional model domain for SDM-Site Forsmark. Two percent of the released particles exit along deformation zones.
- The taliks positioned at the topographic lows in front of the ice sheet margin to the east (outside the regional model domain). The taliks catch about 98% of the released particles.

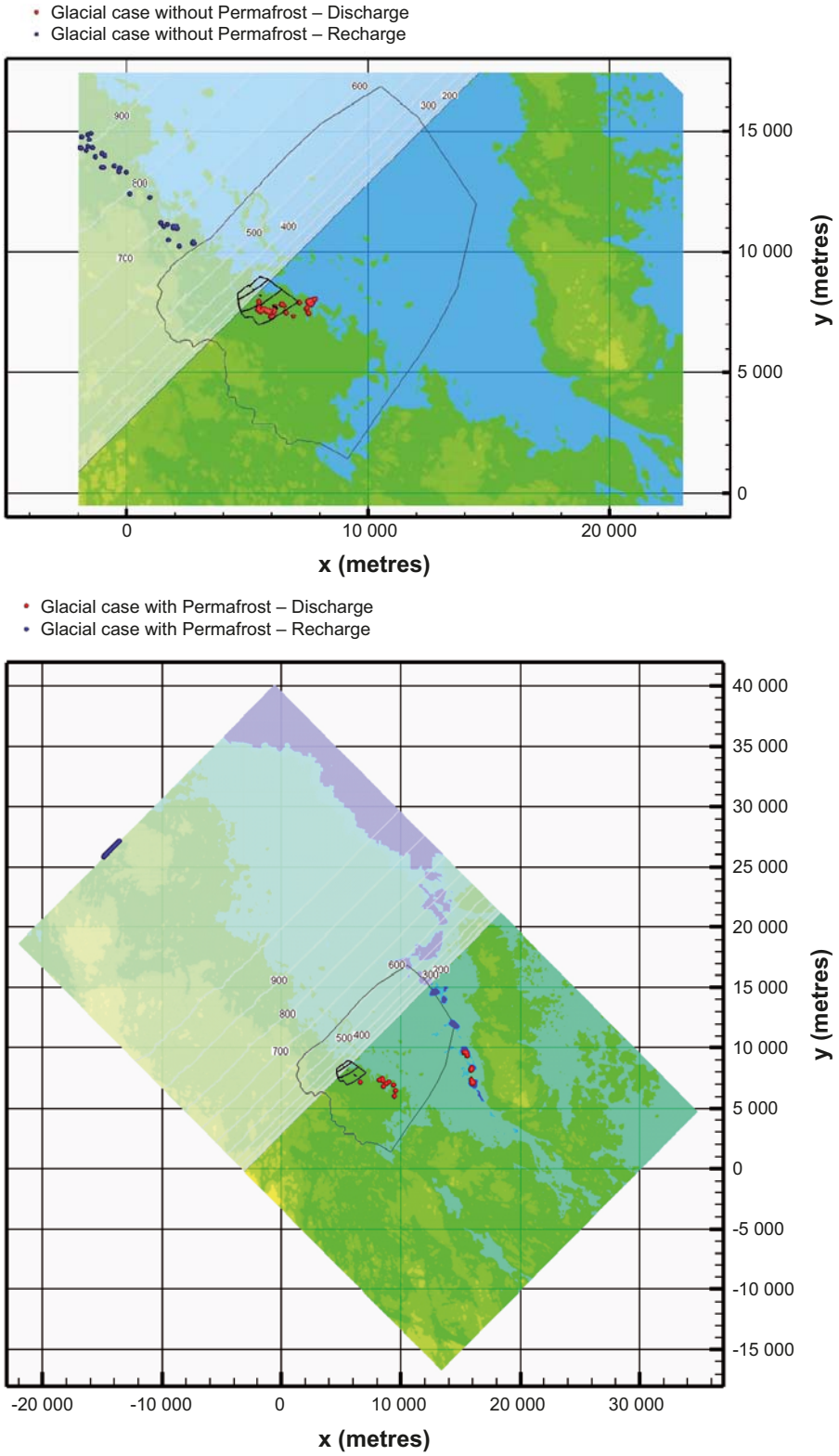


***Figure 6-11.*** *Recharge (blue) and discharge (red) locations of the 6,916 particles released at repository depth when the margin of the advancing ice sheet profile is at ice front location II. Top: Glacial case without permafrost. Bottom: Glacial case with permafrost and taliks. The taliks are positioned at the topographic lows in front of the ice sheet margin to the east (outside the regional model domain).*

### 6.4.3 Performance measures

The performance measures of interest are the Darcy flux (and equivalent flow rate) at each deposition hole position, and the flow-related transport properties along flow paths from the deposition hole positions, i.e. the advective travel time and flow-related transport resistance. In principle, these are directly obtained from the super-regional model /Vidstrand et al. 2010/ for all ice front locations. However, the repository structures are not explicitly included in this model, and hence results for the different release paths Q1, Q2 and Q3 are not obtained. By transferring boundary conditions from the super-regional scale model to the combined repository-scale and site-scale models of /Joyce et al. 2010/ where the repository is included, all performance measures needed for subsequent radionuclide transport calculations are obtained.

In Figure 6-12 and Figure 6-13, the Darcy flux and flow-related transport resistance are shown for the Q1 path for the glacial case without permafrost for a situation where the ice front is located close to the centre of the repository area (ice front location II). It is observed that the median Darcy flux is increased by approximately an order of magnitude. A corresponding decrease of the flow-related transport resistance is observed. Also, the results indicate that the high Darcy fluxes are more influenced by the glacial boundary conditions than the low values; e.g., the 90$^{th}$ percentile is more shifted than the 10$^{th}$ percentile. Thus, it appears that regions with low flow are relatively less affected by the high gradients induced by the ice sheet than regions with high flows.

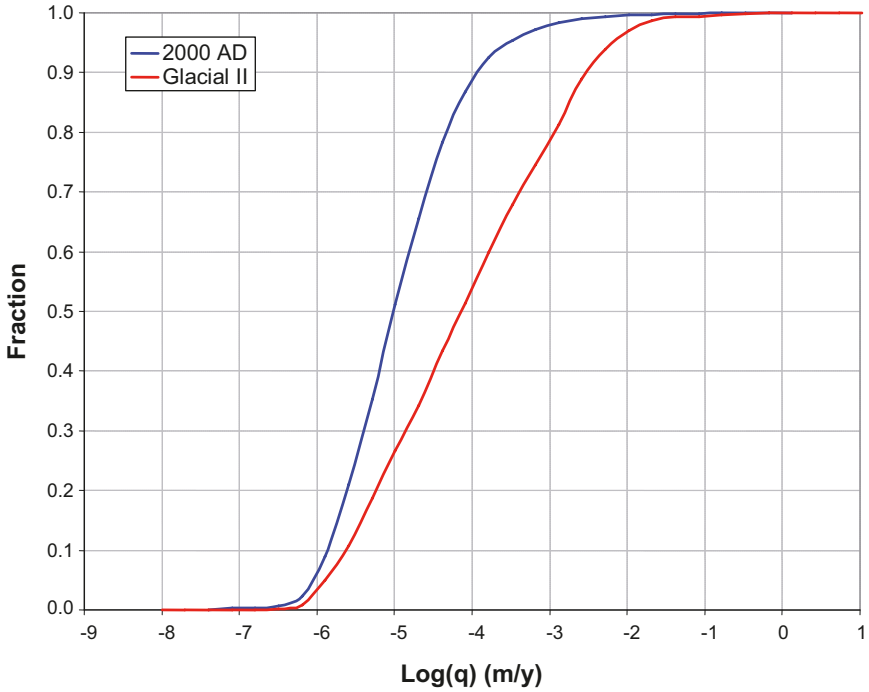


***Figure 6-12.*** *Cumulative distribution function plot of the Darcy flux (q) for the Q1 path for the hydrogeological base case at 2000 AD (2000 AD) and the Glacial Case without Permafrost when the ice sheet margin is at ice front location II (Glacial II).*

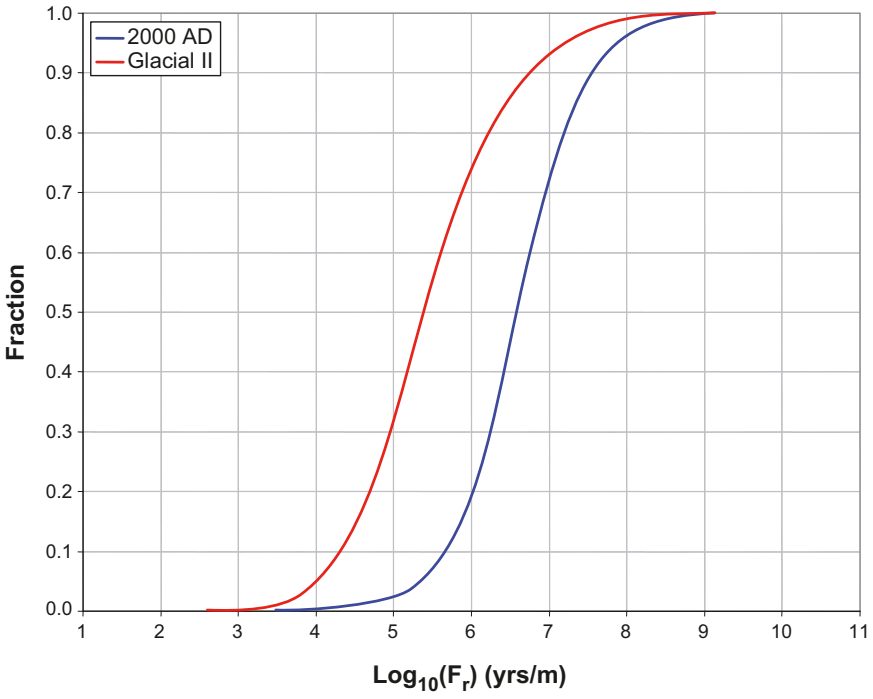


***Figure 6-13.*** *Cumulative distribution function plot of the flow-related transport resistance (F) for the Q1 path for the hydrogeological base case at 2000 AD (2000 AD) and the Glacial Case without Permafrost when the ice sheet margin is at ice front location II (Glacial II).*

### 6.4.4 Penetration of glacial melt water

In principle, the future groundwater chemistry, specifically salinity, is provided by the super-regional scale groundwater flow simulation reported above. However, the super-regional scale model has a fairly coarse discretisation, which does not allow an assessment of the groundwater chemistry evolution on a deposition hole scale. Thus, an alternative assessment of the evolution of the groundwater chemistry, and specifically the potential for penetration of dilute water, is made.

The combined repository-scale and site-scale models of /Joyce et al. 2010/ with boundary conditions from the super-regional scale model of /Vidstrand et al. 2010/ are used. The cases with an advancing ice sheet margin without permafrost for ice-front locations II and V are analysed. In order to assess the potential for penetration of diluted water, an injection of glacial meltwater along all recharge paths is considered for these two ice front locations. Similar simplifying assumptions as used for the temperate period calculations presented in Section 5.4.5 are adopted here. Along the flow paths, the only mitigating process considered is the out diffusion of salt from the matrix affecting the penetration of the glacial meltwater front. It is assumed that the salt concentration of the matrix water is in equilibrium with the fracture water prior to the injection of glacial meltwater with a salt concentration of 0 g/L. The simplifying nature of these assumptions are discussed in Section 2.5. In Figure 6-14 and Figure 6-15, the temporal distribution for all deposition hole positions to obtain ten per cent of the initial water concentration is shown for ice front location II and V, respectively. The initial salt concentration of the fracture water before the onset of the glacial period is estimated to be 3 g/L, see Section 10.4.7 of the SR-Site Main report. Ten per cent of the initial concentration thus corresponds to 0.3 g/L, which coincides with the value assumed to represent dilute conditions with potential buffer erosion. The vertical lines represent the assumed approximate duration of the periods. For ice front location II, i.e. close to the centre of the repository area, the assumed durations are 20 and 100 years. The longer duration is an estimate for an advancing ice front, whereas 20 years is an estimate for a retreating ice front; however, all results presented in the figure are based on a flow field obtained for an advancing ice sheet. For ice-front location V, i.e. the glacial maximum case (LGM), two time durations are assumed, 20,000 and 100,000 years. It is observed that approximately two per cent of deposition hole positions experience dilute conditions during an advancing ice front and also during an assumed period of 100,000 years corresponding to glacial maximum conditions.

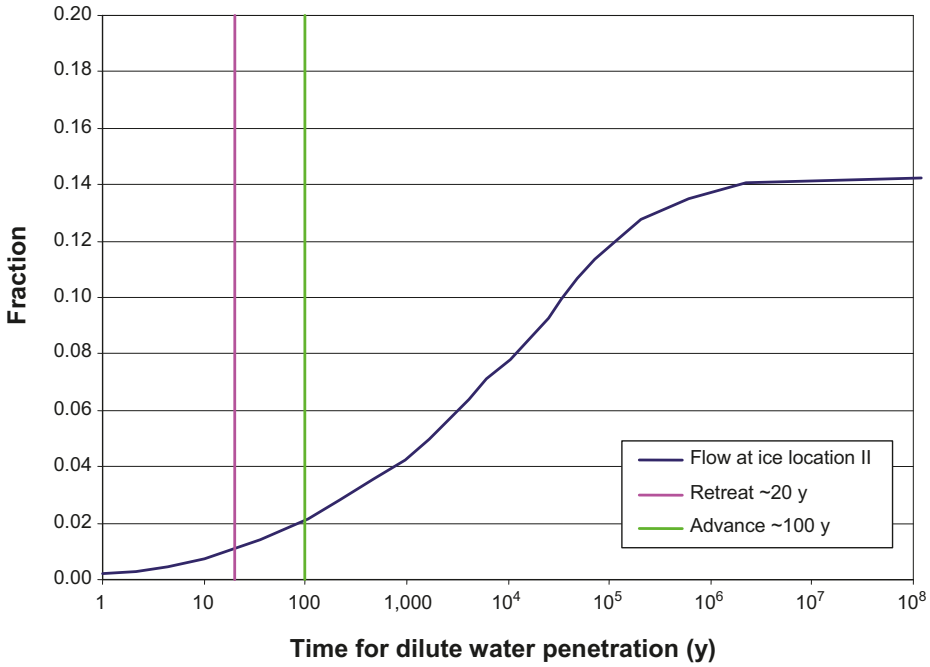


***Figure 6-14.*** *Temporal distribution for all deposition holes to obtain ten per cent of the initial water concentration for an ice sheet margin that is at rest at ice-front location II for 20 years and 100 years.*

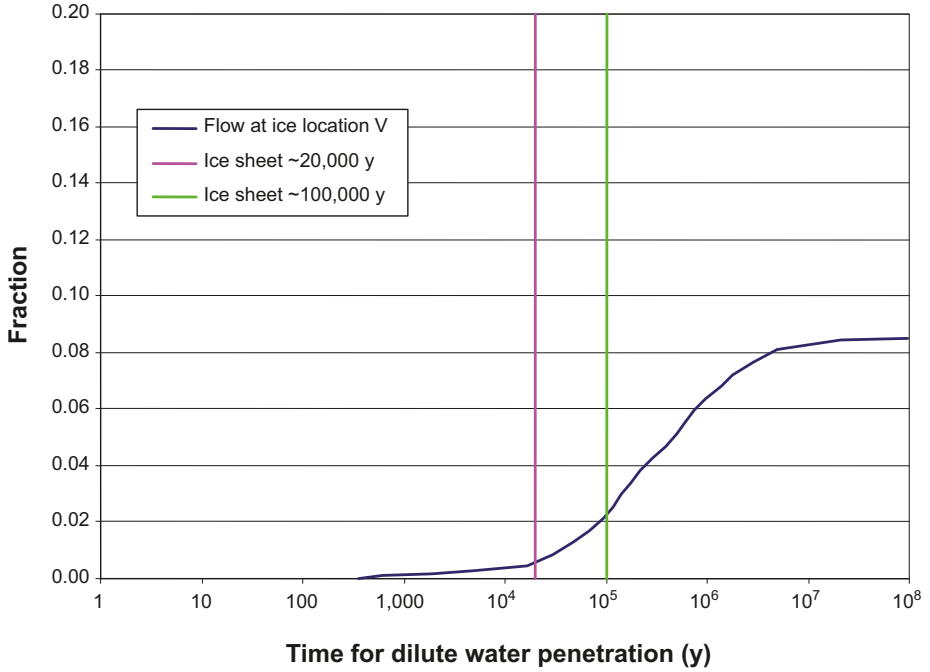


***Figure 6-15.*** *Temporal distribution for all deposition holes to obtain ten per cent of the initial water concentration for two assumed durations of complete ice coverage, 20,000 years and 100,000 years.*

The calculations provided here are bounding estimates; as shown in the results above for the temporal evolution during a glacial cycle, the salinity in the system is in fact restored at repository depth due to up-coning effects. Also, as discussed in Section 2.5 but not accounted for here, water-rock interactions will also modify the water chemistry. Thus, penetration of dilute water with zero concentration for an extended period of time is a conservative assumption.

### 6.4.5 EDZ and crown space

In the hydrogeological base case model, a continuous excavation damaged zone (EDZ) is implemented in all tunnels (both deposition tunnels and other tunnels) under the tunnel floor. The EDZ has a transmissivity value of $T = 1 \cdot 10^{-8}$ m$^2$/s and a thickness of 0.3 m. In order to assess the sensitivity in performance measures on tunnel properties, four alternative cases are analysed. Two of these have higher EDZ transmissivities ($T = 1 \cdot 10^{-7}$ m$^2$/s and $T = 1 \cdot 10^{-6}$ m$^2$/s, respectively), one case has no EDZ, and the final case has the base case EDZ properties, but is combined with a crown space under the tunnel ceiling. The crown space represents a consolidation of the backfill material. In the model, the crown space is implemented as a 0.1 m thick zone with a high conductivity value ($K = 1 \cdot 10^{-3}$ m/s) and a porosity equal to unity.

The Darcy flux for the Q2 path is shown in Figure 6-16. Since the Q2 path corresponds to the EDZ path, no result exists per definition for the case with the EDZ removed. The figure clearly shows, as expected, that an increase in the EDZ transmissivity implies an increase in the associated Darcy flux in the EDZ. The crown space implies a small reduction of the Darcy flux in the EDZ; i.e. the flow is redistributed to the crown space from the EDZ.

The flow-related transport resistance of the Q3 path is shown in Figure 6-17. It is observed that more favourable results are obtained when the EDZ is removed, whereas all other cases imply less favourable conditions. The existence of a crown space is by far the most unfavourable situation. Also worth noticing is that the crown space seems to have a stronger influence for the glacial conditions than for the temperate conditions (Section 5.3.5). This is likely due to the modified flow direction and larger flows to be accommodated during the glacial flow regime; the flow is thus preferentially directed to the high permeability crown space. With flow paths preferentially going through the crown space, less flow-related transport resistance is accumulated in the fractured rock.

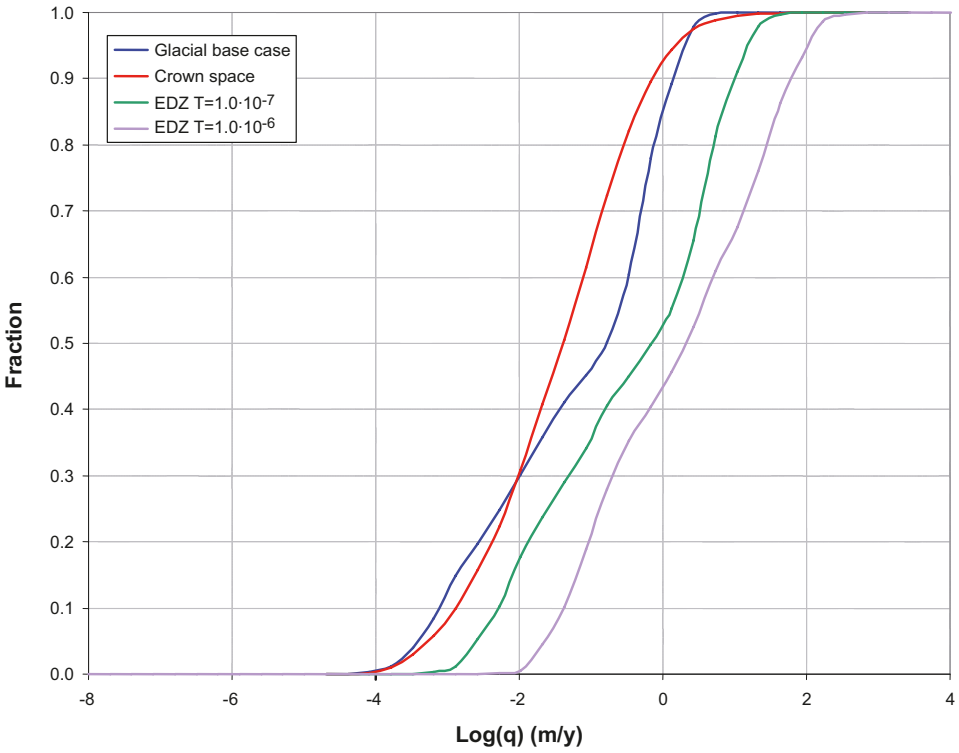


***Figure 6-16.*** *Cumulative distribution function plot of the Darcy flux (q) at ice front location II for release path Q2 for the hydrogeological base case model (Glacial base case), the crown space model (Crown space), the EDZ $T = 1 \cdot 10^{-7}$ m$^2$/s model , and the EDZ $T = 1 \cdot 10^{-6}$ m$^2$/s model. (Modified after Figure E-56 in /Joyce et al. 2010/.)*

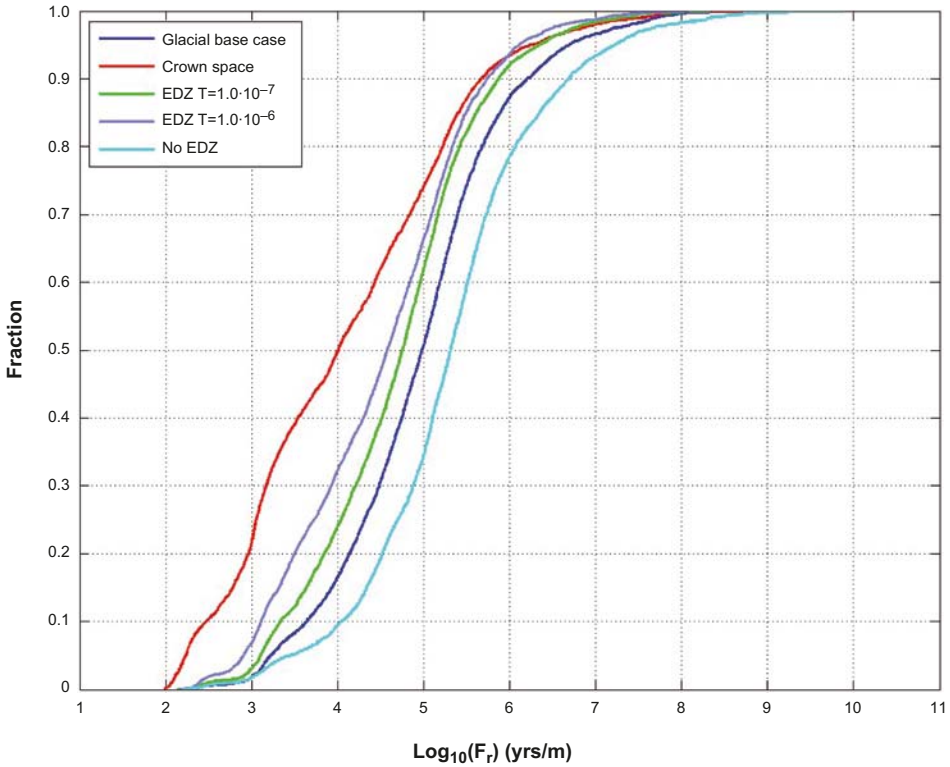


***Figure 6-17.*** *Cumulative distribution function plot of the flow-related transport resistance (F) at ice front location II for release path Q3 for the hydrogeological base case model (Glacial base case), the crown space model (Crown space), the EDZ T = 1·10⁻⁷ m²/s model, the EDZ T = 1·10⁻⁶ m²/s model, and the No EDZ model.*

### 6.4.6 Site related variants

#### *N-S ice advance direction*

Figure 6-18 displays the Darcy fluxes at measurement localities 2 and 4 for the two different ice advance directions. The evolutions and magnitudes are quite similar. Thus, the simulation results reported by /Vidstrand et al. 2010/ suggest minor differences, of insignificant importance for SR-Site, between these two cases.

#### *THM properties*

The simulation results reported by /Vidstrand et al. 2010/ suggest insignificant differences in the peak Darcy fluxes values between an undistorted permeability field and a stress-distorted (increased) permeability field, see Figure 6-19. The stress-distored permeability field uses values based on the THM modelling reported by /Hökmark et al. 2010/.

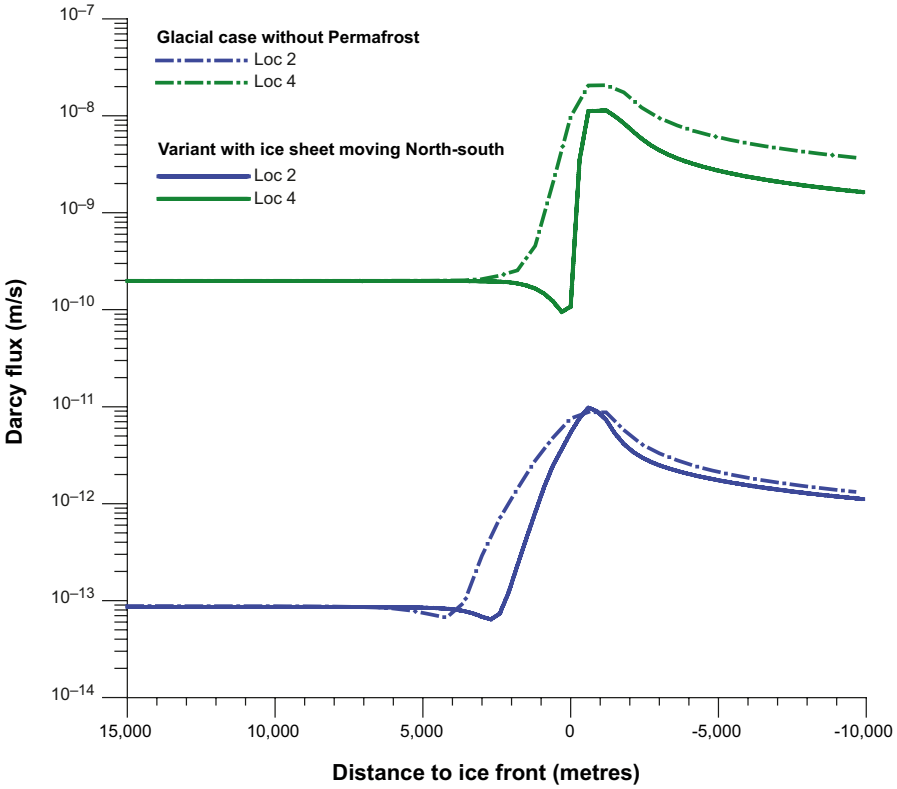


***Figure 6-18.*** *Comparison between the Darcy flux at ML 2 and ML 4 during glaciation for the two ice sheet movement directions considered; Dashed line = NW-SE, Solid lines = N-S. Positive distance values mean that the ice sheet margin has not yet arrived at the measurement localities.*

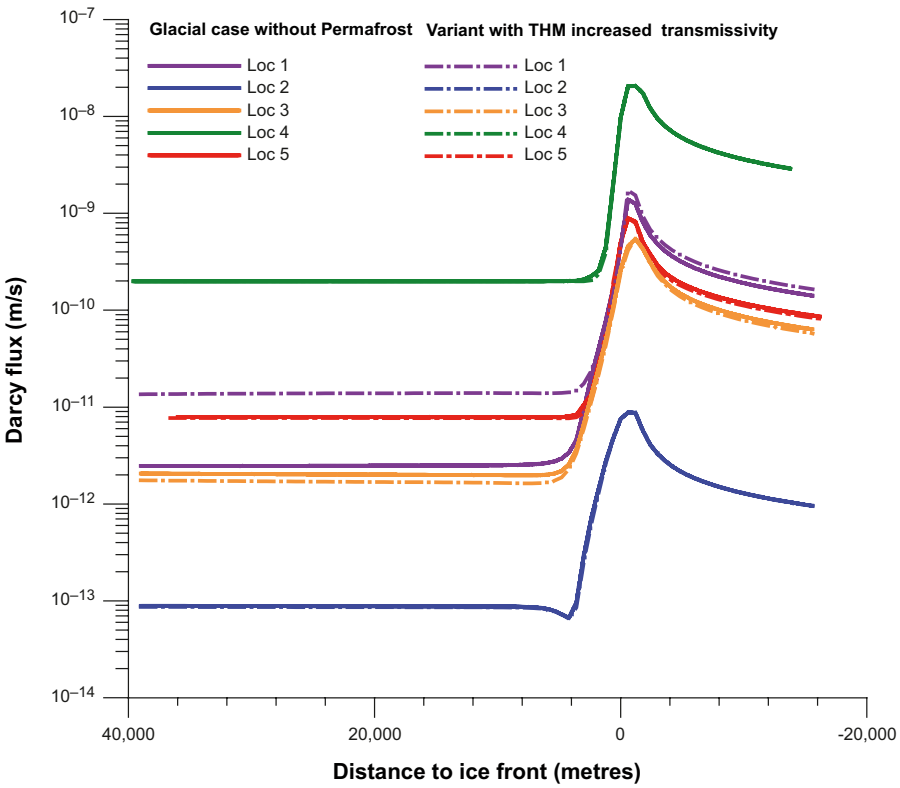


***Figure 6-19.*** *Comparison between the Darcy flux at ML 1–5 during glaciation for the two permeability conditions considered; Dashed lines = Disturbed permeability, Solid lines = undisturbed permeability. Positive distance values mean that the ice sheet margin has not yet arrived at the measurement localities.*

### 6.4.7 Comparison of the Darcy flux at different time slots during glaciation and deglaciation.

Figure 6-20 shows the minimum, median and maximum values of the Darcy flux at all deposition hole positions during the main "climate events" during the simulated period (IFL 0 → IFL V → IFL 0) of periglacial and glacial climate conditions. These main "climate events" are:

- Temperate (used as a reference to which the other results below are scaled (normalised) against).
- Glacial without permafrost.
- Glacial maximum.
- Submerged.
- Permafrost.
- Glacial with permafrost and a 2 km long tongue.
- Glacial with permafrost but no tongue.

The climate condition glacial without permafrost provides the highest maximum as well as highest median value of all simulated climate events. Relative to the median temperate period value, the median value of glacial without permafrost is almost two orders of magnitude higher. The maximum value of glacial without permafrost value is also almost two orders of magnitude higher than the maximum temperate period value.

In the radionuclide transport calculations of SR-Site, see Chapter 13 of the SR-Site Main report, one approach to incorporate flow changes during the climate evolution is to take the flow paths and performance measures obtained from the combined repository-scale and site-scale models, and scale the measures by factors that are obtained by scaling all different periods in Figure 6-20 by the temperate period values. The result is shown in Figure 6-21. Here it is observed that when conditions of only permafrost prevail, or when the domain is submerged, the smallest Darcy fluxes of all climate situations and also the smallest scaling factors are obtained. The values for these two cases are below the temperate period value.

Two issues of particular importance in SR-Site are buffer erosion and canister corrosion over a glacial cycle, see SR-Site Main report Sections 10.3 and 10.4. Figure 6-22 shows normalised average values of the three powers of the Darcy flux that are of interest, ($q$, $q^{0.41}$, $q^{0.5}$). These are obtained by averaging the Darcy flux values calculated from the "Glacial Case without Permafrost" over a full glacial cycle (120,000 years) and then normalise against the corresponding temperate value. It is observed that for measurement locality ML 2, which is located inside the repository footprint, the normalised average value is about 0.8; i.e. the Darcy flux averaged over the 120,000 year glacial cycle is below the corresponding value of the temperate period. In comparison, the normalised average value is greater than 1.0 for measurement localities ML 1 and ML 3 that are located outside the repository footprint close to deformation zones that strike parallel to the flow direction of the ice sheet.

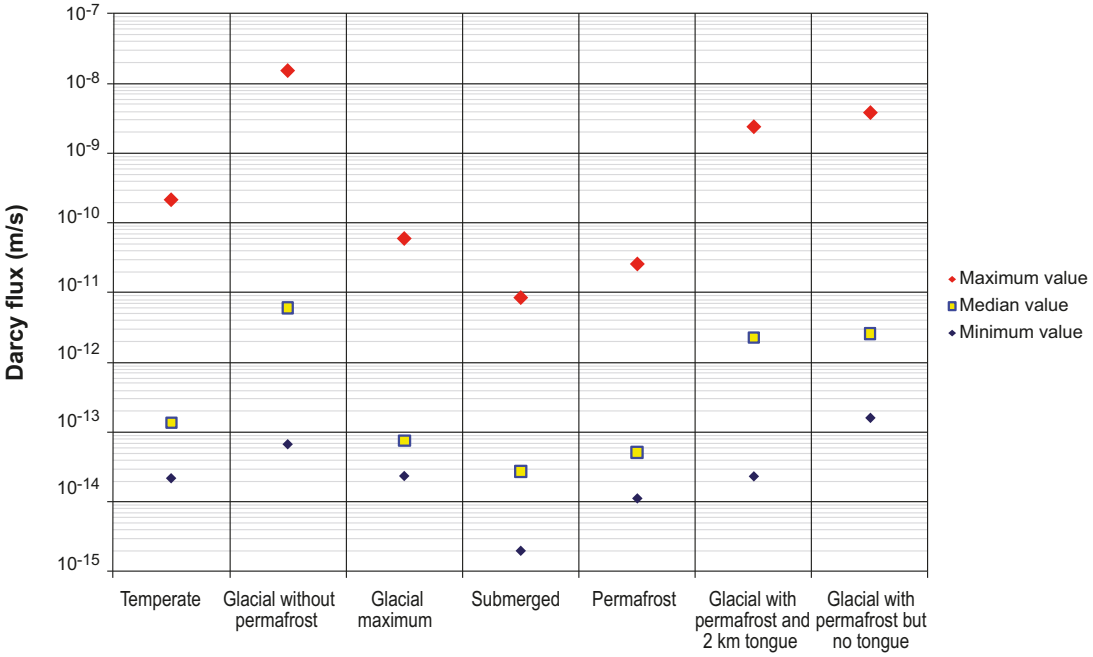


***Figure 6-20.*** *Estimated Darcy fluxes for the main climate situations considered during the simulated period (IFL 0 → IFL V → IFL 0) of periglacial and glacial climate conditions.*

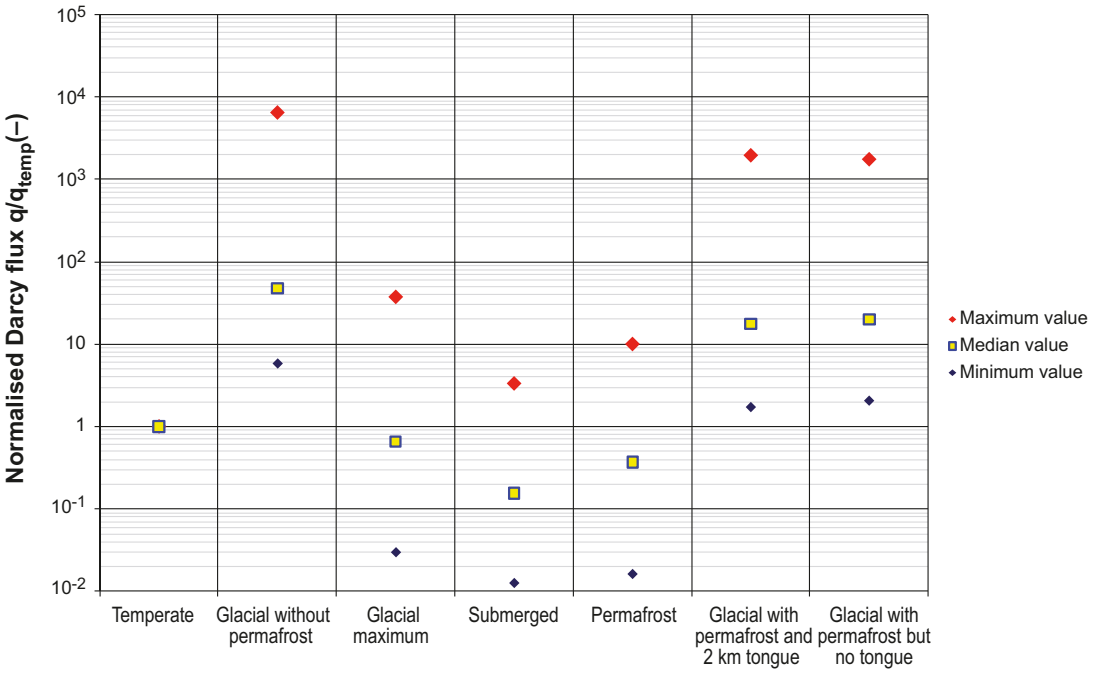


***Figure 6-21.*** *Estimated Darcy flux scaling (multiplication) factors for the main climate situations considered in a full glacial cycle.*

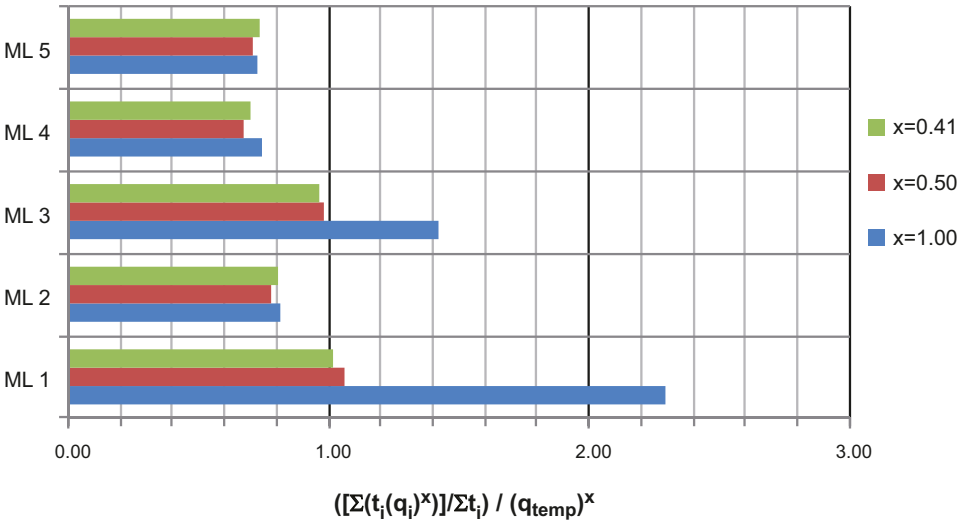


***Figure 6-22.*** *Plot of three kinds of powers of the Darcy flux ($q$, $q^{0.41}$, $q^{0.5}$) averaged over a full glacial cycle and normalised against the corresponding temperate value ($q$, $q^{0.41}$, $q^{0.5})_{temp}$. ML = measurement locality. These averages are used in buffer erosion and canister corrosion calculations, see Sections 10.4.8 and 10.4.9 in SR-Site Main report for details. The glacial period within the glacial cycle is based on the case with glacial conditions without permafrost.*

## 6.5 Assumptions, simplifications and uncertainties

Main assumptions, simplifications and uncertainties related to the study of the evolution for the remaining part of the reference glacial cycle are:

- /Vidstrand et al. 2010/ assume a specified head at all locations under the ice sheet at all times, which is a common assumption in this field of science. Nonetheless, it is not clear that the water pressure at the ice-subsurface interface should be related to the ice sheet thickness under all circumstances as it implies an infinite source of water. For instance, the pressure field may be affected by structures at the ice-subsurface interface, e.g., ice tunnels that carry melt water to the ice sheet margin. The role of ice tunnels are not considered in SR-Site based on the arguments discussed in the Climate report. Another general simplification is in the particle tracking, which is made for a steady-state flow condition although the boundary conditions are constantly and rapidly changing in comparison to the advective travel times. That is, the calculated performance measures such as advective travel time and flow-related transport resistance would increase if the boundary conditions are changing during the particle tracking as the flow paths get longer.
- Several processes take place during a glacial cycle that affect the groundwater salinity. A number of processes are accounted for in /Vidstrand et al. 2010/; however the body of these are of hydrological (physical) nature rather than chemical. A process not accounted for in /Vidstrand et al. 2010/ is the out-freezing of salt (salt rejection) during permafrost growth. In the analysis of penetration of glacial meltwater, water-rock interaction processes are neglected. Regardless of the case studied, an ice sheet without permafrost or an ice sheet with permafrost, a number of particles recharge at the upstream boundary of the model domain, which suggests that the model domain is too short to give a fully undisturbed view of all recharge locations. Nevertheless, it may be concluded that the present-day topographic water divides, which play an important role for the recharge and discharge during temperate conditions, are significantly diminished during glacial conditions. In contrast, the discharge locations are predominantly found well within the physical boundaries of the model domain and, as a matter of fact, often very close to the margin of the ice sheet. The differences seen in the discharge pattern between the two glacial cases are largely caused by the varying hydraulic properties and boundary conditions. The uncertainty in the occurrence of taliks, which may act as major discharge areas in the case of permafrost in the periglacial area in front of the ice sheet margin, is discussed in /SKB 2010a/.

- The same uncertainties in resulting performance measures as in the temperate simulations apply to the simulations based on the combined repository-scale and site-scale models using glacial boundary conditions. In addition, the transfer of boundary conditions from the super-regional model to these smaller scale models implemented in a different numerical flow code implies uncertainties.
- Concerning penetration of glacial melt water, it is shown in Figure 6-14 that there may be some well connected deposition hole positions where the transport resistance is so low that dilute groundwater will penetrate to repository depths. The assessment of penetration of dilute water should be considered an approximate quantification. The same uncertainties as listed for the corresponding analyses performed for temperate conditions apply here. Specifically, steady-state flow fields are used, and no mixing or water-rock interactions are considered. The results of the analysis of penetration of glacial melt water are propagated for further assessment. Concerning EDZ and crown space, the same uncertainties as listed above for performance measures apply here.
- None of the studied site-related variants provide significantly different results to those of the base case, i.e. the case with a steep ice sheet profile without permafrost moving from NW to SE. It is noted that the use of the theoretical maximum ice sheet profile during the post-LGM stage is probably a considerable exaggeration of the conditions during deglaciation (retreat) compared to the reference evolution suggested in /SKB 2010a/. Furthermore, it is noted that the applied change in transmissivity in the hydro-mechanical variant case exceeds the change suggested in the THM modelling within the SR-Site project.
- An advancing ice sheet with permafrost ahead is considered a more realistic case than an ice sheet without permafrost. However, none of the two permafrost cases studied render significantly different results than the base case, i.e. an advancing ice sheet without permafrost. It is noted that the simulations with ice sheet and permafrost combined had to be stopped at ice front location IV (IFL IV) to avoid numerical instabilities. These arise when the ice sheet margin gets close to the downstream boundary and the discharge at ground surface in the periglacial area is prohibited due to the permafrost growth.
- The comparison of the Darcy flux at different time slots during glaciation and deglaciation is merely a different way of illustrating the main results. Thus, no additional uncertainties per se are introduced in this comparison. However, the outlined methodology of using scaling factors for the performance measures representing the different climate regimes clearly is a simplification of the real development depicted in /SKB 2010a/, and hence implies an additional uncertainty. For the subsequent assessment, it is suggested that an ice sheet with permafrost in front of the ice sheet margin is used for the pre-LGM stage, and a retreating ice sheet with submerged ground conditions in front of the ice sheet margin for the post-LGM stage.

# 7 Integration between time periods and disciplines

The different modelling studies deal with different time periods. In order to assess the full time evolution, the results from the different modelling studies have to be combined and put into a common context. Specifically, a few important couplings between the studies/time periods exist; these are an evaluation of deposition hole positions with potentially high flows during both conditions of repository operation and during subsequent saturated conditions, a consistency check of the simulated matrix diffusion effects in the two codes used, and a consistency check of performance measures calculated in the super-regional model for glacial conditions with corresponding performance measures calculated in the finer-resolution models with boundary conditions transferred from the super-regional model.

Finally, a brief listing is made of the other disciplines within SR-Site where results from the bedrock hydrogeological modelling are used.

## 7.1 Flow correlation between open and saturated repository conditions

The flow models used in the Excavation and operational phase /Svensson and Follin 2010/ and in the Temperate period /Joyce et al. 2010/ both use the same model domain, the same parameterisation of discrete deformation zones, and the same realisation of the stochastic fracture network. Also, both models have the repository included explicitly in the models, albeit using different delivery formats[7]. Thus, both models contain the same site and repository data.

In Chapter 4, it is shown and discussed how the Equivalent Discontinuous Porous Medium (EDPM) approach of /Svensson and Follin 2010/ is a preferable approach over the traditional Equivalent Continuous Porous Medium (ECPM) approach when inflow to individual deposition holes are considered in a low permeability environment. This is due to the fact that deposition holes with no fracture intersections in the EDPM model can be resolved as truly no-flowing since no background conductivity is required. With the EDPM approach, exactly the same deposition holes are connected as in the discrete fracture network model of /Joyce et al. 2010/. This provides a possibility to evaluate, on a per deposition hole basis, how inflows during the operational phase correlate with flows through the deposition holes during saturated conditions.

As pointed out in Chapter 4, inflow rejection criteria are originally defined in order to mitigate problems with erosion of backfill material. However, if deposition holes with high inflows during the operational phase are excluded, and a positive correlation exists between inflows during the operational phase and flows during saturated conditions, inflow rejection criteria will also have a positive effect on long term safety.

In Figure 7-1 below, a scatter plot of all deposition holes (6,916 deposition holes) are shown with inflow during the operational phase on the x-axis, and the corresponding Darcy flux during saturated conditions on the y-axis. The plot is for grouted conditions (i.e. grout is applied for the operational phase simulation) as this is a more realistic situation and likely also causes a possible correlation to somewhat deteriorate. Deposition holes that have an inflow smaller than $10^{-6}$ L/min but a Darcy flux larger than $10^{-8}$ m/y are indicated on the y-axis of the plot. Deposition holes that have a Darcy flux smaller than $10^{-8}$ m/y but an inflow larger than $10^{-6}$ L/min are indicated on the x-axis. Deposition holes that have inflows smaller than $10^{-6}$ L/min and a Darcy flux smaller than $10^{-8}$ m/y are indicated at the origin of the plot.

In Figure 7-1 it is seen that 372 (252+120 where 117+135=252) deposition holes have inflows larger than $10^{-6}$ L/min. These are the positions that have failed the combined inflow rejection criteria, namely that a hole should have an inflow rate larger than 0.1 L/min (indicated by the dashed vertical line in the plot), or have an inflow rate larger than 1% of the total flow rate in the deposition tunnel including

[7] /Svensson and Follin 2010/ use imported CAD files, whereas /Joyce et al. 2010/ use an equivalent implementation thereof.

all its deposition holes. It is noted that a majority of these deposition holes have an inflow below 0.1 l/min; i.e. they fail the second criterion (related to 1% of the the total flow rate in the deposition tunnel including all its deposition holes). Also seen in the figure is that there are 6,544 (4,788+1,756) deposition holes that have an inflow below $10^{-6}$ L/min; hence, in total all 6,916 (372+6,544) deposition holes are identified in the figure.

Deposition holes failing the "FPC or EFPC" criterion, see Section 3.2 for details concerning FPC and EFPC, are indicated with red markers in Figure 7-1. It is seen that 141 (135+6) out of the 372 (252+120) positions that fail the inflow rejection criteria also are identified by the EFPC. However, the EFPC also identifies 471 (425+46) positions that have inflows below $10^{-6}$ L/min.

From a long-term safety point of view, one would like to avoid deposition holes with high Darcy flux values, say as an illustrative example values above $10^{-3}$ m/y. If the "FPC or EFPC" criterion is applied, essentially all deposition hole positions with high Darcy fluxes during saturated conditions are identified (only a few values with Darcy flux around $10^{-2}$ m/y are not identified). However, the criterion also identifies a number of positions with lower values; these deposition holes would be abandoned applying this criterion even if not strictly motivated from a hydrogeological long term safety point of view. Since the "FPC or EFPC" criterion in practice may be hard to apply, it is of interest to evaluate if an inflow rejection criterion would be equally successful.

If the inflow criterion "Q1 or Q2" is applied instead of the "FPC or EFPC" criterion, it is seen that all deposition holes except one (the highest value on the y-axis) are found if Darcy fluxes greater than $10^{-3}$ m/y are considered. However, if the threshold value to avoid would be a Darcy flux of $10^{-4}$ m/y, there are a number of additional deposition holes that the inflow rejection criterion would not be able to identify (blue markers on the y-axis between $10^{-4}$ and $10^{-3}$ m/y). Furthermore, if the inflow criterion only considers an inflow rate larger than 0.1 L/min, the number of deposition holes not identified would also increase. Finally, it is observed that the inflow criterion identifies a number of deposition holes that do not constitute a problem for long term safety, e.g., 120 holes with Darcy flux below $10^{-8}$ m/y are identified. However, since the total number of deposition hole positions identified by the "FPC or EFPC" criterion is higher than the number identified by the inflow rejection criteria (612 vs 372), and both methods identify the most problematic positions, one can conclude that the inflow rejection criteria are more efficient.

To summarise, there is a positive correlation between inflows during open conditions and Darcy flux during saturated conditions for the deposition holes. Specifically, there are no, or very few, deposition holes with high Darcy fluxes that would not also have a high enough inflow during open conditions to fail a plausible inflow rejection criterion. Conversely, however, there are a number of deposition holes with inflows that fail the inflow criterion, but that have very low Darcy fluxes. Thus, given the correlation structure, it seems realistic to be able to identify deposition holes with unfavourable characteristics for long term safety by the application of inflow rejection criteria during open repository conditions (i.e. during the operational phase). However, the application of inflow rejection criteria will likely also result in rejection of some deposition holes that do not have unfavourable characteristics, but the same holds true for "FPC or EFPC" criterion, see discussion above. To conclude, inflow rejection criteria appear as a good complement to the "FPC or EFPC" criterion in terms of identifying unfavourable deposition hole positions in terms of Darcy flux during saturated conditions. It is noted that the "FPC or EFPC" criterion also has relevance for reducing risk associated with e.g. earthquakes; hence, the inflow rejection criteria alone may not be sufficient to identify unsuitable deposition hole positions. A combination of both types of criteria likely needs to be considered in the future.

It is noted that during open repository conditions, the largest gradients are found at the rim of the repository whereas the tunnels within the repository footprint are characterised by lower gradients. This results in larger inflows into the tunnels at the rim of the repository as seen in Figure 4-4. Also, one may hypothesise that this feature of uneven driving forces affects the inflow pattern into individual deposition holes presented in Figure 4-6. Thus, a perfect correlation in flows between open repository and saturated conditions should not be expected. Furthermore, even if a deposition hole constitutes a dead-end in the network of fractures and tunnels, it may be part of the connected fracture system during open conditions since the deposition hole will be at atmospheric pressure and hence be a sink in the system, see /Svensson and Follin 2010/ for details. This also implies that deposition holes that are active during open conditions may have no flow during saturated conditions, and hence result in less overall correlation in flows between the two time periods.

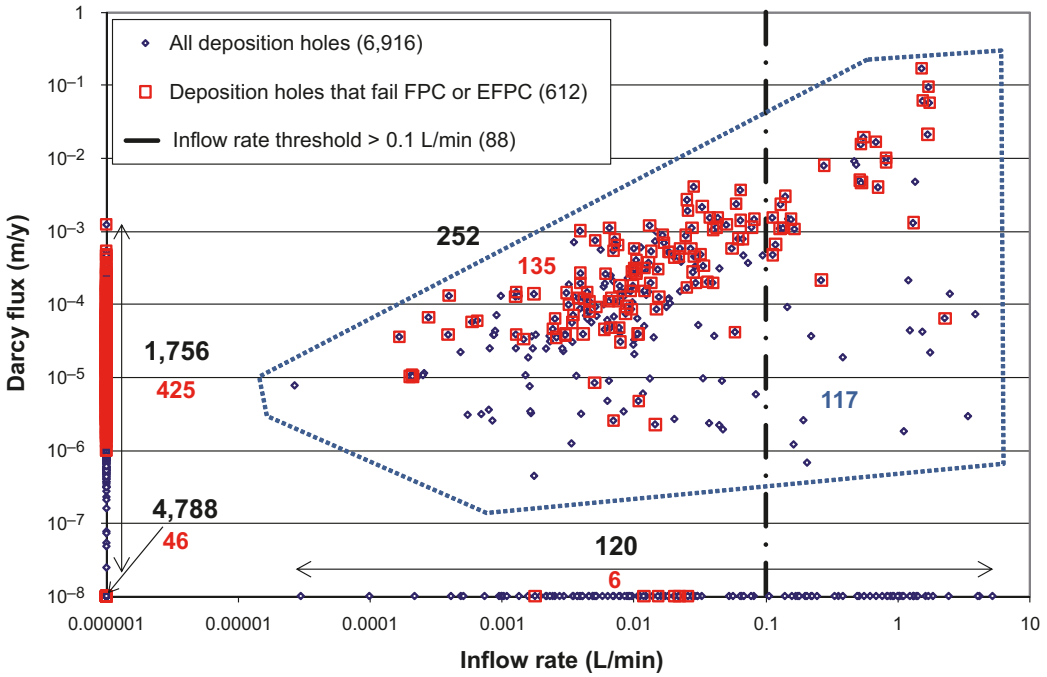


***Figure 7-1.*** *Scatter plot between inflow rate in deposition holes during open repository conditions with grouting and Darcy flux through the deposition holes during saturated repository conditions. See text for details concerning the numbers in the plot.*

## 7.2 Quantification of matrix diffusion effects

Matrix diffusion of dissolved salts is included in all groundwater flow modelling studies conducted for SR-Site. However, it is only during the initial period after closure studied by /Joyce et al. 2010/ and during the remaining part of the glacial cycle studied by /Vidstrand et al. 2010/ that matrix diffusion has a noticeable effect on the fracture water salinity. This is due to the long time needed to penetrate deep into the matrix porewater.

The groundwater flow modelling conducted by /Joyce et al. 2010/ uses the advection-dispersion equation for the advective solute transport. Matrix diffusion is based on a semi-analytical model developed by /Carrera et al. 1998/ and enhanced by /Hoch and Jackson 2004/. The penetration depth of the matrix diffusion process can be estimated from a simple 1D solution to Fick's equation, i.e.:

$$C\,(x,\,t) = C_0\; erfc\;[x/(2\sqrt{D_p t})] \qquad (7\text{-}1)$$

where $C(x,t)$ is the salinity [–] at distance $x$ [L] and time $t$ [T], $C_0$ is concentration at the boundary (fracture) and $D_p$ is the pore diffusivity [$L^2T^{-1}$],

$$D_p = D_e/\phi_m \qquad (7\text{-}2)$$

where $D_p$ is the effective diffusivity [$L^2T^{-1}$] and $\phi_m$ is the matrix porosity [–].

For a salinity ratio of 1%, i.e. $C(x,t)/C_0 \approx 0.01$, the penetration depth becomes:

$$x = 1.8\;[2\sqrt{D_p t}] \qquad (7\text{-}3)$$

The groundwater flow modelling conducted by /Vidstrand et al. 2010/ uses an advection-diffusion equation for the mobile solute transport. Matrix diffusion is based on the multi-rate model developed by /Haggerty and Gorelick 1995/. This model does not invoke classic single-rate transport parameters such as pore diffusivity and matrix porosity. However, as in the case of /Joyce et al. 2010/, the penetration depth of the remotest diffusive exchange rate $\alpha_{min}$ [$T^{-1}$] can be estimated from Equation 7-3, i.e.:

$$x = 1.8\;[2\sqrt{(D_p/\alpha_{min})}] \qquad (7\text{-}4)$$

Inserting $D_e = 4 \cdot 10^{-14}$–$4 \cdot 10^{-15}$ m²/s and $\phi_m = 3.7 \cdot 10^{-3}$, see Appendices C and F in /Joyce et al. 2010/, into Equation 7-3 renders penetration depths of approximately 2–6 m in a 10,000 years perspective. Inserting the same values of $D_e$ and $\phi_m$ together with $\alpha_{min} = 4 \cdot 10^{-12}$ s$^{-1}$, see Section 4.2.4 in /Vidstrand et al. 2010/, into Equation 7-4 renders the same range of penetration depths. In conclusion, the matrix diffusion models used in SR-Site suggest fairly similar penetration depths. As the spacing between conductive fractures is very large at repository depth, it is envisaged that the deep matrix porewater will not fully interact with fracture water on the time scales simulated by /Joyce et al. 2010/ or /Vidstrand et al. 2010/. This hypothesis is based on Figure 7-2, which shows chloride concentrations in matrix porewater and in fracture water from samples gathered in the target volume at Forsmark.

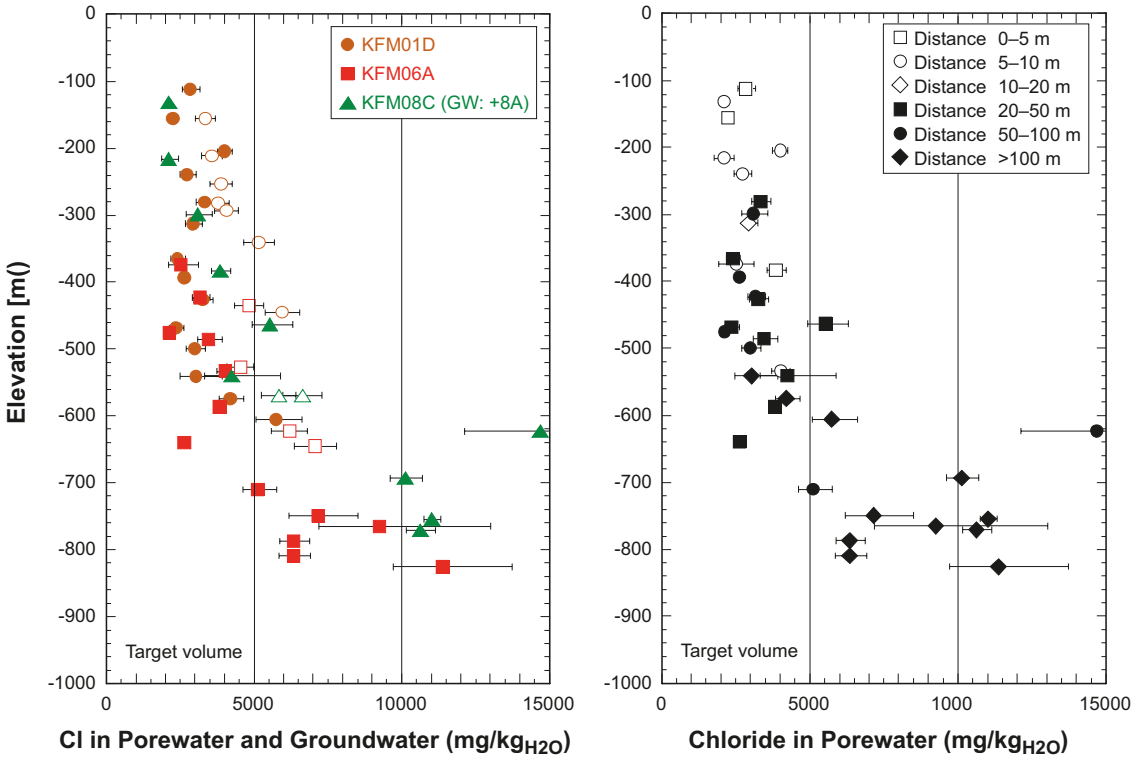


***Figure 7-2.*** *Chloride concentrations in matrix porewater (closed symbols) as a function of the borehole from which the core sample was collected (left) and the distance between the porewater sample and the nearest water conducting facture (right) detected with the PFL method versus elevation (m RHB 70) for the target volume bedrock. Chloride concentrations of fracture water (open symbols in right panels) collected from the same boreholes are given for comparison. See Figure 2-1 for allocation of target volume. (Modified after Figure 7-4 in /Waber et al. 2009/.)*

## 7.3 Consistency between models used in temperate and glacial period analyses

In both /Joyce et al. 2010/ and /Vidstrand et al. 2010/, performance measures are calculated for conditions both with and without an ice sheet present. The cases in /Vidstrand et al. 2010/ without an ice sheet can be considered to represent temperate conditions, even if the initial conditions used imply that the situation modelled does not represent present-day conditions. In the study of /Joyce et al. 2010/, boundary conditions from /Vidstrand et al. 2010/ representing cases with the ice sheet in close proximity to the repository are modelled. Corresponding cases are calculated in the super-regional scale model of /Vidstrand et al. 2010/. Hence, comparisons of these cases can be done and light can be shed on the consistency in results.

### 7.3.1 Temperate period results

In order to compare how the two models react to the glacial boundary conditions, it is of interest to first compare the results for temperate conditions. In Figure 7-3, the Darcy flux at deposition hole positions is shown. The red curve shows the results obtained from the simulations conducted with DarcyTools (ECPM) on a super-regional scale, and the blue curve shows the results from the simulations conducted with ConnectFlow (DFN) on a repository scale. The results are in a reasonable agreement given the differences in flow concept and model scale. Specifically it is noted that the ECPM model does not capture the lowest Darcy flux values and that the distribution is steeper. However, the tail of high values is captured well in the ECPM model when compared to the DFN model; the high-end tail is the one of interest and concern for applications within SR-Site.

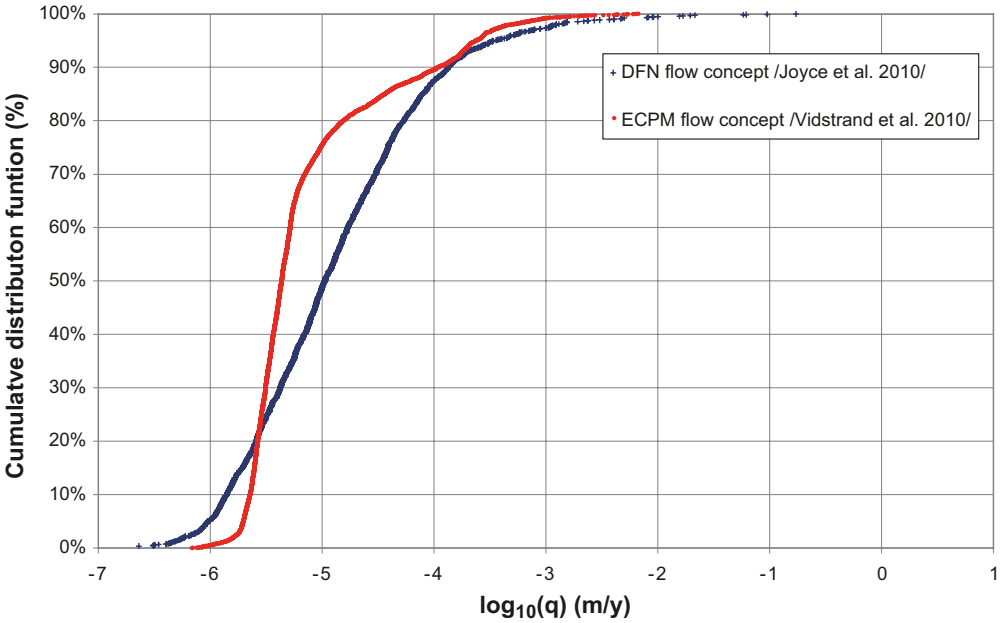


***Figure 7-3.*** *Cumulative distribution function plot of the Darcy flux (q) at deposition hole positions during temperate climate conditions from the models of /Joyce et al. 2010/ and /Vidstrand et al. 2010/, respectively. The results from /Joyce et al. 2010/ are based on the Q1 release path in the repository-scale model; the distribution only includes those deposition hole positions that have particles successfully reaching the model top boundary.*

### 7.3.2 Glacial period results

In Figure 6-12 and Figure 6-13 the Darcy flux and flow-related transport resistance resulting from the model by /Joyce et al. 2010/ using boundary conditions from /Vidstrand et al. 2010/ are shown for the Q1 path for the case with an advancing ice sheet margin without permafrost when the ice front is in close proximity to the repository (ice-front location II). The results are compared to the corresponding results at 2,000 AD. It is observed that the median Darcy flux is increased by approximately an order of magnitude. A corresponding decrease of the flow-related transport resistance is observed.

Corresponding results produced directly in the super-regional scale model of /Vidstrand et al. 2010/ are shown in Figure 7-4 and Figure 7-5, respectively. For the flow-related transport resistance it is observed that the super-regional model predicts a larger difference between the temperate and ice front location II models; i.e. the relative effect of the ice sheet appears stronger in the super-regional model.

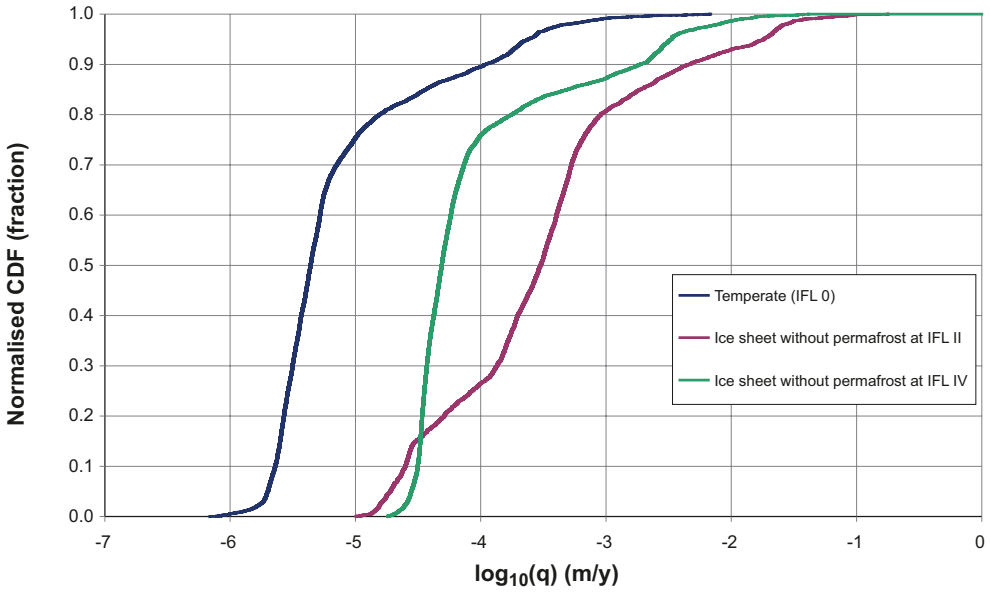


*Figure 7-4. Cumulative distribution function plots of Darcy flux (q) for the temperate case (IFL 0) and the Glacial case without permafrost when the ice sheet margin is at ice front locations II and IV, respectively.*

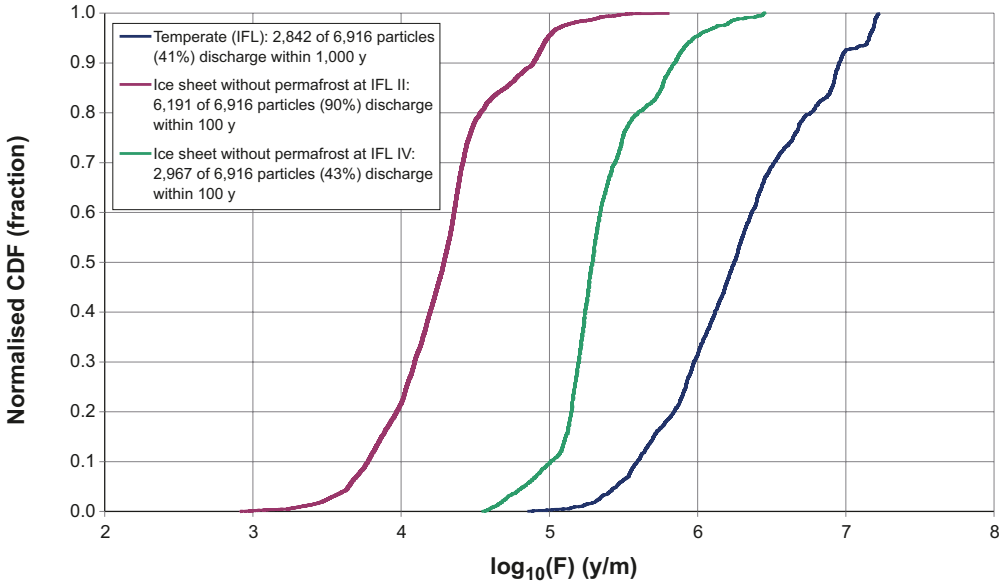


*Figure 7-5. Cumulative distribution function plots of flow-related transport resistance (F) for the temperate case (IFL 0) and the Glacial case without permafrost when the ice sheet margin is at ice-front locations II and IV, respectively.*

This is due to the fact that the super-regional model is treated as a continuum, whereas the combined repository-scale and site-scale models are based on a discrete description of the rock. The sparsely fractured rock characterising the Forsmark site at depth is better represented by a discrete representation; hence, the relatively weaker response to the ice sheet in the combined repository-scale and site-scale models is also considered to be a more correct feature of the modelled system. It is thus noted that a choice of conservatism is made when the flow factors presented in Section 6.4.7, based on results from the super-regional model, are applied in subsequent transport analyses.

## 7.4 Use of hydrogeological results in other disciplines within SR-Site

The results from the bedrock hydrogeological simulations summarised in this report are used in different applications and disciplines within SR-Site. Some of the applications are already mentioned in Chapters 4, 5 and 6. Below, a fuller list is provided including also some complementary analyses performed for direct use within the other disciplines.

### 7.4.1 Rock shear movement and climate evolution

It is noted that some hydrogeological arguments or input are used in the description of rock shear movement, and in the development of the climate evolution. Concerning rock shear movement, see Section 10.4.5 of the SR-Site Main report /SKB 2011/, it is argued that the critical fractures concerning shear movement likely coincides with the most water conductive fractures in the hydrogeological description. Concerning the development of the climate evolution, some of the descriptions in Section 4.5 of the Climate report /SKB 2010a/ are based on, or written in line with, the quantitative results of /Vidstrand et al. 2010/.

### 7.4.2 Corrosion

The Darcy flux values from the temperate phase modelling /Joyce et al. 2010/ are used in the calculations of canister corrosion. The applications are presented in /SKB 2010h/ and summarised in the SR-Site Main report Sections 10.3.13, 10.4.9, 12.6.2 and Chapter 14.

### 7.4.3 Buffer and backfill erosion

For the case where there are strong hydraulic gradients in a fracture intersecting a deposition hole, it could be imagined that buffer could be lost by shearing of particles from the bentonite gel by seeping water. Figure 7-6 shows the shear stress as a function of the hydraulic gradient based on a model for the shear stress as a function of the hydraulic gradient and fracture aperture /Neretnieks et al. 2009/ and the output from hydrogeological modelling from the glacial case without permafrost in /Vidstrand et al. 2010/. The interpretation of the results is presented in Section 10.4.8 in the SR-Site Main report. Hydrogeological results are also used in Section 10.3.11 of the SR-Site Main report when assessing buffer and backfill erosion during temperate climate conditions.

### 7.4.4 Geochemical analyses

Geochemical analyses are performed in SR-Site Main report /SKB 2011/ in Section 10.3.7 for temperate conditions using the fractions of reference waters from /Joyce et al. 2010/ and in Section 10.4.7 for glacial and periglacial conditions using the salinity distributions from /Vidstrand et al. 2010/. In these applications, the groundwater chemistry evolution is analysed. In Section 12.6.2 of the Main report, oxygen penetration is analysed based on the corresponding hydrogeological results.

Furthermore, hydrogeological data is used to argue that sulphide concentrations are not correlated to fracture transmissivity /Tullborg et al. 2010/.

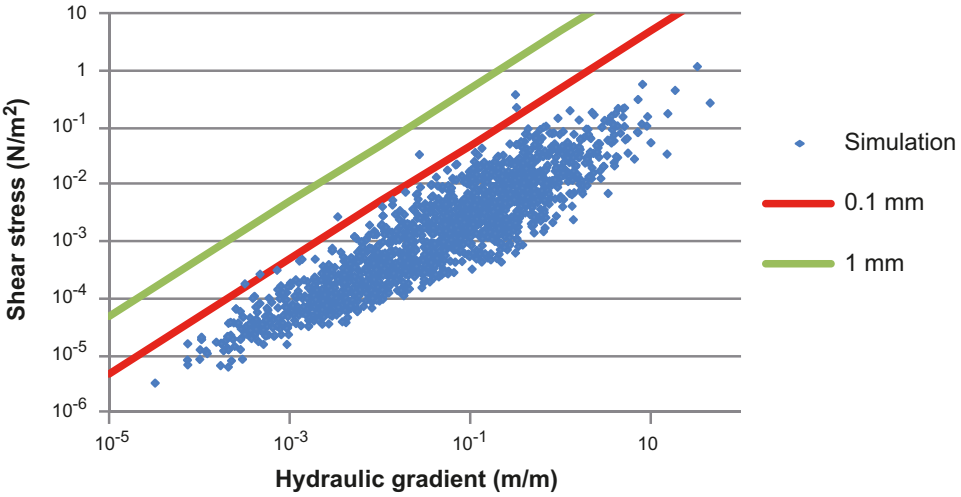


***Figure 7-6.*** *Plot of the shear stress at gel/water interface during glaciation as a function of hydraulic gradient for two different aperture values (0.1 mm and 1 mm) using a model in /Neretnieks et al. 2009/ together with data from /Vidstrand et al. 2010/. The gradients shown come from the glacial case without permafrost when the ice sheet margin is at ice-front location II.*

### 7.4.5 Biosphere analyses

The biosphere exit locations from the regional-scale model of /Joyce et al. 2010/ are used as input when identifying biosphere objects in space and time. The analysis is presented in Section 13.2.2 of the SR-Site Main report. It is noted that results and information from both SDM-Site and the surface hydrological modelling of SR-Site are used extensively in the biosphere analyses as conceptual support and direct input data.

### 7.4.6 Surface hydrology

Surface hydrology is modelled in SR-Site with the modelling tool MIKE SHE /DHI Software 2008/. The parameterisation of the bedrock is based on the hydrogeological base case as presented in the present report. Furthermore, particle tracking results from the ConnectFlow model at elevation –40 m have been exported to the MIKE SHE application for the study of flow paths in the surface system. Also, discharge locations in the MIKE SHE model are compared to discharge locations in the temperate model /Bosson et al. 2010/.

The hydrogeological properties of the rock exported from ConnectFlow to MIKE SHE consist of hydraulic conductivity, specific storage and porosity.

### 7.4.7 Radionuclide transport in nearfield and farfield

The radionuclide transport calculations within SR-Site are described in detail in /SKB 2010d/ and summarised in the SR-Site Main report in Chapter 13.

In the nearfield calculations, the input from the hydrogeological modelling is the equivalent flow rates. In the farfield calculations, the input is the advective travel time and flow-related transport resistance. It is noted that the ConnectFlow application exports both flow-path integrated and segment-based values of advective travel time and flow-related transport resistance for use in different farfield radionuclide transport codes. When segment based values are exported, an account is also made whether a segment resides in tunnels, fractured rock (HRD), deformation zones (HCD) or in soils (HSD; including also rock described as a continuum). This enables an analysis of the retention potential of the different units of the flow system, see /SKB 2010d/ for details.

### 7.4.8 Supporting arguments and feedback to reference design

In Sections 14.3.2 and 15.5.13 of the SR-Site Main report, supporting arguments for safety are discussed and feedback to the design are presented. The results presented in Section 7.1 of the present report are used as a basis for discussions on a more direct and easily observable criterion than “FPC or EFPC” that could be used as a complement to further reduce the final calculated risk in the assessment.

# 8 Summary and conclusions

## 8.1 Summary

In the present report, the bedrock hydrogeological modelling studies performed within SR-Site are summarised and put into a safety assessment context. The methodology used is presented together with the numerical model setups, and results are discussed in light of the issues to be addressed in the safety assessment.

The main objective of the report is to bridge the individual groundwater flow modelling studies of the different time periods with the overall assessment made in the SR-Site Main report. Thus, the present report both provides a summary of the individual modelling reports, and uses the detailed results from these individual studies to provide an integrated assessment of the issues addressed within SR-Site.

## 8.2 Conclusions

Conclusions on a detailed level associated with numerical modelling issues are presented in the individual modelling reports. Here, conclusions with relevance for the use of results from the groundwater flow modelling in the safety assessment are provided. First, conclusions related to the different time periods studied are given. Second, conclusions related to the integration between time periods are provided.

Main conclusions from the study of the excavation and operational phases are:

- During the operation of the repository, a dilution occurs around most parts of the repository. That is, less saline water is drawn towards repository depth due to the lowering of the groundwater table.
- The results indicate that the recharge area is located mainly right above the repository. The radius of influence away from the perimeter of the open repository does not exceed a few hundred metres.
- The total inflow varies from 8 to 51 L/s depending on the stage of operation and the level of grouting efficiency.
- When inflow into individual deposition holes is studied, it is important to capture the discontinuous characteristics of the fractured rock. That is, the utilised equivalent discontinuous porous medium (EDPM) approach is shown to be better suited for this application than a traditional continuous (ECPM) approach. It is shown that 141 out of 372 deposition holes failing inflow criterion “Q1 or Q2” using the EDPM approach also are identified by the “FPC or EFPC” criterion. Thus, the “FPC or EFPC” criterion identifies less than half of the deposition hole positions failing the inflow rejection criteria. However, both “FPC or EFPC” and the inflow rejection criteria appear to capture the deposition holes with most unfavourable conditions. Future studies of the formal use of inflow rejection criteria are suggested based on the preliminary findings within SR-Site. However, it is noted that the “FPC or EFPC” criterion also has relevance for reducing risks associated with e.g. earthquakes; hence, inflow rejection criteria alone may not be sufficient to identify unsuitable deposition hole positions. A combination of both types of criteria likely needs to be considered in the future.
- There appears to be substantial variability between realisations when number and location of deposition holes rejected by inflow criteria are considered. This is due to the fact that the inflows are governed by the stochastic fracture network. The variability can likely only be reduced when deterministic knowledge about fractures intersecting deposition holes is obtained during construction of a repository.

Main conclusions from the study of the period with temperate climate conditions are:

- It will take several hundred years for the repository backfill to reach full saturation. The temperate period is on the order of 10,000 years, hence this initial period of unsaturated conditions covers only a small part of it, and the assumption of saturated conditions within the rest of the simulations of the temperate period can be defended.
- The salinity at repository depth develops during the temperate period towards more dilute conditions due to the flushing by meteoric water following the shoreline displacement.
- The discharge from the repository evolves over time; the near-future discharge locations (3000 AD, 4000 AD and 5000 AD) follow the retreating shoreline. The far-future discharge locations (6000 AD through to 12,000 AD) congregate on the north-eastern model boundary.
- Flow paths tend to become longer with the retreating shoreline. This generally implies longer travel times and larger flow-related transport resistance values with time.
- Roughly 70 per cent of the 6,916 deposition hole positions do not have a flowing fracture intersecting the deposition hole. When the "FPC or EFPC" criterion is applied, roughly 10 per cent of the deposition holes are rejected, leaving the number of deposition holes with a flowing fracture to be roughly 20 per cent of the total number of deposition holes.
- There appears to be some variability between realisations. Specifically, concerning flow-related transport resistance and advective travel time, it is seen that the median and upper percentiles are quite stable between realisations, whereas some realisations have a pronounced lower tail. However, the Darcy flux is more stable between realisations. Also, for all performance measures, the Q1 path is characterised by less variability between realisations than the Q2 and Q3 paths, respectively. The reason is large stochastic fractures intersecting the deposition tunnels and hence the Q2 and Q3 paths in individual realisations.
- The results indicate that approximately two per cent of the deposition hole positions will experience dilute conditions within the Global warming variant whereas approximately one per cent will experience dilute conditions during the first ten thousand years of the initial temperate period.
- An increase in the excavation damaged zone (EDZ) transmissivity implies an increase in the associated Darcy flux. The existence of a crown space in the backfilled tunnels implies only marginal changes in the Darcy fluxes of the different release paths. Concerning the flow-related transport resistance, the case with no EDZ provides most favourable conditions. With an increased EDZ transmissivity or a crown space, less favourable conditions prevail. The effect of EDZ and crown space on the flow-related transport resistance is most pronounced for the Q3 path.
- The Darcy flux and flow-related transport resistance are dependent on the chosen transmissivity-size relationship with up to about half an order of magnitude variation between variants. The other SDM-Site related model variants (possible deformation zones, unmodified vertical hydraulic conductivity, extended spatial variability) yield only small changes in performance measures.
- The effect of open boreholes is small on performance measures even if the groundwater flow pattern is affected and the flow pathways of the released particles change. When ensemble statistics of all deposition hole positions is considered, the change in performance measures generally stays within 20 per cent comparing the borehole case to the hydrogeological base case.

Main conclusions from the study of the period with periglacial and glacial climate conditions (remaining part of the reference glacial cycle) are:

- The influence of the present-day topographic water divides on the flow regime is significantly diminished during periglacial and glacial climate conditions.
- The Darcy flux increases dramatically during the two ice-front passages, glaciation (advance, pre-LGM) and deglaciation (retreat, post-LGM). It is observed that inside the repository footprint, the normalised average value of the Darcy flux during a full glacial cycle is about 0.8; i.e. the Darcy flux averaged over the 120,000 year glacial cycle is below the corresponding value of the temperate period.

- The passage of the ice sheet margin across the site during glaciation (pre-LGM) is characterised by an initial upconing of saline water followed by an out flushing of this water resulting in lower salinities at repository depth than during the initial temperate conditions. However, during the subsequent stage, i.e. when the site is completely covered by the ice sheet (LGM), a gradual increase in fracture water salinity at repository depth occurs. This gain of the "salt water interface" is due to an accommodation of the buoyancy forces to the very weak top boundary condition of an almost uniform ice sheet thickness, and to the slow, but continuous advective transport of salt from below.
- The passage during deglaciation (post-LGM) is also characterised by an upconing and flushing event, but the effects are considerably smaller than during the advance. The reason for this is twofold; (i) the speed of the retreating ice sheet margin is faster than the speed of the advancing ice sheet margin, and (ii) the subglacial area in front of the retreating ice sheet margin is submerged. These conditions reduce the duration and the magnitude of the hydraulic gradient across the ice sheet margin significantly.
- Regarding the exchange of salt between the fracture water and the matrix porewater, the exchange appears to be from the matrix porewater to the fracture water for a limited period of time only coinciding with the passages of the ice sheet margin. During the long period of complete ice coverage the conditions are the opposite. In conclusion, low fracture water salinities, i.e. dilute conditions, are mainly found in conjunction with the ice front passages. The results obtained indicate that fracture water salinities reach values below ten per cent of the values at temperate conditions for a limited period of time only.
- The results indicate that approximately two per cent of the deposition hole positions will experience dilute conditions for an advancing ice sheet margin that is at rest right above the repository for 100 years.
- The results indicate that approximately two per cent of the deposition hole positions will experience dilute conditions during an assumed duration of 100,000 years of complete ice coverage.
- The discharge locations are predominantly found well within the physical boundaries of the model domain and often very close to the ice sheet margin. The differences seen between the two glacial cases studied depend on the handling of permafrost. If permafrost is included, the majority of the discharge occurs in taliks located in the periglacial area.

Integrated modelling conclusions are:

- The application of inflow rejection criteria during open repository conditions has a good potential to identify deposition hole positions with unfavourable conditions during saturated conditions.
- Inflow rejection criteria appear as a good complement to the "FPC or EFPC" criterion in terms of identifying unfavourable deposition hole locations.
- Matrix diffusion is parametrised consistently between the two model codes and applications, yielding similar matrix penetration depths for the considered simulation times. Also, the calculated penetration depths appear consistent with the present site understading implying that only the rock matrix in fairly close proximity to the fractures interact with the fracture water.
- The ECPM model application appears to yield a stronger glacial effect at repository depth than the discrete DFN model application. The sparsely fractured rock characterising the Forsmark site at depth is better represented by a discrete representation; hence, the relatively weaker response to the ice sheet in the combined repository-scale and site-scale models is considered to be a correct feature of the modelled system.
- The repository structures are not explicitly included in the super-regional model by /Vidstrand et al. 2010/, and hence results for the different release paths Q1, Q2 and Q3 are not obtained. By transferring boundary conditions from the super-regional scale model of /Vidstrand et al. 2010/ to the combined repository-scale and site-scale models of /Joyce et al. 2010/, where the repository is included, performance measures during periglacial and glacial climate conditions are obtained.

# 9 References

SKB's (Svensk Kärnbränslehantering AB) publications can be found at www.skb.se/publications.


**Bosson E, Sassner M, Sabel U, Gustafsson L-G, 2010.** Modelling of present and future hydrology and solute transport at Forsmark. SR-Site Biosphere. SKB R-10-02, Svensk Kärnbränslehantering AB.

**Börgesson L, Fälth B, Hernelind J, 2006.** Water saturation phase of the buffer and backfill in the KBS-3V concept. Special emphasis given to the influence of the backfill on the wetting of the buffer. SKB TR-06-14, Svensk Kärnbränslehantering AB.

**Carrera J, Sanchez-Vila X, Benet I, Medina A, Galarza G, Guimera J, 1998.** On Matrix Diffusion: Formulations, Solution Methods, Quantitative Effects, Hydrogeology Journal 6, No. 1, 178-190.

**Cordes C, Kinzelbach W, 1992.** Continuous groundwater velocity fields and path lines in linear, bilinear, and trilinear finite elements. Water Resources Research, 28, pp 2903–2911.

**Crawford J, 2008.** Bedrock transport properties Forsmark. Site descriptive modelling, SDM-Site Forsmark. SKB R-08-48, Svensk Kärnbränslehantering AB.

**Dershowitz W, Winberg A, Hermanson J, Byegård J, Tullborg E-L, Andersson P, Mazurek M, 2003.** Äspö Hard Rock Laboratory. Äspö Task Force on modelling of groundwater flow and transport of solutes. Task 6c. A semi-synthetic model of block scale conductive structures at the Äspö HRL. SKB IPR-03-13, Svensk Kärnbränslehantering AB.

**DHI Software, 2008.** MIKE SHE – User manual. DHI Water & Environment, Hørsholm, Denmark.

**Enssle C P, Poppei J, 2010.** Implementation and testing of an improved methodology to simultate resaturation processes with DarcyTools. SKB R-09-54, Svensk Kärnbränslehantering AB.

**Follin S, 2008.** Bedrock hydrogeology Forsmark. Site descriptive modelling, SDM-Site Forsmark. SKB R-08-95, Svensk Kärnbränslehantering AB.

**Follin S, Levén J, Hartley L, Jackson P, Joyce S, Roberts D, Swift B, 2007a.** Hydrogeological characterisation and modelling of deformation zones and fracture domains, Forsmark modelling stage 2.2. SKB R-07-48, Svensk Kärnbränslehantering AB.

**Follin S, Johansson P-O, Hartley L, Jackson P, Roberts D, Marsic N, 2007b.** Hydrogeological conceptual model development and numerical modelling using CONNECTFLOW, Forsmark modelling stage 2.2. SKB R-07-49, Svensk Kärnbränslehantering AB.

**Follin S, Hartley L, Jackson P, Roberts D, Marsic N, 2008.** Hydrogeological conceptual model development and numerical modelling using CONNECTFLOW, Forsmark modelling stage 2.3. SKB R-08-23, Svensk Kärnbränslehantering AB.

**Haggerty R, Gorelick S M, 1995.** Multiple-rate mass transfer for modeling diffusion and surface reactions i media with pore-scale heterogeneity. Water Resources Research, 31, pp 2383–2400.

**Hartikainen J, Kouhia R, Wallroth T, 2010.** Permafrost simulations at Forsmark using a numerical 2D thermo-hydro-chemical model. SKB TR-09-17, Svensk Kärnbränslehantering AB.

**Hartley L, Cox I, Holton D, Hunter F, Joyce S, Gylling B, Lindgren M, 2004.** Groundwater flow and radionuclide transport modelling using CONNECTFLOW in support of the SR Can assessment. SKB R-04-61, Svensk Kärnbränslehantering AB.

**Hartley L, Hoch A, Jackson P, Joyce S, McCarthy R, Rodwell W, Swift B, Marsic N, 2006.** Groundwater flow and transport modelling during the temperate period for the SR-Can assessment. Forsmark area – version 1.2. SKB R-06-98, Svensk Kärnbränslehantering AB.

**Hjerne C, Nordqvist R, Harrström J, 2010.** Compilation and analyses of results from cross-hole tracer tests with conservative tracers. SKB R-09-28, Svensk Kärnbränslehantering AB.

**Hoch A R, Jackson C P, 2004.** Rock-matrix diffusion in transport of salinity. Implementation in ConnectFlow. SKB R-04-78, Svensk Kärnbränslehantering AB.

**Hökmark H, Lönnqvist M, Fälth B, 2010.** THM-issues in repository rock. Thermal, mechanical, thermo-mechanical and hydro-mechanical evolution of the rock at the Forsmark and Laxemar sites. SKB TR-10-23, Svensk Kärnbränslehantering AB.

**Joyce S, Simpson T, Hartley L, Applegate D, Hoek J, Jackson P, Swan D, Marsic N, Follin S, 2010.** Groundwater flow modelling of periods with temperate climate conditions – Forsmark. SKB R-09-20, Svensk Kärnbränslehantering AB.

**Laaksoharju M, Smellie J, Tullborg E-L, Gimeno M, Hallbäck L, Molinero J, Waber N, 2008.** Bedrock hydrogeochemistry Forsmark. Site descriptive modelling, SDM-Site Forsmark. SKB R-08-47, Svensk Kärnbränslehantering AB.

**Longcheng L, Moreno L, Neretnieks I, Gylling B, 2010.** A safety assessment approach using coupled NEAR3D and CHAN3D – Forsmark. SKB R-10-69, Svensk Kärnbränslehantering AB.

**Lönnqvist M, Hökmark H, 2010.** Assessment of potential for glacially induced hydraulic jacking at different depths. SKB R-09-35, Svensk Kärnbränslehantering AB.

**Munier R, 2006.** Using observations in deposition tunnels to avoid intersections with critical fractures in deposition holes. SKB R-06-54, Svensk Kärnbränslehantering AB.

**Munier R, 2010.** Full perimeter intersection criteria. Definitions and implementations in SR-Site. SKB TR-10-21, Svensk Kärnbränslehantering AB.

**Mårtensson E, Gustafsson L-G, 2010.** Hydrological and hydrogeological effects of an open repository in Forsmark. Final MIKE SHE flow modelling results for the Environmental Impact Assessment. SKB R-10-18, Svensk Kärnbränslehantering AB.

**Neretnieks I, Liu L, Moreno L, 2009.** Mechanisms and models for bentonite erosion. SKB TR-09-35, Svensk Kärnbränslehantering AB.

**Olofsson I, Simeonov A, Stephens M, Follin S, Nilsson A-C, Röshoff K, Lindberg U, Lanaro F, Fredriksson A, Persson L, 2007.** Site descriptive modelling Forsmark, stage 2.2. A fracture domain concept as a basis for the statistical modelling of fractures and minor deformation zones, and inter-disciplinary coordination. SKB R-07-15, Svensk Kärnbränslehantering AB.

**Salas J, Gimeno M J, Auqué L, Molinero J, Gómez J, Juárez I, 2010.** SR-Site – hydrogeochemical evolution of the Forsmark site. SKB TR-10-58, Svensk Kärnbränslehantering AB.

**Selroos J O, Walker D D, Ström A, Gylling B, Follin S, 2002.** Comparison of alternative modelling approaches for groundwater flow in fractured rock. Journal of Hydrology, 257, pp 174–188.

**Serco, 2008a.** ConnectFlow Release 9.6 Technical Summary Document. SA/ENV/CONNECTFLOW/15, Serco Assurance, UK.

**Serco, 2008b.** NAMMU Release 9.6 Technical Summary Document. SA/ENV/CONNECTFLOW/8, Serco Assurance, UK.

**Serco, 2008c.** NAPSAC Release 9.6 Technical Summary Document. SA/ENV/CONNECTFLOW/12, Serco Assurance, UK.

**Serco, 2008d.** NAMMU Release 9.6 Verificiation Document. SA/ENV/CONNECTFLOW/9, Serco Assurance, UK.

**Serco, 2008e.** NAPSAC Release 9.6 Verificiation Document. SA/ENV/CONNECTFLOW/13, Serco Assurance, UK.

**Serco, 2008f.** ConnectFlow Release 9.6 Verificiation Document. SA/ENV/CONNECTFLOW/16, Serco Assurance, UK.

**Serco, 2011.** NAMMU Technical Summary, Release 10.1, Serco Report SA/ENV/CONNECTFLOW/8.

**Sidborn M, Sandström B, Tullborg E-L, Delos A, Molinero J, Hallbeck L, Pedersen K, 2010.** SR-Site: Oxygen ingress in the rock at Forsmark during a glacial cycle. SKB TR-10-57, Svensk Kärnbränslehantering AB.

**SKB, 2005a.** Preliminary site description Forsmark area – version 1.2. SKB R-05-18, Svensk Kärnbränslehantering AB.

**SKB, 2005b.** Forsmark site investigation. Programme for further investigations of geosphere and biosphere. SKB R-05-14, Svensk Kärnbränslehantering AB.

**SKB, 2008.** Site description of Forsmark at completion of the site investigation phase. SDM-Site Forsmark. SKB TR-08-05, Svensk Kärnbränslehantering AB.

**SKB, 2009a.** Design premises for a KBS-3V repository based on results from the safety assessment SR-Can and some subsequent analyses. SKB TR-09-22, Svensk Kärnbränslehantering AB.

**SKB, 2009b.** Underground design Forsmark. Layout D2. SKB R-08-116, Svensk Kärnbränslehantering AB.

**SKB, 2010a.** Climate and climate-related issues for the safety assessment SR-Site. SKB TR-10-49, Svensk Kärnbränslehantering AB.

**SKB, 2010b.** Data report for the safety assessment SR-Site. SKB TR-10-52, Svensk Kärnbränslehantering AB.

**SKB, 2010c.** Geosphere process report for the safety assessment SR-Site. SKB TR-10-48, Svensk Kärnbränslehantering AB.

**SKB, 2010d.** Radionuclide transport report for the safety assessment SR-Site. SKB TR-10-50, Svensk Kärnbränslehantering.

**SKB, 2010e.** Design, construction and initial state of the underground openings. SKB TR-10-18, Svensk Kärnbränslehantering AB.

**SKB, 2010f.** Design, production and initial state of the backfill and plug in deposition tunnels. SKB TR-10-16, Svensk Kärnbränslehantering AB.

**SKB, 2010g.** Model summary report for the safety assessment SR-Site. SKB TR-10-51, Svensk Kärnbränslehantering AB.

**SKB, 2010h.** Corrosion calculations report for the safety assessment SR-Site. SKB TR-10-66, Svensk Kärnbränslehantering AB.

**SKB, 2011.** Long-term safety for the final repository for spent nuclear fuel at Forsmark. Main report of the SR-Site project. SKB TR-11-01, Svensk Kärnbränslehantering AB.

**Stephens M B, Fox A, La Pointe P R, Simeonov A, Isaksson H, Hermanson J, Öhman J, 2007.** Geology Forsmark. Site descriptive modelling Forsmark stage 2.2. SKB R-07-45, Svensk Kärnbränslehantering AB.

**Svensson U, 2010.** DarcyTools Version 3.4 – Verification, validation and demonstration. SKB R-10-71, Svensk Kärnbränslehantering AB.

**Svensson U, Ferry M, 2010.** DarcyTools Version 3.4 – User's Guide. SKB R-10-72, Svensk Kärnbränslehantering AB.

**Svensson U, Follin S, 2010.** Groundwater flow modelling of the excavation and operational phases – Forsmark. SKB R-09-19, Svensk Kärnbränslehantering AB.

**Svensson U, Ferry M, Kuylenstierna H-O, 2010.** DarcyTools Version 3.4 – Concepts, methods and equations. SKB R-07-38, Svensk Kärnbränslehantering AB.

**Tullborg E-L, Smellie J, Nilsson A-C, Gimeno M J, Auqué L F, Brüchert V, Molinero J, 2010.** SR-Site – sulphide content in the groundwater at Forsmark. SKB TR-10-39, Svensk Kärnbränslehantering AB.

**Vidstrand P, Follin S, Zugec N, 2010.** Groundwater flow modelling of periods with periglacial and glacial climate conditions – Forsmark. SKB R-09-21, Svensk Kärnbränslehantering AB.

**Waber H N, Gimmi T, Smellie J A T, 2009.** Porewater in the rock matrix. Site descriptive modelling SDM-Site Forsmark. SKB R-08-105, Svensk Kärnbränslehantering AB.

**Öhman J, Follin S, 2010.** Site investigation SFR. Hydrogeological modelling of SFR. Model version 0.2. SKB R-10-03, Svensk Kärnbränslehantering AB.

# Appendix A

## Extended hydrogeological DFN

**Table A-1. Preliminary hydrogeological DFN parameters of the hydraulic rock domains outside the candidate area. (Source: Appendix A in /Öhman and Follin 2010/.)**

| Fracture domain (m RHB 70) | Fracture set name | Orientation set pole: (trend, plunge), conc. | Size model, power-law ($r_0$, $k_r$) (m, –) | Intensity, ($P_{32}$), valid size interval: ($r_0$, 169 m) ($m^2/m^3$) | Parameter values for a correlated transmissivity model: $T = a\ r^b$ (*a*,*b*) |
|---|---|---|---|---|---|
| > –60 | EW | (3, 7) 12.6 | (0.038, 3.45) | 2.597 | ($6.0 \cdot 10^{-9}$, 1.29) |
| | NW | (233, 12) 13.2 | (0.038, 3.10) | 1.153 | ($8.0 \cdot 10^{-9}$, 1.13) |
| | NE | (128, 8) 11.7 | (0.038, 3.45) | 1.339 | ($1.0 \cdot 10^{-9}$, 1.25 |
| | HZ | (116, 85) 27.6 | (0.038, 2.60) | 1.059 | ($2.0 \cdot 10^{-8}$, 1.48) |
| | GD | (232, 85) 6.5 | (0.038, 2.79) | 1.865 | ($3.7 \cdot 10^{-8}$, 1.16) |
| –60 to –245 | EW | (5, 13) 8.5 | (0.038, 3.45) | 1.407 | ($6.0 \cdot 10^{-9}$, 1.29) |
| | NW | (234, 6) 12.3 | (0.038, 2.95) | 0.856 | ($8.0 \cdot 10^{-9}$, 1.13) |
| | NE | (128, 6) 11.5 | (0.038, 3.45) | 1.033 | ($1.0 \cdot 10^{-8}$, 1.25) |
| | HZ | (137, 84) 7.1 | (0.038, 2.55) | 0.848 | ($2.1 \cdot 10^{-9}$, 1.85) |
| | GD | (354, 85) 7.1 | (0.038, 2.72) | 1.204 | ($4.0 \cdot 10^{-9}$, 1.05) |
| < –245 | EW | (3, 20) 9.7 | (0.038, 3.45) | 0.918 | ($6.0 \cdot 10^{-9}$, 1.29) |
| | NW | (233, 7) 14.9 | (0.038, 3.10) | 0.867 | ($8.0 \cdot 10^{-9}$, 1.13) |
| | NE | (305, 0) 11.2 | (0.038, 3.45) | 1.023 | ($1.0 \cdot 10^{-8}$, 1.25) |
| | HZ | (128, 81) 27.9 | (0.038, 2.75) | 0.595 | ($1.4 \cdot 10^{-9}$, 1.45) |
| | GD | (269, 85) 6.6 | (0.038, 2.70) | 1.283 | ($2.2 \cdot 10^{-9}$, 0.90) |

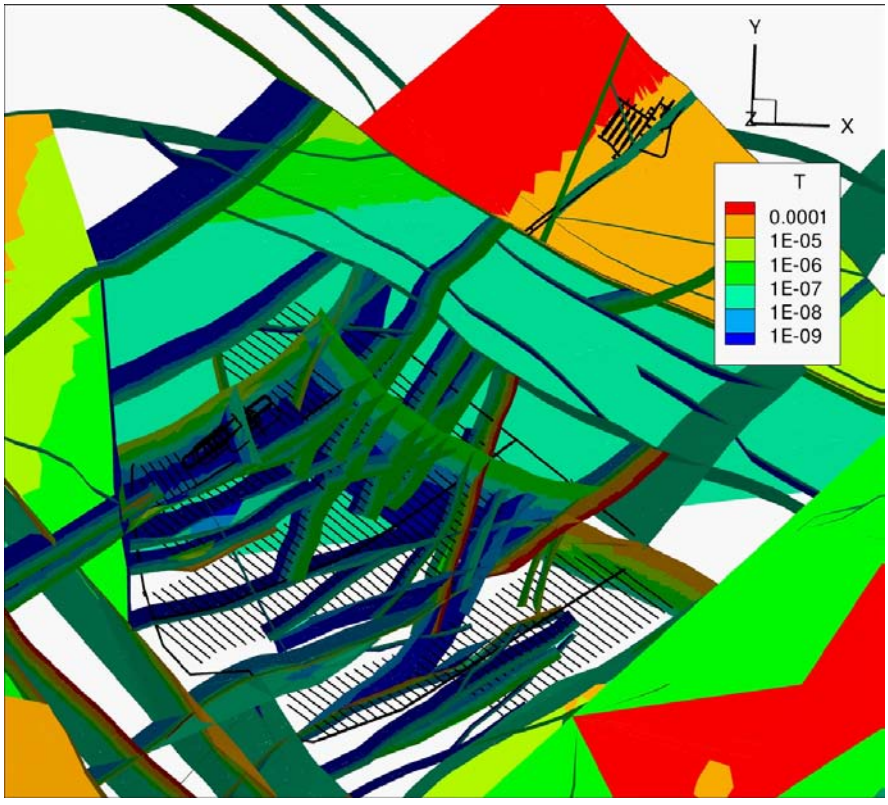


***Figure A-1.*** *View showing a final repository for spent nuclear fuel at Forsmark and SFR, the existing repository for short-lived radioactive waste. The shortest distance between the two repositories is less than 1 km. The y-axis points towards north. In this image, the deformation zones have homogeneous hydraulic properties with depth dependency according to Equation 2-1. In addition, some zones are deleted for visibility.*